

Investigation of Halogenate Complexes Stabilized
by Fluorido, Chlorine Monofluoride, and
Perfluoro-*tert*-Butoxy Ligands

Inaugural-Dissertation
to obtain the academic degree
Doctor rerum naturalium (Dr. rer. nat.)

submitted to the Department of Biology, Pharmacy, Chemistry
of Freie Universität Berlin

by

Patrick Pröhm

2021

The work for this dissertation was done in the group of Prof. Sebastian Hasenstab-Riedel from October 2017 until November 2021 at the Institute of Chemistry and Biochemistry at Freie Universität Berlin.

I declare that this dissertation is my own work except where stated contrary. This dissertation has not been submitted to obtain any other degree.

Patrick Pröhm

First referee: Prof. Dr. Sebastian Hasenstab-Riedel

Second referee: Prof. Dr. Berthold Hoge

Date of disputation: 11 March 2022

Acknowledgements

Firstly, I want to express my great thanks to Prof. Dr. Sebastian Hasenstab-Riedel who not only provided me with the opportunity to undertake my doctoral thesis in his research group but was also helpful and supportive at any time regarding my research and also personally.

Additionally, I want to thank Prof. Dr. Berthold Hoge for assessing this thesis as a second referee.

Also I would like to thank my collaboration partners for their hard work to genuinely improve my projects and publications: Caspar J. Schattenberg, Dr. Robert Müller and Prof. Dr. Martin Kaupp.

I want to thank my students Jonas R. Schmid and Willi R. Berg for their high commitment during their research internship, bachelor's and master's theses. My gratitude also goes to Dr. Karsten Sonnenberg, Dr. Simon Steinhauer, Dr. Daniel Franz, Susanne Rupf, Patrick Voßnacker and Kurt Hoffmann for crystal measurements. Furthermore, I want to express my gratitude to Dr. Alberto Pérez-Bitrián, Dr. Julia Bader und Dr. Alex Plajer for proofreading this dissertation.

Furthermore, I want to thank all my academic mentors, advisors, assistants and tutors who greatly taught and inspired me in all fields of chemistry. You helped me to become the chemist I am. In addition, I owe gratitude to the whole AG Riedel with its current and former members because it has created a friendly, homely atmosphere and welcomed me during my first days in Berlin. Throughout my time you were always helpful with scientific advice and experimental help. I really enjoyed the many coffee breaks, BBQs and *Feierabendbiere* with you. Moreover, my thanks goes to Kurt Hoffmann for being a great lab mate. I want to thank you for a great time with fruitful scientific discussions, and many other good conversations and for being indulgent to me when I did not clean my glassware in time. The FCI is acknowledged for providing Ph. D. funding (Kekulé Fellowship).

Finally I want to thank my family, my friends and my beloved fiancée for always supporting and encouraging me as well as for being patient with me. Without you this work would not have been possible.

Abstract

The synthesis and follow-up chemistry of classical and non-classical fluoridochlorates and -bromates is investigated. Here, an efficient synthetic method for the synthesis of soluble di- and tetrafluoridohalogenates(I/III) of bromine and chlorine is presented. Tetraalkylammonium halides are fluorinated with dilute fluorine or chlorine monofluoride (10 % in Ar) in acetonitrile or propionitrile. For the first time, difluoridochlorate(I) and -bromate(I) salts are fully characterized by Raman and NMR spectroscopy as well as by single crystal X-ray diffraction. The data are supported by quantum-chemical calculations. Their potential application as halogenation reagents is studied with different organic and inorganic substrates. These include nitriles and tetracyanoborate which reacted to their corresponding trifluoromethyl compounds, diaryldisulfides were fully fluorinated to pentafluorosulfanyl aryls, noble metals dissolved under formation of fluoro- and bromido metallates and the reaction with carbon monoxide yielded carbonyl fluoride.

Furthermore, these compounds are used as substrates in ligand exchange reactions with perfluoro-*tert*-butyl hypochlorite to install the perfluoro-*tert*-butoxy ligand on a positively charged halogen atom. The isolation of halogen(I) species with this ligand was possible for chlorine, bromine and iodine, while the oxidation state +III was only reached for bromine and iodine. During the attempted synthesis of a Cl(III) compound, ligand oxidation under formation of perfluoro-*tert*-butyl hypofluorite and -peroxide was observed. The steric bulk of the ligands in tetrakis(perfluoro-*tert*-butoxy)iodate(III) effectively shields the iodine center from further oxidation with dilute fluorine. Additionally, the non-classical polyinterhalide $[\text{F}(\text{ClF})_3]^-$ was synthesized from the reaction of tetramethylammonium chloride with an excess of chlorine monofluoride. This compound was thoroughly characterized by Raman spectroscopy and single crystal X-ray diffraction, supported by quantum-chemical calculations. Surprisingly, its calculated global minimum structure is trigonal planar with D_{3h} symmetry instead of the trigonal pyramidal C_{3v} symmetric structure, which is predicted by the VSEPR model and also found in several other polyhalides and -interhalides. The structure giving factor is traced back to the central fluorine atom and its unique electronic properties.

Kurzzusammenfassung

Es wird eine effiziente Synthese für organisch lösliche Tetrafluoridohalogenate(I/III) von Brom und Chlor vorgestellt. Dabei werden Tetraalkylammoniumhalogenide mit verdünntem Fluor oder Chlormonofluorid (10 % in Ar) in Acetonitril oder Propionitril fluoriert. Erstmals wurden Difluoridochlorat(I) und Difluoridobromat(I)-Salze vollständig mittels Raman- und NMR-Spektroskopie sowie Einkristall-Röntgenbeugung untersucht. Sämtliche Daten sind durch quantenchemische Berechnungen gestützt. Die Reaktivitäten der Verbindungen wurden anhand von organischen und anorganischen Substraten eruiert. Dabei wurden Nitrile und Tetracyanidobromat in die entsprechenden Trifluoromethylverbindungen überführt, Diaryldisulfide reagierten zu Pentafluorsulfanylarylen, Edelmetalle lösten sich unter Bildung von Fluorido- und Bromidometallaten auf und Kohlenstoffmonoxid reagierte zu Carbonylfluorid.

Weiterhin wurden diese Verbindungen als Edukte in Ligandenaustauschreaktionen mit Perfluoro-*tert*-butylhypochlorit verwendet, um den Perfluoro-*tert*-butoxyliganden am positiv geladenen Halogenzentrum einzuführen. Mit diesem Liganden konnten Halogen(I)-Verbindungen von Chlor, Brom und Iod isoliert werden, wobei die Oxidationsstufe +III lediglich für Brom und Iod erreicht werden konnte. Während der Syntheseversuche einer Cl(III)-Spezies wurde der Ligand oxidiert unter Bildung von Perfluoro-*tert*-butylhypofluorit und -peroxid. Der sterische Anspruch des Liganden in Tetrakis(perfluoro-*tert*-butyl)iodat(III) verhinderte die Oxidation des Iodzentrums mittels verdünntem Fluor.

Schlussendlich wurde das nicht-klassische Polyinterhalogenid $[F(ClF)_3]^-$ ausgehend von Tetramethylammoniumchlorid und einem Überschuss Chlormonofluorid synthetisiert. Die Substanz wurde mittels Raman-Spektroskopie und Röntgenbeugung am Einkristall charakterisiert, sowie quantenchemisch untersucht. Überraschenderweise wurde eine trigonal-planare Struktur mit D_{3h} -Symmetrie als globale Minimumsstruktur berechnet, anstelle der vom VSEPR Modell vorhergesagten und in zahlreichen anderen Poly- und Polyinterhalogeniden gefundenen trigonal-pyramidalen, C_{3v} -symmetrischen Struktur. Das zentrale Fluoratom konnte auf Grund seiner einzigartigen elektronischen Eigenschaften als Ursache für die unterschiedliche Struktur ausgemacht werden.

List of Abbreviations

- 3c-4e** 3-center-4-electron
- ρ** electron density
- aHF** anhydrous hydrogen fluoride
- B3LYP** Becke, 3-parameter, Lee-Yang-Parr
- BLW** block-localized wavefunction method
- BMP** 1-butyl-1-methyl-pyrrolidinium
- cat** cation
- CCDC** Cambridge Crystallographic Data Centre
- e-waste** electrical waste
- ED** energy decomposition
- ESP** electrostatic potential
- et al.*** et alii
- EtCN** propionitrile
- Et** ethyl
- GVB** generalized valence bond
- HF** Hartree-Fock
- HMIM** 1-hexyl-3-methyl-imidazolium
- IL** ionic liquid
- IR** infrared
- lat. vib.** lattice vibration
- MeCN** acetonitrile
- Me** methyl
- MO** molecular orbital
- MP2** Møller-Plesset perturbation theory second order

NMR nuclear magnetic resonance

OETPP octaethyltetraphenylporphyrin

OS oxidation state

pip 1,1,3,3,5,5-hexamethyl piperidinium

PNP hexaphenyldiphosphazanium

Pr propyl

py pyridine

QTAIM quantum theory of atoms in molecules

R-21 dichlorofluoromethane

sh shoulder (in IR spectroscopy)

ttmgn 1,2,4,5-tetrakis(tetramethylguanidinylnaphthalene

UV/VIS ultraviolet/visible

VB valence bond

VSEPR valence shell electron pair repulsion

WCA weakly coordinating anion

Contents

1. Introduction	1
1.1. Polyhalides	1
1.1.1. Trihalides	1
1.1.2. Larger Polyhalides	2
1.1.3. Bonding Situation	3
1.2. Polyinterhalides	6
1.2.1. Classical Polyinterhalides	6
1.2.2. Non-classical Polyinterhalides	21
1.3. Halogenate Complexes with other Ligand Systems	24
2. Objectives	29
3. Publications	31
3.1. Improved Access to Organo-Soluble Di- and Tetrafluoridochlorate(I/III) Salts	31
3.2. Soluble Fluoridobromates as Well-Behaved Strong Fluorination Reagents	37
3.3. Non-classical polyinterhalides of chlorine monofluoride: experimental and theoretical characterization of $[\text{F}(\text{ClF})_3]^-$	42
3.4. Investigation of Bis(Perfluoro- <i>tert</i> -Butoxy) Halogenates(I/III)	47
4. Conclusion and Outlook	55
4.1. Conclusion	55
4.2. Outlook	58
5. References	61
6. List of Publications	69
A. Supporting Information of Publications	73
A.1. Improved Access to Organo-Soluble Di- and Tetrafluoridochlorate(I/III) Salts	73
A.2. Soluble Fluoridobromates as Well-Behaved Strong Fluorination Reagents	93
A.3. Non-classical polyinterhalides of chlorine monofluoride: experimental and theoretical characterization of $[\text{F}(\text{ClF})_3]^-$	108
A.4. Investigation of Bis(Perfluoro- <i>tert</i> -Butoxy)Halogenates(I/III)	123

1. Introduction

Halogenates are anionic complexes with halogens as a central atom according to the IUPAC recommendation.^[1] Different ligand classes are known in these complexes. Simple examples are halogen atoms or dihalogens themselves. The formed homoatomic anionic complexes, purely consisting of group 17 elements, are called polyhalides. If the anion is built of different halogens, it is referred to as a polyinterhalide. Within the group of polyinterhalides one can differentiate between compounds with a positive oxidation state on the central atom (classical polyinterhalides) and those in which the more electronegative halogen is the central atom, consequently having a negative oxidation state (non-classical polyinterhalides).^[2] Another class, similar to polyhalides ($[X(X_2)_n]^- \equiv [X_{2n+1}]^-$), are poly(hydrogen halide) halogenates ($[X(HX)_n]^-$) built from halide anions and hydrogen halide ligands which are held together by hydrogen instead of halogen bonds.^[3-12] Oxido is another widely known ligand for halogens, present in halogen oxoacids and their corresponding anions $[XO_n]^-$.^[13-17] Larger ligands are mainly based on anions of acids such as nitrate, fluorosulfate, perchlorate, trifluoroacetate and, the only formal alcohol, tetrakis(hydroxymethyl)ammonium. They will be discussed in detail in the following chapters.

1.1. Polyhalides

1.1.1. Trihalides

Trihalides $[X_3]^-$ exist for all four halogens fluorine, chlorine, bromine and iodine. Generally, the triatomic anions are linear with small deviations from the 180° bonding angle and varying degrees of asymmetry, i.e. differences between the two X–X bond lengths, depending on interactions with the surroundings. The trifluoride ion $[F_3]^-$ was only characterized in rare gas matrices and by mass spectrometry as an alkali metal complex or as the free ion.^[18-23]

The trichloride ion $[Cl_3]^-$ was first prepared by CHATTAWAY and HOYLE in 1923 by the reaction of tetraethylammonium chloride $[NEt_4]Cl$ with chlorine Cl_2 .^[24] Since then, several salts with other cations have been characterized by spectroscopic and crystallographic methods.^[25-32] If asymmetric or longer alkyl-chain-containing cations such as $[NEt_3Me]^+$, $[HMIM]^+$, $[BMP]^+$ or $[C_4H_9py]^+$, to only mention a few examples, are used, ionic liquids (ILs) are formed.^[33-35] They are applied for the dissolution of metals and alloys, including Fe, Cu, In, Zn, Ga, Au, Ge, Sb, InAs, GaAs and SmCo, which is used in high-temperature magnets.^[33,34] Additionally, trichloride ILs can be used to oxidatively dissolve UO_2 under formation of $[UO_2Cl_4]^{2-}$, an important step during the synthesis of nuclear fuels.^[36] Furthermore, $[NEt_3Me][Cl_3]$ can be used for the synthesis of phosgene under mild conditions, an important intermediate for the industrial synthesis of polycarbonates and polyurethanes.^[35]

The tribromide anion $[Br_3]^-$ was synthesized from the reaction of bromide salts with elemental bromine. The CCDC contains 101 structurally characterized tribromide salts, ranging from many

fully symmetric structures to highly asymmetric ones.^[37,38] They find applications in commercial zinc/bromine redox flow batteries,^[39] as well as manifold application in synthetic chemistry as bromination reagents. Possible substrates are ferrocene^[40] and other aromatic compounds,^[41] unsaturated carboxylic acids,^[42] ketones,^[43] alkenes and alkynes.^[44]

The simplest, oldest and probably most widely known polyhalide is the triiodide anion $[I_3]^-$. Its oldest description can be dated back to 1819 and since then triiodides were applied in different fields.^[45] For instance, solutions of potassium triiodide in water (Lugol's iodine) or ethanol/water mixtures are used for medical disinfection purposes and were applied as an antidote for poisoning.^[46,47] Additionally, the triiodide intercalates into the starch helix forming an intensely blue colored charge-transfer complex, which is used as an indicator in iodometric titrations.^[48] Triiodides are also used as charge carriers in dye sensitized solar cells^[49] and as halogenation reagents.^[40]

1.1.2. Larger Polyhalides

Additionally to the trihalides, larger polyhalide anions are known for all four halogens. The valence shell electron pair repulsion (VSEPR) model (Figure 1) predicts a v-shape structure with C_{2v} symmetry for $[X_5]^-$ which was experimentally reported for $[ttmgn-Br_4(BF_2)_2][Br_5]_2 \cdot 0.65Br_2$ ^[50] and in four $[I_5]^-$ -containing compounds.^[51–55] Distortion can also lead to a hockey-stick structure with C_s symmetry in which a trihalide is weakly coordinated by a dihalogen molecule as becomes evident in $[PPh_2Cl_2][Cl_3 \cdot Cl_2]$ ^[56] and four $[I_3 \cdot I_2]^-$ structures.^[55,57–59] $[F_5]^-$ was only spectroscopically studied under cryogenic conditions with matrix-isolation spectroscopy, suggesting a symmetric structure. However, high-level quantum-chemical calculations in the gas-phase suggested a hockey-stick structure as the global minimum structure.^[60]

$[X_7]^-$ is expected to form a trigonal pyramidal structure but for chlorine only a network structure with the composition $[CCl(NMe_2)_2][Cl_7]$ is known.^[61] Two structures of $[Br_7]^-$ were reported with the cations $[PPh_3Br]^+$ ^[62] and $[(o-SCH_3C_6H_4)_3PBr]^+$.^[63] In $[PPh_4][I_7]$ ^[64] and $[Cu(OETPP)][I_7]$ ^[65] the heptaiodide anions exist as isolated ions while several other formally $[I_7]^-$ containing compounds consist of anionic network structures.^[55] This network-forming behavior is often observed for polyhalides with a high halogen content.^[37,55]

Nonachloride anions are known in $[NPr_4][Cl_9]$ and $[Cp^*Fe][Cl_9 \cdot HF]$.^[61] The former has the expected tetrahedral structure of the anion while in the latter an HF molecule coordinates to the central halogen as a fifth ligand forming a trigonal bipyramidal structure.^[61] The heavier congener $[Br_9]^-$ is known with different tetraalkylammonium and imidazolium-based cations.^[66–68] The most isolated salts contain the $[NPr_4]^+$ cation and can be used as a selective bromination reagent for olefins, alkynes, ketones and aromatics.^[67,69] The known nonaiodides do not form tetrahedral anions but rather extended network structures.^[55]

$[X_{11}]^-$ structures are known for chlorine and bromine. For chlorine, two structures are known, one with isolated undecachloride anions in $[PNP][Cl_{11}] \cdot Cl_2$, which adopts a square pyramidal geometry, and a one-dimensional polymer chain in $[AsPh_4][Cl_{11}]$.^[70] Bromine also forms square pyramidal anions in the compound $[PNP][Br_{11}]$.^[71]

Amongst the polyhalides an octahedral $[X_{13}]^-$ is only known for chlorine in the compound $[PNP][Cl_{13}]$ which makes it the polyhalide with the highest halogen to halide ratio.^[70] In addition

to the mentioned monoanions, dianionic polyhalides also exist for chlorine, bromine and iodine and for the latter even tri- and tetraanions.^[37,55]

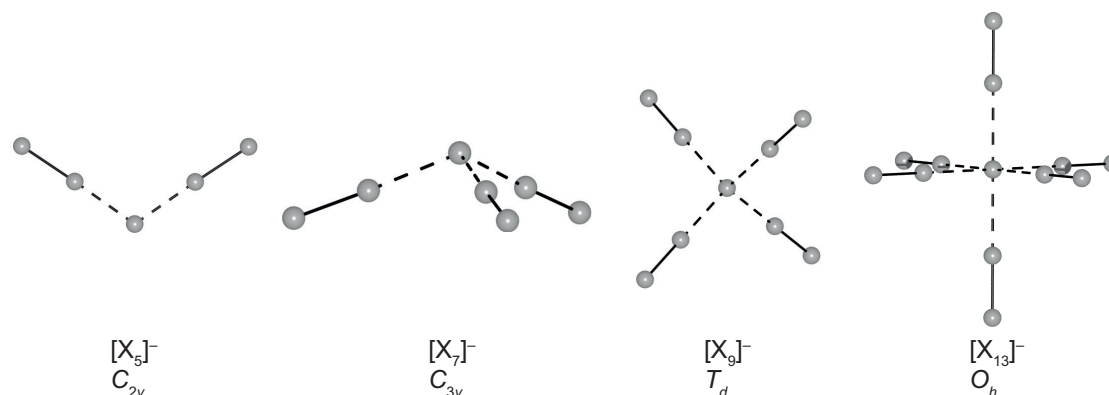


Figure 1. Structures of polyhalides $[X_n]^-$ $n = 5, 7, 9, 13$ and their symmetry predicted by the VSEPR model.^[37]

1.1.3. Bonding Situation

The bonding situation in polyhalides has been subject of much debate due to the fact that the simplest polyhalide, the trihalide anion, has 22 valence electrons, a number that is not trivially incorporated in a Lewis formula.^[72] Different models for the bonding were extensively discussed in the literature and will be shortly introduced in the following.

An MO theory approach describes the bonding situation of $D_{\infty h}$ symmetric trihalides using a 3-center-4-electron (3c-4e) bond with the scheme suggested by PIMENTEL and RUNDLE still being the textbook model (Figure 2a).^[73,74] The three p-orbitals along the molecule's main axis combine to a bonding (Ψ_1), non-bonding (Ψ_2) and antibonding (Ψ_3) molecular orbital (MO) with rising energies. Four electrons fill the lower two MOs, Ψ_1 and Ψ_2 , leaving the third Ψ_3 unoccupied. Hoffmann *et al.* refined the model by taking s-p mixing and π interactions into account.^[72] Their refined MO scheme is shown in Figure 2b. Here, σ_u is similar to Ψ_1 and σ_u^* is similar to Ψ_3 . The extent of mixing depends on the relative energies s_C , p_C and $n_1 \pm n_2$. An important effect is the destabilization of σ_g^* in comparison to $n_1 + n_2$.^[72] In principle, the same bonding explanation holds for triatomic classical polyinterhalides $[YXY]^-$.^[75] In line with that, CHRISTE *et al.* proposed a 3c-4e bond as the most likely model for the bonding in $[ClF_2]^-$.^[76]

However, DUNNING *et al.* pointed out some inconsistencies within the 3c-4e bonding model as an explanation for hypervalency in late p-block elements, including halogens.^[77,78] Therefore, they used the generalized valence bond (GVB) theory to explain the bonding and bond formation of the series $[ClF_n]^-$ ($n = 1-6$) with recoupled pair bonds and recoupled pair bond dyads.^[79] The bonding of $[ClF_2]^-$ is explained starting from a closed-shell chloride ion Cl^- in which the 3p electron pairs are recoupled. Each doubly occupied 3p orbital (from the HF wavefunction) is replaced with a singly occupied spatially polarized lobe orbital in the GVB wavefunction (Figure 3). Addition of one fluorine atom leads to a recoupled pair bond between chlorine and fluorine in $[ClF]^-$, formed from a 3p lobe orbital (Cl^-) and a singly occupied 2p orbital (F).^[79] For the addition of a second fluorine atom two possibilities exist. Either a recoupled pair bond dyad

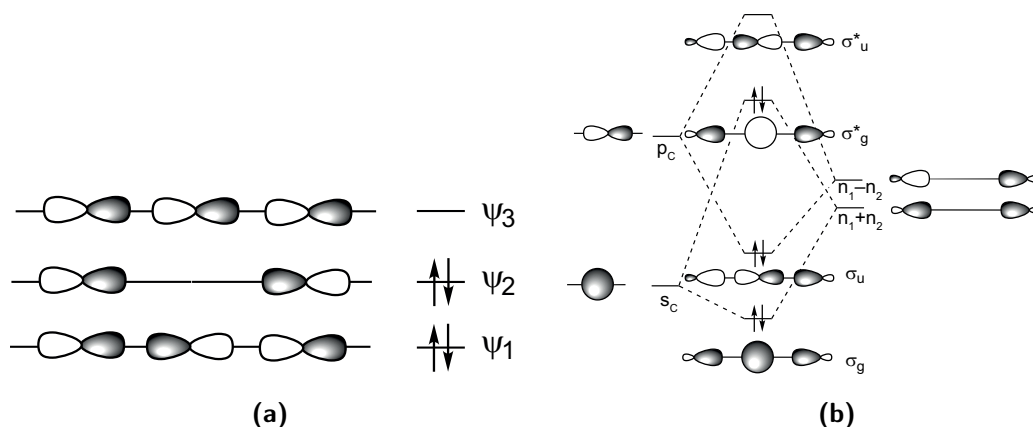
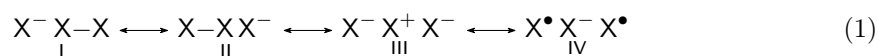


Figure 2. (a) Molecular orbital diagram for a 3c-4e bond by Pimentel and Rundle.^[74] (b) Molecular orbital diagram for a 3c-4e bond by Hoffmann taking s-p mixing into account.^[72]

is formed requiring a collinear arrangement, or a bent, excited state with two recoupled pair bonds. However, formation of a full dyad is more favorable, explaining the linear ground state of $[\text{ClF}_2]^-$.^[79] This model for the triatomic $[\text{ClF}_2]^-$ can be expanded to larger fluoridochlorate anions to explain their bonding. In case of $[\text{ClF}_4]^-$ and $[\text{ClF}_6]^-$, two and three recoupled pair bond dyads are formed, respectively.^[79]

It was shown by the block-localized wavefunction method (BLW) (a variant of the valence bond (VB) method) in combination with an energy decomposition (ED) approach that the charge-transfer contribution to the bonding is dominant in the trihalides $[\text{Cl}_3]^-$ and $[\text{Br}_3]^-$. Here, Pauli repulsion outweighs electrostatic attraction due to short distances between the nuclei making the "frozen energy" term in the ED repulsive for symmetric gas-phase optimized structures.^[80] The charge transfer part can be interpreted as the (covalent) donor-acceptor interaction between the halide lone pair with the antibonding σ^* dihalogen orbital.^[80] This is manifested experimentally in an increase of the dihalogen bond length and a red-shift of its valence mode in the Raman spectrum.^[81] In other words, the charge transfer is largest for symmetric trihalides and decreases continuously with growing asymmetry of the polyhalide.^[80] The frozen energy term becomes less repulsive, and in some cases even attractive.^[80] However, quantum theory of atoms in molecules (QTAIM) of theoretically and experimentally determined electron densities (ρ) shows that the Laplacian of the electron density $\nabla^2\rho$ is small and positive which is indicative of closed-shell interactions.^[32] This seeming dilemma is solved by the charge-shift bond for which positive Laplacians are expected.^[32,82] The high charge-shift energy is obtained from the mixing of three of the resonance structures (I, II and IV) that describe the bonding (eq. 1).^[32] Charge-shift bonds occur due to electron repulsion of σ bonds or lone pairs, making them particularly important for halogen-containing systems.



The bonding in larger polyhalide and polyinterhalide anions can be explained with halogen bonding, sometimes referred to as σ -hole interactions.^[37] The σ -hole is an area of positive electrostatic potential located on an atom, in this case a halogen, in the extension of the bonding

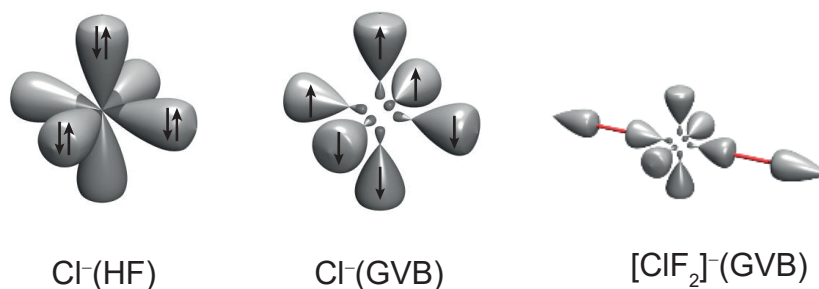


Figure 3. HF (left) and GVB (middle) orbitals of Cl^- . The GVB orbitals of the ground state of $[\text{ClF}_2]^-$ are shown on the right.^[79]

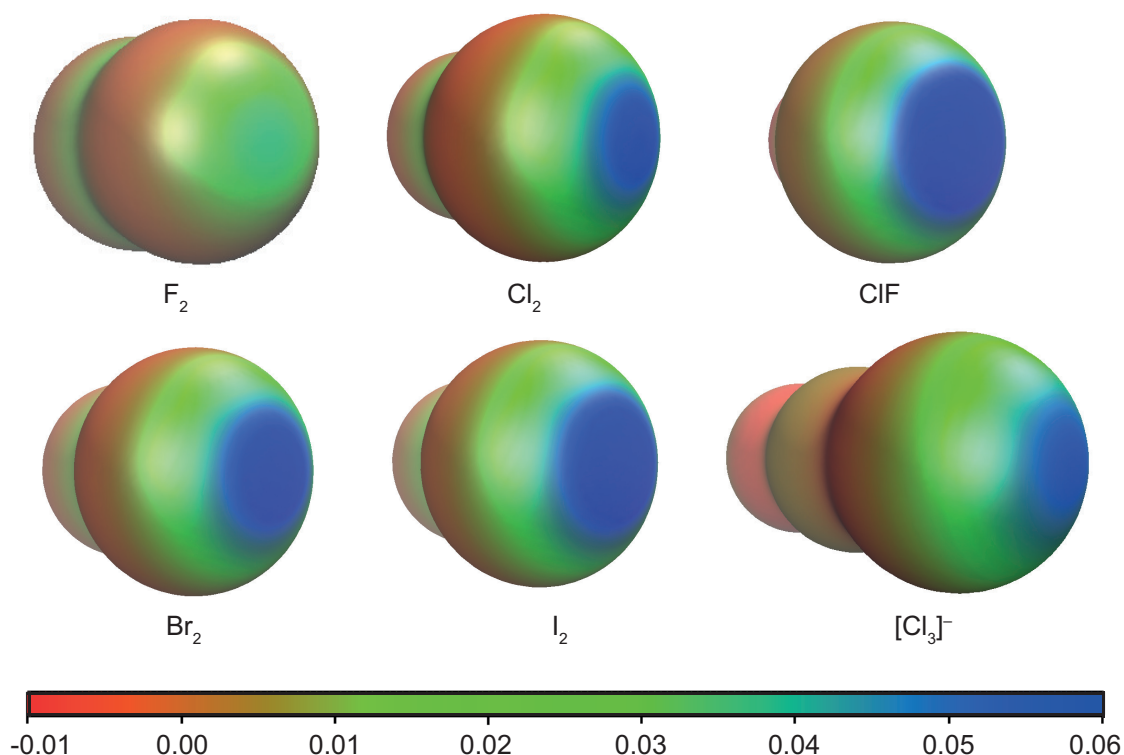


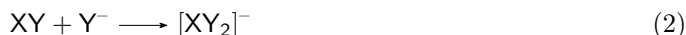
Figure 4. Electrostatic potentials (ESPs) plotted on the isosurface of the electron density (iso = 0.0035 a.u.) of F_2 , Cl_2 , Br_2 , I_2 , ClF (chlorine site) and $[\text{Cl}_3]^-$. Color bar is not valid for the trihalide anion.

axis.^[83–85] Figure 4 shows the electrostatic potentials (ESPs) mapped on an isosurface of the electron density for all four dihalogens F_2 , Cl_2 , Br_2 and I_2 . Bases can interact with this positive region of the halogen and as the σ -hole gets more pronounced for the heavier halogens, the interactions with bases become stronger.^[37,84] In addition to this region of positive electrostatic potential, a negative charge belt is observed perpendicular to the bonding axis with which electrophiles can interact. In other words, the σ -hole is another representation of the anisotropic charge distribution in a halogen, which is, to some extent, unexpected since dihalogens do not have a dipole moment.^[37] It can be increased by the addition of electronegative substituents as indicated by the larger σ -hole of ClF in comparison to Cl_2 (Figure 4).^[84,86] Similar to the dihalo-

gen molecules, the trihalide anions also have an anisotropic charge distribution. The negative charge of the anion is largely localized on the outer atoms on a charge belt perpendicular to the bonding axis. The σ -hole is again located on the bonding axis. A dihalogen molecule can interact with the charge belt and form an $[X_5]^-$ anion with a v-shape structure via halogen bonding. Further coordination of X_2 molecules leads to larger polyhalide systems with the general formula $[X_{2n+1}]^-$. Despite being a simple guide to the right structure, the electrostatic σ -hole interactions are not the dominant part in the bonding.^[80] Although dropping with increasing size of the anion, the charge-transfer energy remains dominant in polybromides and polychlorides.^[80]

1.2. Polyinterhalides

Polyinterhalides are polyhalogen anions that consist of at least two different halogens. Only taking the trihalides into account the amount of possible structures is 40 (including their different isomers).^[87] However, the number of "chemically reasonable" structures is drastically reduced, not only due to the formation of the most stable isomer, but also because different oxidation potentials of the halogens hamper the synthesis of several possible compounds. In practice, most polyinterhalides contain only two different halogens.^[37] Only a few examples of polyinterhalides, containing the three halogens Br, Cl and I, have been characterized, including $[\text{BrICl}]^-$, $[\text{I}_2\text{Br}_2\text{Cl}_4]^{2-}$, $[\text{I}_3\text{BrCl}_4]^{2-}$, $[\text{I}_4\text{Br}_2\text{Cl}_2]^{2-}$, $[\text{I}_2\text{Br}_4\text{Cl}_2]^{2-}$ and $[\text{I}_3\text{Br}_3\text{Cl}_2]^{2-}$.^[88,89] There are two conceptually different synthetic procedures for the synthesis of polyinterhalides. In the first one, the central halogen is already in the final oxidation state. A neutral interhalogen (e.g. bromine chloride BrCl) reacts with a (lighter) halide anion (e.g. chloride Cl^-) in a Lewis acid base type reaction to form the classical polyinterhalide (e.g. $[\text{BrCl}_2]^-$, Eq. 2). If more interhalogen is used, non-classical polyinterhalides can be formed (Eq. 3). In the second synthetic approach, a halide anion (e.g. iodide I^-) is exposed to a lighter dihalogen (e.g. chlorine Cl_2 , Eq. 4). Depending on the stoichiometry, the iodine(I) species dichloridoiodate(I) $[\text{ICl}_2]^-$ or the iodine(III) species tetrachloroiodate(III) $[\text{ICl}_4]^-$ is formed. In the following, the focus will be on binary fluorine-containing polyinterhalides.



1.2.1. Classical Polyinterhalides

Classical fluorine containing polyinterhalides exist for all three halogens chlorine, bromine and iodine. For Cl, Br and I fluoridohalogenates with the composition $[\text{XF}_n]^-$, $n = 2, 4, 6$ are known.^[76,90–92,94–96] Additionally, for I, also $[\text{IF}_8]^-$ ^[97] and $[\text{IF}_5]^{2-}$ ^[93] are reported (Table 1). In case of chlorine the difluorodichlorate(I) $[\text{ClF}_2]^-$ was synthesized from the reaction of chlorine monofluoride ClF with the corresponding metal fluorides KF , RbF and CsF or with nitrosyl fluoride NOF , leading to the corresponding K^+ , Rb^+ , Cs^+ or $[\text{NO}]^+$ salts.^[76,98] Additionally, the metal salts can be obtained from a salt metathesis between the metal fluoride and nitrosyl difluorodichlorate(I).^[98] These compounds were characterized by vibrational spectroscopy.

Table 1. Known classical fluorine containing polyinterhalides $[\text{XF}_n]^-$. Structures marked with an asterisk are only characterized spectroscopically.

n	Cl	Br	I
2	$[\text{ClF}_2]^{-*}$ [76]	$[\text{BrF}_2]^{-*}$ [90]	$[\text{IF}_2]^{-}$ [91]
4	$[\text{ClF}_4]^{-}$ [91]	$[\text{BrF}_4]^{-}$ [92]	$[\text{IF}_4]^{-}$ [91]
5	-	-	$[\text{IF}_5]^{2-*}$ [93]
6	$[\text{ClF}_6]^{-*}$ [94]	$[\text{BrF}_6]^{-}$ [95]	$[\text{IF}_6]^{-}$ [96]
8	-	-	$[\text{IF}_8]^{-}$ [97]

$\text{Rb}[\text{ClF}_2]$ showed two lines in the IR spectrum at 661 cm^{-1} and 470 cm^{-1} , corresponding to the antisymmetric and symmetric valence vibration of the $D_{\infty h}$ symmetric anionic moiety.^[99] The Raman spectrum of the compound showed a single line at 475 cm^{-1} for the symmetric valence mode.^[99] Vibrational data for the $[\text{ClF}_2]^-$ anion with different cations, as well as calculated frequencies are largely in agreement with each other (Table 2). The antisymmetric valence mode of the Cs^+ salt is observed at 636 cm^{-1} and of the $[\text{NO}]^+$ salt at 635 cm^{-1} . The symmetric valence mode of the Cs^+ salt splits into two lines at 510 cm^{-1} and 478 cm^{-1} .^[99] For the K^+ salt the symmetric stretching mode is observed at 475 cm^{-1} .^[99] The calculated frequencies (CCSD(T)/def2-TZVPP) of $[\text{ClF}_2]^-$ are predicted at 477 cm^{-1} (antisymmetric valence mode) and 453 cm^{-1} (symmetric valence mode).^[87] However, a structural characterization by means of X-ray or neutron diffraction is not known. The reactivity of the difluoridochlorate(I) anion remains basically unexplored.

Table 2. Vibrational spectroscopic data of the $[\text{ClF}_2]^-$ anion with different counterions. Assignment in the point group $D_{\infty h}$. Values given in cm^{-1} .

	Cs^+	Rb^+	K^+	$[\text{NO}]^+$	calc ^a
A_{1g}	510, 478	470, 475	475	-	453
A_{1u}	636	661	-	635	477
Ref.	[99]	[99]	[99]	[99]	[87]

^a CCSD(T)/def2-TZVPP

The tetrafluoridochlorate(III) anion $[\text{ClF}_4]^-$ can be synthesized from the reaction of chlorine trifluoride ClF_3 with the alkali metal fluorides potassium fluoride KF , rubidium fluoride RbF and caesium fluoride CsF as well as nitrosyl fluoride NOF .^[100,101] When the alkali metal chlorides KCl , RbCl or CsCl are exposed to elemental fluorine F_2 at elevated temperature and pressure, the corresponding alkali metal tetrafluoridochlorates(III) are also formed.^[102,103] After salt metathesis between hardly soluble $\text{Cs}[\text{ClF}_4]$ and either 1,1,3,3,5,5-hexamethyl piperidinium (pip) fluoride or tetramethylammonium fluoride $[\text{NMe}_4]\text{F}$ the more soluble $[\text{pip}][\text{ClF}_4]$ or $[\text{NMe}_4][\text{ClF}_4]$ can be obtained.^[91,104] Due to the better solubility of these salts in standard organic solvents such as acetonitrile (MeCN) or propionitrile (EtCN), the $[\text{ClF}_4]^-$ anion was not only characterized by vibrational spectroscopy, but also by ^{19}F NMR spectroscopy and single crystal structure analysis.

Figures 5a and 5b show the structure in the solid state of $[\text{pip}][\text{ClF}_4]$ and $[\text{NO}][\text{ClF}_4]$.^[91] The solid-state structures confirmed the anticipated D_{4h} structure of the anion. More recently, the crystal structures of the alkali metal salts $\text{K}[\text{ClF}_4]$, $\text{Rb}[\text{ClF}_4]$ and $\text{Cs}[\text{ClF}_4]$ were also determined (Figures 5c and 5d).^[105] The most asymmetric anionic moiety is found in $[\text{NO}][\text{ClF}_4]$ due to interactions with the cation (Figure 5b). The Cl–F bond lengths are 172.7(1) pm and 187.4(1) pm (Table 3). The most symmetric example is $\text{K}[\text{ClF}_4]$, with four equidistant Cl–F bond lengths. The cation is coordinated by eight fluorine atoms in a distorted square-antiprismatic fashion (Figure 5c).^[105] The crystal structures of the rubidium and caesium salt are isotypic with two inequivalent Cl–F bonds each and distorted anti-cuboctahedral coordination of twelve fluorine atoms around the cations (Figure 5d).^[105]

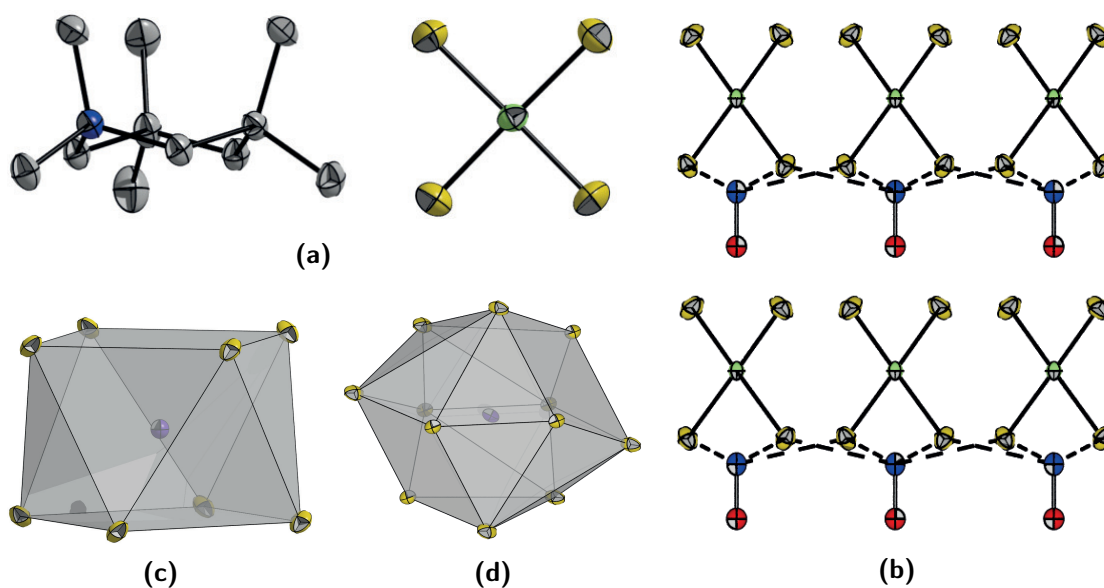


Figure 5. Solid-state structures of compounds containing the $[\text{ClF}_4]^-$ anion. Thermal ellipsoids at 50 % probability level. Color code: gray = carbon, blue = nitrogen, green = chlorine, yellow = fluorine, red = oxygen, violet = potassium, purple = rubidium. (a) Molecular structure in the solid-state of $[\text{pip}][\text{ClF}_4]$.^[91] Hydrogen atoms omitted for clarity. (b) Crystal packing of $[\text{NO}][\text{ClF}_4]$.^[91] Dashed lines indicate short cation-anion contacts. (c) Coordination polyhedron of potassium in $\text{K}[\text{ClF}_4]$.^[105] (d) Coordination polyhedron of rubidium in $\text{Rb}[\text{ClF}_4]$.^[105]

Table 4 gives an overview of the vibrational spectroscopic data of all known $[\text{ClF}_4]^-$ salts. IR spectra are reported for $[\text{ClF}_4]^-$ salts with the inorganic cations Cs^+ , Rb^+ , K^+ , and $[\text{NO}]^+$, as well as with the organic cations $[\text{pip}]^+$ and $[\text{NMe}_4]^+$. Overall, they have two bands, attributed to the antisymmetric stretching mode (E_u symmetry in the D_{4h} point group) between 745 and 482 cm^{-1} (Rb^+)^[109] which is split in two bands in some cases. The second band is a wagging mode with A_{2u} symmetry between 498 ($[\text{NO}]^+$)^[108] and 413 cm^{-1} (Rb^+).^[105] For the Cs^+ salt three IR spectra are reported, which however differ significantly in the E_u mode. The first spectrum by CHRISTE and co-workers from 1966 has a split band at 742 and 430 cm^{-1} ^[108] while they reported only one broad band at 590 cm^{-1} four years later.^[107] A spectrum reported in 2020 by KRAUS *et al.* also has a split band at 552 and 491 cm^{-1} .^[105] Differences in the A_{2u} mode are less pronounced (Table 4). For the Rb^+ salt also two different IR spectra exist, again with striking discrepancies in the E_u mode. A spectrum reported by CHRISTE *et al.* has two bands at 745 and 430 cm^{-1} ^[109] while in the spectrum by the KRAUS group two bands at 559 and 482 cm^{-1} are observed.^[105]

Table 3. Structural parameters of the $[\text{ClF}_4]^-$ anion with different counterions determined from single crystal X-ray diffraction. Bond lengths given in [pm], bond angles given in $[\circ]$.

space group	Cs^+	Rb^+	K^+	$[\text{NO}]^+$	$[\text{pip}]^+$	calc. ^a
	$I4/mcm$	$C2/c$	$C2/c$	$I4/cm$	$I4_1/cd$	-
Cl–F1	179.4(4)	180.34(9)	179.81(5)	187.4(1)	175.9(2)	180.6
Cl–F2	179.2(5)	179.30(9)	-	172.7(1)	181.4(1)	-
Cl–F3	-	-	-	-	177.1(1)	-
Cl–F4	-	-	-	-	181.3(1)	-
F1–Cl–F2	89.1(2)	89.33(4)	89.79(3)	89.36(5)	89.94(7)	90
F2–Cl–F3	90.9(2)	90.67(4)	90.21(3)	91.32(9)	89.94(7)	-
F3–Cl–F4	-	-	-	-	91.16(7)	-
F4–Cl–F1	-	-	-	-	89.98(7)	-
Ref.	[105]	[105]	[105]	[91]	[91]	[106]

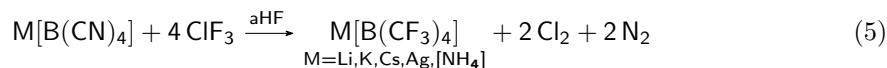
^a CCSD(T)/aug-cc-pVTZ**Table 4.** Vibrational spectroscopic data of the $[\text{ClF}_4]^-$ anion with different counterions. Assignment in the point group D_{4h} . Values given in cm^{-1} .

	Cs^+		Rb^+		K^+	$[\text{NO}]^+$	$[\text{pip}]^+$	$[\text{NMe}_4]^+$	calc. ^a
	E_u	590	742 552(sh)	745 559(sh)	498	676	549	550	635.0
A_{1g}	505	- 501	505 503	515	-	501	508	507.6	
A_{2u}	425	478 414	486 413	424	498	494	425	425.8	
B_{2g}	417	- 414	417 415	416	-	409	415	418.6	
B_{1g}	288	- 284	288 288	272 265	-	276.5	278	262.5	
Ref.	[107] [108]	[105]	[109] [105]	[105]	[108]	[91]	[104]	[106]	

^a MP2/aug-cc-pVTZ

The corresponding A_{2u} band differs by 73 cm^{-1} .^[105,109] The deviations in the spectra could have different reasons. Firstly, the reaction between the metal fluorides and ClF_3 could be incomplete due to the poor solubility of the starting materials and products. Secondly, the IR spectra by CHRISTE and co-workers were measured as nujol mulls or between AgCl or polyethylene disks^[108] and the compounds may have reacted with the carrier material due to the immense reactivity of $[\text{ClF}_4]^-$. The data reported by KRAUS *et al.* were measured on a diamond ATR unit inside a glovebox which makes reactions during the measurement unlikely. Additionally, their data are supported by periodic DFT calculations. The Raman spectra of the $[\text{ClF}_4]^-$ salts are all very similar, consisting of three bands. The first one corresponds to the in-phase symmetric stretching vibration (A_{1g}) between 515 cm^{-1} (K^+) and 501 cm^{-1} (Cs^+ , $[\text{pip}]^+$).^[105] The second band is found between 417 cm^{-1} ^[109] (Rb^+) and 414 cm^{-1} ^[105] (Cs^+) and corresponds to the out-of-phase symmetric stretching mode. The third band is associated to the scissoring mode (B_{1g}) and is found between 288 cm^{-1} ^[105,107] (Cs^+ , Rb^+) and 265 cm^{-1} ^[105] (K^+). In the latter case the band is split and has a second maximum at 272 cm^{-1} .^[105] The ^{19}F NMR spectra of $[\text{NMe}_4][\text{ClF}_4]$ and $[\text{pip}][\text{ClF}_4]$ show one resonance each at 66.8 ppm ^[104] and 68.5 ppm ,^[91] respectively. The

follow-up chemistry of $[\text{ClF}_4]^-$ has not been studied so far. This is probably associated with the limited access to soluble sources of the anion. However, the neutral, more reactive chlorine trifluoride ClF_3 has some applications as a reactant, for example as a cleaning and etching agent in the semiconductor industry.^[110–115] Additionally, it can be used for the synthesis of uranium hexafluoride UF_6 , an important intermediate in the uranium enrichment process.^[116] Apart from these more technical applications, ClF_3 is also used for the synthesis of the weakly coordinating anion (WCA) $[\text{B}(\text{CF}_3)_4]^-$. In an uncommon transformation, tetracyanidoborate $[\text{B}(\text{CN})_4]^-$ is exposed to ClF_3 in anhydrous hydrogen fluoride (aHF) and the cyanido ligands are cleanly transformed into trifluoromethyl groups under elimination of chlorine Cl_2 and nitrogen N_2 (Eq. 5).^[117] Reactions of ClF_3 with hydrocarbons are reported to be explosive, however, fluorination of 1-methylcyclohexane with ClF_3 is surprisingly smooth and selective under high dilution in an inert solvent and at low temperatures.^[118]



The hexafluoridochlorate(V) anion $[\text{ClF}_6]^-$ was synthesized as the tetramethylammonium salt from the reaction of tetramethylammonium fluoride $[\text{NMe}_4]\text{F}$ and chlorine pentafluoride ClF_5 in MeCN.^[94] The mass balance of the shock, temperature, and photolytically sensitive solid indicated formation of $[\text{NMe}_4][\text{ClF}_6]$.^[94] When caesium was used as the cation, removal of the solvent left only CsF as the non-volatile starting material behind.^[94] Therefore, the Raman spectrum had to be recorded from the reaction mixture of CsF and ClF_5 in frozen MeCN. It shows three bands in the Cl–F region at 525 cm^{-1} , 348 cm^{-1} and 289 cm^{-1} .^[94] They are assigned to the in-phase symmetric stretching vibration (A_{1g}), the out-of-phase stretching vibration (E_g) and the scissoring vibration (T_{2g}) of the octahedral molecule. They are in good agreement with calculated bands for octahedral $[\text{ClF}_6]^-$ (504.2 , 347.7 , 258.9 cm^{-1}).^[119] The signals rapidly decayed under irradiation of the Raman laser beam at $-110 \text{ }^\circ\text{C}$ in frozen MeCN, giving rise to bands associated with $[\text{ClF}_4]^-$. The presence of three bands indicates that the molecular structure is indeed octahedral, meaning that the lone pair at the chlorine atom is sterically inactive.^[94]

For the heavier congener bromine, the difluoridobromate(I) $[\text{BrF}_2]^-$ was only characterized spectroscopically. It was synthesized as the Cs^+ salt both by oxidation of caesium bromide CsBr with xenon difluoride XeF_2 , as well as from the comproportionation reaction of bromine trifluoride BrF_3 , bromine Br_2 and caesium fluoride CsF.^[90,91] However, none of the methods yielded pure samples and their analytical data are contradictory (Table 5). For the sample prepared from CsF, BrF_3 and Br_2 four bands were reported in the Raman spectrum at 596 (ν_{as}), 562 (ν_{as}), 442 (ν_{sy}), 198 cm^{-1} (δ).^[120] The $\text{D}_{\infty h}$ symmetric molecule has four fundamental vibrations from which one is degenerate and only one is Raman active. However, it is known that the selection rules and degeneracy can be broken by coordination to a cation.^[99,121–123] The sample prepared by oxidation with XeF_2 by SEPPELT showed two bands in the Raman spectrum at 465.5 cm^{-1} (ν_{sy}) and at 92 cm^{-1} (lat. vib.).^[91] Salt metathesis with $[\text{pip}]\text{F}$ yielded a soluble sample with a ^{19}F NMR chemical shift of -210 ppm .^[91] Apart from the caesium salt, the $[\text{NMe}_4]^+$ salt was also described. It was observed by MINKWITZ *et al.* as a decomposition product of $[\text{NMe}_4][\text{Br}(\text{OCF}_3)_2]$, which readily eliminates carbonyl fluoride COF_2 and forms the $[\text{BrF}_2]^-$ anion.^[124] The compound showed two Raman bands in the Br–F region at 470 cm^{-1} ($2\delta(\text{F–Br–F})$) and 460 cm^{-1} (ν_{sy}) and two IR bands at 450 cm^{-1} (ν_{as}) and 236 cm^{-1} ($\delta(\text{F–Br–F})$).^[124] The reported ^{19}F NMR

chemical shift ($\delta = -41.6$ ppm), however, is in contradiction to the value reported by SEPPELT.

Table 5. Comparison of different synthetic routes to $[\text{BrF}_2]^-$ -containing salts with their reported analytical data. Raman data given in cm^{-1} , ^{19}F NMR data given in ppm.

Synthetic route	Analytical data	
	Raman ^a	NMR
$3 \text{CsF} + \text{Br}_2 + \text{BrF}_3 \longrightarrow 3 \text{Cs}[\text{BrF}_2]$	596 (ν_{as}), 562 (ν_{as}), 442 (ν_{sy}), 198 (δ)	-
$\text{CsBr} + \text{XeF}_2 \xrightarrow{-\text{Xe}} \text{Cs}[\text{BrF}_2]$	465.5 (ν_{sy})	-210 ^b
$[\text{NMe}_4][\text{Br}(\text{OCF}_3)_2] \xrightarrow{-2 \text{COF}_2} [\text{NMe}_4][\text{BrF}_2]$	470 (2δ), 460 (ν_{sy})	-41.6

^a cation and lattice vibrations omitted

^b obtained after salt metathesis with $[\text{pip}]\text{F}$

Amongst all binary fluoridohalogenates, tetrafluoridobromate(III) ($[\text{BrF}_4]^-$) is the most in-depth studied molecule. It is known with a variety of counterions, including Na^+ ,^[125] K^+ ,^[92,126–131] Rb^+ ,^[95,132] Cs^+ ,^[130,133–135] Ag^+ ,^[136] $[\text{NO}]^+$,^[130] $[\text{NO}_2]^+$,^[130] $[\text{NMe}_4]^+$,^[104] $[\text{NF}_4]^+$ ^[137] and as the only dication Ba^{2+} .^[136,138] The metal salts were synthesized from the reaction of bromine trifluoride BrF_3 and the corresponding metal fluorides or metal chlorides. If metal chlorides are used, bromine and chlorine are released during the reaction.^[136] The nitrosonium ($[\text{NO}]^+$) and nitronium ($[\text{NO}_2]^+$) salts were synthesized from the reaction of BrF_3 with NOF or NO_2F . The $[\text{NMe}_4]^+$ and $[\text{NF}_4]^+$ salts can be obtained from salt metathesis between $\text{Cs}[\text{BrF}_4]$ and $[\text{NMe}_4]\text{F}$ or $[\text{NF}_4][\text{SbF}_6]$, respectively. Table 6 gives an overview of the vibrational spectroscopic data of different $[\text{BrF}_4]^-$ salts. The reported spectra are overall consistent, showing five bands for the D_{4h} symmetric anion, two in the IR and three in the Raman spectrum. For the caesium, potassium and tetrafluoroammonium salts their IR spectra show a broad band for the E_u vibration between 580 and 410 cm^{-1} (Cs^+ and K^+) and from 500 to 430 cm^{-1} ($[\text{NF}_4]^+$).^[130,137] In cases of the nitrosonium cation and the barium dication, the A_{2u} umbrella vibration is not observed. The three Raman active bands are in good agreement with each other and with the calculated data between 520 and 555 cm^{-1} (A_{1g}), 449 and 461 cm^{-1} (B_{2g}), as well as 240 and 266 cm^{-1} (B_{1g}). The ^{19}F NMR spectra of $[\text{NMe}_4][\text{BrF}_4]$ and $\text{Cs}[\text{BrF}_4]$ show one resonance at -37 ppm each.^[104]

Table 6. Vibrational spectroscopic data of the $[\text{BrF}_4]^-$ anion with different counterions. Assignment in the point group D_{4h} . Values given in cm^{-1} .

	Cs^+	Rb^+	K^+	Na^+	$[\text{NO}]^+$	$[\text{NF}_4]^+$	$[\text{NMe}_4]^+$	Ba^{2+}	calc. ^a
A_{1g}	523	529	531	531	527	535	520	555	520.8
E_u	580-410	413	580-410	403	542	500-430	480	509	516.5
B_{2g}	449	452	454	462	461	466	448	452	446.6
A_{2u}	317	316	325	320	-	325	315	-	322.6
B_{1g}	246	241	242	262,246	235	258	240	266	233.5
Ref.	[130]	[132]	[130]	[125]	[130]	[137]	[104]	[138]	[106]

^a MP2/aug-cc-pVTZ

Solid-state structures of $[\text{BrF}_4]^-$ salts are known of $\text{Na}[\text{BrF}_4]$,^[125] $\text{K}[\text{BrF}_4]$,^[131] $\text{Rb}[\text{BrF}_4]$,^[132] $\text{Cs}[\text{BrF}_4]$ ^[135] and $\text{Ba}[\text{BrF}_4]_2$.^[125] The first three structures are isotypic (space group $I4/mcm$) (Figures 6a and 6b) with one crystallographically independent Br–F bond each, all of them very similar in length (Na^+ : 189.9(1),^[125] K^+ : 189.24(9),^[131] Rb : 193.2(8) pm,^[132] Table 7). The cation is coordinated by eight fluorine atoms in a cuboid coordination polyhedron (Figure 6b). The caesium salt has two crystallographically independent anionic moieties, one with two crystallographically independent Br–F bonds and a second with only one.^[135] Here, the coordination sphere is an anticuboctahedron (Figure 6c). The most asymmetric tetrafluorobromate(III) anion, however, is found in the barium(II) compound (Figure 6d). Here, the shortest Br–F bond measures 180.1(4) pm, the longest 193.5(2) pm.^[125] Apart from X-ray diffraction, neutron diffraction was used to determine the structure of $\text{K}[\text{BrF}_4]$ with very similar results.^[128] Overall, the experimental structural parameters agree well with the calculated values (Br–F = 189.94 pm, F–Br–F = 90°).^[106]

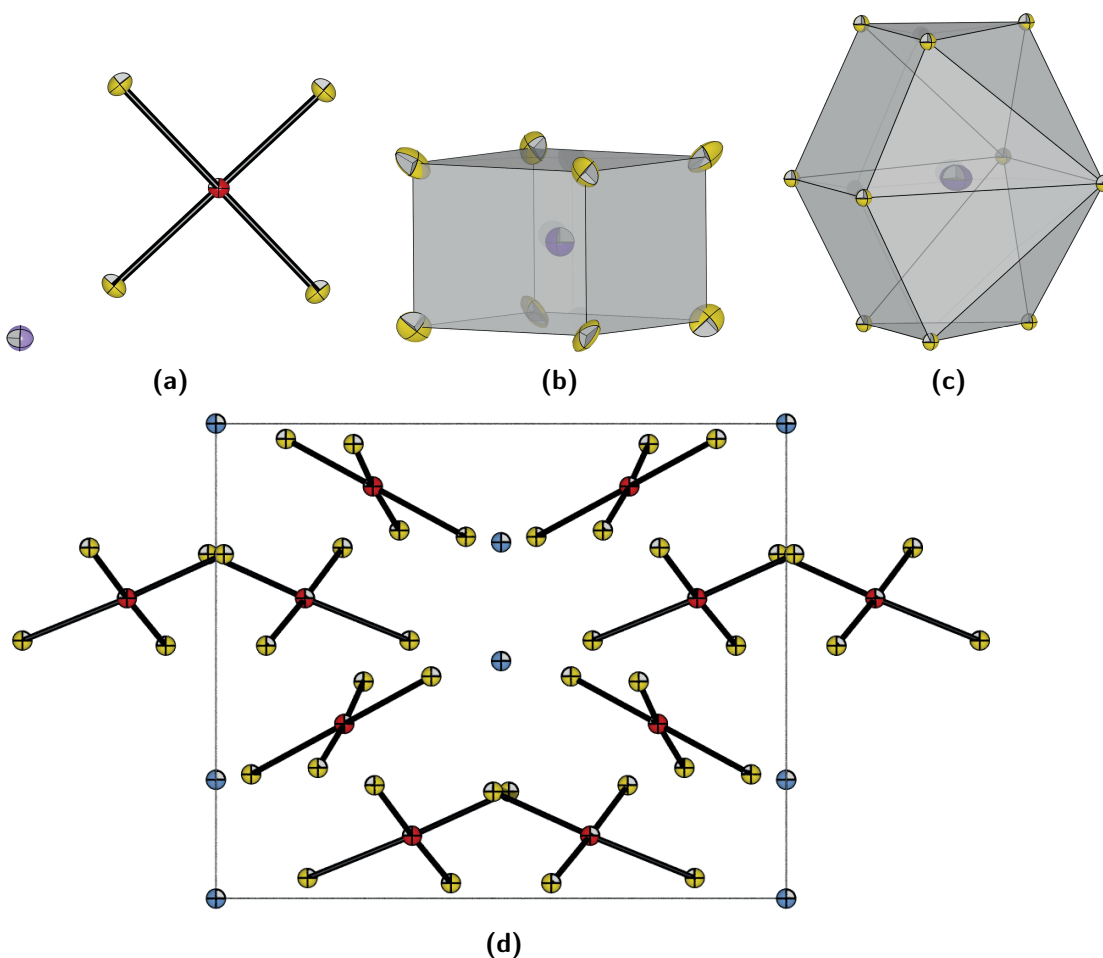


Figure 6. Solid-state structures of compounds containing the $[\text{BrF}_4]^-$ anion. Thermal ellipsoids at 50 % probability level. Color code: red = bromine, yellow = fluorine, lilac = sodium, purple = rubidium, violet = caesium, blue = barium. (a) Molecular structure in the solid-state of $\text{Na}[\text{BrF}_4]$.^[125] (b) Coordination polyhedron of rubidium in $\text{Rb}[\text{BrF}_4]$.^[95] (c) Coordination polyhedron of caesium in $\text{Cs}[\text{BrF}_4]$.^[135] (d) Unit cell of $\text{Ba}[\text{BrF}_4]_2$.^[138]

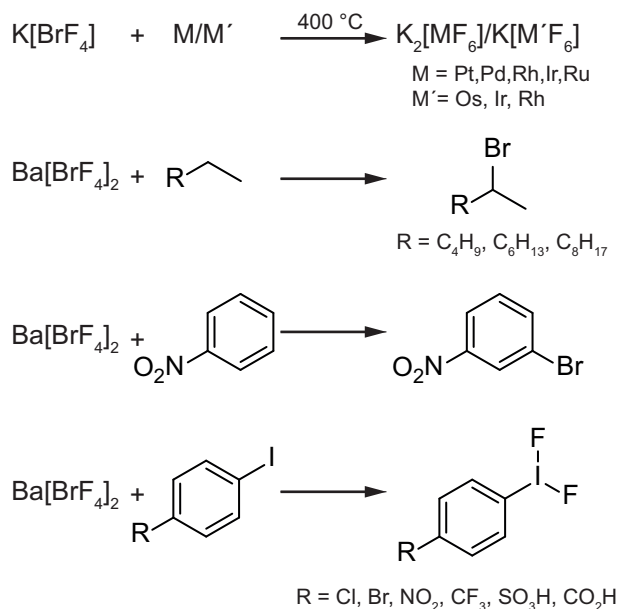
Table 7. Structural parameters of the $[\text{BrF}_4]^-$ anion with different counterions determined by single crystal X-ray diffraction. Bond lengths given in [pm], bond angles given in $[\circ]$.

space group	Cs^+ ^a <i>Immm</i>	Rb^+ <i>I4/mcm</i>	K^+ <i>I4/mcm</i>	Na^+ <i>I4/mcm</i>	Ba^{2+} <i>I4</i>	calc. ^b -
Br-F1	188.5(1) 189.1(1)	193.2(8)	189.24(9)	189.9(1)	180.1(4)	189.94
Br-F2	- 190.2(2)	-	-	-	185.6(4)	-
Br-F3	-	-	-	-	190.1(4)	-
Br-F4	-	-	-	-	193.5(2)	-
F1-Br-F2	92.04(7) 90.0	90.4(3)	90.02(3)	90.75(4)	93.1(2)	90
F2-Br-F3	87.96(7) 90.0	89.6(3)	89.98(5)	89.25(8)	85.1(2)	-
F3-Br-F4	-	-	-	-	90.0(1)	-
F4-Br-F1	-	-	-	-	91.8(2)	-
Ref.	[135]	[132]	[131]	[125]	[125]	[106]

^a two anionic moieties in the asymmetric unit^b CCSD(T)/aug-cc-pVTZ

Despite their high reactivity and toxicity, tetrafluoridobromates(III) are considered promising tools for the recovery of precious materials, especially noble metals, from solids. This process, known as urban mining, is becoming more and more important since prices for raw materials as well as waste production are steadily increasing.^[139] In 2019, 53.6 Mt of electrical waste (e-waste) were generated.^[140] Adverse health effects on humans in connection with e-waste are severe and include, amongst many others, adverse birth outcomes for infants, altered neurodevelopment, adverse learning and behavioral outcomes for children, as well as DNA damage and male reproductive and genital disorders for informal recycling workers.^[140] The chemical recovery of noble metals is inherently challenging due to the inertness of these metals. Therefore, harsh conditions and strongly oxidizing reagents such as *aqua regia* are employed. However, the release of toxic nitrogen oxides is a drawback.^[141] Additionally, nitric acid often leads to the formation of metastannic acid when exposed to tin-containing materials, which makes the isolation of the desired component difficult.^[141] Therefore, the usage of $\text{K}[\text{BrF}_4]$ as a relatively safe agent for the conversion of elemental noble metals such as ruthenium, osmium, rhodium, iridium, palladium and platinum into their fluoridometallates was studied.^[141–143] In a standard experiment $\text{K}[\text{BrF}_4]$ and the metal under study were pressed into pellets and heated to 400 °C in a nickel ampule for several hours. The reaction products were fluorido metallates $\text{K}_2[\text{MF}_6]$ for $\text{M} = \text{Pt}, \text{Pd}, \text{Rh}$ and $\text{K}[\text{MF}_6]$ for $\text{M} = \text{Os}$ or their mixtures for $\text{M} = \text{Ir}, \text{Ru}$, which can be further processed by standard wet-chemical procedures (Scheme 1).^[142] $\text{Ba}[\text{BrF}_4]_2$ can be used in organic chemistry for the bromination of alkanes such as hexane, octane and decane (Scheme 1). The reaction occurs selectively in two position without any fluorination and only minor amounts (<10 %) of doubly brominated products are observed.^[144] Reaction with simple aryl compounds such as benzene, toluene or nitrobenzene leads to electrophilic bromination of the aromatic system, in case of

nitrobenzene or nitrotoluene selectively in *meta* position (Scheme 1). For more electron-rich systems (benzene and toluene), product mixtures with doubly brominated and partially fluorinated or C–C coupled products are observed.^[145] Additionally, it can be used for the synthesis of hypervalent difluoroiodoarenes (Scheme 1).^[146]



Scheme 1. Reactions of $[\text{BrF}_4]^-$ salts noble metals and organic substrates.

Bromine in oxidation state +V is found in the hexafluorobromate(V) anion $[\text{BrF}_6]^-$. It is known as the potassium,^[147] rubidium,^[147] caesium,^[95,133,147,148] pip^[149] and tetramethylammonium salt.^[104] Crystal structures of the Cs^+ and $[\text{pip}]^+$ salt were determined by X-ray diffraction (Figure 7), however, the structure of $[\text{pip}][\text{BrF}_6]$ is of poor quality.^[149] Nevertheless, both structures clearly point towards an octahedral shape of the anionic moiety, meaning that the remaining lone pair at the bromine atom is sterically inactive, similarly to the lighter homologue $[\text{ClF}_6]^-$. In $\text{Cs}[\text{BrF}_6]$ all Br–F bonds are equivalent with a bond length of 185.4(1) pm and three linear, perpendicular F–Br–F units.^[95] In $[\text{pip}][\text{BrF}_6]$ the Br–F bond lengths vary between 187.3(2) and 181.4(2) pm. The most bent F–Br–F unit has a bonding angle of 177.5°. However, the authors note that due to excessive disorder in the crystal especially the bonding angle may well be meaningless.^[149] The crystal packing of $\text{Cs}[\text{BrF}_6]$ shows cuboctahedral coordination of the fluorine atoms around the cations leading to an alternating packing between anion octahedra and cation cuboctahedra (Figure 7b). The ^{19}F NMR spectra of $\text{Cs}[\text{BrF}_6]$ and $[\text{NMe}_4][\text{BrF}_6]$ show singlet resonances at 94 ppm, independent of the measuring temperature.^[104] In case of $[\text{pip}][\text{BrF}_6]$ the fine structure of the signal, two overlapping 1:1:1:1 quartets due to $^1J(^{19}\text{F}, ^{79/81}\text{Br})$ coupling, is resolved.^[149]

Vibrational spectroscopic data are available for all three salts. Quantum-chemical calculations (MP2/aug-cc-pVTZ) predict six bands for the O_h symmetric $[\text{BrF}_6]^-$ anion at 564.5 (A_{1g}), 575.9 (T_{1u}), 442.9 (E_g), 235.0 (T_{2g}), 211.3 (T_{1u}) and 166.7 cm^{-1} (T_{2u}) (Table 8).^[106] The Raman spectrum of $\text{Cs}[\text{BrF}_6]$ in MeCN solution has three bands at 565 (A_{1g}), 450 (E_g) and 240 cm^{-1} (T_{2g})^[148] which are in good agreement with the predicted spectrum and the spectra of solid $\text{Cs}[\text{BrF}_6]$ (562, 451, 243 cm^{-1}),^[147] $[\text{pip}][\text{BrF}_6]$ (561, 445, 241 cm^{-1})^[149] and $[\text{NMe}_4][\text{BrF}_6]$ (562,

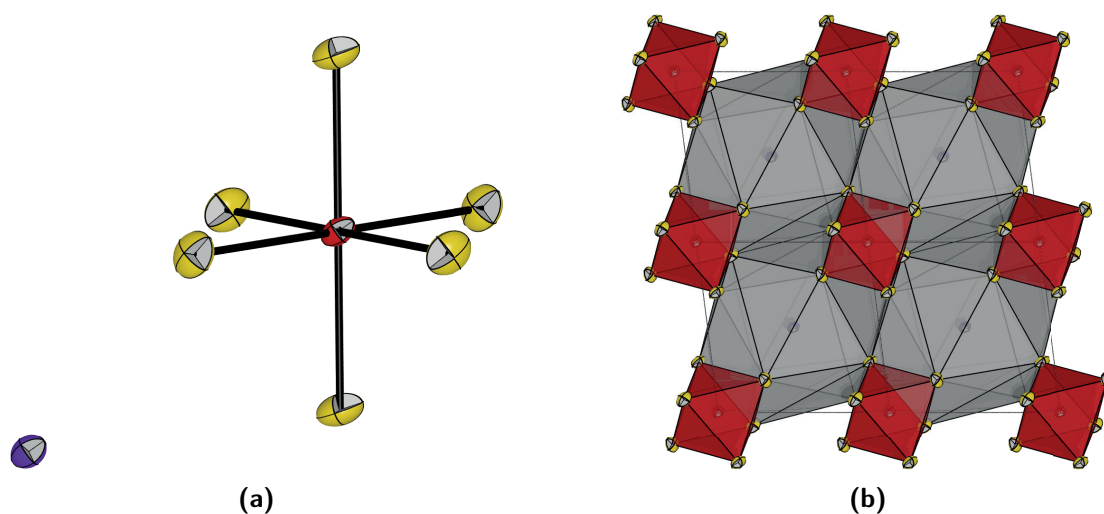


Figure 7. Solid-state structure of $\text{Cs}[\text{BrF}_6]$.^[95] Thermal ellipsoids at 50 % probability level. Color code: red = bromine, yellow = fluorine, violet = caesium. (a) Molecular structure in the solid-state of $\text{Cs}[\text{BrF}_6]$. (b) Coordination polyhedra of caesium (gray) and bromine (red) in $\text{Cs}[\text{BrF}_6]$.

Table 8. Vibrational spectroscopic data of the $[\text{BrF}_6]^-$ anion with different counterions. Assignment in the point group O_h . Values given in cm^{-1} .

	K^+	Rb^+	Cs^+		$[\text{pip}]^+$	$[\text{NMe}_4]^+$	calc. ^c
A_{1g}	568	568	562 ^a	565 ^b	561	562	564.5
T_{1u}	- ^d	- ^d	- ^d	-	472	490	575.9
E_g	454	456	451 ^a	450 ^b	445	451	442.9
T_{2g}	250	250	243 ^a	240 ^b	241	239	235.0
T_{1u}	204	203	193	-	-	-	211.3
T_{2u}	138	144	156	-	-	-	166.7
Ref.	[147]	[147]	[147]	[148]	[149]	[104]	[106]

^a solid

^b solution in MeCN

^c MP2/aug-cc-pVTZ

^d The authors noted a strong absorption around 400 cm^{-1} .

$451, 239 \text{ cm}^{-1}$).^[104] IR bands of the latter two compounds show one anion band at 472 ^[149] and 490 cm^{-1} ,^[104] respectively. These bands show relatively high deviations from the calculated band at 572.8 cm^{-1} .^[119] These results, especially the Raman spectrum in solution without any crystal effects, underpin the octahedral structure of the anion.

The largest number of fluoridohalogenates is known for iodine. The $[\text{IF}_2]^-$ anion was synthesized through four different routes. Firstly, the ligand exchange reaction of tetraethylammonium dichloridoiodate(I), $[\text{NEt}_4][\text{ICl}_2]$, with AgF in MeCN (Eq. 6).^[150] Secondly, the reaction of tetraethylammonium fluoride $[\text{NEt}_4]\text{F}$ with iodine monofluoride IF (Eq. 7).^[151] Thirdly, the reaction of pip fluoride, iodine I_2 and xenon difluoride XeF_2 (Eq. 8)^[91] and lastly, the fluorination reaction of $[\text{NMe}_4]\text{I}$ with XeF_2 (Eq. 9).^[152] For the first reaction, no spectroscopic data were reported and the product was purely analyzed by elemental analysis. However, NAUMANN *et al.*

later confirmed the synthetic procedure.^[151] Additionally, they suggested the second route as an alternative synthesis and provided spectroscopic data for their product. However, the synthesis of anhydrous $[\text{NEt}_4]\text{F}$ via the same procedure as the one described for $[\text{NMe}_4]\text{F}$ ^[153] in the publication^[151] appears unlikely due to the well-known Hofmann degradation of β -hydrogen-containing ammonium salts.^[154] The third synthetic procedure is more elegant because (i) a stable alkylammonium fluoride salt is used and (ii) it avoids the isolation of unstable IF .^[155] From that route single crystals suitable for X-ray diffraction were obtained (Figure 8a). The I–F bond lengths are 208.2(3) and 207.5(3) pm, with an F–I–F bond angle of 177.8(1)°. Route four is probably the most straightforward because it uses only commercially available starting materials. Raman spectroscopic data of $[\text{pip}][\text{IF}_2]$ (447.5 (A_{1g}) and 112.5 cm^{-1} (lattice vibration) for the anionic moiety)^[91] agree with those reported for $[\text{NEt}_4][\text{IF}_2]$ (445 (A_{1g}) and 111 cm^{-1} (lattice vibration)) and $[\text{NMe}_4][\text{IF}_2]$ (446 cm^{-1} (A_{1g}))^[152] as well as with the calculated value for the symmetric stretching vibration at the CCSD(T)/aug-cc-pVTZ level (460.7 cm^{-1} , Table 9).^[87] IR data are available for $[\text{NEt}_4][\text{IF}_2]$ (462 and 206 cm^{-1}) and $[\text{NMe}_4][\text{IF}_2]$ (397 cm^{-1}). The calculated value (CCSD(T)/aug-cc-pVTZ) for the antisymmetric vibration is 426.0 cm^{-1} ,^[87] which is in between the band reported for the $[\text{NMe}_4]^+$ and the $[\text{NEt}_4]^+$ salts. Additionally, the reported ^{19}F NMR spectroscopic data have large differences: -286 ppm^[91] (EtCN) for $[\text{pip}][\text{IF}_2]$, -282 ppm^[152] (MeCN) for $[\text{NMe}_4][\text{IF}_2]$ and -126.1 ppm^[151] (MeCN) for $[\text{NEt}_4][\text{IF}_2]$. From this, one can conclude that only reactions 8 and 9 lead to clean products. IR data from experiments in solid argon matrices for the ion pairs $\text{M}[\text{IF}_2]$ ($\text{M}=\text{Na}, \text{K}, \text{Rb}, \text{Cs}$), obtained from the codeposition of metal iodides MI and fluorine F_2 at 15 K, gave rise to bands at 520 (Na), 506 (K), 503 (Rb), and 504 cm^{-1} (Cs).^[156] The apparent differences in the spectra obtained from bulk material are probably due to strong interactions within the ion pair.

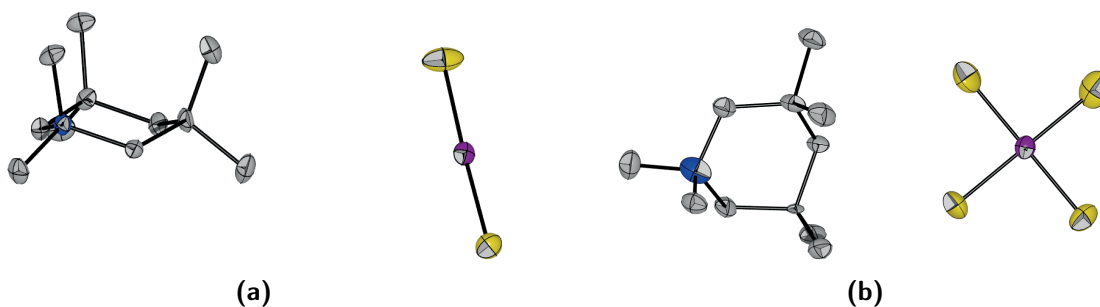
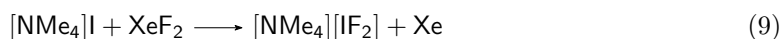
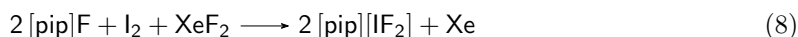
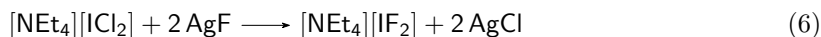


Figure 8. Solid-state structures of (a) $[\text{pip}][\text{IF}_2]$ and (b) $[\text{pip}][\text{IF}_4]$.^[91] Hydrogen atoms and co-crystallized $[\text{pip}][\text{F}(\text{HF})_2]$ are omitted for clarity. Only one ion pair of the asymmetric unit is shown. Thermal ellipsoids at 50 % probability level. Color code: gray = carbon, blue = nitrogen, violet = iodine, yellow = fluorine.

Table 9. Vibrational spectroscopic data of the $[\text{IF}_2]^-$ anion with different counterions. Assignment in the point group $D_{\infty h}$. Lattice vibration omitted. Values given in cm^{-1} .

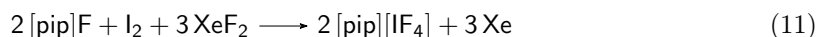
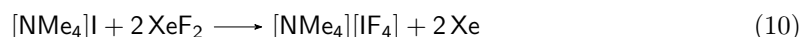
	$[\text{NEt}_4]^+$	$[\text{pip}]^+$	$[\text{NMe}_4]^+$	calc. ^a
A_{1g}	445	447.5	446	460.7
A_{1u}	462	-	397	426.0
Ref.	[151]	[91]	[152]	[87]

^a CCSD(T)/aug-cc-pVTZ**Table 10.** Vibrational spectroscopic data of the $[\text{IF}_4]^-$ anion with different counterions. Assignment in the point group D_{4h} . Values given in cm^{-1} .

	Cs^+	$[\text{pip}]^+$	$[\text{NMe}_4]^+$	calc. ^a
A_{1g}	522	573.5	515	517.1
E_u	448	-	449	474.4
B_{2g}	455	461.0	457	459.5
A_{2u}	271	-	267	281.0
B_{1g}	195	213.0	197	195.9
Ref.	[157]	[91]	[93]	[119]

^a CCSD(T)/aug-cc-pVTZ

For iodine in oxidation state +III, two different anions are known, $[\text{IF}_4]^-$ and $[\text{IF}_5]^{2-}$. For several years an $[\text{IF}_6]^{3-}$ trianion was believed to exist, but later identified to be a mixture of $[\text{IF}_5]^{2-}$ and F^- .^[93] The synthesis of alkali metal tetrafluoroiodate(III) was described in 1960 from the reaction of potassium iodide KI, rubidium iodide RbI and caesium iodide CsI with iodine pentafluoride IF_5 in the cold,^[158] and in 1961 by direct fluorination of RbI.^[102] However, both reports lack spectroscopic data and products were purely analyzed by elemental analysis. A synthetic procedure starting from CsF and iodine trifluoride IF_3 , first described in 1968,^[159] was later used to generate vibrational spectroscopic data.^[157] As for the lighter congeners, the Raman spectrum of $\text{Cs}[\text{IF}_4]$ has three lines at 522, 455 and 195 cm^{-1} , corresponding to the A_{1g} , B_{2g} and B_{1g} vibrations of the D_{4h} symmetric molecule.^[157] The IR spectrum showed two lines at 448 and 271 cm^{-1} corresponding to the E_u and A_{2u} vibrations, respectively.^[157] The IR ($449, 267 \text{ cm}^{-1}$) and Raman ($515, 457, 197 \text{ cm}^{-1}$) data of $[\text{NMe}_4][\text{IF}_4]$ are very similar (Table 10). The sample was obtained from the reaction of $[\text{NMe}_4]\text{I}$ and XeF_2 (Eq. 10). The crystal structure of the tetrafluoroiodate(III) anion was obtained from a sample of $[\text{pip}][\text{IF}_4]$ (Figure 8b) which was synthesized through the reaction of $[\text{pip}]\text{F}$, I_2 and XeF_2 (Eq.11).^[91] The I–F bond lengths vary between 200.0(4) and 201.8(3) pm.^[91] The F–I–F bond angles are all 90 and 180° , respectively, within the estimated standard deviation.^[91] The ^{19}F NMR spectra of the alkylammonium salts show resonances at $-106.5 \text{ ppm}^{[93]}$ ($[\text{NMe}_4]^+$) and -106 ppm ($[\text{pip}]^+$).^[91]



The pentafluoroiodate(III) dianion $[\text{IF}_5]^{2-}$ was synthesized from $[\text{NMe}_4][\text{IF}_4]$ and $[\text{NMe}_4]\text{F}$ in MeCN.^[93] Due to its limited solubility, the compound was identified by its vibrational spectra in comparison with quantum-chemical calculations. It has a pentagonal planar coordination sphere with D_{5h} symmetry, similar to the isoelectronic $[\text{XeF}_5]^-$.^[160] It showed two bands in the IR spectrum ($335, 245 \text{ cm}^{-1}$) with a third lower intensity band probably hidden under the broad 335 cm^{-1} band, as well as three bands in the Raman spectrum at 474, 366 and 322 cm^{-1} .^[93] With this compound unambiguously identified by vibrational spectroscopy in combination with quantum-chemical calculations, the assumed compound $\text{Cs}_3[\text{IF}_6]$ was identified as a mixture of CsF and $\text{Cs}_2[\text{IF}_5]$.^[93]

Iodine pentafluoride IF_5 forms adducts with KF , RbF , CsF , NOF and $[\text{NMe}_4]\text{F}$,^[96,161] in which the amounts of IF_5 varies (between 1.7 equivalents for RbF and 3 equivalents for CsF and $[\text{NMe}_4]\text{F}$). However, removal of excess IF_5 down to one equivalent is possible by heating the samples in vacuum to yield hexafluoroiodate(V) $[\text{IF}_6]^-$ salts.^[96,161] The vibrational spectra of these compounds showed a variety of bands (Table 11), many of them observed in both IR and Raman spectra. This is in sharp contrast to the vibrational spectra of the lighter congeners $[\text{BrF}_6]^-$ and $[\text{ClF}_6]^-$ (*vide supra*), indicating that the structure of $[\text{IF}_6]^-$ differs. The crystal structure determination by X-ray diffraction (Figure 10) proved that the coordination of the iodine center is indeed non-octahedral but has C_{3v} symmetry, meaning that the electron pair at the iodine atom is sterically active.^[96] Structure optimizations (CCSD(T)/aug-cc-pVTZ) found three minima close in energy with C_{3v} , C_{2v} and O_h symmetry (Figure 9) from which the C_{3v} symmetric structure is the global minimum.^[119] The calculated vibrational frequencies based on this structure are in good agreement with the experimentally determined bands (Table 11). The reason for the different steric activity of the lone pair in the $[\text{XF}_6]^-$ ($\text{X} = \text{Cl}, \text{Br}, \text{I}$) series is the increasing halogen–fluorine bond length. For chlorine and bromine, the halogen–fluorine bonds are too short for a sterically active lone pair and therefore it resides in an A_{1g} symmetric orbital. In contrast, for iodine the I–F bond is sufficiently long to allow for steric activity of the lone pair.^[119] An interesting intermediate case is the XeF_6 molecule, which has an Xe–F bond length in between those of $[\text{BrF}_6]^-$ and $[\text{IF}_6]^-$. Here the structure is believed to be C_{3v} symmetric but highly fluxional, with the O_h symmetric structure comparable in energy.^[119] In the crystal structure of $[\text{NMe}_4][\text{IF}_6]$ two anions are asymmetrically μ_2 -bridged over two fluorine atoms (Figure 10c). The long bridging interaction is 282(1) pm, whereas the short bond has a length of 211(1) pm. The terminal I–F bond distances vary between 182(1) and 198.3(6) pm. The anions in $[\text{NO}][\text{IF}_6]$ form a tetrameric moiety (Figure 10b). Here, the iodine centers are located on the corners of a tetrahedron and each face of the tetrahedron is overcapped by a μ_3 -bridging fluorine atom. The distances between the iodine and bridging fluorine atoms are in the range of 260.9(4) to 276.9(4) pm.^[96] The ^{19}F NMR spectrum of $\text{Cs}[\text{IF}_6]$ shows a single resonance at 13 ppm, indicating a fluxional C_{3v} structure of the anion.^[148]

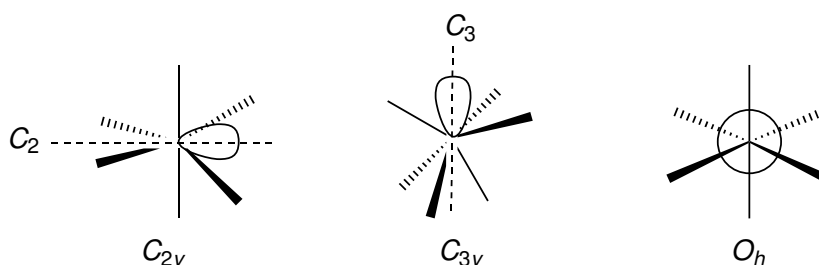


Figure 9. Schematic structures of $[\text{XF}_6]^-$ with their corresponding symmetry.

The only known octafluoridohalogenate is formed with iodine, $[\text{IF}_8]^-$. It is known as the Cs^+ , $[\text{NO}]^+ \cdot 2 \text{NOF}$, $[\text{NO}_2]^+$ and $[\text{NMe}_4]^+$ salt, all obtained by reaction of the corresponding cation fluorides with iodine heptafluoride IF_7 .^[97,162–164] The crystal structures of the $[\text{NMe}_4]^+$ and $[\text{NO}]^+ \cdot 2 \text{NOF}$ salts (Figure 11) reveal that the anion has a square antiprismatic molecular geometry with D_{4d} symmetry. The I–F bond lengths in the $[\text{NO}]^+$ are in the range of 188.4(4) to 190.4(4) pm.^[97] The vibrational spectroscopic data are summarized in Table 12 with an overall

Table 11. Vibrational spectroscopic data of the $[\text{IF}_6]^-$ anion with different counterions^[161] in comparison with calculated values of the C_{3v} symmetric anion. Values given in cm^{-1} .

	Cs^+		Rb^+		K^+		calc. ^{a[119]}
	IR	Raman	IR	Raman	IR	Raman	
A_1	620	620	620	622	625	628	662
	-	451	-	447	-	450	448
	-	347	-	348	-	342	355
	-	199	-	208	-	209	206
A_2	-	-	288	292	290	293	244
E	599	599	599	598	609	607	603
	570-500	554	570-500	562	570-500	554	
		527		528		528	
		502		501		501	
	390	391	391	391	393	392	371
	335	-	337	-	341	-	352
	260	275	260	270	268	268	231
	-	-	-	-	-	183	-
-	-	-	-	-	-	58	

^a HF/aug-cc-pVTZ, scaling factor of 0.891

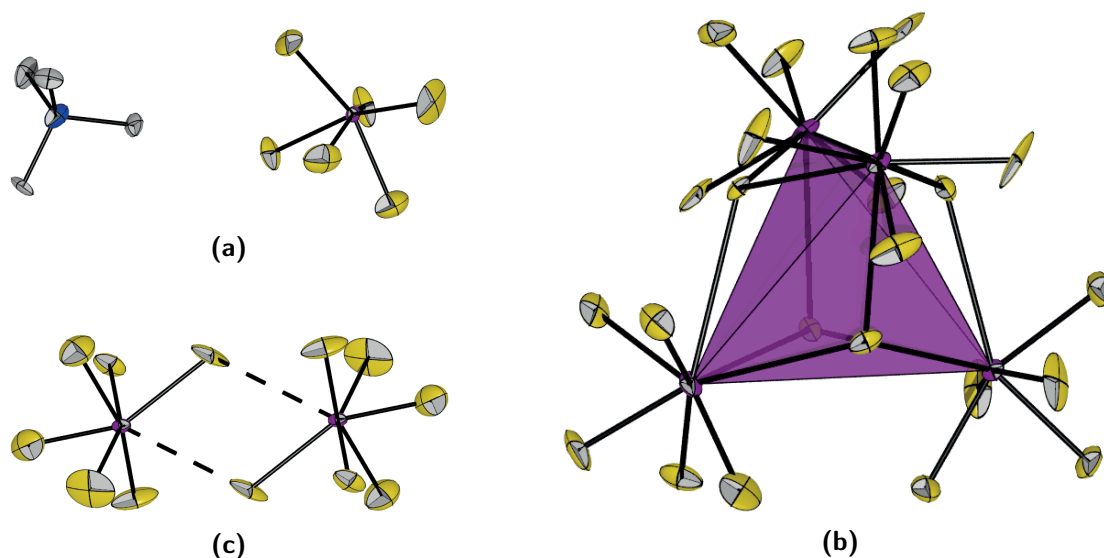


Figure 10. Solid-state structures of compounds containing the $[\text{IF}_6]^-$ anion. Thermal ellipsoids at 50 % probability level. Hydrogen atoms are omitted for clarity. Color code: gray = carbon, blue = nitrogen, violet = iodine, yellow = fluorine. (a) Solid-state structure of $[\text{NMe}_4][\text{IF}_6]$. (b) Tetrameric structure formed by the anionic moiety of $[\text{NO}][\text{IF}_6]$ (c) Dimeric structure formed by the anionic moiety of $[\text{NMe}_4][\text{IF}_6]$.^[96]

good agreement with the calculated values. The ^{19}F NMR spectrum of $[\text{NMe}_4][\text{IF}_8]$ shows a multiplet at 248.6 ppm.

Tables 13 and 14 summarize the bond lengths and ^{19}F NMR shifts of all known fluoridohalogenates depending on the central halogen and their oxidation state. The bond distances increase with the atomic number due to the increasing atomic radius of the halogens and they decrease with rising oxidation state due to higher electrostatics. The ^{19}F NMR chemical shifts show an upfield shift for heavier halogens and a downfield shift with increasing oxidation state.

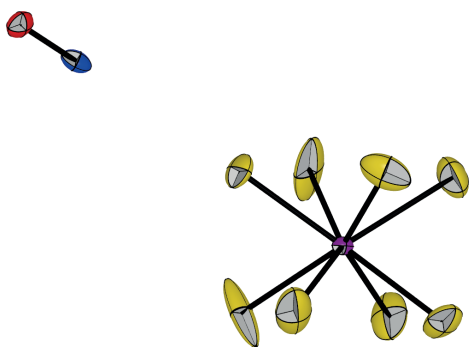


Figure 11. Solid-state structure of $[\text{NO}][\text{IF}_8]\cdot 2 \text{NOF}$.^[97] Co-crystallized NOF is omitted for clarity. Only one of two ion pairs of the asymmetric unit is shown. Thermal ellipsoids at 50 % probability level. Color code: blue = nitrogen, red = oxygen, violet = iodine, yellow = fluorine.

Table 12. Vibrational spectroscopic data of the $[\text{IF}_8]^-$ anion with different counterions^a in comparison with calculated values of the D_{4d} symmetric anion. Values given in cm^{-1} .

	Cs^+	$[\text{NO}]^+$	$[\text{NMe}_4]^+$	calc. ^b
E_3	655	650	660	540
A_1	594	594	595,588	590
B_2	-	-	590	597
E_1	-	-	590	604
E_2	461	467	463	465
E_3	415	418	419	410
A_1	403	418	410	413
E_1	-	-	410	419
B_2	-	-	410	404
-	375	339	380	-
E_1	-	-	314	346
	270	246		
B_1	200	-	-	218
E_2	-	-	119	114
Ref.	[162]	[162]	[164]	[119]

^a for $[\text{NO}_2]^+$ only one IR band at 600 cm^{-1} is reported.^[163]

^b MP2/aug-cc-pVTZ

Table 13. Summarized X–F bond lengths of $[\text{XF}_n]^-$ anions (X = Cl, Br, I) depending on the oxidation state of the central halogen atom. Values given in pm.

ox. state	Cl	Br	I
+I	-	-	207.5(3)-208.2(3) ^[91]
+III	172.7(1)-187.4(1) ^[91]	180.1(4)-193.5(2) ^[138]	200.0(4)-201.8(3) ^[91]
+V	-	181.4(2)-187.3(2) ^[149]	182(1)-211(1) ^[96]
+VII	-	-	188.4(4)-190.4(4) ^[97]

Table 14. Summarized ^{19}F NMR chemical shifts of $[\text{XF}_n]^-$ anions ($\text{X} = \text{Cl}, \text{Br}, \text{I}$) depending on the oxidation state of the central halogen atom. Entries in parentheses are incorrect and were corrected later. Values given in ppm.

ox. state	Cl	Br	I
+I	-	$(-41.6),^{[124]} -210^{[91]}$	$(-126.1),^{[151]} -282,^{[152]} -286^{[91]}$
+III	$66.8,^{[104]} 68.5^{[91]}$	$-37^{[104]}$	$-106.5,^{[93]} -106^{[91]}$
+V	-	$94^{[104]}$	$13^{[148]}$
+VII	-	-	$248.6^{[164]}$

1.2.2. Non-classical Polyinterhalides

As mentioned above, non-classical polyinterhalides consist of a more electronegative central halogen and less electronegative halogen or interhalogen ligands. Consequently, potential central atoms are F, Cl and Br. Potential ligands include Cl_2 , ClF , ClF_3 , ClF_5 , Br_2 , BrF , BrF_3 , BrF_5 , BrCl , I_2 , IF , IF_3 , IF_5 , IF_7 , ICl , ICl_3 , IBr and IBr_3 . Despite the seemingly huge amount of theoretically possible anions only a moderate number of compounds have been synthesized thus far.^[2,37] Several reasons can justify this: (i) many combinations of central halide and ligand lead to redox reactions and therefore do not yield stable anions, (ii) the availability and practical handling of several starting materials is difficult, especially non-solvated fluoride salts which are soluble in organic solvents, as well as highly reactive halogen fluorides. Therefore, I will focus on fluorine-containing non-classical polyinterhalides.

According to a report from 2015, $[\text{NEt}_4]\text{F}$ reacts with iodine and bromine under formation of $[\text{NEt}_4][\text{I}_2\text{F}]$ and $[\text{NEt}_4][\text{Br}_2\text{F}]$.^[165] The authors provide UV/Vis and IR spectroscopic data of the products and compare the experimental spectra with computational results. However, the vibrational spectroscopic data do not include the region expected for the anion bands (below 400 cm^{-1}). Therefore this report has to be treated with care. More reliable reports are found for the reaction of bromine with caesium fluoride by SEPPELT and co-workers. They measured crystal structures and Raman spectra of a halogen richer $\text{CsF}\cdot\text{Br}_2$ and a less halogen-rich compound $2\text{CsF}\cdot\text{Br}_2$.^[166,167] The former was obtained from exposure of CsF to an excess of Br_2 .^[166,167] From this compound bromine can be removed in vacuum until a 2:1 ratio of CsF to Br_2 is reached.^[167] Figure 12 shows the unit cells of both compounds. The $\text{Br}-\text{Br}$ bond lengths are slightly elongated ($\text{CsF}\cdot\text{Br}_2$ $232.4(2)\text{ pm}$, $2\text{CsF}\cdot\text{Br}_2$ $239(2)\text{ pm}$) in comparison to elemental bromine ($228.6(3)\text{ pm}$),^[168] but less than in asymmetric $\text{Cs}[\text{Br}_3]$ ($244.0(6)$, $269.8(6)\text{ pm}$).^[169] The larger bond elongation in $2\text{CsF}\cdot\text{Br}_2$ is expected because the donation of charge density from two fluoride ions into the antibonding σ^* MO of the $\text{Br}-\text{Br}$ bond is larger than from only one. The $\text{Br}-\text{F}$ bond lengths are $252.0(1)$ and $252(1)$, respectively. This is relatively long for a $\text{Br}-\text{F}$ bond ($\text{Br}-\text{F}$ bond length in BrF is 175.9 pm).^[170] The Raman spectra of the samples show one line each, at 292.5 and 287.0 cm^{-1} pm , respectively, which is attributed to the $\text{Br}-\text{Br}$ vibration.^[167] Since these data point to a relatively weak interaction between Br_2 and F^- , the compounds are probably better described as intercalation compounds of Br_2 in the CsF lattice.^[166,167] Exchanging the halide salt (e.g. for RbF) or the halogen (e.g. for Cl_2 or I_2) did not lead to non-classical polyinterhalide compounds. In case of chlorine, no reaction was observed and in case of iodine, polyiodides such as $[\text{I}_8]^{2-}$ were formed from disproportionation reactions.^[167]

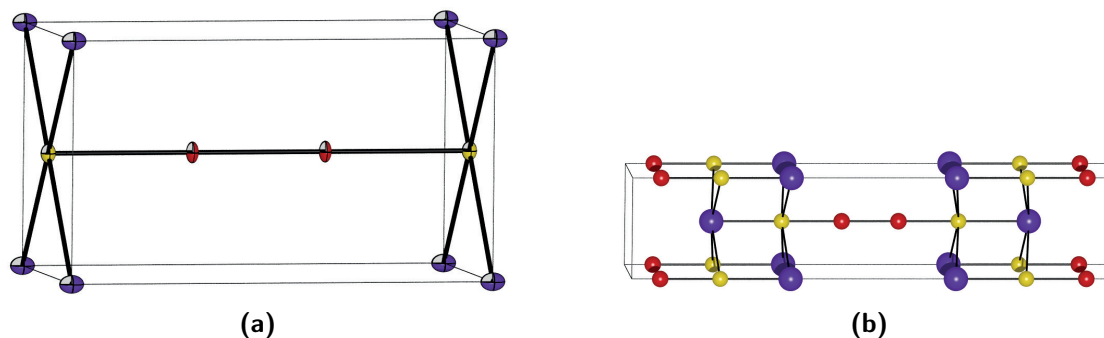


Figure 12. Unit cells of (a) $\text{CsF}\cdot\text{Br}_2$, thermal ellipsoids at 50 % probability level, (b) $2 \text{CsF}\cdot\text{Br}_2$. Color code: purple = caesium, yellow = fluorine, red = bromine.^[166,167]

Bromine trifluoride is known to act as a ligand in various compounds with the general formula $[\text{cat}][\text{F}(\text{BrF}_3)_n]$ ($n = 2, 3, 4$). The solvolysis of $\text{Cs}[\text{BrF}_4]$ in BrF_3 was reported to yield $\text{Cs}[\text{F}(\text{BrF}_3)_3]$.^[171] Removal of one equivalent of BrF_3 in vacuum at elevated temperatures enabled the isolation of $\text{Cs}[\text{F}(\text{BrF}_3)_2]$.^[171] Moreover, the reaction of equimolar amounts of $\text{Cs}[\text{BrF}_4]$ and BrF_3 also led to the same species.^[172] Later, KRAUS and co-workers showed that CsCl and RbCl are also suitable starting materials for the synthesis of these compounds.^[134,173] Furthermore, solvolysis of PbF_2 in BrF_3 led to $[\text{PbF}][\text{F}(\text{BrF}_3)_2]$.^[174] The compounds are all characterized by vibrational spectroscopy (Table 15) and X-ray diffraction (Figure 13a). The structural analysis revealed that the $[\text{F}(\text{BrF}_3)_2]^-$ anion neither has a linear $\text{Br}-\text{F}-\text{Br}$ bridging fragment nor is it planar, as anticipated earlier.^[171] The $\text{Br}-\text{F}-\text{Br}$ bonding angle is between $105.6(5)$ and $140.27(6)^\circ$ whereas the twisting angle between the two connected $\{\text{BrF}_4\}$ units is in the range of $61.90(4)$ to $85.2(3)^\circ$.^[173,174] The $\text{Br}-\text{F}$ bonds can be sorted into three categories. The bridging fluorine atoms have the longest $\text{Br}-\text{F}$ distances ($211.5(2)$ – $225(1)$ pm^[174]), whereas the fluorine atoms *trans* to the bridging fluorine have the shortest ($174(1)$ – $178.0(2)$ pm^[173]). These findings are well reproduced in the vibrational spectra (Table 15): The bridging $\text{Br}-\text{F}$ stretching mode is observed at lower energies than the $\text{Br}-\text{F}_{cis}$, and the $\text{Br}-\text{F}_{trans}$ is the most blue shifted.^[171,173,174] For the coordination of a third equivalent of BrF_3 three different donor fluorine atoms exist, the bridging $\mu_2\text{-F}$, F_{trans} or F_{cis} . Although $[\text{F}(\text{BrF}_3)_3]^-$ was first predicted to have a chain-line coordination via F_{trans} ,^[171] quantum-chemical calculations showed that a coordination via F_{cis} is the global minimum.^[175] Vibrational spectroscopic data (Table 15) and X-ray diffraction (Figure 13b) show that in reality all three BrF_3 moieties are coordinated to the same fluorine atom, forming a $\mu_3\text{-F}$ bridging fluorine.^[173] The $[\text{F}(\text{BrF}_3)_3]^-$ anion exists in $\text{Rb}[\text{F}(\text{BrF}_3)_3]$, $\text{Cs}[\text{F}(\text{BrF}_3)_3]$, $\text{Ba}_2[\text{F}(\text{BrF}_3)_3]_2[\text{F}(\text{BrF}_3)_4]_2$, as well as $\text{Ba}[\text{F}(\text{BrF}_3)_3]_2\cdot\text{BrF}_3$,^[171,173,176] and was synthesized via the solvolysis of RbCl , CsCl , CsF and BaCl_2 in BrF_3 . As in $[\text{F}(\text{BrF}_3)_2]^-$, the $\text{Br}-\text{F}$ bond lengths fall in three categories: $\text{Br}-\mu_3\text{-F}$ ($230.93(6)$ – $233.9(6)$ pm),^[176] $\text{Br}-\text{F}_{cis}$ ($182(1)$ – $187.8(7)$ pm)^[173] and $\text{Br}-\text{F}_{trans}$ ($172.3(3)$ – $176.7(7)$ pm^[173]). Coordination of a third equivalent of BrF_3 therefore leads to an elongation of the $\text{Br}-\mu\text{-F}$ bonds and a shortening of the other $\text{Br}-\text{F}$ bonds, which approach the bond lengths of gaseous BrF_3 (172.10 and 181.00 pm).^[177] The decreasing distortion of the BrF_3 ligands upon further coordination can be rationalized through the increasingly shared bonding electron density, similar to larger polyhalides.^[37] The coordination of a fourth equivalent of BrF_3 is calculated to form a chain-like structure.^[175] However, experimentally de-

terminated structures (Figure 13c and 13d) obtained from the reaction of BaCl_2 with BrF_3 show branched arrangements of the BrF_3 units. The compound $\text{Ba}_2[\text{F}(\text{BrF}_3)_2]_2[\text{F}(\text{BrF}_3)_4]_2$ has two isomeric $[\text{F}(\text{BrF}_3)_4]^-$ anions, one in which a BrF_3 ligand is coordinated to a $[\text{F}(\text{BrF}_3)_3]^-$ anion on a *cis*-F (Figure 13c), with a corresponding $\text{Br}-\text{F}$ distance of 239.1(8) pm,^[176] and another in which a $[\text{F}(\text{BrF}_3)_2]^-$ is coordinated by two BrF_3 ligands on opposite *cis* fluorine atoms. The bonds connecting these two ligands with the backbone are even longer (240.8(9), 266(2) pm) than the $\text{Br}-\mu_2\text{-F}$ and $\text{Br}-\mu_3\text{-F}$ bonds discussed above.^[176]

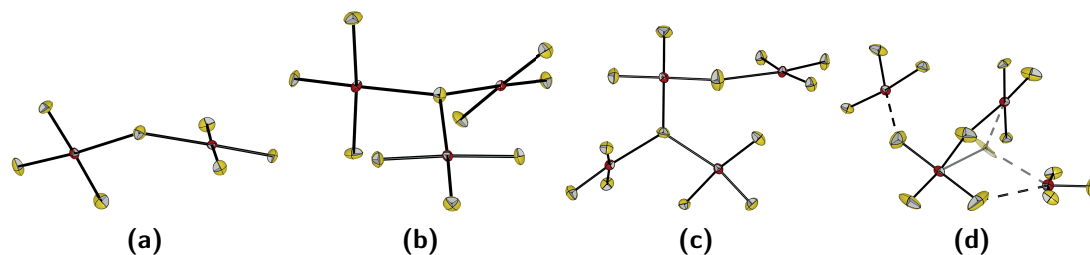


Figure 13. Molecular structures of the anionic moieties of (a) $\text{Rb}[\text{F}(\text{BrF}_3)_2]$, (b) $\text{Rb}[\text{F}(\text{BrF}_3)_3]$, (c) one isomer of $[\text{F}(\text{BrF}_3)_4]^-$ in $\text{Ba}_2[\text{F}(\text{BrF}_3)_2]_2[\text{F}(\text{BrF}_3)_4]_2$, (d) other isomer of $[\text{F}(\text{BrF}_3)_4]^-$ in $\text{Ba}_2[\text{F}(\text{BrF}_3)_2]_2[\text{F}(\text{BrF}_3)_4]_2$. Thermal ellipsoids at 50 % probability level, disorder shown with transparency. Color code: red = bromine, yellow = fluorine.^[173,176]

Table 15. Raman spectroscopic data of the $[\text{F}(\text{BrF}_3)_2]^-$ and $[\text{F}(\text{BrF}_3)_3]^-$ anions with different counterions. Values given in cm^{-1} .

Assignment ^a	$[\text{F}(\text{BrF}_3)_2]^-$			$[\text{F}(\text{BrF}_3)_3]^-$	
	Rb^+	$\text{Cs}^{+\text{b}}$	$[\text{PbF}]^+$	Rb^+	$\text{Cs}^{+\text{b}}$
	-	848	-	-	-
$\nu_{\text{sy}}(\text{Br}-\text{F}_{\text{trans}})$	616	608	660	647	647
$\nu_{\text{as}}(\text{Br}-\text{F}_{\text{trans}})$	589	584	631	631,617	620
$\nu_{\text{as}}(\text{Br}-\text{F}_{\text{cis}})$	549	520	545,522,504	566,555	570
$\nu_{\text{sy}}(\text{Br}-\text{F}_{\text{cis}})$	522,500	517,503	592	540,529	535,518,506
	-	473	-	-	472,380
$\nu(\text{Br}-\text{F}_{\mu})$	350-300	303,340	341	-	-
$\nu(\text{Br}-\text{F}_{\mu})+\delta(\text{Br}-\text{F}_{\mu})$	280-260	287,274	340-280	320-240	317,304,252
libration + δ	-	188,147	273-116	-	-
lat. vib.	-	78,68	111-26	-	-
	-	-	-	-	188,142,120,94,80
Ref.	[173]	[171]	[174]	[173]	[171]

^a according to [173], [174] based on periodic DFT calculations.

^b no comprehensive assignment available

The only non-classical chlorine fluorine polyinterhalide is $\text{Cs}[\text{F}(\text{ClF}_3)_3]$.^[178] It was synthesized by solvolysis of CsF in ClF_3 . The structure of the anionic moiety (Figure 14a) is similar to that of the heavier homologue $[\text{F}(\text{BrF}_3)_3]^-$, also containing a μ_3 -bridging fluorine atom which is coordinated by three ClF_3 ligands. As for the corresponding bromine compound, the chlorine fluorine bond lengths fall into three different regimes: $\mu_3\text{-F}-\text{Cl}$ distances are between 224.3(2) to 226.5(2) pm, $\text{F}_{\text{cis}}-\text{Cl}$ are in the range of 173.0(2) to 174.7(2) pm and $\text{F}_{\text{trans}}-\text{Cl}$ are between

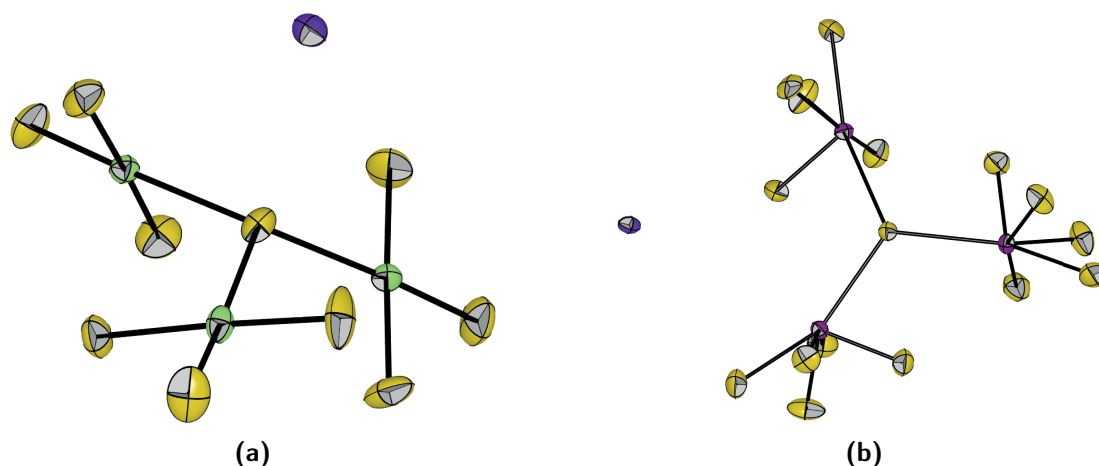


Figure 14. Molecular structures of (a) $\text{Cs}[\text{F}(\text{ClF}_3)_3]$, (b) $\text{Cs}[\text{F}(\text{IF}_5)_3]$. Thermal ellipsoids at 50 % probability level. Color code: green = chlorine, yellow = fluorine, violet = iodine, purple = caesium.

160.0(2) to 161.5(2) pm.^[178] Interestingly, the optimized structure in the gas-phase is fully planar, whereas in the actual structure the bridging fluorine atom lies 52.2(2) pm above the plane of the chlorine atoms. The Raman spectrum has five bands assigned to the anion at 761, 699, 498 334 and 315 cm^{-1} , which are in good agreement with the calculated spectrum.^[178]

In the case of iodine the best characterized compound is $\text{Cs}[\text{F}(\text{IF}_5)_3]$. It was synthesized by reaction of CsF with excess IF_5 and was studied with vibrational spectroscopy and single crystal X-ray diffraction (Figure 14b).^[95,161] Additionally, the crystal structure of the potassium salt is known^[95] and the vibrational spectra of a mixture of $\text{Rb}[\text{IF}_6]$ and $\text{Rb}[\text{F}(\text{IF}_5)_3]$ were reported.^[161] The structures in the solid state again contain a bridging $\mu_3\text{-F}$ atom which is coordinated by three IF_5 units. As for $[\text{IF}_6]^-$, the electron pair at iodine is structurally active. The $\mu_3\text{-F-I}$ bond lengths are in the range of 247(1) to 252.5(3) pm.^[95] The terminal I-F stretching modes (677 and 635 cm^{-1} (IR), 674 and 635 cm^{-1} (Raman)) are blue shifted in comparison to $[\text{IF}_6]^-$.^[161] Additionally, a compound with the composition $\text{CuF}_2 \cdot 4 \text{ MeCN} \cdot 4 \text{ IF}_5$ was synthesized from CuF_2 and IF_5 in MeCN.^[179] The potential anions in the compound are two $[\text{F}(\text{IF}_5)_2]^-$ or one $[\text{IF}_6]^-$ and $[\text{F}(\text{IF}_5)_3]^-$. The Raman spectrum showed a band at 687 cm^{-1} assigned to the terminal I-F stretching mode which is even more blue shifted than in the well-established $\text{Cs}[\text{F}(\text{IF}_5)_3]$. This, together with the fact that CHRISTE never observed $[\text{F}(\text{IF}_5)_2]^-$ but only mixtures of $[\text{IF}_6]^-$ and $[\text{F}(\text{IF}_5)_3]^-$ points to either the aforementioned anion mixture or weakly bound complexes.^[161]

1.3. Halogenate Complexes with other Ligand Systems

In addition to fluorine, a handful of other elements are potential ligands for halogens in positive oxidation states. Since the formal oxidation state (OS) is purely governed by electronegativity differences, the assessment for potential elements is fairly easy.^[180] In case of chlorine, only fluorine and oxygen (and nitrogen depending on the electronegativity scale used) are potential ligands to realize positive oxidation states, leaving noble gases aside. For bromine the aforementioned elements plus chlorine come under consideration and for iodine, both chlorine and bromine. Binary oxohalogenate anions $[\text{XO}_n]^-$ ($n = 1-4$) are well-known, as they are the cor-

responding bases of the halogen oxo-acids.^[13–15] Amongst them, hypochlorite $[\text{ClO}]^-$ -containing salts such as $\text{Na}[\text{ClO}]$, $\text{K}[\text{ClO}]$ or $\text{Ca}[\text{ClO}]_2$ are the most widely used substances, as they are the main component of industrial bleach.^[181] Ternary fluoridooxohalogenates $[\text{XF}_n\text{O}_m]^-$ ($n = 2, 4$; $m = 1, 2$) exist for chlorine, bromine and iodine, and OS +V appears to be most favorable, since $[\text{XOF}_4]^-$ and $[\text{XO}_2\text{F}_2]^-$ ($X = \text{Cl}, \text{Br}, \text{I}$) are the only known anions of this kind apart from $[\text{IO}_2\text{F}_4]^-$.^[182,183] Two binary nitrogen halogenate anions are known, $[\text{I}_2\text{N}_3]^-$ and $[\text{I}(\text{N}_3)_2]^-$. The latter is known as the $[\text{PPh}_4]^+$,^[184] and $[\text{NMe}_4]^+$ ^[184,185] salt. It is synthesized from the corresponding cation azides $[\text{cat}][\text{N}_3]$ with iodine azide IN_3 .^[184,185] The I–N stretching modes in the IR spectrum are observed at 250 and 237 cm^{-1} ($[\text{NMe}]^+$) and 285 and 269 cm^{-1} ($[\text{PPh}_4]^+$).^[184] A solid-state structure of the tetraphenylphosphonium salt is reported (Figure 15).^[184]

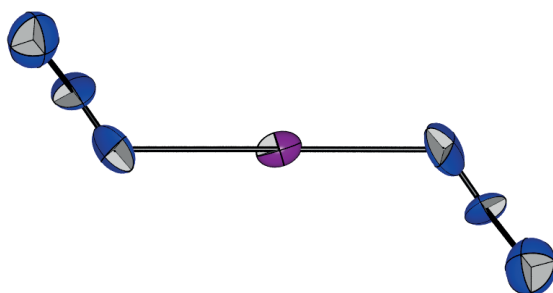


Figure 15. Solid-state structure of the anionic moiety of $[\text{PPh}_4][\text{I}(\text{N}_3)_2]$.^[184] Thermal ellipsoids at 50 % probability level. Color code: blue = nitrogen, violet = iodine.

Table 16. Literature-known examples of symmetric halogenate complexes with polyatomic ligands.

	NO_3	SO_3F	ClO_4	O_2CCF_3	OCF_3
Br	$[\text{Br}(\text{NO}_3)_2]^-$	$[\text{Br}(\text{SO}_3\text{F})_4]^-$	$[\text{Br}(\text{ClO}_4)_2]^-$	-	$[\text{Br}(\text{OCF}_3)_2]^-$
I	$[\text{I}(\text{NO}_3)_2]^-$ $[\text{I}(\text{NO}_3)_4]^-$	$[\text{I}(\text{SO}_3\text{F})_4]^-$	$[\text{I}(\text{ClO}_4)_4]^-$	$[\text{I}(\text{O}_2\text{CCF}_3)_4]^-$	-
Ref.	[186]	[187]	[188, 189]	[190]	[124]

So far only compounds with monoatomic ligands were discussed. Nevertheless, a few halogenate complexes with polyatomic ligands exist for bromine and iodine (Table 16). To date, examples for chlorine are still absent. The first reported compounds $\text{K}[\text{Br}(\text{SO}_3\text{F})_4]$, $\text{K}[\text{I}(\text{SO}_3\text{F})_4]$ and $\text{Na}[\text{I}(\text{SO}_3\text{F})_4]$ were synthesized from peroxydisulfuryl difluoride $\text{S}_2\text{O}_6\text{F}_2$ with KI , NaI and KBr , respectively (Eq. 12).^[187,191] Later, synthetic routes using potassium bromate(V) $\text{K}[\text{BrO}_3]$ (Eq. 13) and potassium tetrachloroiodate(III) $\text{K}[\text{ICl}_4]$ (Eq. 14) were found.^[191] The Raman spectra show three bands associated with X–O vibrations at $447/440/442\text{ cm}^{-1}$, $399/394/397\text{ cm}^{-1}$ and $270/252/260\text{ cm}^{-1}$ for $\text{K}[\text{Br}(\text{SO}_3\text{F})_4]/\text{Na}[\text{I}(\text{SO}_3\text{F})_4]/\text{K}[\text{I}(\text{SO}_3\text{F})_4]$, respectively, which can be assigned to the in-phase symmetric stretching, the out-of-phase symmetric stretching and a deformation mode.^[191] This fits well to the corresponding fluoridohalogenates(III) $\text{K}[\text{BrF}_4]$ ($531, 454, 242\text{ cm}^{-1}$)^[130] and $\text{Cs}[\text{IF}_4]$ (Table 17) ($522, 455, 195\text{ cm}^{-1}$).^[157] Another closely related group of compounds are the nitrido halogenates $[\text{NMe}_4][\text{I}(\text{NO}_3)_4]$, $[\text{NMe}_4][\text{I}(\text{NO}_3)_2]$ and $[\text{NMe}_4][\text{Br}(\text{NO}_3)_2]$, with Br(I), I(III) and I(I) centers. The I(I) compound was synthesized from tetramethylammonium dichloridoiodate(I) $[\text{NMe}_4][\text{ICl}_2]$ and silver(I) nitrate $\text{Ag}[\text{NO}_3]$ under el-

emination of silver chloride AgCl (Eq. 15).^[186] If tetramethylammonium tetrachloridoiodate(III) $[\text{NMe}_4][\text{ICl}_4]$ is used as a starting material, all four chlorido ligands can be exchanged to yield $[\text{NMe}_4][\text{I}(\text{NO}_3)_4]$ (Eq. 15).^[186] A second preparative procedure employs chlorine nitrate ClNO_3 instead of $\text{Ag}[\text{NO}_3]$, which leads to the generation of elemental chlorine during the reaction (Eq. 16). Both compounds were characterized by elemental analysis, conductivity measurements, UV/VIS and IR spectroscopy. The IR spectra confirm the absence of ionic nitrate in all cases, but unfortunately do not show the region for the X–O vibrations below 600 cm^{-1} .^[186] The lighter homologue $[\text{Br}(\text{NO}_3)_2]^-$ is known as the $[\text{NO}_2]^+$,^[192] Cs^+ ^[193] and $[\text{NMe}_4]^+$ ^[186] salt. The latter two were synthesized from the corresponding dichloridobromate(I) salts $[\text{cat}][\text{BrCl}_2]$ and ClNO_3 (Eq.17).^[186,193] The nityl salt was either synthesized from bromine nitrate BrNO_3 and dinitrogen pentoxide N_2O_5 (Eq. 18),^[193] or from bromine fluorine dioxide BrO_2F and nitrogen dioxide NO_2 (Eq. 19).^[192] Overall, the Raman spectroscopic data (Table 18) are consistent with the calculated data, however, the assignment shows discrepancies especially for the most intense band at $732/747/746\text{ cm}^{-1}$. CHRISTE^[193] assigned this band to an O–N–O deformation mode whereas SEPPELT^[192] assigned it to the symmetric BrO_2 stretching mode. This vibration is observed at 298 cm^{-1} in the Cs^+ salt according to CHRISTE (no value given for the the $[\text{NO}_2]^+$ compound).^[193] The fact that the calculated band at 728 cm^{-1} can be assigned to the $\nu_s(\text{BrO}_2)$ vibration, however, strongly supports the assignment by SEPPELT.^[192] In addition to the Raman spectroscopic data, a crystal structure of $[\text{NO}_2][\text{Br}(\text{NO}_3)_2]$ is known (Figure 16). It shows a linear coordination of the Br(I) center with two identical Br–O bond lengths ($205.1(2)\text{ pm}$).^[192]

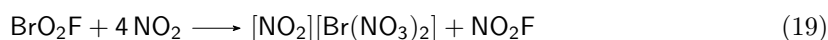
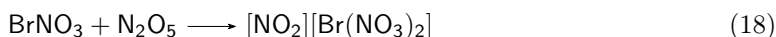
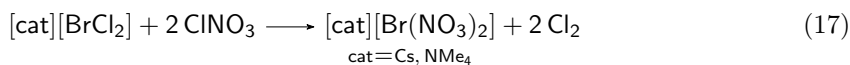
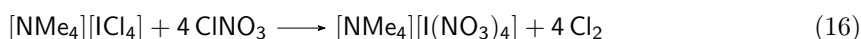
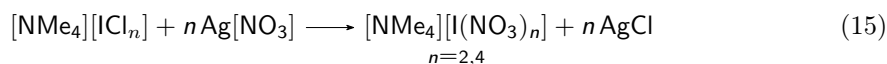
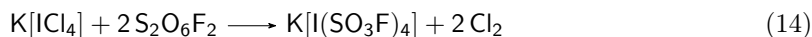
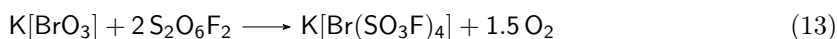
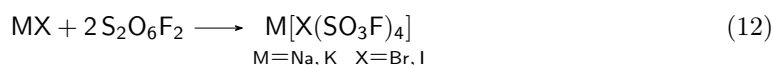


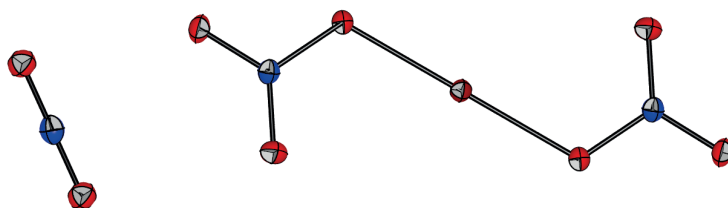
Table 17. Raman spectroscopic data of $\text{K}[\text{Br}(\text{SO}_3\text{F})_4]$, $\text{Na}[\text{I}(\text{SO}_3\text{F})_4]$ and $\text{K}[\text{I}(\text{SO}_3\text{F})_4]$ in comparison with $\text{K}[\text{BrF}_4]$ and $\text{Cs}[\text{IF}_4]$. Values given in cm^{-1} .

	$\text{K}[\text{Br}(\text{SO}_3\text{F})_4]$	$\text{Na}[\text{I}(\text{SO}_3\text{F})_4]$	$\text{K}[\text{I}(\text{SO}_3\text{F})_4]$	$\text{K}[\text{BrF}_4]$	$\text{Cs}[\text{IF}_4]$
ν_{sy} in-phase	447	440	442	531	522
ν_{sy} in-phase	399	394	397	454	455
δ	270	252	260	242	195
Ref.	[191]	[191]	[191]	[130]	[157]

In addition to the two already discussed ligands derived from inorganic acids, also two perchlo-

Table 18. Raman spectroscopic data of the $[\text{Br}(\text{NO}_3)_2]^-$ anion with different counterions. Values given in cm^{-1} .

Assignment ^a	Cs^+	$[\text{NO}_2]^{+\text{b}}$	calc. ^c	
$\nu_{\text{as}}(\text{NO}_2)$ out-of-phase	1530	1569, 1529, 1493	1528	1548
$\nu_{\text{s}}(\text{NO}_2)$ in-phase	1283	1308, 1283	1282	1312
$\nu_{\text{as}}(\text{NO}_2)$ in-phase	-	1130, 1118, 1103	-	-
$\nu_{\text{s}}(\text{NO}_2)$ out-of-phase	975, 960	982, 964	964	985
	-	-	910	953 ^d
$\delta_{\text{sciss}}(\text{NO}_2)$	791	787	-	806
$\delta_{\text{as}}(\text{O}-\text{N}-\text{O})$ in plane	732	747	746	728
$\delta(\text{O}-\text{N}-\text{O})$ out of plane	697	700	697	700
	-	-	507	-
$\nu_{\text{as}}(\text{O}-\text{N})$	460	480	-	-
$\nu_{\text{as}}(\text{BrO}_2)$	400	400	-	-
$\nu_{\text{s}}(\text{O}-\text{N})$	317	315	314	278
$\nu_{\text{s}}(\text{BrO}_2)$	298	-	-	264 ^d
	230	-	-	218 ^d
	-	175	179	- ^e
	157	162	151	- ^e
	128	126	-	- ^e
	110	105	-	- ^e
	87	93	-	- ^e
	53	-	-	- ^e
Ref.	[193]	[193]	[192]	[192]

^a according to Ref. [193] for $[\text{NO}_2][\text{Br}(\text{NO}_3)_2]$ ^b cation vibration at $1395/1407 \text{ cm}^{-1}$, respectively^c B3LYP^d no calculated Raman intensity^e five bands below 200 reported ambiguously**Figure 16.** Solid-state structure of $[\text{NO}_2][\text{Br}(\text{NO}_3)_2]$.^[192] Thermal ellipsoids at 50 % probability level. Color code: blue = nitrogen, red = oxygen, brown = bromine.

rate halogenates are known, namely $\text{Cs}[\text{Br}(\text{ClO}_4)_2]$ and $\text{Cs}[\text{I}(\text{ClO}_4)_4]$.^[188,189] They were synthesized from the corresponding caesium halide salts with an excess of chlorine perchlorate ClClO_4 . Both compounds were characterized by means of vibrational spectroscopy, indicating a monodentate coordination of the ligands with linear $\text{O}-\text{X}-\text{O}$ ($\text{X} = \text{Br}, \text{I}$) units. For $[\text{I}(\text{ClO}_4)_4]^-$ the symmetric in-phase and out-of-phase stretching modes of the $\{\text{IO}_4\}$ unit are assigned to bands at 261 and 240 cm^{-1} , respectively.^[189] The symmetric $\text{Br}-\text{O}$ stretching modes in $[\text{Br}(\text{ClO}_4)_2]^-$

were assigned to the bands at 633, 625 and 450 cm^{-1} .^[188] The assignment for the $[\text{I}(\text{ClO}_4)_4]^-$ anion seems surprising because (i) $\text{K}[\text{I}(\text{SO}_3\text{F})_4]$ has I–O stretching bands at 442 and 397 cm^{-1} and (ii) the structurally related $\text{Cs}[\text{IF}_4]^-$ has symmetric stretching modes at 522 and 455 cm^{-1} , respectively, indicating that the assignment in $[\text{I}(\text{ClO}_4)_4]^-$ may be erroneous. Trifluoroacetate holds as an example for an organic ligand in the compound $\text{Cs}[\text{I}(\text{O}_2\text{CCF}_3)_4]$. It was synthesized from the reaction of $\text{Cs}[\text{IF}_4]$ with trifluoroacetic anhydride.^[190] In the same paper the authors report on the synthesis of $\text{Cs}_3[\text{I}(\text{O}_2\text{CCF}_3)_6]$ starting from $\text{Cs}_3[\text{IF}_6]$, but as already mentioned, this compound was identified as a mixture of CsF and $\text{Cs}_2[\text{IF}_5]$ (*vide supra*). Therefore, reports regarding this compound have to be treated with care. For $[\text{I}(\text{O}_2\text{CCF}_3)_4]^-$, Raman bands of the $\{\text{IO}_4\}$ -unit can be observed for the symmetric out-of-phase stretching (604 cm^{-1}), for the symmetric in-phase stretching (501, 490 cm^{-1}) and for the deformation mode (306, 130 cm^{-1}). The antisymmetric stretching mode was observed at 470 cm^{-1} in the IR spectrum.^[194] Based on the vibrational spectra a monodentate coordination is most likely, in agreement with the earlier discussed nitrate and perchlorate compounds.^[194] In the last example the ligands are not derived from an acid but from the alcohol trifluoromethanol. $[\text{NMe}_4][\text{Br}(\text{OCF}_3)_2]$ was synthesized from $[\text{NMe}_4]\text{Cl}$ or $[\text{NMe}_4][\text{BrCl}_2]$ with trifluoromethylhypochlorite ClOCF_3 .^[195] It is well characterized by vibrational and NMR spectroscopy, as well as by mass spectrometry. The symmetric and antisymmetric O–Br–O stretching modes were observed at 383 and 308 cm^{-1} , respectively.^[195] Compared to $[\text{Br}(\text{NO}_3)_2]^-$, it fits to the assignment by CHRISTE ($\nu_s = 298$, $\nu_{\text{as}} = 400$ cm^{-1}).^[193] The ^{19}F NMR spectrum shows a singlet at -54.8 ppm, which is in the typical area for OCF_3 groups. The compound is relatively unstable since loss of carbonyl fluoride starts at -70 °C leaving the $[\text{BrF}_2]^-$ anion behind, a known phenomenon of OCF_3 groups.^[124]

2. Objectives

As presented above, fluoridohalogenates have been known since the 1950s. In the past years, they have experienced a renaissance, in which the focus has slowly shifted away from pure synthesis to exploration of their applications. However, some white spots on the map of classical fluoridohalogenates have remained until today. For instance, the characterization of the difluoridochlorate(I) and -bromate(I) anions is still incomplete with no crystal structures and no or inconclusive NMR data. Therefore, one scientific goal will be the synthesis and unambiguous identification of the difluoridochlorate(I) and -bromate(I) anions to complete the series of fluoridohalogenates.

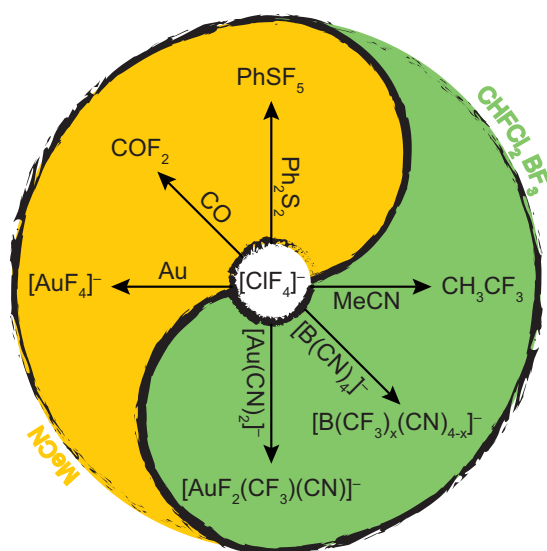
Despite all previous knowledge of the synthesis of fluoridohalogenates with higher fluorine content (especially tetrafluoridohalogenates), the follow-up chemistry of tetrafluoridobromate(III) has started to be explored only recently. Reactivity studies concerned with tetrafluoridochlorate(III) are not known. This is probably attributed to the limited availability of organo-soluble sources of these salts. Therefore, the second objective of this work will be the development of a method that grants easy access to soluble sources of tetrafluoridochlorate(III) and -bromate(III) which enables the study of their follow-up chemistry.

Amongst the non-classical polyinterhalides of chlorine and fluorine, only one compound is known for which an unexpected gas-phase structure is predicted. Therefore, this work intends to synthesize further examples of non-classical chlorido-fluorido polyinterhalides and study their bonding situation in comparison to known systems.

Examples of halogenate complexes with halogens in positive OS and larger, polyatomic ligand systems are quite rare and their characterization is often limited, with only one known solid-state structure of a Br(I) anion. Examples with a central chlorine atom are not known. Therefore, a systematic approach for the stabilization of positively charged halogen atoms with polyatomic ligand systems will be studied.

3. Publications

3.1. Improved Access to Organo-Soluble Di- and Tetrafluoridochlorate(I/III) Salts



Patrick Pröhm, Jonas R. Schmid, Karsten Sonnenberg, Patrick Voßnacker, Simon Steinhauer, Caspar J. Schattenberg, Robert Müller, Martin Kaupp, Sebastian Riedel*

Angew. Chem. Int. Ed. **2020**, *59*, 16002;

Angew. Chem. **2020**, *132*, 16136.

DOI: 10.1002/anie.202006268

DOI: 10.1002/ange.202006268

©The Authors. Published by Wiley-VCH GmbH

Author Contribution:

Patrick Pröhm designed the project, performed experiments, analyzed data and wrote the manuscript. Jonas R. Schmid performed experiments during his internship under supervision of Patrick Pröhm. Karsten Sonnenberg measured and refined crystal structures. Simon Steinhauer designed the project and revised the manuscript. Patrick Voßnacker, Caspar J. Schattenberg, Robert Müller and Martin Kaupp performed quantum-chemical calculations and prepared the computational part of the manuscript. Sebastian Riedel supervised the project and revised the manuscript.

Chlorine Fluorides

Improved Access to Organo-Soluble Di- and Tetrafluoridochlorate-(I)/(III) Salts

P. Pröhm, J. R. Schmid, K. Sonnenberg, P. Voßnacker, S. Steinhauer, C. J. Schattenberg, R. Müller, M. Kaupp, and S. Riedel*

Abstract: A facile one-pot gram-scale synthesis of tetraalkylammonium tetrafluoridochlorate(III) $[cat][ClF_4]$ ($[cat] = [NEt_3Me]^+$, $[NEt_4]^+$) is described. An acetonitrile solution of the corresponding alkylammonium chloride salt is fluorinated with diluted fluorine at low temperatures. The reaction proceeds via the $[ClF_2]^-$ anion which is structurally characterized for the first time. The potential application of $[ClF_4]^-$ salts as fluorinating agents is evaluated by the reaction with diphenyl disulfide, Ph_2S_2 , to pentafluorosulfanyl benzene, $PhSF_5$. The CN moieties in acetonitrile and $[B(CN)_4]^-$ are transferred in CF_3 groups. Exposure of carbon monoxide, CO, leads to the formation of carbonyl fluoride, COF_2 , and elemental gold is dissolved under the formation of tetrafluoridoaurate $[AuF_4]^-$.

Chlorine fluorides (ClF , ClF_3 , ClF_5) are amongst the most reactive compounds known.^[1] These very strongly oxidizing gases should only be handled in special equipment made from metal, including stainless steel, copper, nickel, Monel and other Cu/Ni alloys or from perfluorinated polymers such as PTFE, KEL-F or PFA. Especially ClF_3 and ClF_5 can under certain conditions exceed the reactivity of elemental fluorine. Exposure to organic material leads to violent reactions in many cases and only carefully chosen reaction conditions (especially dilution of the chlorine fluoride) can avoid dangerous explosions; however, acetonitrile is known to be resistant against bromo and chloro fluorine compounds.^[2] ClF_3 reacts with nitrosyl fluoride or alkali metal fluorides under formation of the corresponding tetrafluoridochlorate-(III) salts.^[3,4] Alkali metal tetrafluoridochlorates can also be formed via exposure of the corresponding alkali metal

How to cite: *Angew. Chem. Int. Ed.* **2020**, *59*, 16002–16006
 International Edition: doi.org/10.1002/anie.202006268
 German Edition: doi.org/10.1002/ange.202006268

chlorides (CsCl, RbCl, KCl) towards elemental fluorine at elevated temperatures.^[5] More soluble tetrafluoridochlorate-(III) salts, for example, alkylammonium salts, can be obtained by salt metathesis with the corresponding alkylammonium fluorides in propionitrile at low temperatures.^[3] However, only few examples of stable anhydrous alkylammonium fluorides are known.^[6] Nevertheless, cation metathesis was used to synthesize the tetramethylammonium and 1,1,3,3,5,5-hexamethylpiperidinium (pip) tetrafluoridochlorate(III) salts.^[3,7] Additionally, $[NMe_4][ClF_4]$ was observed as a decomposition product of $[NMe_4][ClF_6]$.^[8] The difluoridochlorate(I) anion, $[ClF_2]^-$, is so far only reported with a limited amount of counter ions (K^+ , Rb^+ , Cs^+ , NO^+) and only characterized by vibrational spectroscopy.^[9,10] To the best of our knowledge the chemistry of di- and tetrafluoridochlorates was only studied rudimentarily. Hence, we present a ClF_5 -free, gram scale synthesis of organo-soluble tetraalkylammonium tetrafluoridochlorate and explore its chemical properties. We exposed triethylmethylammonium chloride $[NEt_3Me]Cl$ to dilute fluorine (10% in argon) in acetonitrile or propionitrile at low temperatures [Equation (1)]. In the beginning of the fluorination a slight yellow color of the solution was observed. We hypothesize that small amounts of chlorine are formed. However, it was not possible to detect any vibrational band of Cl_2 via Raman spectroscopy. In the process of further fluorination the solution decolorized again. For the synthesis of highly concentrated solutions we used $[NEt_3Me][Cl_3]$ ^[11] as a starting material due to its enhanced solubility in acetonitrile in comparison to tetraalkylammonium chlorides like $[NEt_4]Cl$ or $[NMe_4]Cl$. It is worth mentioning that all starting materials are commercially available and the reaction proceeds in standard laboratory glassware in contrast to the reported synthesis with ClF_3 .



We characterized the obtained solution by Raman and ^{19}F NMR spectroscopy. The ^{19}F NMR spectrum (Figure S2 in the Supporting Information) shows one main resonance at 67 ppm for $[ClF_4]^-$ which is in good agreement with previously reported values (66.8 ppm).^[7] The Raman spectrum (Figure 1) measured at $-196^\circ C$ shows, besides the bands of the cation and solvent, three bands at 500 cm^{-1} , 408 cm^{-1} and 278 cm^{-1} , which are attributed to the a_{1g} , the b_{1g} , and the b_{2g} vibration in the D_{4h} symmetric molecule in agreement with literature values (508 cm^{-1} , 415 cm^{-1} , 278 cm^{-1}).^[7,12]

By exchange of the cation to tetraethylammonium $[NEt_4]^+$ we were able to grow single crystals suitable for single crystal X-Ray diffraction. $[NEt_4][ClF_4]$ crystallizes in

* M. Sc. P. Pröhm, J. R. Schmid, Dr. K. Sonnenberg,
 M. Sc. P. Voßnacker, Dr. S. Steinhauer, Prof. Dr. S. Riedel
 Freie Universität Berlin, Institut of Chemistry and Biochemistry
 Fabeckstr. 34/36, 14195 Berlin (Germany)
 E-mail: s.riedel@fu-berlin.de

M. Sc. C. J. Schattenberg, Dr. R. Müller, Prof. Dr. M. Kaupp
 Technische Universität Berlin, Department of Chemistry: Theoretical
 Chemistry
 Sekr. C7, Strasse des 17. Juni 135, 10623 Berlin (Germany)
 E-mail: martin.kaupp@tu-berlin.de

Supporting information and the ORCID identification number(s) for the author(s) of this article can be found under:
<https://doi.org/10.1002/anie.202006268>.

© 2020 The Authors. Published by Wiley-VCH Verlag GmbH & Co. KGaA. This is an open access article under the terms of the Creative Commons Attribution License, which permits use, distribution and reproduction in any medium, provided the original work is properly cited.

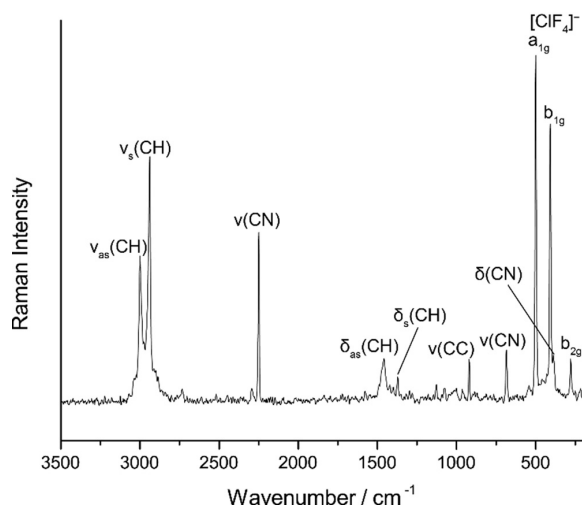


Figure 1. Raman spectrum of $[\text{NEt}_3\text{Me}][\text{ClF}_4]$ in acetonitrile at -196°C .

the space group $C2/c$. The chlorine atom occupies the Wyckhoff position $4c$ (site symmetry $P\bar{1}$). The $[\text{ClF}_4]^-$ is only slightly distorted from D_{4h} symmetry with two crystallographically inequivalent Cl–F bonds, $d(\text{Cl}–\text{F}1) = 180.6(2)$ pm and $d(\text{Cl}–\text{F}2) = 179.3(2)$ pm and rectangular bond angles $\angle(\text{F}1–\text{Cl}–\text{F}2) = 90.01(5)^\circ$ and $\angle(\text{F}2–\text{Cl}–\text{F}1') = 89.99(5)^\circ$, see Figure 2. Overall, the anion is in good agreement with the structures reported in the literature ($[\text{cat}][\text{ClF}_4]$, $[\text{cat}] = \text{K}^+$, Rb^+ , Cs^+ , NO^+ , $[\text{pip}]^+$) and is only slightly less distorted than in the reported structures of $[\text{pip}][\text{ClF}_4]$ and $[\text{NO}][\text{ClF}_4]$ (see Table S2).^[3] The shortest cation anion contact is an F–H hydrogen bridge and was determined to 242.3(1) pm, the corresponding $\text{F}\cdots(\text{H})–\text{C}$ distance was determined to 336.5(3) pm. Additionally, we calculated the Hirshfeld surface which is also showing a short cation anion contact (Figure S16).

The addition of 1.2 equiv. fluorine to a solution of $[\text{NEt}_3\text{Me}]\text{Cl}$ in acetonitrile yields a mixture of $[\text{ClF}_2]^-$ and $[\text{ClF}_4]^-$ anions. Again, we were able to characterize this mixture by vibrational and ^{19}F NMR spectroscopy. The Raman spectrum (Figure 3) of this mixture at -196°C shows the characteristic bands of $[\text{ClF}_4]^-$ and additionally

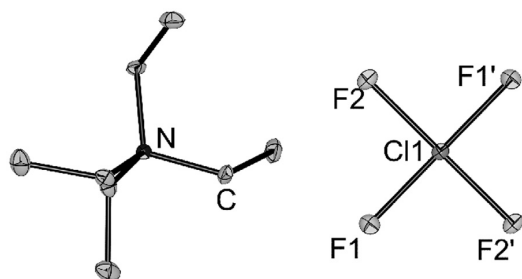


Figure 2. Crystal structure $[\text{NEt}_3\text{Me}][\text{ClF}_4]$. Displacement ellipsoids are shown at 50% probability at 100 K. Selected bond lengths [pm] and bond angles $^\circ$: $\text{F}1–\text{Cl}1$ 179.2(2), $\text{F}2–\text{Cl}1$ 180.6(2), $\text{F}1–\text{Cl}1–\text{F}2$ 89.99(5), $\text{F}2–\text{Cl}1–\text{F}1'$ 90.01(5). Hydrogen atoms omitted for clarity.^[29]

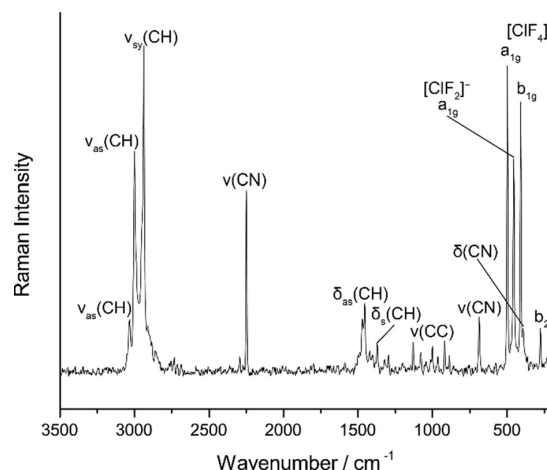


Figure 3. Raman spectrum of $[\text{NEt}_3\text{Me}]_3[\text{ClF}_4][\text{ClF}_2]_2$ in acetonitrile at -196°C .

one band at 455 cm^{-1} which can be assigned to the symmetric stretch vibration of $[\text{ClF}_2]^-$, similar to those reported for solid KClF_2 (475 cm^{-1}) and RbClF_2 (476 cm^{-1}).^[10] The harmonic frequency of the symmetric stretching mode for free $[\text{ClF}_2]^-$ is calculated to 453 cm^{-1} (CCSD(T)/def2-TZVPP) which is in good agreement with our assignment.^[13] The differences between the value reported by us and the literature values can be explained by the stronger coordination of the alkali metal cation in the solid-state in comparison with the tetraalkylammonium cation.

The ^{19}F NMR spectrum (Figure S3) shows two signals. The one at 67 ppm can be assigned to the $[\text{ClF}_4]^-$ anion (see above). We assigned the second signal at -125 ppm to the $[\text{ClF}_2]^-$ anion since the Raman spectrum showed the corresponding band at 455 cm^{-1} before and after the measurement of the NMR spectrum.

Table 1 provides our computed ^{19}F shifts for the full series of anions $[\text{XF}_n]^-$ ($\text{X} = \text{Cl}, \text{Br}, \text{I}; n = 2, 4, 6$), using two functionals (the B3LYP global hybrid and the LH12ct-SsifPW92 local hybrid) that have been shown to provide superior ^{19}F shieldings compared to B3LYP.^[14,15] The computations used BP86-D3(BJ)(COSMO, CH_3CN)/def2-TZVPPD structures and DFT(COSMO, CH_3CN)-GIAO//pcSseg-4/ANO-RCC-unc shielding computations (with pcSseg-4 basis sets for F, Cl, Br and the uncontracted ANO-RCC basis for I; see Supporting Information for further computational details and additional data). The available experimental data for $n = 4, 6$ are reproduced rather well at the two levels used. As shown by separate four-component relativistic computations (Table S5 in Supporting Information), both spin-orbit and scalar relativistic effects are small, in most cases a few ppm, at most about 13 ppm for $[\text{IF}_2]^-$. The small spin-orbit effects can be understood from an inefficient transfer mechanism to the fluorine nuclei.^[16] However, the computed ^{19}F shifts for the difluoridohalide anions are too shielded by 60–100 ppm (more so for B3LYP than for LH12ct-SsifPW92). This is clearly outside the error margins of these two density functionals or of relativistic contribu-

Table 1: Calculated ^{19}F NMR chemical shifts relative to CFCl_3 (in ppm) of $[\text{XF}_n]^-$ ($\text{X} = \text{Cl}, \text{Br}, \text{I}; n = 2, 4, 6$) in comparison with experimental values.

Molecule	δ_{exp}	$\delta_{\text{BHLYP}}^{\text{[a]}}$	$\delta_{\text{LH12ct-sifPW92}}^{\text{[a]}}$
$[\text{ClF}_2]^-$	-125 ^[b]	-202	-174
$[\text{ClF}_4]^-$	67 ^[7]	68	61
$[\text{ClF}_6]^-$	–	278	249
$[\text{BrF}_2]^-$	-210 ^[3a]	-296	-273
$[\text{BrF}_4]^-$	-37 ^[8]	-42	-45
$[\text{BrF}_6]^-$	94 ^[8]	129	112
$[\text{IF}_2]^-$	-286, -282 ^[3a, 17]	-360	-348
$[\text{IF}_4]^-$	-106 ^[3a, 18]	-111	-117
$[\text{IF}_6]^-$	13 ^[19]	30	14

[a] DFT(COSMO, CH_3CN)-GIAO/pcSseg-4/ANO-RCC-unc//BP86-D3-(B)(COSMO, CH_3CN)/def2-TZVPPD data. [b] This work.

tions. Closer inspection reveals that the highly negative fluorine charges in the difluorido anions give rise to specific $\text{F}\cdots\text{H}-\text{C}$ interactions with the acetonitrile solvent, which is not the case for the four- and six-coordinate cases. These strong interactions are not covered by the implicit COSMO solvent model but become apparent when using more explicit treatments of solvation. Detailed studies of these interesting fluoro-specific interactions are underway and will be reported elsewhere.

By slowly cooling a reaction mixture of $[\text{NEt}_3\text{Me}]\text{Cl}$ with 1.2 equiv. fluorine in acetonitrile, single crystals of $[\text{NEt}_3\text{Me}]_3[\text{ClF}_4][\text{ClF}_2]_2$ were obtained (for further details see Supporting Information, Figure S17). Replacing F_2 by ClF as a fluorination agent we were able to synthesize neat $[\text{NEt}_3\text{Me}][\text{ClF}_2]$. The Raman spectrum (Figure S6) shows one main band at 457 cm^{-1} which is in good agreement with data from $[\text{NEt}_3\text{Me}]_3[\text{ClF}_4][\text{ClF}_2]_2$ (455 cm^{-1}). The compound crystallizes in the space group $P12_1/c1$ (Figure 4). The two anionic moieties $\text{F1Cl1F1}'$ and $\text{F2Acl2F2A}'$ are both half occupied with Cl1 on Wyckhoff position 2b (site symmetry $P\bar{1}$) and Cl2 on Wyckhoff position 2c (site symmetry $P\bar{1}$). The $\text{Cl}-\text{F}$ bond lengths are $185.24(6)\text{ pm}$ ($\text{Cl1}-\text{F1}$) and $184.6(2)\text{ pm}$ ($\text{Cl2}-\text{F2A}$). The calculated bond length of the free $[\text{ClF}_2]^-$ is 186.8 pm (CCSD(T)/def2-TZVPP).^[13] The bonding situation

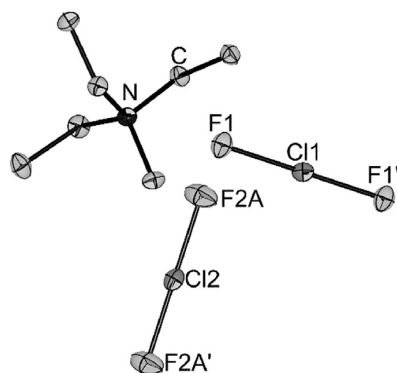


Figure 4. Crystal structure of $[\text{NEt}_3\text{Me}][\text{ClF}_2]$. Displacement ellipsoids are shown at 50% probability at 100 K. Selected bond lengths [pm]: $\text{F1}-\text{Cl1}$ 185.24(6), $\text{F2A}-\text{Cl2}$ 184.6(2). Hydrogen atoms omitted for clarity.^[29]

is best described by a 3-center-4-electron bond. The $\text{Cl}-\text{F}$ bond lengths in $[\text{ClF}_2]^-$ are significantly elongated in comparison with solid ClF ($162.8(1)\text{ pm}$).^[20] It is well-known from polyhalide chemistry that the bond length of a dihalogen is elongated upon coordination by a Lewis base due to the donation of electron density into the $\sigma^*(\text{Cl}-\text{F})$ orbital.^[12, 21] As anticipated, the $[\text{ClF}_2]^-$ anion is computed to be more thermochemically stable towards halogen loss than $[\text{Cl}_3]^-$ and $[\text{F}(\text{Cl})_2]^-$ which is due to more ionic interactions of the ClF moiety in comparison to Cl_2 .^[12, 22]

We examined the stability of $[\text{NEt}_3\text{Me}][\text{ClF}_4]$ in acetonitrile solution via ^{19}F NMR spectroscopy. Surprisingly, it showed only slow decomposition at room temperature over a month via fluorination of the organic solvent and the cation. However, the isolated solid is significantly more reactive. We observed explosions in several cases at temperatures above -40°C . Consequently, we avoided the isolation of larger quantities of $[\text{NEt}_3\text{Me}][\text{ClF}_4]$ and instead worked with solutions in propionitrile or acetonitrile with concentrations in the range of 0.66 mol l^{-1} to 8.8 mol l^{-1} .

We envisioned $[\text{NEt}_3\text{Me}][\text{ClF}_4]$ as a fluorinating and oxidation reagent for the synthesis of highly fluorinated moieties such as trifluoromethyl ($-\text{CF}_3$), pentafluorosulfanyl ($-\text{SF}_5$) or fluoridometallates ($[\text{MF}_n]^-$). Trifluoromethyl and pentafluorosulfanyl derivatives have a growing importance in pharmaceutical- and agrochemistry.^[23, 24, 25] Recently, Togni and co-workers reported on a non-gaseous reagent to access aryl tetrafluorido- λ^6 -sulfanyl chlorides ($\text{Ar}-\text{SF}_4\text{Cl}$), a key intermediate for the synthesis of pentafluorosulfanyl aryls ($\text{Ar}-\text{SF}_5$).^[24] Beier and co-workers recently studied the direct fluorination with dilute elemental fluorine and disulfides to directly obtain pentafluorosulfanyl aryls, a process with industrial application.^[25] As a proof of concept we exposed diphenyl disulfide, Ph_2S_2 , to a solution of $[\text{NEt}_3\text{Me}][\text{ClF}_4]$ in propionitrile at -50°C to directly obtain phenylsulfur pentafluoride, PhSF_5 . As by-products the *cis*- and *trans*- PhSF_4Cl were observed (Table 2 Entry 1, for further details see Supporting Information). PhSF_5 can be prepared in pure form by removal of both PhSF_4Cl isomers by hydrolysis. Simultaneously, residual fluorochlorates are hydrolysed.^[26]

Addition of the Lewis acid boron trifluoride, BF_3 , to a solution of $[\text{NEt}_3\text{Me}][\text{ClF}_4]$ in acetonitrile led to the formation of CH_3CF_3 , the CN activation product of the solvent acetonitrile, amongst other components. To increase the selectivity of this reaction, we synthesized the acetonitrile- BF_3 complex and substituted the solvent, from nitrile-based solvents to chlorofluorocarbons. Dichlorofluoromethane (CHFCl_2 , R-21) turns out to be sufficiently stable towards

Table 2: Reactivity Studies with $[\text{NEt}_3\text{Me}][\text{ClF}_4]$.

Entry	Substrate	Lewis acid	Product
1	Ph_2S_2	–	PhSF_5 , PhSF_4Cl
2	MeCN	BF_3	MeCF_3
3	$[\text{B}(\text{CN})_4]^-$	BF_3	$[\text{B}(\text{CF}_3)_x(\text{CN})_{4-x}]^-$
4	$[\text{Au}(\text{CN})_2]^-$	BF_3	<i>cis</i> - $[\text{AuF}_2(\text{CF}_3)(\text{CN})]^-$ ^[a]
5	Au	–	$[\text{AuF}_4]^-$
6	CO	–	COF_2

[a] Minor product.

F_2 and $[ClF_4]^-$ and also dissolves the starting material $[NEt_3Me]Cl$. Combination of two dichlorofluoromethane solutions containing $[NEt_3Me][ClF_4]$ and $MeCN \cdot BF_3$ leads to the formation of CH_3CF_3 (Table 2 Entry 2, for further details see Supporting Information). This is reminiscent of the reaction between succinonitrile and BrF_3 .^[27] We also examined the reactivity towards the tetracyanidoborate anion $[B(CN)_4]^-$. With addition of the Lewis acid BF_3 we observed the conversion of the cyanido ligands to trifluoromethyl ligands. This result is analogous to the synthesis of $[B(CF_3)_4]^-$ from $[B(CN)_4]^-$ and ClF_3 in anhydrous HF.^[28] However, we did not achieve full conversion but a distribution of different borate anions with trifluoromethyl and cyanido ligands $[B(CF_3)_x(CN)_{4-x}]^-$ (Table 2 Entry 3, for further details see Supporting Information). Additionally, we exposed the $[BF_3(CN)]^-$ anion to $[NEt_3Me][ClF_4]$ but only fluorination to $[BF_4]^-$ was observed. The reaction of $[NEt_3Me][ClF_4]$ with dicyanidoaurate(I) $[Au(CN)_2]^-$ is not selective, however, we were able to identify one $Au-CF_3$ containing product in the reaction mixture via NMR spectroscopy, that is, *cis*- $[AuF_2(CF_3)(CN)]^-$ (Table 2 Entry 4, for further details see Supporting Information). Another promising application for $[NEt_3Me][ClF_4]$ is the dissolution of noble metals such as gold. After the addition of a piece of elemental gold, the solution containing $[ClF_4]^-$ turns yellow. The ^{19}F NMR spectroscopic analysis reveals the formation of mainly $[AuF_4]^-$ (Table 2 Entry 5, for further details see Supporting Information) and traces of other chloridofluoridoaurates ($[AuF_3Cl]^-$ and *cis*- $[AuF_2Cl_2]^-$ see Figure S12). Exposure of $[NEt_3Me][ClF_4]$ in propionitrile to an atmosphere of CO results in the formation of carbonyl fluoride (COF_2) within 30 min (Table 2 Entry 6, for further details see Supporting Information).

In conclusion, we developed a facile and fast synthetic procedure to obtain a soluble source of highly reactive $[ClF_4]^-$ in the form of $[NEt_3Me][ClF_4]$ avoiding gaseous ClF_3 which tends to react explosively when exposed to organic matter. We characterized this compound by NMR and Raman spectroscopy and, additionally, single crystal X-Ray diffraction for the analogous $[NEt_4][ClF_4]$. Furthermore, we presented the first structural and ^{19}F NMR spectroscopic proof of the $[ClF_4]^-$ anion. All experimental results are supported by quantum-chemical calculations. Additionally, we showed several applications of $[NEt_3Me][ClF_4]$ as a highly reactive fluorinating agent for the transformation of aryl disulfides into the corresponding pentafluorosulfanyl aryls, nitriles and cyanido complexes into the corresponding trifluoromethyl compounds, carbon monoxide into carbonyl fluoride and the dissolution of elemental gold. In further studies we will explore a broader substrate scope to develop a widely applicable fluorinating reagent for organic and inorganic chemists.

Caution! Fluorine, even under dilute conditions, is extraordinarily reactive and can react violently with organic materials under the formation of HF. Similarly, tetrafluoridochlorate(III) and difluoridochlorate(I) are strongly oxidizing compounds, which can decompose violently under certain conditions when exposed to organic materials. Exposure to acidic compounds (e.g. water or boron trifluoride) greatly enhances the reactivity due to the in situ formation

of ClF_3 . Additionally, precipitation also greatly enhances the reactivity of tetrafluoridochlorate(III) and difluoridochlorate(I) compounds, leading to explosions at temperatures above $-40^\circ C$. Usage of PFA, FEP or PTFE may lower the risk of injury.

Acknowledgements

We gratefully acknowledge the ZEDAT at Freie Universität Berlin for providing computing resources. Additionally, we are grateful for donations of chemicals from the Solvay company. SPP 1708 is acknowledged for funding. Furthermore, PP acknowledges VCI for providing PhD funding (Kekulé Fellowship). Funded by the Deutsche Forschungsgemeinschaft (DFG, German Research Foundation)—Project-ID 387284271—SFB 1349. Open access funding enabled and organized by Projekt DEAL.

Conflict of interest

The authors declare no conflict of interest.

Keywords: chlorine fluorides · fluorination reagents · strong oxidizers

- [1] D. Naumann, *Fluor und Fluorverbindungen*, Steinkopff, Heidelberg, **1980**.
- [2] a) K. R. Brower, *J. Fluorine Chem.* **1986**, *31*, 333; b) F. Kraus, *Nachr. Chem.* **2019**, *67*, 17; c) G. Schiemann, K. Bromme, B. Cornils, *Chem. Ber.* **1965**, *98*, 3410; d) G. Schiemann, M. Kühnhold, B. Cornils, *Liebigs Ann. Chem.* **1968**, *714*, 62; e) H. Meinert, U. Groß, *Z. Chem.* **1969**, *9*, 190.
- [3] a) X. Zhang, K. Seppelt, *Z. Anorg. Allg. Chem.* **1997**, *623*, 491; b) B. Scheibe, S. I. Ivlev, A. J. Karttunen, F. Kraus, *Eur. J. Inorg. Chem.* **2020**, 1319.
- [4] a) E. D. Whitney, R. O. MacLaren, T. J. Hurley, C. E. Fogle, *J. Am. Chem. Soc.* **1964**, *86*, 4340; b) E. D. Whitney, R. O. MacLaren, C. E. Fogle, T. J. Hurley, *J. Am. Chem. Soc.* **1964**, *86*, 2583; c) K. O. Christe, J. P. Guertin, *Inorg. Chem.* **1966**, *5*, 473; d) K. O. Christe in *IUPAC, XXIVth Int. Cong. Pure Appl. Chem.* **1974**, 115.
- [5] a) L. B. Asprey, J. L. Margrave, M. E. Silverthorn, *J. Am. Chem. Soc.* **1961**, *83*, 2955; b) D. H. Kelly, B. Post, R. W. Mason, *J. Am. Chem. Soc.* **1963**, *85*, 307.
- [6] a) K. O. Christe, W. W. Wilson, R. D. Wilson, R. Bau, J. A. Feng, *J. Am. Chem. Soc.* **1990**, *112*, 7619; b) A. R. Mahjoub, X. Zhang, K. Seppelt, *Chem. Eur. J.* **1995**, *1*, 261; c) H. Sun, S. G. DiMaggio, *J. Am. Chem. Soc.* **2005**, *127*, 2050; d) S. Elias, N. Karton-Lifshin, L. Yehezkel, N. Ashkenazi, I. Columbus, Y. Zafrani, *Org. Lett.* **2017**, *19*, 3039.
- [7] W. W. Wilson, K. O. Christe, *Inorg. Chem.* **1989**, *28*, 4172.
- [8] K. O. Christe, W. W. Wilson, R. V. Chirakal, J. C. P. Sanders, G. J. Schrobilgen, *Inorg. Chem.* **1990**, *29*, 3506.
- [9] a) K. O. Christe, J. P. Guertin, *Inorg. Chem.* **1965**, *4*, 905; b) K. O. Christe, J. P. Guertin, *Inorg. Chem.* **1965**, *4*, 1785.
- [10] K. O. Christe, W. Sawodny, J. P. Guertin, *Inorg. Chem.* **1967**, *6*, 1159.
- [11] R. Brückner, *Dissertation*, Freie Universität Berlin, Berlin, **2016**.
- [12] K. O. Christe, W. Sawodny, *Z. Anorg. Allg. Chem.* **1968**, *357*, 125.
- [13] F. A. Redeker, A. Kropman, C. Müller, S. E. Zewge, H. Beckers, B. Paulus, S. Riedel, *J. Fluorine Chem.* **2018**, *216*, 81.

- [14] C. J. Schattenberg, K. Reiter, F. Weigend, M. Kaupp, *J. Chem. Theory Comput.* **2020**, *16*, 931.
- [15] T. Kupka, *Magn. Reson. Chem.* **2009**, *47*, 959.
- [16] M. Kaupp, O. L. Malkina, V. G. Malkin, P. Pyykkö, *Chem. Eur. J.* **1998**, *4*, 118.
- [17] K. O. Christe, W. W. Wilson, G. W. Drake, M. A. Petrie, J. A. Boatz, *J. Fluorine Chem.* **1998**, *88*, 185.
- [18] K. O. Christe, W. W. Wilson, G. W. Drake, D. A. Dixon, J. A. Boatz, R. Z. Gnann, *J. Am. Chem. Soc.* **1998**, *120*, 4711.
- [19] K. O. Christe, W. W. Wilson, *Inorg. Chem.* **1989**, *28*, 3275.
- [20] R. Boese, A. D. Boese, D. Bläser, M. Y. Antipin, A. Ellern, K. Seppelt, *Angew. Chem. Int. Ed. Engl.* **1997**, *36*, 1489; *Angew. Chem.* **1997**, *109*, 1538.
- [21] a) B. Schmidt, K. Sonnenberg, H. Beckers, S. Steinhauer, S. Riedel, *Angew. Chem. Int. Ed.* **2018**, *57*, 9141; *Angew. Chem.* **2018**, *130*, 9279; b) K. Sonnenberg, P. Pröhm, N. Schwarze, C. Müller, H. Beckers, S. Riedel, *Angew. Chem. Int. Ed.* **2018**, *57*, 9136; *Angew. Chem.* **2018**, *130*, 9274; c) S. I. Ivlev, A. J. Karttunen, R. Ostvald, F. Kraus, *Z. Anorg. Allg. Chem.* **2015**, *641*, 2593; d) S. I. Ivlev, A. J. Karttunen, R. V. Ostvald, F. Kraus, *Chem. Commun.* **2016**, *52*, 12040; e) K. Sonnenberg, L. Mann, F. A. Redeker, B. Schmidt, S. Riedel, *Angew. Chem. Int. Ed.* **2020**, *59*, 5464; *Angew. Chem.* **2020**, *132*, 5506.
- [22] a) T. J. Van Huis, J. M. Galbraith, H. F. Schaeffer, *Mol. Phys.* **1996**, *89*, 607; b) A. B. Sannigrahi, S. D. Peyerimhoff, *Chem. Phys. Lett.* **1985**, *119*, 119; c) L. Chen, D. E. Woon, T. H. Dunning, *Comput. Theor. Chem.* **2017**, *1116*, 73; d) K. S. Thanthiriwatte, J. M. Spruell, D. A. Dixon, K. O. Christe, H. D. B. Jenkins, *Inorg. Chem.* **2014**, *53*, 8136.
- [23] a) D. Lentz, K. Seppelt in *Chemistry of hypervalent compounds* (Ed.: K. y. Akiba), Wiley-VCH, Weinheim, **1999**; b) H. L. Yale, *J. Med. Chem.* **1959**, *1*, 121; c) T. Umemoto, L. M. Garrick, N. Saito, *Beilstein J. Org. Chem.* **2012**, *8*, 461; d) P. R. Savoie, J. T. Welch, *Chem. Rev.* **2015**, *115*, 1130.
- [24] C. R. Pitts, D. Bornemann, P. Liebing, N. Santschi, A. Togni, *Angew. Chem. Int. Ed.* **2019**, *58*, 1950; *Angew. Chem.* **2019**, *131*, 1970.
- [25] J. Ajenjo, B. Klepetářová, M. Greenhall, D. Bím, M. Culka, L. Rulíšek, P. Beier, *Chem. Eur. J.* **2019**, *25*, 11375.
- [26] W.-T. Tsai, *J. Hazard. Mater.* **2011**, *190*, 1.
- [27] M. T. Baker, J. A. Ruzicka, J. H. Tinker, *J. Fluorine Chem.* **1999**, *94*, 123.
- [28] E. Bernhardt, G. Henkel, H. Willner, G. Pawelke, H. Bürger, *Chem. Eur. J.* **2001**, *7*, 4696.
- [29] Deposition Number(s) 1948998 (for [NEt₃][ClF₄]) and 2004243 (for [NEt₃Me][ClF₂]) contain(s) the supplementary crystallographic data for this paper. These data are provided free of charge by the joint Cambridge Crystallographic Data Centre and Fachinformationszentrum Karlsruhe Access Structures service www.ccdc.cam.ac.uk/structures.

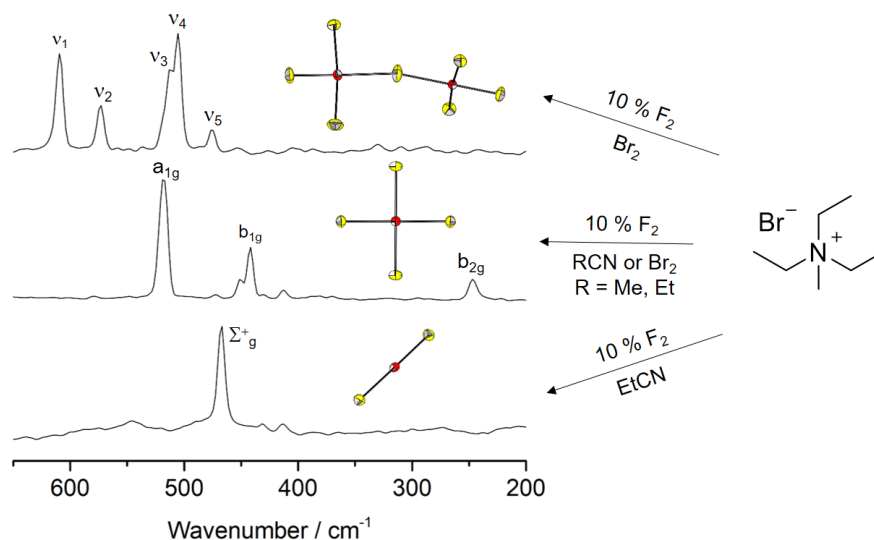
Manuscript received: April 30, 2020

Revised manuscript received: May 18, 2020

Accepted manuscript online: May 27, 2020

Version of record online: July 15, 2020

3.2. Soluble Fluoridobromates as Well-Behaved Strong Fluorination Reagents



Jonas R. Schmid,[†] Patrick Pröhm,[†] Patrick Voßnacker, Günter Thiele, Mathias Ellwanger, Sebastian Riedel*

[†] These authors have contributed equally.

Eur. J. Inorg. Chem. **2020**, *47*, 4497.

DOI: 10.1002/ejic.202000847

©The Authors. Published by Wiley-VCH GmbH

Author Contribution:

Jonas R. Schmid performed experiments and analyzed data during his Master's thesis with support of Patrick Pröhm. Patrick Pröhm designed the project, analyzed data, performed quantum-chemical calculations and wrote the manuscript. Patrick Voßnacker and Günter Thiele measured and refined crystal structures. Mathias Ellwanger designed the project and revised the manuscript. Sebastian Riedel supervised the project and revised the manuscript.

Fluoridobromates | Very Important Paper |

VIP Soluble Fluoridobromates as Well-Behaved Strong Fluorination Reagents

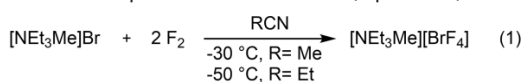
Jonas R. Schmid,^{[a][‡]} Patrick Pröhm,^{[a][‡]} Patrick Voßnacker,^[a] Günter Thiele,^[a] Mathias Ellwanger,^[a] Simon Steinhauer,^[a] and Sebastian Riedel^{[*][a]}

Abstract: We present a facile synthesis of the soluble fluoridobromates $[\text{NEt}_3\text{Me}][\text{BrF}_4]$ and $[\text{NEt}_3\text{Me}][\text{Br}_2\text{F}_7]$ via fluorination of the corresponding bromide salts in acetonitrile, propionitrile or bromine. We structurally characterized the $[\text{BrF}_2]^-$ anion, an inter-

mediate during the synthesis, for the first time. Additionally, the dissolution of noble metals to form the corresponding halometalates as well as the application of $[\text{NEt}_3\text{Me}][\text{BrF}_4]$ as a fluorination agent for disulfides to form pentafluorosulfanyl was studied.

Bromine, like almost any other element, forms binary compounds with fluorine. The neutral compounds and strong oxidizers bromine monofluoride (BrF) and bromine trifluoride (BrF_3) can form anions ($[\text{BrF}_2]^-$ and $[\text{BrF}_4]^-$) upon formal addition of a fluoride ion. The difluoridobromate(I) ($[\text{BrF}_2]^-$) anion is known as its Cs^+ ^[1] and $[\text{NMe}_4]^+$ ^[2] salt. $\text{Cs}[\text{BrF}_2]$ can be synthesized via the exposure of CsBr to XeF_2 or by careful condensation of a mixture of Br_2 and BrF_3 onto CsF .^[1,3] However, these procedures were not suitable to isolate pure samples.^[3] The tetramethylammonium salt was obtained as a decomposition product of $[\text{NMe}_4][\text{Br}(\text{OCF}_3)_2]$.^[2] To date, it is only characterized by vibrational and NMR spectroscopy.^[2,3] Significantly more references regarding the tetrafluoridobromate(III) ($[\text{BrF}_4]^-$) can be found in the literature with several counterions, including Na^+ ,^[4] K^+ ,^[5–7] Rb^+ ,^[8] Cs^+ ,^[7,9,10] Ag^+ ,^[11] NO^+ ,^[10] NO_2^+ ,^[10] $[\text{NMe}_4]^+$,^[12] $[\text{NF}_4]^+$,^[13] and Ba^{2+} .^[11,14] The synthesis is accomplished by exposure of the corresponding fluorides or chlorides to BrF_3 .^[11] If chloride salts are used Cl_2 and Br_2 are generated during the reaction. The tetramethylammonium salt was obtained by a metathesis reaction from $\text{Cs}[\text{BrF}_4]$ and $[\text{NMe}_4]\text{F}$.^[12] If an excess of BrF_3 is used to dissolve RbCl , CsCl , CsF or PbF_2 larger anions of the type $[\text{F}(\text{BrF}_3)_n]^-$ with $n = 2$ or 3 can be isolated. The $[\text{Br}_2\text{F}_7]^-$ with a bridging μ_2 -F atom is known as the Cs^+ ,^[15,16] Rb^+ ^[15,16] and $[\text{PbF}_4]^+$ ^[17] salt. The $[\text{Br}_3\text{F}_{10}]^-$ complex with a bridging μ_3 -F atom exists as the Rb^+ and Cs^+ salt.^[15,16] They were studied via vibrational spectroscopy and X-ray diffraction.

Herein, we present the application of a direct fluorination to synthesize these anions, a method we published recently for the synthesis of di- and tetrafluoridochlorate(I/III).^[18] We used this method for the fluorination of the organic halide salts, *i.e.* tetraethylammonium and triethylmethylammonium bromide, with dilute fluorine in the solvents acetonitrile, propionitrile, or bromine. In analogy to the lighter homologue $[\text{ClF}_4]^-$, triethylmethylammonium tetrafluoridobromate(III) is selectively formed from the exposure of the bromide salt to two equivalents of dilute fluorine (10 % in Ar) in acetonitrile or propionitrile at temperatures below -30°C (Equation 1).



The ^{19}F NMR chemical shift of $[\text{NEt}_3\text{Me}][\text{BrF}_4]$ is -35.1 ppm.^[12] We were able to grow single crystals suitable for X-ray diffraction from a MeCN solution. The molecular structure in the solid-state is in line with already published structures of the $[\text{BrF}_4]^-$

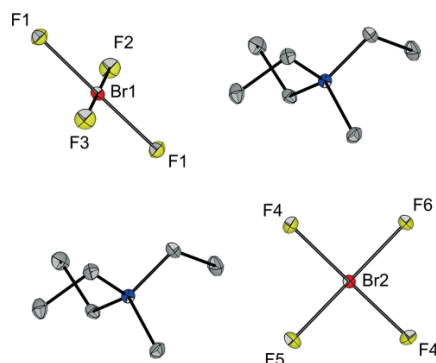


Figure 1. Solid-state structure of $[\text{NEt}_3\text{Me}][\text{BrF}_4]$. Thermal ellipsoids are shown at 50 % probability at 100 K. Color code: yellow = fluorine, red = bromine, grey = carbon, blue = nitrogen. Selected bond lengths [pm] and bond angles [°]: F1–Br1 189.64(1), F2–Br1 190.47(1), F3–Br1 187.87(1), F4–Br2 189.38(1), F5–Br2 188.93(1), F6–Br2 189.33(1); F1–Br1–F2 90.277(2), F1–Br1–F3 89.729(2), F4–Br2–F5 90.189(2), F4–Br2–F6 89.810(2).

[a] J. R. Schmid, P. Pröhm, P. Voßnacker, Dr. G. Thiele, Dr. M. Ellwanger, Dr. S. Steinhauer, Prof. Dr. S. Riedel
Freie Universität Berlin, Institute of Chemistry and Biochemistry,
Fabeckstr. 34/36, 14195 Berlin, Germany
E-mail: s.riedel@fu-berlin.de
<https://www.fluorinechemistry.de>

[‡] These authors have contributed equally.

Supporting information and ORCID(s) from the author(s) for this article are available on the WWW under <https://doi.org/10.1002/ejic.202000847>.

© 2020 The Authors. European Journal of Inorganic Chemistry published by Wiley-VCH GmbH · This is an open access article under the terms of the Creative Commons Attribution License, which permits use, distribution and reproduction in any medium, provided the original work is properly cited.

anion with idealized D_{4h} symmetry (Figure 1).^[5] It crystallizes in the monoclinic space group $P2_1/m$ with two crystallographically inequivalent anions. The single crystal Raman spectrum (Figure 2) shows three bands attributed to the anion at 519, 442 and 247 cm^{-1} corresponding to the a_{1g} , b_{1g} , and b_{2g} vibration.^[7]

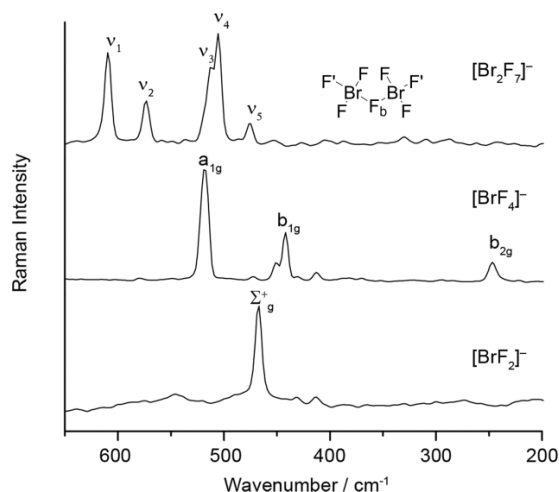
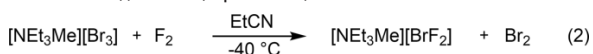


Figure 2. Single crystal Raman spectra of $[\text{NET}_3\text{Me}][\text{Br}_2\text{F}_7]$ (top), $[\text{NET}_3\text{Me}][\text{BrF}_4]$ (middle) and $[\text{NET}_3\text{Me}][\text{BrF}_2]$ (bottom) in the Br–F region. Selected bands [cm^{-1}]: $\nu_1 = 610$ (in phase Br–F' stretching), $\nu_2 = 573$ (out of phase Br–F' stretching), $\nu_3 = 513$ (in phase asymmetric F–Br–F stretching), $\nu_4 = 505$ (out of phase asymmetric F–Br–F stretching), $\nu_5 = 477$ (in phase symmetric F–Br–F stretching), $a_{1g} = 519$, $b_{1g} = 442$, $b_{2g} = 277$, $\Sigma^+_g = 467$.

To avoid side products of the fluorination the reactions were done at -30 °C or below. At these temperatures the solubility of the starting material $[\text{NET}_3\text{Me}]\text{Br}$ can be quite low. However, the solubility can be increased by the addition of one equivalent of bromine to form the well-known tribromide anion. In case of the $[\text{NET}_3\text{Me}]^+$ cation, however, the $[\text{Br}_3]^-$ salt is structurally unknown. Hence, we characterized it via Raman spectroscopy and single-crystal X-ray diffraction. Surprisingly, we realized that in the solid state the $[\text{Br}_6]^{2-}$ dianion had formed. This is not only evident from the molecular structure in the solid state (Figure S2) but also from the Raman spectrum (Figure S1). A polybromide anion with the composition of $[\text{Br}_6]^{2-}$ was previously reported by our group.^[19] However, this structure significantly differs from the previously reported structure. This might be due to the altered cations which show different intermolecular interactions, possibly orchestrating their metrics. In the reported structure the cation possesses a bromine atom which interacts with the anion via halogen bonding (for a detailed discussion see Supporting Information). Raman spectra in acetonitrile solution (Figure S1) suggest the dissociation of the $[\text{Br}_6]^{2-}$ in two $[\text{Br}_3]^-$ fragments when in solution. We used a propionitrile solution of $[\text{NET}_3\text{Me}][\text{Br}_3]$ and exposed it to one equivalent of dilute fluorine (10 % in Ar) to obtain the difluoridobromate(I) anion (Equation 2).



This anion has only been characterized spectroscopically (Raman, IR, ^{19}F NMR) and X-ray diffraction data are to the best of

our knowledge unknown. Slow cooling of the reaction mixture resulted in the growth of single crystals of $[\text{NET}_3\text{Me}][\text{BrF}_2]$. The single crystal Raman spectrum (Figure 2) shows one prominent band at 467 cm^{-1} that corresponds to the symmetric stretching.^[1,2] The molecular structure in the solid-state (Figure 3) indeed shows the idealized $D_{\infty h}$ symmetry of the anion. The two Br–F bond lengths differ only slightly with $d(\text{F1–Br}) = 197.3(1)$ pm and $d(\text{F2–Br}) = 193.2(1)$ pm. The F1–Br–F2 bond angle is 179.34(4)°. We calculated the Hirshfeld surface (Figure S13) which revealed multiple short cation anion contacts. The ^{19}F NMR spectrum (Figure S3) of the reaction solution shows three signals, at -35.8 ppm ($[\text{BrF}_4]^-$), -83.3 ppm (fluorinated solvent) and -216.8 ppm. We attribute the latter to $[\text{BrF}_2]^-$ in good agreement with literature values.^[3] To avoid contamination from a fluorination of the solvent we changed the solvent to elemental bromine. Any occurring fluorination of bromine at 0 °C and ambient pressure leads to the formation of BrF_3 which can function as an oxidizing agent for Br^- . The Raman spectrum (Figure S5) reveals the successful formation of $[\text{BrF}_4]^-$ in bromine. Therefore, the addition of more than two equivalents of fluorine leads to a mixture of $[\text{BrF}_4]^-$ and BrF_3 . These can form a Lewis acid-base adduct, i.e. a higher fluoridobromate(III) as first described by Stein.^[15] We obtained single crystals of $[\text{NET}_3\text{Me}][\text{Br}_2\text{F}_7]$ from a reaction of $[\text{NET}_3\text{Me}]\text{Br}$ with four equivalents of F_2 in bromine and subsequent recrystallization from SO_2ClF (Figure 4). The Raman spectrum (Figure 2) of a single crystal of $[\text{NET}_3\text{Me}][\text{Br}_2\text{F}_7]$ shows bands at 610 cm^{-1} (in phase Br–F' stretching), 573 cm^{-1} (out of phase Br–F' stretching), 513 cm^{-1} (in phase asymmetric F–Br–F stretching), 505 cm^{-1} (out of phase asymmetric F–Br–F stretching) and at 477 cm^{-1} (in phase symmetric F–Br–F stretching) which is in agreement with the data reported by Kraus and Stein.^[15,16] Small differences are attributed to different structural parameters. Most significantly, the Br–F–Br bond angle is wider (166.86(5)° this work, 140.27(6)° $\text{Cs}[\text{Br}_2\text{F}_7]$), as well as the torsion angle between the two planar $[\text{BrF}_4]^-$ fragments (70.11(3)° this work, 61.90(4)° $\text{Cs}[\text{Br}_2\text{F}_7]$). Interestingly, the smaller angles in the Kraus structure are closer to the gas-phase optimized structure (see Table S1). To gain a deeper understanding we performed NBO analyses of the optimized structure [B3LYP-D3(BJ)/def2-TZVPP] as well as of the solid-state structures from this work and from the Kraus group. In the NBO analysis, the bonding between the bridging fluoride atom F_b and the bromine centers is mainly an interaction between the bridging fluoride F_b lone pair and the

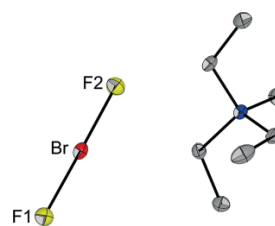


Figure 3. Solid-state structure of $[\text{NET}_3\text{Me}][\text{BrF}_2]$. Thermal ellipsoids are shown at 50 % probability at 100 K. Color code: yellow = fluorine, red = bromine, grey = carbon, blue = nitrogen. Selected bond lengths [pm] and bond angles [°]: F1–Br 197.3(1), F2–Br 193.2(1), F1–Br–F2 179.34(4).

σ^* orbital of the opposite Br–F' bond (Figure 5). The bonding of the perpendicular fluorine ligands is best described as a 3-center-4-electron bond (detailed discussion of the NBO analysis in the Supporting Information).

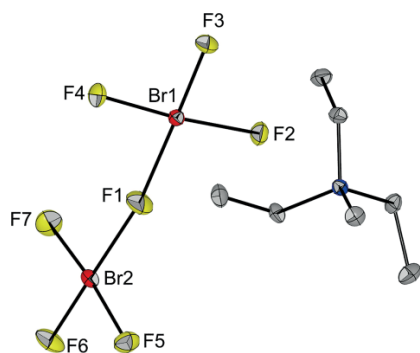


Figure 4. Solid-state structure of $[\text{NEt}_3\text{Me}][\text{Br}_2\text{F}_7]$. Thermal ellipsoids are shown at 50 % probability at 100 K. Color code: yellow = fluorine, red = bromine, grey = carbon, blue = nitrogen. Selected bond lengths [pm] and bond angles [°]: F1–Br1 206.68(7), F1–Br2 218.61(7), F3–Br1 179.18, F6–Br2 176.38(7), F2–Br1 188.10, F7–Br2 184.76(8); Br1–F1–Br2 166.86(5).

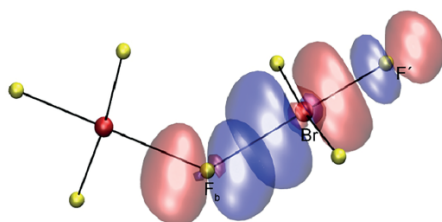
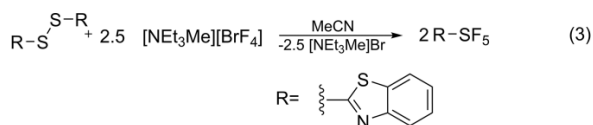


Figure 5. Natural MOs of optimized $[\text{Br}_2\text{F}_7]^-$ [B3LYP-D3(BJ)/def2-TZVPP] showing the strongest interaction between lone pair of the bridging fluorine atom F_b and the $\sigma^*(\text{Br}-\text{F})$.

The isolation of $[\text{Br}_3\text{F}_{10}]^-$ and $[\text{Br}_4\text{F}_{13}]^-$ by direct fluorination of a bromide salt with dilute fluorine in liquid bromine was not successful so far, despite their proposed stability.^[20] The obtained Raman spectra from the reactions of $[\text{NEt}_3\text{Me}]\text{Br}$ with 5 to 8 equivalents of dilute fluorine in the solvent bromine looks promising, however, due to broad bands an unambiguous assignment is not possible. We were able to obtain single crystals from reactions with 4 and 7 eq of F_2 , however, they consisted of $[\text{NEt}_3\text{Me}][\text{Br}_2\text{F}_7]$. Figure S8 shows the Raman spectra of $[\text{NEt}_3\text{Me}]\text{Br}$ after a reaction with 5 to 8 equivalents of dilute F_2 in liquid Br_2 . To achieve sufficient sensitivity for Br–F containing species in the Raman spectrum the excess Br_2 had to be removed at low temperatures.

We studied the chemical properties of an acetonitrile solution of $[\text{NEt}_3\text{Me}][\text{BrF}_4]$, especially with regard to its oxidation and fluorination properties. It has been previously shown that $\text{K}[\text{BrF}_4]$ can be used for the recovery of precious metals in dry chemical reactions at 400 °C, a process referred to as urban mining.^[21] We were able to dissolve elemental silver and gold in an acetonitrile solution of $[\text{NEt}_3\text{Me}][\text{BrF}_4]$ at room temperature by formation of $[\text{NEt}_3\text{Me}][\text{Ag}_2\text{Br}_3]$ and $[\text{NEt}_3\text{Me}][\text{AuF}_4]$. However, the dissolution of Au was rather inefficient and only traces of tetrafluoroaurate(III) were found in the ^{19}F NMR

spectrum. In the case of Ag we were able to grow single crystals of the mentioned silver complex (see Supporting Information). During these experiments we observed slow decomposition reactions with the solvent.^[22] In analogy to the reaction of diphenyl disulfide with $[\text{NEt}_3\text{Me}][\text{ClF}_4]$ we were able to convert a disulfide into the corresponding pentafluorosulfanyl compound (Equation 3).^[18] Here, we used 2,2'-dibenzothiazolyl disulfide because the corresponding SF_5 product could be a valuable intermediate for an SF_5 -transfer reagent.^[23] Previously, the compound was synthesized in a two-step reaction involving IF_5 .^[24] A direct fluorination with dilute fluorine of the disulfide to form the SF_5 product at low temperatures in acetonitrile was not successful.



In conclusion, we used the direct fluorination of triethylmethylammonium bromide in solution to obtain organo-soluble tetraalkylammonium fluoridobromate salts. Depending on the solvent (acetonitrile, propionitrile or bromine) and the amount of fluorine added we obtained different anions. This includes the difluoridobromate(I) $[\text{BrF}_2]^-$ anion which was structurally characterized for the first time. Additionally, the synthesis of the highly soluble tetrafluoridobromate(III) $[\text{BrF}_4]^-$ and heptafluoridobromate(III) $[\text{Br}_2\text{F}_7]^-$ was achieved and we showed the application of $[\text{BrF}_4]^-$ as a fluorination and oxidation agent for disulfides and noble metals such as gold and silver.

Caution! Fluorine, even under dilute conditions, is extraordinarily reactive and can react violently with organic materials under the formation of HF. Similarly, fluoridobromates are strongly oxidizing compounds, which can decompose violently under certain conditions when exposed to organic materials. Exposure to acidic compounds (e.g. water or boron trifluoride) greatly enhances the reactivity due to the in-situ formation of BrF_3 .

Deposition Numbers 2015010, 2015014, 2015013, 2015012, and 2015008 contain the supplementary crystallographic data for this paper. These data are provided free of charge by the joint Cambridge Crystallographic Data Centre and Fachinformationszentrum Karlsruhe Access Structures service www.ccdc.cam.ac.uk/structures.

Acknowledgments

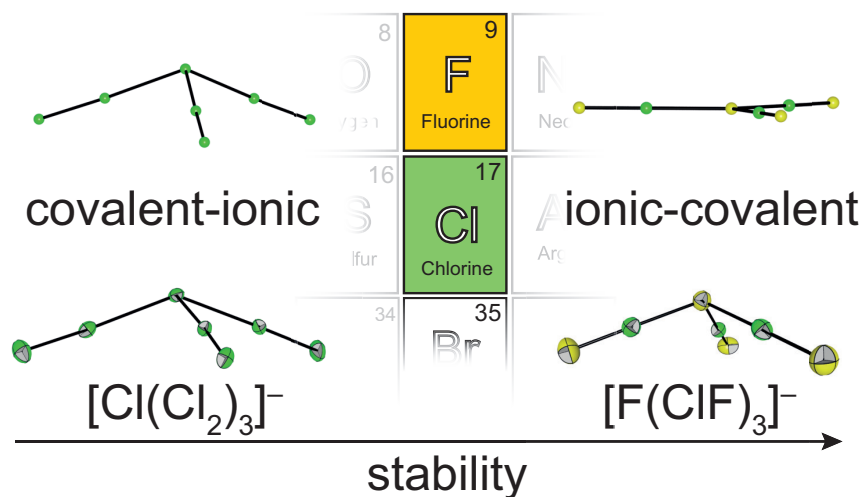
We gratefully acknowledge the ZEDAT at Freie Universität Berlin for providing computing resources. Additionally, we are grateful for donations of chemicals from the Solvay company. The DFG is acknowledged for funding (SPP 1708 and SFB 1349 Project-ID 387284271) as well as ERC HighPotOx (Grant agreement ID: 818862). Furthermore, P. P. acknowledges VCI for providing PhD funding (Kekulé Fellowship) and G. T. acknowledges VCI for financial support (Liebig Fellowship). Open access funding enabled and organized by Projekt DEAL.

Keywords: Bromine fluorides · Strong oxidizers · Fluorination reagents · Halogens · Structure elucidation

- [1] T. Surles, L. A. Quarterman, H. H. Hyman, *J. Inorg. Nucl. Chem.* **1973**, *35*, 668.
- [2] R. Minkwitz, R. Bröchler, R. Ludwig, *Inorg. Chem.* **1997**, *36*, 4280.
- [3] X. Zhang, K. Seppelt, *Z. Anorg. Allg. Chem.* **1997**, 623, 491.
- [4] S. I. Ivlev, R. V. Ostvald, F. Kraus, *Monatsh. Chem.* **2016**, *147*, 1661.
- [5] S. Siegel, *Acta Crystallogr.* **1956**, *9*, 493.
- [6] a) S. Siegel, *Acta Crystallogr.* **1957**, *10*, 380; b) W. G. Sly, R. E. Marsh, *Acta Crystallogr.* **1957**, *10*, 378; c) A. J. Edwards, G. R. Jones, *J. Chem. Soc. A* **1969**, 1936; d) I. Sheft, A. F. Martin, J. J. Katz, *J. Am. Chem. Soc.* **1956**, *78*, 1557.
- [7] K. O. Christe, C. J. Schack, *Inorg. Chem.* **1970**, *9*, 1852.
- [8] a) A. R. Mahjoub, A. Hoser, J. Fuchs, K. Seppelt, *Angew. Chem. Int. Ed. Engl.* **1989**, *28*, 1526; *Angew. Chem.* **1989**, *101*, 1528; b) S. I. Ivlev, A. J. Karttunen, R. Ostvald, F. Kraus, *Z. Anorg. Allg. Chem.* **2015**, *641*, 2593.
- [9] S. Ivlev, P. Woidy, V. Sobolev, I. Gerin, R. Ostvald, F. Kraus, *Z. Anorg. Allg. Chem.* **2013**, *639*, 2846.
- [10] S. I. Ivlev, P. Woidy, I. I. Zherin, R. V. Ostvald, F. Kraus, M. Y. Voytenko, V. V. Shagalov, *Procedia Chem.* **2014**, *11*, 35.
- [11] A. G. Sharpe, H. J. Emeléus, *J. Chem. Soc.* **1948**, *0*, 2135.
- [12] W. W. Wilson, K. O. Christe, *Inorg. Chem.* **1989**, *28*, 4172.
- [13] K. O. Christe, W. W. Wilson, *Inorg. Chem.* **1986**, *25*, 1904.
- [14] S. Ivlev, V. Sobolev, M. Hoelzel, A. J. Karttunen, T. Müller, I. Gerin, R. Ostvald, F. Kraus, *Eur. J. Inorg. Chem.* **2014**, *2014*, 6261.
- [15] L. Stein, *J. Fluorine Chem.* **1985**, *27*, 249.
- [16] S. I. Ivlev, A. J. Karttunen, R. V. Ostvald, F. Kraus, *Chem. Commun.* **2016**, *52*, 12040.
- [17] J. Bandemehr, M. Sachs, S. I. Ivlev, A. J. Karttunen, F. Kraus, *Eur. J. Inorg. Chem.* **2020**, *2020*, 64.
- [18] P. Pröhm, J. R. Schmid, K. Sonnenberg, S. Steinhauer, C. J. Schattenberg, R. Müller, M. Kaupp, P. Voßnacker, S. Riedel, *Angew. Chem. Int. Ed.* **2020**, *59*, 16002; *Angew. Chem.* **2020**, *132*, 16136.
- [19] K. Sonnenberg, P. Pröhm, C. Müller, H. Beckers, S. Steinhauer, D. Lentz, S. Riedel, *Chem. Eur. J.* **2018**, *24*, 1072.
- [20] J. Linnera, S. I. Ivlev, F. Kraus, A. J. Karttunen, *Z. Anorg. Allg. Chem.* **2019**, *645*, 284.
- [21] a) S. I. Ivlev, A. V. Malin, A. J. Karttunen, R. V. Ostvald, F. Kraus, *J. Fluorine Chem.* **2019**, *218*, 11; b) S. Ivlev, P. Woidy, F. Kraus, I. Gerin, R. Ostvald, *Eur. J. Inorg. Chem.* **2013**, *2013*, 4984.
- [22] S. Rozen, *Adv. Synth. Catal.* **2010**, *352*, 2691.
- [23] S. Dix, M. Jakob, M. N. Hopkinson, *Chem. Eur. J.* **2019**, *25*, 7635.
- [24] N. Shibata, N. Saito, WO2018159515, **2018**.

Received: September 8, 2020

3.3. Non-classical polyinterhalides of chlorine monofluoride: experimental and theoretical characterization of $[\text{F}(\text{ClF})_3]^-$



Patrick Pröhm, Nico Schwarze, Carsten Müller, Simon Steinhauer, Helmut Beckers, Susanne M. Rupf, Sebastian Riedel*

Chem. Commun. **2021**, 57, 4834.

DOI: 10.1039/D1CC01088C

Reproduced with permission from the Royal Society of Chemistry.

Author Contribution:

Patrick Pröhm performed the experiments regarding the compound $[\text{NMe}_4][\text{F}(\text{ClF})_4]$, analyzed data, performed quantum-chemical calculation and prepared the manuscript. Nico Schwarze performed experiments regarding the compound $[\text{NPr}_3\text{Me}][\text{Cl}_7]$. Carsten Müller performed quantum-chemical calculations and prepared the manuscript. Simon Steinhauer and Susanne M. Rupf measured and refined the crystal structures. Helmut Beckers and Sebastian Riedel supervised the project and revised the manuscript.



Non-classical polyinterhalides of chlorine monofluoride: experimental and theoretical characterization of $[F(\text{ClF})_3]^-$ †

Patrick Pröhm,¹ Nico Schwarze,¹ Carsten Müller,¹ Simon Steinhauer,¹ Helmut Beckers,¹ Susanne M. Rupf¹ and Sebastian Riedel¹*

Cite this: *Chem. Commun.*, 2021, 57, 4843

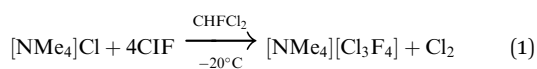
Received 26th February 2021,
Accepted 7th April 2021

DOI: 10.1039/d1cc01088c

rsc.li/chemcomm

We present the synthesis and characterization of the first non-classical Cl(I) polyinterhalide $[\text{NMe}_4][\text{F}(\text{ClF})_3]$ as well as the homologous polychloride $[\text{NPr}_3\text{Me}][\text{Cl}_7]$. Both salts were obtained from the reaction of the corresponding ammonium chlorides with ClF or Cl_2 , respectively. Quantum-chemical investigations predict an unexpected planar structure for the $[\text{F}(\text{ClF})_3]^-$ anion.

Fluoridopolyhalogen chemistry is experiencing a renaissance. In the last few decades, several binary fluoridopolyhalogenates were structurally described. They can be divided into two conceptually different groups, classical and non-classical interhalides.¹ Classical interhalides have a central, more electropositive halogen atom surrounded by more electronegative halogens. The majority of the known fluoridohalides belong to this group, such as $[\text{IF}_2]^-$,^{2,3} $[\text{IF}_4]^-$,^{3,4} $[\text{IF}_6]^-$,⁵ $[\text{IF}_8]^-$,⁶ $[\text{BrF}_2]^-$,^{7,8} $[\text{BrF}_4]^-$,⁸⁻¹¹ $[\text{BrF}_6]^-$,^{10,11} $[\text{ClF}_2]^-$,¹² $[\text{ClF}_4]^-$,^{11,13,14} and $[\text{ClF}_6]^-$.¹⁴ The valence shell pair repulsion (VSEPR) model can well predict the linear structures of the $[\text{XF}_2]^-$ anions and square planar shape of $[\text{XF}_4]^-$, but not the undistorted octahedral structures of the $[\text{XF}_6]^-$ (X = Br, Cl) anions.¹⁰ Non-classical interhalides have more electronegative central halogen atoms surrounded by more electropositive (poly)halogen ligands. The known fluoridohalides of this group are $[\text{F}(\text{IF}_5)_3]^-$,¹⁰ $[\text{F}(\text{BrF}_3)_2]^-$,^{15,16} and $[\text{F}(\text{BrF}_3)_3]^-$.¹⁶ The Kraus group recently synthesized the first non-classical fluoridochlorate(III), the $[\text{F}(\text{ClF}_3)_3]^-$ anion obtained by solvolysis of CsF in ClF_3 .¹⁷



Here, we present an unprecedented Cl(I) compound, $[\text{NMe}_4][\text{F}(\text{ClF})_3]$. With a formal $[\text{F}(\text{ClF})_3]^-$ anion, it belongs to

the non-classical interhalides. It was synthesized *via* the exposure of tetramethylammonium chloride to an excess of chlorine monofluoride in dichlorofluoromethane at low temperatures (eqn (1)). Initially, ClF likely oxidizes the chloride anion to yield elemental chlorine and a fluoride anion, which is eventually coordinated by three ClF molecules.

We were able to grow single crystals suitable for X-ray diffraction at -80°C . $[\text{NMe}_4][\text{F}(\text{ClF})_3]$ crystallized in the orthorhombic space group $Pna2_1$, as shown in Fig. 1. The anion consists of a central fluoride anion F1 coordinated by three ClF molecules in a pyramidal shape. Two of the bond lengths to F1 are almost identical ($d(\text{F1}-\text{Cl2}) = 219.4(2)$ pm, $d(\text{F1}-\text{Cl3}) = 219.5(1)$ pm), whereas the bond to the third ClF ligand is approximately 6 pm shorter ($d(\text{F1}-\text{Cl1}) = 213.9(2)$ pm). The inverse trend is observed for the Cl-F bond lengths of the ligands: $d(\text{Cl1}-\text{F2}) = 169.9(2)$ pm, $d(\text{Cl2}-\text{F3}) = d(\text{Cl3}-\text{F4}) = 168.1(1)$ pm. The Cl-F bond

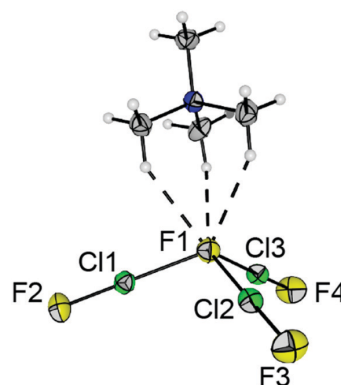


Fig. 1 Section of the solid-state structure of $[\text{NMe}_4][\text{F}(\text{ClF})_3]$. Displacement ellipsoids are shown at the 50% probability level. Color code: yellow = fluorine, green = chlorine, blue = nitrogen, grey = carbon, white = hydrogen. Selected bond lengths [pm] and angles [°]: F1–Cl1 213.9(2), F1–Cl2 219.4(2), F1–Cl3 219.5(1), Cl1–F2 169.9(2), Cl2–F3 168.1(1), Cl3–F4 168.1(1), F1...H in the range of 248 to 250, dihedral angle Cl1–F1–Cl2–Cl3 112.12(9).

Freie Universität Berlin, Department for Chemistry and Biochemistry, Fabeckstr. 34/36, Berlin, Germany. E-mail: s.riedel@fu-berlin.de

† Electronic supplementary information (ESI) available. CCDC 2031712 and 2060326. For ESI and crystallographic data in CIF or other electronic format see DOI: 10.1039/d1cc01088c

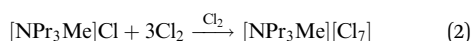


Communication

ChemComm

length of neat ClF in the solid-state is 162.8(1) pm.¹⁸ The elongation of the di- or interhalogen ligand bond is well understood in polyhalide chemistry. It can be attributed to the interaction between the lone pairs of the central fluoride anion with the $\sigma^*(\text{Cl-F})$ orbital in the ligand.¹ Donation of electron density into this antibonding orbital weakens the corresponding bond. Hence, stronger halide-ligand-interactions result in a more pronounced weakening of the ligand bond. The Cl-F1-Cl bond angles are in the range of 103.87(6)° and 108.86(6)°, and the Cl1-F1-Cl2-Cl3 dihedral angle is 112.12(9)°. The counterion $[\text{NMe}_4]^+$ forms three short hydrogen bonds to F1 (see Fig. 1 and Fig. S4 for the Hirshfeld surface, ESI†). Overall, the three hydrogen bonds, together with the three ClF ligands, result in a distorted octahedral coordination sphere for the central F1 anion (Fig. S3, ESI†).

The Raman spectrum of crystalline $[\text{NMe}_4][\text{F}(\text{ClF})_3]$ (Fig. 2, bottom, full spectrum see Fig. S1, ESI†) shows three bands at 675, 641, and 615 cm^{-1} , which are attributed to the stretching vibrations of the Cl-F ligands. The vibrational band of gaseous ClF is reported at 772 cm^{-1} .¹⁹ The red shift is expected due to the weakened inter-ligand bond, consistent with the structural parameters mentioned above. This assignment is supported by periodic solid-state calculations using the CRYSTAL17²⁰ program and the B3LYP DFT functional (Fig. 2, for full spectrum see Fig. S8 and Table S2, for computational details see the ESI†).



The analogous treatment of $[\text{NPr}_3\text{Me}]\text{Cl}$ with elemental chlorine instead of ClF leads to the polychloride anion

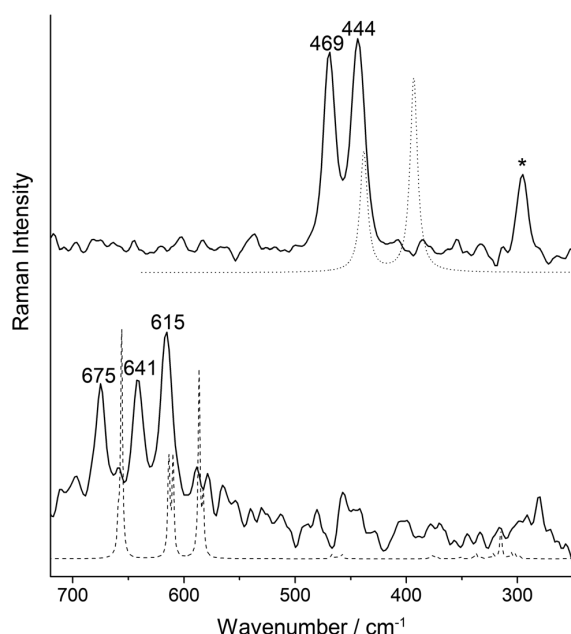


Fig. 2 Comparison of the Raman spectra of $[\text{NMe}_4][\text{F}(\text{ClF})_3]$ (bottom, solid line) and $[\text{NPr}_3\text{Me}][\text{Cl}_7]$ (top, solid line) with their computed spectra obtained at the B3LYP level (dashed line: solid-state calculation, dotted line: gas-phase calculation). The decomposition product $[\text{Cl}_3]^-$ is marked by an asterisk.

formation of $[\text{NPr}_3\text{Me}][\text{Cl}_7]$ (eqn (2)). Fig. 3 shows a section of the solid-state structure of $[\text{NPr}_3\text{Me}][\text{Cl}_7]$. It crystallized in the space group $P\bar{1}$. This structure again shows a pyramidal conformation of the anion. Analogously, it can be interpreted as a complex between a central chloride ion with three dichlorine ligands $[\text{Cl}(\text{Cl}_2)_3]^-$. The bond lengths between the central chloride ion Cl1 and the chlorine ligands are 276.0(1)–277.4(1) pm. The bond lengths within the Cl_2 ligands are 202.7(1)–203.8(1) pm, elongated by 4–5 pm compared to solid Cl_2 (198.4(1) pm).²¹ The anion has two smaller and one significantly larger Cl-Cl-Cl angles: Cl2-Cl1-Cl6: 82.41(2)°, Cl4-Cl1-Cl2: 93.69(2)°, and Cl4-Cl1-Cl6: 140.25(2)°. The Cl2-Cl1-Cl4-Cl6 dihedral angle is 82.55(4)°. There are five close Cl1...H-C contacts to two cations (Fig. 3 and Fig. S5 for the Hirshfeld surface, ESI†). The Raman spectrum of crystalline $[\text{NPr}_3\text{Me}][\text{Cl}_7]$ shows two pronounced inter-ligand Cl-Cl stretching vibrations at 469 and 444 cm^{-1} , which is consistent with the calculated Raman spectrum for the isolated free $[\text{Cl}_7]^-$ anion (Fig. 2, top).

The direct comparison of the $[\text{F}(\text{ClF})_3]^-$ and $[\text{Cl}_7]^-$ solid-state structures reveals a significantly wider dihedral angle and stronger bonds between the central anion and the ligands in the fluoridochlorate. Elimination of a ClF ligand in $[\text{F}(\text{ClF})_3]^-$ is significantly more endothermic than the loss of a Cl_2 ligand in $[\text{Cl}_7]^-$ (Table 1). This is likely due to a higher acidity of ClF and the higher basicity of the central fluoride ion. Calculated halogen-elimination energies for $[\text{F}(\text{Cl}_2)_3]^-$ and the hypothetical $[\text{Cl}(\text{ClF})_3]^-$ show the same trend (Table 1): ClF elimination is always more endothermic than Cl_2 elimination and the dihalogen bond to the fluoride anion is stronger than the corresponding bond to Cl^- .

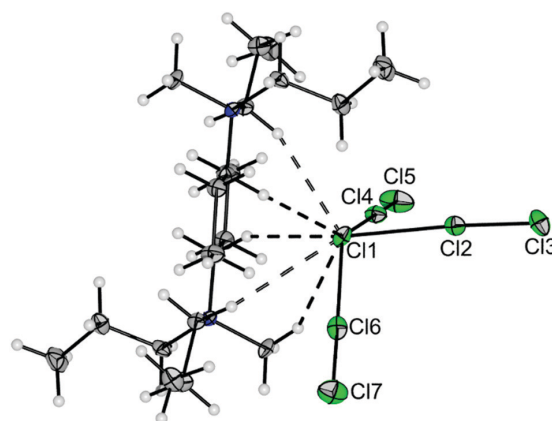


Fig. 3 Section of the solid-state structure of $[\text{NPr}_3\text{Me}][\text{Cl}_7]$ showing one anion and two cations [one at (x, y, z) and one at $(-x, 1 - y, 1 - z)$]. Displacement ellipsoids are shown at the 50% probability level. Color code: green = chlorine, blue = nitrogen, grey = carbon, white = hydrogen. Selected bond lengths [pm] and angles [°]: Cl1-Cl2 277.08(8), Cl1-Cl4 275.97(6), Cl1-Cl6 277.36(6), Cl2-Cl3 203.80(8), Cl4-Cl5 203.28(7), Cl6-Cl7 202.66(8), Cl2-Cl1-Cl6 82.41(2), Cl4-Cl1-Cl2 93.69(2), Cl4-Cl1-Cl6 140.25(2), Cl2-Cl1-Cl4-Cl6 82.55(4), Cl...H in the range 2.77 to 2.90.



Table 1 Thermochemical data for the decomposition of different heptahalides calculated at different computational levels using the def2-TZVPP basis set at the DFT and MP2 levels, and individual basis sets at the CCSD(T) level (see ESI). Energies are given in kJ mol^{-1} . A positive value implies an endothermic reaction

Reaction	B3LYP-D3BJ	SCS-MP2	CCSD(T)
$[F(\text{ClF})_3]^- \rightarrow [F(\text{ClF})_2]^- + \text{ClF}$	68.5	54.9	63.3
$[\text{Cl}(\text{Cl}_2)_3]^- \rightarrow [\text{Cl}(\text{Cl}_2)_2]^- + \text{Cl}_2$	41.8	32.5 ²²	—
$[\text{Cl}(\text{ClF})_3]^- \rightarrow [\text{Cl}(\text{ClF})_2]^- + \text{ClF}$	62.6	34.7	53.1
$[F(\text{Cl}_2)_3]^- \rightarrow [F(\text{Cl}_2)_2]^- + \text{Cl}_2$	48.8	—	48.7

Unlike the free $[\text{Cl}(\text{Cl}_2)_3]^-$ and $[\text{Cl}(\text{ClF})_3]^-$ anions and in contrast to the prediction from the VSEPR model the fluorido-polyhalogenates $[F(\text{ClF})_3]^-$ and $[F(\text{Cl}_2)_3]^-$ anions show planar D_{3h} molecular structures at the CCSD(T)/aug-cc-pVTZ level, indicating that the pyramidal structure of the title compound in the solid state is most likely due to the formation of hydrogen bonds to the counter ion. Indeed, a relaxed surface scan for $[F(\text{ClF})_3]^-$ revealed a rather flat potential surface with a planar minimum and only a small energy (1.5 kJ mol^{-1}) is required for its pyramidalization from a local minimum structure with C_{3v} symmetry to the global minimum with D_{3h} structure (Fig. S6, ESI[†]). Also, the inversion of the $[\text{Cl}(\text{Cl}_2)_3]^-$ anion *via* a planar transition state requires a low energy barrier of only 2 kJ mol^{-1} at the MP2/def2-TZVPP level (Fig. S6, ESI[†]).

While trigonal planar coordination is an unusual exception in the polyhalide chemistry,¹ there are a few known precedents. One example is the free planar $[F(\text{ClF})_3]^-$ anion. In the crystal structure of the Cs salt it shows, however, a distorted C_3 -symmetry with a dihedral angle of $136.4(2)^\circ$.¹⁷ Other examples are the poly(hydrogenhalide)halogenates of the general type $[\text{X}(\text{HY})_3]^-$ (X, Y = F, Cl, Br, I). For the $[F(\text{HF})_3]^-$ anion (X, Y = F) a planar structure was predicted to be slightly more stable, but only the K^+ -salt shows a planar anion, whereas several other solid-state structures show pyramidal anion structures.²³ A relaxed surface scan for $[\text{X}(\text{HF})_3]^-$ (X = F, Cl) revealed trends similar to those for the polyhalide species (Fig. S6, ESI[†]). With X = F, the planar structure is more stable than a pyramidal structure, but with X = Cl, the pyramidal structure is slightly favored (MP2/def2-TZVPP: 0.5 kJ mol^{-1}). Note, very recently a quantum-chemical investigation has been published which predicts a planar tetracoordinated structure of a fluorine atom in *e.g.* $[\text{FIn}_4]^+$ or $[\text{FTl}_4]^+$.²⁴

A natural bond orbital (NBO) analysis for the planar $[F(\text{ClF})_3]^-$ revealed a pure $2p$ -type lone pair on the central fluoride ion perpendicular to the molecular plane, while the two other $2p$ -orbitals (82 kJ mol^{-1}) as well as the $2s$ -orbital (26 kJ mol^{-1}) show correlation with the $\sigma^*(\text{Cl-F})$ orbitals of the ligands (Fig. S7, ESI[†]). For the chloride centered molecules symmetry allowed sp -hybridization is observed at the central ion in addition to overall stronger correlation effects between the central ion and the ligands ($[\text{Cl}(\text{ClF})_3]^-$ 134 kJ mol^{-1} per ligand), ($[F(\text{ClF})_3]^-$ 107 kJ mol^{-1} per ligand). If $[\text{Cl}(\text{ClF})_3]^-$ is forced into a planar geometry the correlation energy per ligand drops by 8 kJ mol^{-1} . This observation is consistent with a general trend in main group chemistry that elements of the

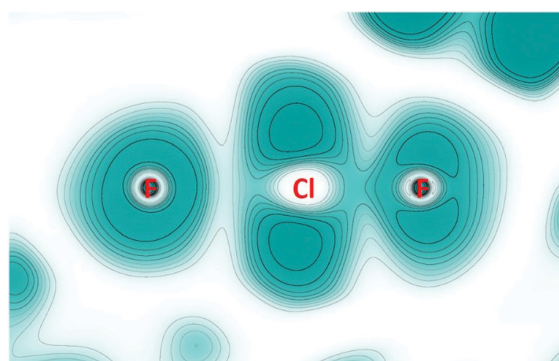


Fig. 4 Electron localization function (ELF) calculated for a plane containing a F–Cl–F unit of the $[F(\text{ClF})_3]^-$ anion. Color is ranging from white (0.0) to blue (1.0). Contours are drawn for values from 0.1 to 1.0 in intervals of 0.1. The fluorine atom to the left is the central atom of the anion. For the chlorine atom, no inner shell is seen due to the use of a pseudopotential.

second period have larger s -valence orbital contributions to their bonds and larger bond angles than the higher homologues.²⁵

The trigonal planar structure of the fluoridohalogenates is also consistent with their high ionic bond character, as shown by an analysis according to the atoms in molecules (AIM) scheme and the electron localization function (ELF) for the $[F(\text{ClF})_3]^-$ anion.

2D-maps of the ELF in a plane containing one F–Cl–F unit (Fig. 4) were obtained from periodic solid-state calculations (for details see the ESI[†]). The valence shell of the central fluoride ion (left in Fig. 4) appears almost symmetrical as expected for a non-covalently bound atom. In contrast, the fluorine atom of the ClF unit (right in Fig. 4), as well as the chlorine atom, shows clear signs of lone pairs. Finally, the different ELF values at the BCPs – 0.6 for the short contact and 0.2 for the long one – confirm that a covalently bound ClF molecule (with large charge-shift contribution) is electrostatically bonded to one fluoride ion.²⁶

A topological AIM analysis indicates that the bond in a ClF ligand has a strong charge-shift character due to the repulsion between electrons in the lone pairs and the σ -bond. This is best depicted by the ratio of the potential and kinetic charge density ($|V|/G$) at the bond critical point (BCP), which is between 1.6 and 1.7 and thus right in the range between ionic (< 1.0) and covalent (> 2.0) interactions. For the longer Cl–F contacts in $[F(\text{ClF})_3]^-$, the electron density at the BCPs (ρ_{BCP}) are significantly lower, indicating a non-shared interaction. The $|V|/G$ is about 1.0, also suggesting that this interaction is mainly of ionic character.

In conclusion, we report on the first non-classical Cl(i) fluoridochlorate. Additionally, we synthesized the corresponding heptachlorate anion. Analysis of the electronic structure and bonding situation revealed an unusual planar minimum structure of the $[F(\text{ClF})_3]^-$ anion. More in-depth quantum-chemical analysis shows the geometry dependence on the central halide ion which can be called fluorine specific.



Caution! Chlorine monofluoride is extraordinarily reactive and can react violently with organic materials under the formation of HF. Similarly, $[\text{NMe}_4][\text{F}(\text{ClF})_3]$ can decompose violently under certain conditions when exposed to organic materials. Exposure to acidic compounds (e.g. water or boron trifluoride) greatly enhances the reactivity.

We gratefully acknowledge the ZEDAT at Freie Universität Berlin for providing computing resources. Additionally, we are grateful for donations of chemicals from the Solvay Company. PP acknowledges VCI for providing PhD funding (Kekulé Fellowship). Funded by Deutsche Forschungsgemeinschaft (DFG, German Research Foundation) Project-ID 387284271 – SFB 1349. We also gratefully acknowledge support of the ERC-CoG project “HighPotOx” – Project-ID 818862.

Conflicts of interest

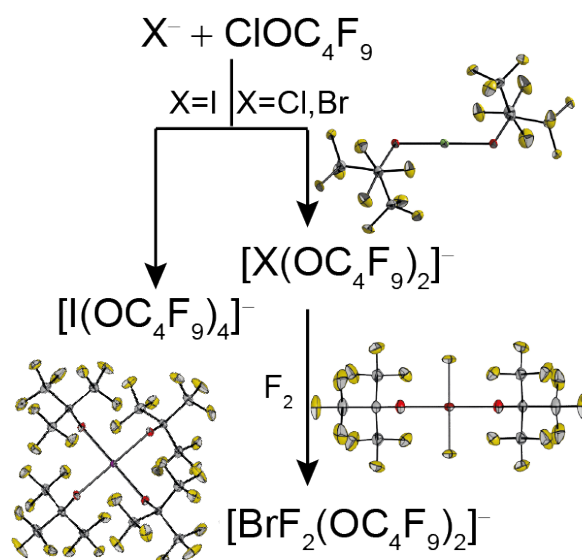
There are no conflicts to declare.

References

- K. Sonnenberg, L. Mann, F. A. Redeker, B. Schmidt and S. Riedel, *Angew. Chem., Int. Ed.*, 2020, **59**, 5464–5493.
- (a) H. Meinert and H. Klamm, *Z. Chem.*, 1965, **5**, 468–469; (b) D. Naumann and A. Meurer, *J. Fluorine Chem.*, 1995, **70**, 83–84.
- X. Zhang and K. Seppelt, *Z. Anorg. Allg. Chem.*, 1997, **623**, 491–500.
- K. O. Christe and D. Naumann, *Inorg. Chem.*, 1973, **12**, 59–62.
- A. R. Mahjoub and K. Seppelt, *Angew. Chem., Int. Ed. Engl.*, 1991, **30**, 323–324.
- (a) C. J. Adams, *Inorg. Nucl. Chem. Lett.*, 1974, **10**, 831–835; (b) A.-R. Mahjoub and K. Seppelt, *Angew. Chem., Int. Ed. Engl.*, 1991, **30**, 876–878.
- (a) R. Minkwitz, R. Bröchler and R. Ludwig, *Inorg. Chem.*, 1997, **36**, 4280–4283; (b) T. Surles, L. A. Quarterman and H. H. Hyman, *J. Inorg. Nucl. Chem.*, 1973, **35**, 668–670.
- J. R. Schmid, P. Pröhm, P. Voßnacker, G. Thiele, M. Ellwanger, S. Steinhauer and S. Riedel, *Eur. J. Inorg. Chem.*, 2020, 4497–4500.
- (a) A. G. Sharpe and H. J. Emeléus, *J. Chem. Soc.*, 1948, **0**, 2135–2138; (b) S. Siegel, *Acta Crystallogr.*, 1957, **10**, 380; (c) K. O. Christe and C. J. Schack, *Inorg. Chem.*, 1970, **9**, 1852–1858; (d) K. O. Christe and W. W. Wilson, *Inorg. Chem.*, 1986, **25**, 1904–1906; (e) S. Ivlev, P. Woidy, V. Sobolev, I. Gerin, R. Ostvald and F. Kraus, *Z. Anorg. Allg. Chem.*, 2013, **639**, 2846–2850; (f) S. I. Ivlev, R. V. Ostvald and F. Kraus, *Monatsh. Chem.*, 2016, **147**, 1661–1668; (g) S. Siegel, *Acta Crystallogr.*, 1956, **9**, 493–495; (h) S. I. Ivlev, P. Woidy, I. I. Zherin, R. V. Ostvald, F. Kraus, M. Y. Voytenko and V. V. Shagalov, *Procedia Chem.*, 2014, **11**, 35–42; (i) S. I. Ivlev, A. J. Karttunen, R. Ostvald and F. Kraus, *Z. Anorg. Allg. Chem.*, 2015, **641**, 2593–2598; (j) S. Ivlev, V. Sobolev, M. Hoelzel, A. J. Karttunen, T. Müller, I. Gerin, R. Ostvald and F. Kraus, *Eur. J. Inorg. Chem.*, 2014, 6261–6267; (k) A. J. Edwards and G. R. Jones, *J. Chem. Soc. A*, 1936, 1969.
- A. R. Mahjoub, A. Hoser, J. Fuchs and K. Seppelt, *Angew. Chem., Int. Ed. Engl.*, 1989, **28**, 1526–1527.
- W. W. Wilson and K. O. Christe, *Inorg. Chem.*, 1989, **28**, 4172–4175.
- (a) K. O. Christe and J. P. Guertin, *Inorg. Chem.*, 1965, **4**, 905–908; (b) K. O. Christe and J. P. Guertin, *Inorg. Chem.*, 1965, **4**, 1785–1787; (c) K. O. Christe, W. Sawodny and J. P. Guertin, *Inorg. Chem.*, 1967, **6**, 1159–1162; (d) P. Pröhm, J. R. Schmid, K. Sonnenberg, S. Steinhauer, C. J. Schattner, R. Müller, M. Kaupp, P. Voßnacker and S. Riedel, *Angew. Chem., Int. Ed.*, 2020, **59**, 16002.
- (a) L. B. Asprey, J. L. Margrave and M. E. Silverthorn, *J. Am. Chem. Soc.*, 1961, **83**, 2955–2956; (b) D. H. Kelly, B. Post and R. W. Mason, *J. Am. Chem. Soc.*, 1963, **85**, 307–308; (c) E. D. Whitney, R. O. MacLaren, T. J. Hurley and C. E. Fogle, *J. Am. Chem. Soc.*, 1964, **86**, 4340–4342; (d) E. D. Whitney, R. O. MacLaren, C. E. Fogle and T. J. Hurley, *J. Am. Chem. Soc.*, 1964, **86**, 2583–2586; (e) K. O. Christe and J. P. Guertin, *Inorg. Chem.*, 1966, **5**, 473–476; (f) K. O. Christe, *XXIVth International Congress of Pure and Applied Chemistry*, Elsevier, 1974, p. 115; (g) B. Scheibe, S. I. Ivlev, A. J. Karttunen and F. Kraus, *Eur. J. Inorg. Chem.*, 2020, 477; (h) I. Sheft, A. F. Martin and J. J. Katz, *J. Am. Chem. Soc.*, 1956, **78**, 1557–1559.
- K. O. Christe, W. W. Wilson, R. V. Chirakal, J. C. P. Sanders and G. J. Schrobilgen, *Inorg. Chem.*, 1990, **29**, 3506–3511.
- (a) L. Stein, *J. Fluorine Chem.*, 1985, **27**, 249–256; (b) J. Bandemehr, M. Sachs, S. I. Ivlev, A. J. Karttunen and F. Kraus, *Eur. J. Inorg. Chem.*, 2020, 64–70.
- S. I. Ivlev, A. J. Karttunen, R. V. Ostvald and F. Kraus, *Chem. Commun.*, 2016, **52**, 12040–12043.
- B. Scheibe, A. J. Karttunen, U. Müller and F. Kraus, *Angew. Chem., Int. Ed.*, 2020, **59**, 18116–18119.
- R. Boese, A. D. Boese, D. Bläser, M. Y. Antipin, A. Ellern and K. Seppelt, *Angew. Chem., Int. Ed. Engl.*, 1997, **36**, 1489–1492.
- E. A. Jones, T. F. Parkinson and T. G. Burke, *Z. Naturforsch., A: Phys. Sci.*, 1950, **18**, 235–236.
- R. Dovesi, A. Erba, R. Orlando, C. M. Zicovich-Wilson, B. Civalleri, L. Maschio, M. Rérat, S. Casassa, J. Baima, S. Salustro and B. Kirtman, *Wiley Interdiscip. Rev.: Comput. Mol. Sci.*, 2018, **8**, e1360.
- B. M. Powell, K. M. Heal and B. H. Torrie, *Mol. Phys.*, 1984, **53**, 929–939.
- R. Brückner, H. Haller, M. Ellwanger and S. Riedel, *Chem. – Eur. J.*, 2012, **18**, 5741–5747.
- (a) D. Mootz and W. Poll, *Z. Naturforsch., B: Chem. Sci.*, 1984, **39**, 1300–1305; (b) D. Mootz and W. Poll, *Z. Naturforsch., B: Chem. Sci.*, 1984, **39**, 290–297; (c) D. Mootz and D. Boenigk, *J. Am. Chem. Soc.*, 1986, **108**, 6634–6636; (d) D. Mootz and D. Boenigk, *Z. Anorg. Allg. Chem.*, 1987, **544**, 159–166.
- G. Castillo-Toraya, M. Orozco-Ic, E. Dzib, X. Zarate, F. Ortiz-Chi, Z.-h. Cui, J. Barroso and G. Merino, *Chem. Sci.*, 2021, DOI: 10.1039/D1SC01325D.
- (a) H. Hartl, J. Schnier, J. Jander and H. Schulz, *Z. Anorg. Allg. Chem.*, 1975, **413**, 61–71; (b) S. C. Nyburg, G. A. Ozin and S. T. Szymański, *Acta Crystallogr., Sect. B: Struct. Crystallogr. Cryst. Chem.*, 1972, **28**, 2885; (c) L. Zhao, S. Pan, N. Holzmann, P. Schwerdtfeger and G. Frenking, *Chem. Rev.*, 2019, **119**, 8781–8845.
- S. Shaik, D. Danovich, W. Wu and P. C. Hiberty, *Nat. Chem.*, 2009, **1**, 443–449.



3.4. Investigation of Bis(Perfluoro-*tert*-Butoxy) Halogenates(I/III)



Patrick Pröhm, Willi Berg, Susanne M. Rupf, Patrick Voßnacker, Sebastian Riedel*

Chem. Eur. J. **2021** (accepted article)

DOI: 10.1002/chem.202103325

©The Authors. Published by Wiley-VCH GmbH.

Author Contribution:

Patrick Pröhm designed the project, performed experiments, analyzed data, performed quantum-chemical calculations and wrote the manuscript. Willi Berg performed experiments during his Bachelor's thesis under supervision of Patrick Pröhm. Susanne M. Rupf and Patrick Voßnacker measured and refined crystal structures. Sebastian Riedel supervised the project and revised the manuscript.

Investigation of Bis(Perfluoro-*tert*-Butoxy) Halogenates(I/III)

Patrick Pröhm,^[a] Willi R. Berg,^[a] Susanne M. Rupf,^[a] Patrick Voßnacker,^[a] and Sebastian Riedel^{]*[a]}

Dedicated to Otto Ruff in occasion of his 150th birthday.

Abstract: A systematic study of halogenate(I/III) anions with polyatomic ligands is presented. The bis(perfluoro-*tert*-butoxy) halogenates(I) $[\text{X}(\text{OC}_4\text{F}_9)_2]^-$, X=Cl, Br, I, of chlorine, bromine, and iodine are prepared as their tetraethylammonium salts and characterized with IR, Raman, and NMR spectroscopic methods, as well as single-crystal X-ray diffraction analyses. Spectroscopic data are supported by quantum-chemical calculations. Additionally, the bonding situation of the species in question are analyzed and

discussed. Furthermore, the oxidation to the corresponding halogenate(III) derivatives was studied. For $[\text{Br}(\text{OC}_4\text{F}_9)_2]^-$, oxidation with elemental fluorine gave $[\text{BrF}_2(\text{OC}_4\text{F}_9)_2]^-$. Iodide was directly oxidized by ClOC_4F_9 to the I^{III} species $[\text{I}(\text{OC}_4\text{F}_9)_4]^-$, which is a surprisingly inert anion that might be used as a weakly coordinating anion (WCA) in the future. For $[\text{Cl}(\text{OC}_4\text{F}_9)_2]^-$, the decomposition products of the synthetic approaches towards a chlorine(III) system were analyzed.

Introduction

Halogen compounds with halogens in positive oxidation states and alcoholate ligands are rare, especially amongst the lighter halogens bromine^[1,2] and chlorine.^[3–5] Partially positively charged halogen compounds with other ligands such as fluoro or oxido are more abundant, however in comparison to compounds with partially negatively charged halogens still rare.^[6] Despite their relatively low abundance they play an important role in modern synthetic chemistry. Hypervalent iodine compounds are widely used as reagents in organic and polymer chemistry.^[7] Bromine trifluoride can be used for a variety of bromination and fluorination reactions of organic molecules and its fluoro complex tetrafluoridobromate(III) is a promising tool for the recovery of scarce elements by urban mining.^[8] Hypochlorite is the main component of industrially used bleach^[9] and its organic esters are used for synthetical purposes, for example, the synthesis of perfluorinated peroxides.^[3] However, little is known about partially positively charged halogens with larger ligand systems. In case of multiatomic oxygen-based ligands, organic hypohalites are the most common compounds. They are neutral compounds composed of an alcoholate fragment and a halogen in the oxidation state +I. Hypochlorites with different alcohol moieties

are known, including OMe,^[4] OEt,^[4] OiPr,^[5] OtBu.^[5] Additionally, fully fluorinated versions of these hypochlorites exist.^[3] Generally, they are more reactive than their non-fluorinated counterparts. While non-fluorinated hypochlorites are typically prepared in aqueous solutions, their perfluorinated counterparts are synthesized with ClF under strict exclusion of moisture. The hypobromites BrOCF_3 ^[11] and BrOC_4F_9 ^[2] are briefly described in the literature, however, they are significantly less stable than their chlorine counterparts.^[1,2] Examples for higher oxidation states than +I with multiatomic ligands are even more scarce. Neutral representatives include $\text{C}_6\text{F}_5\text{BrF}_2$ and $\text{C}_6\text{F}_5\text{BrF}_4$.^[10]

Due to the high oxidation potential of partially positively charged halogen anions are often more stable than their neutral or cationic counterparts. Therefore, it appears surprising that virtually nothing is known about such anions with the exception of a quite instable intermediate reported by Minkwitz in 1997, $[\text{NMe}_4][\text{Br}(\text{OCF}_3)_2]$.^[11] It was synthesized via exposure of $[\text{NMe}_4]\text{Br}$ or $[\text{NMe}_4][\text{BrCl}_2]$ to ClOCF_3 . However, decomposition of the anion under loss of carbonyl fluoride and formation of $[\text{BrF}_2]^-$ began already at -70 °C, a known problem of α -fluoroalcohol moieties.^[11] Anions with polyatomic inorganic ligands such as OSO_2F , ONO_2 , OCIO_3 and O_2CCF_3 are described in $[\text{NMe}_4][\text{I}(\text{ONO}_2)_2]$,^[12] $[\text{NMe}_4][\text{I}(\text{ONO}_2)_4]$,^[12] $[\text{NMe}_4][\text{Br}(\text{ONO}_2)_2]$,^[12] $\text{KI}(\text{OSO}_2\text{F})_4$,^[13] $\text{K}[\text{Br}(\text{OSO}_2\text{F})_4]$,^[13] $\text{Cs}[\text{I}(\text{OCIO}_3)_4]$,^[14] $\text{Cs}[\text{Br}(\text{OCIO}_3)_2]$ ^[15] and $\text{Cs}[\text{I}(\text{O}_2\text{CCF}_3)_4]$,^[16] however, their characterization is often limited to elemental analysis and MIR spectra in case of ONO_2 without the crucial region of the halogen oxygen vibrations. The only known crystal structure was recently reported by Seppelt for $[\text{NO}_2][\text{Br}(\text{ONO}_2)_2]$.^[17]

Here we present the first systematic study of halogenate(I/III) anions of chlorine, bromine and iodine using the perfluorinated OtBu^F as a potent ligand system to stabilize such oxidizing compounds (Figure 1). We believe this is a fundamental work for the understanding of hypervalent halogen molecules.

[a] P. Pröhm, W. R. Berg, S. M. Rupf, P. Voßnacker, Prof. Dr. S. Riedel
 Department of Chemistry and Biochemistry-Inorganic Chemistry
 Freie Universität Berlin
 Fabeckstrasse 34/36, 14195 Berlin (Germany)
 E-mail: s.riedel@fu-berlin.de

Supporting information for this article is available on the WWW under <https://doi.org/10.1002/chem.202103325>

© 2021 The Authors. Chemistry - A European Journal published by Wiley-VCH GmbH. This is an open access article under the terms of the Creative Commons Attribution License, which permits use, distribution and reproduction in any medium, provided the original work is properly cited.

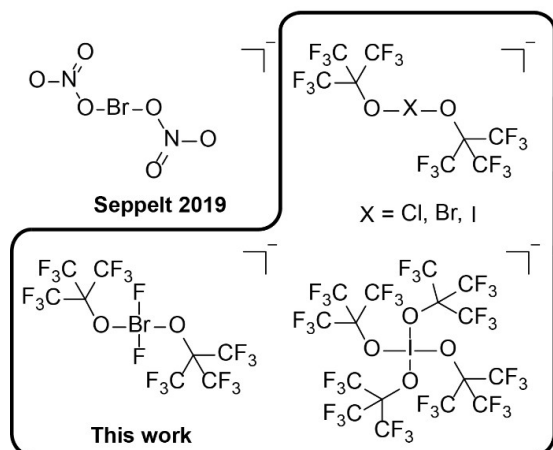
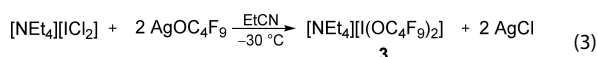
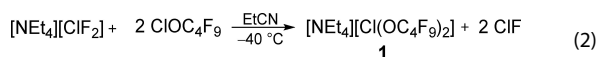
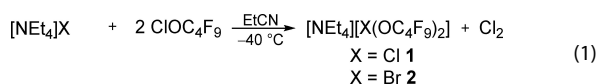


Figure 1. Comparison between the structurally characterized halogenate anions with polyatomic ligands.

Results and Discussion



We were able to synthesize the halogenate(I) salts $[\text{NEt}_4][\text{X}(\text{OC}_4\text{F}_9)_2]$, X=Cl, Br, I, for the three halogens chlorine, bromine and iodine. For chlorine and bromine the corresponding halide salts tetraethylammonium chloride or bromide were oxidized by perfluoro-*tert*-butoxyhypo-chlorite, ClOC_4F_9 , in propionitrile at -40°C (Eq. (1)) to yield $[\text{NEt}_4][\text{Cl}(\text{OC}_4\text{F}_9)_2]$ (**1**) and $[\text{NEt}_4][\text{Br}(\text{OC}_4\text{F}_9)_2]$ (**2**) under elimination of elemental chlorine. For **1**, $[\text{NEt}_4][\text{ClF}_2]$ was also a suitable starting material (Eq. (2)). In this case no oxidation reaction of the halogen is necessary and the fluoro ligands are exchanged for perfluoro-*tert*-butoxy ligands under elimination of ClF. $[\text{NEt}_4][\text{I}(\text{OC}_4\text{F}_9)_2]$ was obtained from the reaction of $[\text{NEt}_4][\text{ICl}_2]$ with AgOC_4F_9 in propionitrile at -30°C (Eq. (3)). Here, the ligand exchange was accomplished by precipitation of AgCl.

We obtained single crystals suitable for X-ray diffraction for all three compounds by slowly cooling solutions in propionitrile (**1** and **2**) or DCM (**3**) to -80°C . Interestingly, the compounds are all isotypic and crystallized in the monoclinic space group $P2_1$ (see Figure 2 for **1**, for **2** and **3** see Figures S14 and S15). Table 1 gives an overview of the halogen oxygen bond lengths and angle in the three crystal structures. Overall, the anions are nearly inversion symmetric with bond angles close to 180° and nearly equally long X–O1 and X–O2 bond distances. As

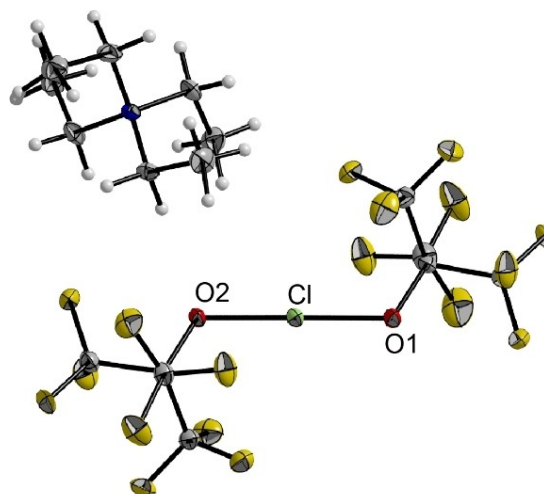


Figure 2. Molecular structure of $[\text{NEt}_4][\text{Cl}(\text{OC}_4\text{F}_9)_2]$. 1. Displacement ellipsoids are shown at 50% probability level. Color code: yellow = fluorine, grey = carbon, red = oxygen, green = chlorine, blue = nitrogen. Compounds **2** and **3** are isotypic (cf. Supporting Information).

Table 1. Selected structural parameters of **1**, **2** and **3**, determined from their crystal structures in comparison with calculated parameters (italic). Bond lengths are given in [pm], bond angles in [°].

	X	X–O1	X–O2	O1–X–O2
1	Cl	195.6(2)	<i>197.7</i>	179.4(1)
2	Br	205.1(4)	<i>209.3</i>	179.5(2)
3	I	218.5(6)	<i>221.7</i>	179.8(3)

expected, the oxygen halogen bond length increases from chlorine to iodine due to the increasing atomic radii of the halogens. Comparing the oxygen halogen bond lengths with the very recently determined bond lengths from the crystal structures of $[\text{ClO}]^-$ (168.6(1) pm) and $[\text{BrO}]^-$ (182.0(3) pm) it becomes obvious that the bonding in the $[\text{X}(\text{OC}_4\text{F}_9)_2]^-$ anions is significantly weaker than the bonding in the hypohalite anions $[\text{XO}]^-$.^[18] In case of **2**, a related structure is known, $[\text{NO}_2][\text{Br}(\text{ONO}_2)_2]$.^[17] Its Br–O bond lengths are well comparable (205.1(1) pm) and the O–Br–O angle is 180° , indicating a similar bonding situation. Additionally, we obtained Raman and IR data of compounds **1–3**. Overall, the spectra are very similar to each other. The Raman spectra (Figure S3) show the symmetric X–O stretching modes at 511 cm^{-1} (**1**), 513 cm^{-1} (**2**) and 513 cm^{-1} (**3**) (Table 2), with a slight blue shift when increasing the atomic number, whereas the X–O deformation mode experiences a red shift (459 cm^{-1} (**1**), 452 cm^{-1} (**2**), 431 cm^{-1} (**3**)). The IR spectra (Figure S6) are dominated by antisymmetric C–F valence vibrations in the area between 1300 and 1150 cm^{-1} , followed by C–O valence and deformation modes between 1150 and 900 cm^{-1} . Below 600 cm^{-1} several halogen oxygen modes as well as C–F deformation modes are observed. Like the symmetric X–O stretching modes, also the antisymmetric stretching modes experience a slight blue shift with increasing

Table 2. Vibrational spectroscopic data of [NEt₄][Cl(OC₄F₉)₂] (1), [NEt₄][Br(OC₄F₉)₂] (2), [NEt₄][I(OC₄F₉)₂] (3), [NEt₄][I(OC₄F₉)₄] (4) and [NEt₄][BrF₂(OC₄F₉)₂] (5). Calculated data were obtained on the B3LYP-D3(BJ)/def2-TZVPP level.

	ν _{sy} (XO)		ν _{as} (XO)		ν _{sy} (BrF)		ν _{as} (BrF)	
	Exp.	Calc.	Exp.	Calc.	Exp.	Calc.	Exp.	Calc.
1	511	504	505	499	–	–	–	–
2	513	504	507	500	–	–	–	–
3	513	503	510	500	–	–	–	–
4	519 ^[a] 541 ^[b]	505 ^[a] 539 ^[b]	510	506	–	–	–	–
5	521	509	515	504	477	473	515	502

[a] out-of-phase; [b] in-phase.

atomic number of the halogen from 505 cm⁻¹ (1) over 507 cm⁻¹ (2) to 510 cm⁻¹ (3). The blue shifts indicate stronger bonding between the oxygen and halogen atoms when going to the heavier halogens. We confirmed this conclusion by calculating the energies of the decomposition reaction of [X(OC₄F₉)₂]⁻ into XOC₄F₉ and [C₄F₉O]⁻ (X=Cl, Br, I). Indeed, we found that the decomposition reaction is the least endoenergetic for X=Cl, while for X=Br it is 30 kJ mol⁻¹ more endoenergetic and for X=I even 57 kJ/mol. The stronger bonding for the heavier elements can be rationalized with stronger ionic contributions to the bonding. The natural population analysis (NPA) predicted a rise of the partial positive charge on the central halogen when going from chlorine to iodine (Cl=0.19, Br=0.31, I=0.44). This trend is easily understood when taking the decreasing electronegativity and ionization potential of the halogens into account. The charge of the halogens in the [X(OC₄F₉)₂]⁻ series is very similar to the charges in the [XF₂]⁻ series (Cl=0.23, Br=0.32, I=0.43). According to the natural bond orbital (NBO) analysis the bonding in the {O–X–O} core is a 3-center-4-electron bond for all three molecules, similar to the fluoridohalogenates(I).



Due to the seemingly strong analogy between [X(OC₄F₉)₂]⁻ and [XF₂]⁻ we investigated the synthesis of the OC₄F₉ analogues of [XF₄]⁻ anions with the central halogen in oxidation state +III. In contrast to the reaction of ClOC₄F₉ with Cl⁻ and Br⁻ which generated halogenate(I) compounds, the reaction of tetraethylammonium iodide [NEt₄]I with four or more equivalents of ClOC₄F₉ under generation of chlorine yielded [NEt₄][I(OC₄F₉)₄] (4) with iodine in the desired oxidation state +III (Eq. (4)). Single crystals were obtained by slowly cooling a propionitrile solution to -80 °C. 4 crystallized in the monoclinic space group P2₁/n with two ion pairs in the antisymmetric unit (Figure 3). The I–O bond lengths are in the range of 211.7(2) pm to 213.1(2) pm (calc: 214.7 pm) and therefore 5–7 pm shorter than in the I^I compound 3. The bond angles are between 88.58(7) (O1–I1–O2) and 91.34(7) (O4–I1–O1). As for the halogenate(I) compounds, the IR spectrum (Figure S4) shows several prominent C–F valence vibrations in the area between 1300 cm⁻¹ and 900 cm⁻¹. The antisymmetric I–O valence vibrations are found at 511 cm⁻¹, highly coupled with the C–F

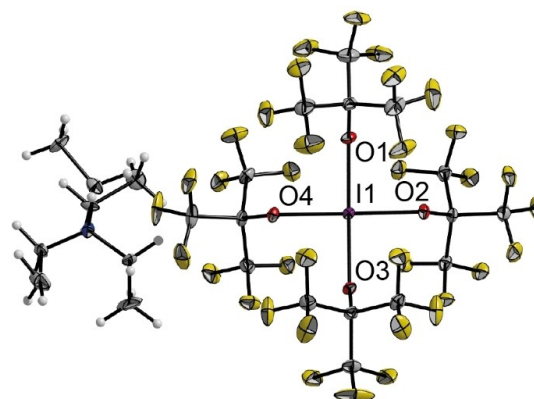
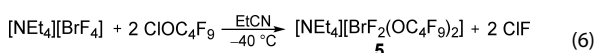
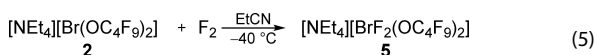


Figure 3. Molecular structure of [NEt₄][I(OC₄F₉)₄] 4. One ion pair of the asymmetric unit is shown. Displacement ellipsoids are shown at 50% probability level. Disorder in the cation omitted for clarity. Color code: yellow = fluorine, grey = carbon, red = oxygen, purple = iodine, blue = nitrogen. Selected bond lengths [pm] and angles [°]: I1–O1 213.1(2), I1–O2 211.7(2), I1–O3 212.4(2), I1–O4 212.7(2), O1–I1–O2 88.58(7), O2–I1–O3 90.85(7), O3–I1–O4 89.22(7), O4–I1–O1 91.34(7).

deformation modes in the ligand backbone. In the area below 400 cm⁻¹ I–O deformation modes are observed, again coupled with the ligand. The Raman spectrum (Figure S7) shows the in-phase symmetric I–O valence modes at 541 cm⁻¹ and the out-of-phase mode at 519 cm⁻¹. In comparison to the corresponding I^I species 3, the symmetric I–O modes are slightly blue shifted (Δν_{sy}=28 cm⁻¹ for the in-phase mode of 4) indicating a stronger bonding in 4 than in 3. Again, we calculated the decomposition reaction of [I(OC₄F₉)₄]⁻ into I(OC₄F₉)₃ and [C₄F₉O]⁻ and found that it is more endoenergetic by 57 kJ/mol than the respective decomposition of 3. According to the NBO analysis the bonding situation is best described by two perpendicular 3-center-4-electron bonds and the NPA predicted a charge of 1.7 for the iodine center.

In the area below 700 cm⁻¹ a variety of valence and deformation modes of the {IO₄} unit are observed. At higher energies (900 cm⁻¹ to 1300 cm⁻¹) weak bands corresponding to C–O and C–F vibrations are detected. We unsuccessfully tried to oxidize the iodine center further by adding stoichiometric and excess diluted fluorine. This is somewhat surprising because the addition of three equivalents of diluted fluorine (10%) to a solution of [NEt₃Me]I in propionitrile readily yields [NEt₃Me][IF₆] (see discussion in Supporting Information). Additionally, among the binary iodine fluorides the oxidation state +V is the most preferred one.^[19] However, the crystal structure of 4 depicted as a space-filling model (Figure S12) reveals that the iodine center is sterically completely shielded by the ligands which is reminiscent of the aluminum derivative [Al(OC₄F₉)₄]⁻ which is widely used as a WCA.^[20] The estimated thermochemical volume of 4 is 698 Å³ (see Supporting Information for details). This is similar to the volume of the aluminate [Al(OC₄F₉)₄]⁻ (776 Å³).^[21] Additionally, we calculated the electrostatic potential (ESP) mapped on the electron density (Figure S13). It showed a well distributed negative charge without

any concentrated charge spots. Therefore, we envision this anion to be a potent metal-free WCA. Amongst the substances discussed in this work, $[\text{NEt}_4][\text{I}(\text{OC}_4\text{F}_9)_4]$ is the most stable one. It can be stored at room temperature under Ar and for short amounts of time handled at ambient atmosphere (Figures S16 and S17). Hydrolysis under formation of I_2 occurs within several minutes in comparison to immediate decomposition of the lighter homologues. Synthesis of a mixed ligand I^{III} anion from the reaction of $[\text{NEt}_4][\text{ICl}_2]$ with two equivalents of ClOC_4F_9 yielded two anionic species, $[\text{ICl}_4]^-$ and $[\text{I}(\text{OC}_4\text{F}_9)_4]^-$, indicating dismutation of the ligands. Quantum-chemical calculations confirm that the symmetric anions are indeed energetically more favorable than two equivalents of $[\text{ICl}_2(\text{OC}_4\text{F}_9)_2]^-$.



Additionally, we studied the reactivity of the lighter homologues 1 and 2. The Br^{I} compound 2 can be oxidized with dilute fluorine (10% in Ar) to yield the Br^{III} compound $[\text{NEt}_4][\text{BrF}_2(\text{OC}_4\text{F}_9)_2]$ 5 (Eq. (5)). The reaction is reminiscent of the fluorination of Cl^- and Br^- to the tetrafluorido halogenates(III) under similar conditions.^[22,23] Interestingly, we obtained the same compound from the ligand exchange reaction between $[\text{NEt}_4][\text{BrF}_4]$ and ClOC_4F_9 under elimination of two equivalents of ClF (Eq. (6)).

Again, we were able to characterize the compound by single crystal X-ray diffraction (Figure 4). 5 crystallized in the monoclinic space group $I2/m$. The bromine center is positioned on a center of inversion, rendering the anion inversion symmetric. The Br–O distances are 199.4(2) pm (calc: 204.7 pm). The shortening by 5.5 ppm and 5.7 pm in comparison to 2 can be rationalized by the higher charge on the bromine leading to stronger ionic contributions in the bonding. The Br–F bonds have a length of 189.3(2) pm (calc: 190.1 pm). This is very similar to the Br–F bond lengths in $[\text{NEt}_3\text{Me}][\text{BrF}_4]$ with 188.93(1) pm to 190.47(1) pm.^[23] Therefore we assume that the bonding situation in the anion of 2 is closely related to the bonding situation in $[\text{BrF}_4]^-$. This can also be deduced from the Raman

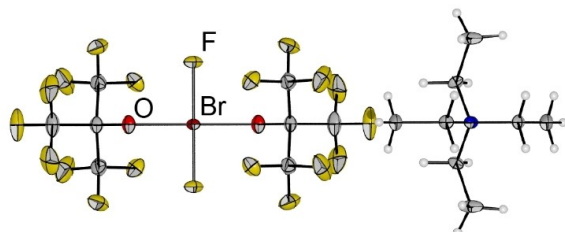


Figure 4. Molecular structure of $[\text{NEt}_4][\text{BrF}_2(\text{OC}_4\text{F}_9)_2]$ 5. Displacement ellipsoids are shown at 50% probability level. Disorder in the cation omitted for clarity. Color code: yellow = fluorine, grey = carbon, red = oxygen, dark red = bromine, blue = nitrogen. Selected bond lengths [pm]: Br–O 199.4(2), Br–F 189.3(2).

spectrum (Figure S5). A breathing mode-like vibration, i.e. $\nu_{\text{sy}}(\text{BrO})$ in-phase coupled with $\nu_{\text{sy}}(\text{BrF})$, is observed at 521 cm^{-1} (Table 2). Additionally, the symmetric Br–F stretching mode is observed at 477 cm^{-1} as the dominant vibration in the spectrum. This is in excellent agreement with the a_{1g} and b_{1g} vibrations of $[\text{BrF}_4]^-$ at 519 cm^{-1} and 442 cm^{-1} .^[23] In comparison with the Br^{I} species 2 the $\nu_{\text{sy}}(\text{BrO})$ mode is slightly blue shifted by 8 cm^{-1} due to the stronger bond formation which is in line with the structural data of the crystal structure. The NPA analysis shows a charge of +1.40 at the bromine which is significantly increased in comparison to 2 (+0.31), however, it is comparable to the natural charge of Br in $[\text{BrF}_4]^-$ (+1.46). Therefore, it can be assumed that the ionic contributions are increased in 5 in comparison to 2. According to the NBO analysis the bonding of the $\{\text{BrF}_2\text{O}_2\}$ core is best described by two perpendicular 3-center-4-electron bonds. The IR spectrum shows both antisymmetric Br–F and Br–O stretching modes at 515 cm^{-1} (Table 2). In case of $[\text{NMe}_4][\text{BrF}_4]$ the corresponding mode is observed at 480 cm^{-1} .^[24] At lower energies the spectrum shows several wagging modes of the BrF_2 unit, coupled with the ligand backbone, however, the most intense band at 288 cm^{-1} is in agreement with the out-of-plane vibration of $[\text{NMe}_4][\text{BrF}_4]$ at 315 cm^{-1} .^[24] The most intense IR bands (Figure S8) are observed between 900 and 1300 cm^{-1} and correspond to the $\nu_{\text{as}}(\text{CF})$ modes.

Analogous to the oxidation of 2 we performed a similar reaction with the Cl^{I} derivative 1. However, in contrast to exclusive oxidation of the chlorine center we observed cleavage of the Cl–O bond. The reaction products were identified as the hypofluorite FOC_4F_9 and tetraethylammonium tetrafluoridochlorate(III) $[\text{NEt}_4][\text{ClF}_4]$. From the reaction of $[\text{NEt}_4][\text{ClF}_4]$ with ClOC_4F_9 we obtained the bis(perfluoro-tert-butyl)peroxide $(\text{C}_4\text{F}_9\text{O})_2$.^[25] From these results we concluded that Cl^{III} is too strongly oxidizing to tolerate alcoholate ligands like OC_4F_9 .

Conclusion

The synthesis and characterization of halogenate anions $[\text{X}(\text{OC}_4\text{F}_9)_2]^-$ for the three halogens $\text{X}=\text{Cl}$, Br , and I in their oxidation state +I is presented. Their bonding situation was analyzed and differences in the bonding were elucidated showing more ionic contributions to the bonding for the heavier halogens. Additionally, their reactivity was studied by oxidizing the Br^{I} derivative with dilute fluorine. The resulting compound is a rare example of a Br^{III} anion with a polyatomic ligand system. At this point, sharp differences between the Br^{I} and the Cl^{I} compound manifested because fluorination of the latter led to a cleavage of the Cl–O bond instead of an oxidation of the halogen center.

In the case of iodine, the I^{III} compound $[\text{I}(\text{OC}_4\text{F}_9)_4]^-$ was obtained directly from the oxidation of iodide with ClOC_4F_9 . The steric bulk of the perfluoroalcoholate ligands shielded the iodine center rendering it the most stable compound of the series (stable at RT and ambient atmosphere) and even showed resistance towards elemental fluorine. This anion is envisioned

to be a potent, metal-free candidate as a WCA for certain applications.

Experimental Section

All experiments were performed under rigorous exclusion of moisture and oxygen using standard Schlenk techniques. Solids were handled in a dry box under argon atmosphere ($O_2 < 0.5$ ppm, $H_2O < 0.5$ ppm). Fluorination experiments were performed with a stainless steel vacuum line, previously passivated with F_2 . Propionitrile was dried over Sicapent® prior to use and stored over molecular sieve 3 Å. $[NEt_4]Cl$, $[NEt_4]Br$ and $[NEt_4]I$ were dried overnight at 120 °C under dynamic vacuum. All other chemicals were used as purchased. CIO_4F_9 ^[26] and $AgOC_4F_9$ ^[27] were synthesized as described elsewhere. Raman spectra were recorded on a Bruker MultiRAM II equipped with a low-temperature Ge detector (1064 nm, 30–80 mW, resolution 4 cm^{-1}). Spectra of single crystals were recorded at –196 °C using the Bruker RamanScope III. IR spectra were recorded on a Nicolet i550 Advance FTIR by Thermo Fisher Scientific equipped with an ATR unit, with a Ge on KBr beamsplitter and a DLATGS-KBr detector for MIR and a solid-substrate beamsplitter with a DLATGS-PE detector for FIR. For low-temperature measurements we used a metal cylinder cooled by a cold N_2 stream (see Figures S1 and S2 for details). NMR spectra were recorded on a JEOL 400 MHz ECS or ECZ spectrometer. All reported chemical shifts are referenced to the δ values given in IUPAC recommendations of 2008 using the 2H signal of the deuterated solvent as internal reference.^[28] For external locking acetone- d_6 was flame sealed in a glass capillary and the lock oscillator frequency was adjusted to give $\delta(^1H) = 7.26$ ppm for a $CHCl_3$ sample locked on the capillary. Crystal data were collected on a Bruker D8 Venture diffractometer with a Photon 100 CMOS area detector with MoK α radiation. Single crystals were picked at –80 °C under nitrogen atmosphere and mounted on a 0.15 mm Mitegen micromount using perfluoroether oil diluted with perfluoro-hexane. The structures were solved with the ShelXT^[29] structure solution program using intrinsic phasing and refined with the ShelXL^[30] refinement package using least squares minimizations by using OLEX2.4^[31] For visualization the Diamond V3.0 program was used.^[32]

Deposition Numbers 2105613 (for 1), 2105583 (for 2), 2105590 (for 3), 2105589 (for 4), 2105582 (for 5) and 2105587 (for 6) contain the supplementary crystallographic data for this paper. These data are provided free of charge by the joint Cambridge Crystallographic Data Centre and Fachinformationszentrum Karlsruhe Access Structures service.

For structure optimizations and thermochemical data, the program package Turbomole V7.3^[33] was used with the DFT hybrid functional B3LYP^[34] and dispersion correction by Grimme (D3)^[35] and Becke-Johnson damping (BJ)^[36] with the triple- ζ basis set def2-TZVPP^[37] and the effective core potential def2-ECP^[38] for I. As a validation for minimum structures, harmonic frequencies were calculated as implemented. NBO analyses were performed with the Gaussian G16^[39] software package and NBO 7.0.^[40] Raman spectra were calculated with a 1064 nm excitation. Raman intensities are given for unpolarized radiation.

Synthesis of $[NEt_4][Cl(OC_4F_9)_2]$ 1: **Route A:** tetraethylammonium chloride (50.0 mg, 0.302 mmol, 1 eq) was dissolved in propionitrile (0.8 ml). Perfluoro-*tert*-butyl hypochlorite (324 mg, 1.20 mmol, 4 eq) was added at –196 °C. The reaction mixture was allowed to warm to –40 °C and stirred for 15 min. After slowly cooling to –80 °C the product was obtained as single crystals. **Route B:** A solution of $[NEt_4][ClF_2]$ (61.5 mg, 0.302 mmol, 2 eq) in propionitrile (0.7 ml) was

prepared as described elsewhere.^[22] Perfluoro-*tert*-butyl hypochlorite (163 mg, 0.603 mmol, 2 eq) was added at –196 °C. The reaction mixture was allowed to warm to –40 °C and stirred for 15 min. After slowly cooling to –80 °C the product was obtained as single crystals. 1H NMR (400 MHz, EtCN, ext. acetone- d_6 , 223 K): $\delta/ppm = 3.86$ (q, $^3J(^1H,^1H) = 7.6$ Hz, 8H, CH_2). ^{19}F NMR (376 MHz, EtCN, ext. acetone- d_6 , 223 K): $\delta/ppm = -74.7$. IR (ATR, 233 K) $\tilde{\nu}/cm^{-1} = 2996, 2961, 1490, 1457, 1445, 1397, 1369, 1236, 1212, 1176, 1154, 1105, 1055, 978, 959, 787, 764, 732, 723, 668, 578, 535, 505, 489, 366, 336, 318, 253, 174, 144$. Raman (crystal, 1064 nm, 77 K) $\tilde{\nu}/cm^{-1} = 3019, 3005, 2996, 2954, 2900, 1468, 1301, 1102, 1003, 758, 679, 668, 576, 537, 527, 460, 422, 352, 338, 323, 294, 280, 212, 178, 117, 94, 73$. CCDC number: 2105613.

Synthesis of $[NEt_4][Br(OC_4F_9)_2]$ 2: tetraethylammonium bromide (20.0 mg, 0.095 mmol, 1 eq) was dissolved in propionitrile (0.6 ml). Perfluoro-*tert*-butyl hypochlorite (154 mg, 0.570 mmol, 6 eq) was added at –196 °C. The reaction mixture was allowed to warm to –40 °C and stirred for 15 min. After slowly cooling to –80 °C the product was obtained as single crystals. 1H NMR (400 MHz, CD_3CN , 243 K): $\delta/ppm = 2.33$ (q, $^3J(^1H,^1H) = 7.6$ Hz, 8H, CH_2), 1.13 (tt, $^3J(^1H,^1H) = 7.6$ Hz, $^3J(^{14}N,^1H) = 1.9$ Hz, 12H, CH_3). ^{19}F NMR (376 MHz, CD_3CN , 243 K): $\delta/ppm = -72.9$ (s). IR (ATR, 233 K) $\tilde{\nu}/cm^{-1} = 2995, 2961, 1490, 1242, 1207, 1176, 1156, 1112, 1071, 1054, 1000, 976, 959, 788, 764, 730, 723, 671, 576, 535, 507, 475, 362, 335, 293, 288, 280, 222, 161, 131$. Raman (crystal, 1064 nm, 77 K) $\tilde{\nu}/cm^{-1} = 3032, 2992, 2969, 2952, 1468, 1302, 1157, 1120, 999, 767, 676, 576, 536, 513, 452, 422, 322, 285, 267, 224, 213, 197, 117, 83$. CCDC number: 2105583.

Synthesis of $[NEt_4][I(OC_4F_9)_2]$ 3: $AgOC_4F_9$ (131.0 mg, 0.381 mmol, 2.5 eq) was dissolved in EtCN (5 ml), cooled to –30 °C and added to a cooled (–30 °C) solution of tetraethylammonium dichloroiodate(I) (50.0 mg, 0.152 mmol, 1 eq) in EtCN (5 ml). The reaction mixture was stirred for 30 min at –30 °C, then for 30 min at RT. Then it was filtered and the solvent removed. The residual solid was washed with hexane three times (10 ml each). Single crystals were obtained by cooling a DCM solution to –80 °C after 1 night. IR (ATR, 298 K) $\tilde{\nu}/cm^{-1} = 3004, 1488, 1396, 1250, 1204, 1155, 1139, 1053, 1002, 785, 722, 676, 617, 565, 533, 510, 473, 453, 347, 305, 267, 219, 201, 148$. Raman (1064 nm, 298 K) $\tilde{\nu}/cm^{-1} = 3004, 2954, 2904, 1464, 1301, 1265, 1071, 1003, 973, 907, 894, 766, 679, 571, 536, 513, 421, 353, 335, 319, 293, 266, 214, 180, 150, 110$. CCDC number: 2105590.

Synthesis of $[NEt_4][I(OC_4F_9)_4]$ 4: tetraethylammonium iodide (50.0 mg, 0.195 mmol, 1 eq) was dissolved in propionitrile (0.9 ml). Perfluoro-*tert*-butyl hypochlorite (262 mg, 0.972 mmol, 5 eq) was added at –196 °C. The reaction mixture was allowed to warm to RT and stirred for 15 min. All volatiles were removed under vacuum and the product was obtained as a colorless solid. 1H NMR (400 MHz, CD_3CN , 298 K): $\delta/ppm = 3.15$ (q, $^3J(^1H,^1H) = 7.3$ Hz, 8H, CH_2), 1.20 (tt, $^3J(^1H,^1H) = 7.3$ Hz, $^3J(^{14}N,^1H) = 1.9$ Hz, 12H, CH_3). ^{19}F NMR (376 MHz, CD_3CN , 243 K): $\delta/ppm = -74.2$ (s). IR (ATR, 233 K) $\tilde{\nu}/cm^{-1} = 3023, 3008, 1487, 1443, 1397, 1305, 1287, 1252, 1236, 1221, 1163, 1116, 1097, 999, 965, 783, 767, 725, 669, 573, 536, 510, 427, 357, 333, 319, 295, 274, 216, 187, 172, 151$. Raman (1064 nm, 298 K) $\tilde{\nu}/cm^{-1} = 3006, 2969, 2952, 2895, 1467, 1354, 1291, 1227, 1155, 1117, 969, 772, 686, 575, 541, 519, 467, 451, 416, 366, 323, 300, 281, 227, 191, 157, 110, 81$. CCDC number: 2105589.

Synthesis of $[NEt_4][BrF_2(OC_4F_9)_2]$ 5: **Route A:** 2 (160 mg, 0.238 mmol, 1 eq) was dissolved in propionitrile (3 ml) at –30 °C. Dilute fluorine (10 % in Ar) was bubbled through the solution for 3 min at a flow rate of 20 $ml\ min^{-1}$ at –35 °C. After slowly cooling to –80 °C the product was obtained as single crystals. **Route B:** A solution of $[NEt_4][BrF_4]$ (55 mg, 0.190 mol, 1 eq) in propionitrile (1 ml) was prepared as described elsewhere.^[19] Perfluoro-*tert*-butyl hypochlorite (308 mg, 1.14 mmol, 6 eq) was added at –196 °C. The reaction

mixture was allowed to warm to -40 °C and stirred for 15 min. After slowly cooling to -80 °C the product was obtained as single crystals. IR (ATR, 233 K) $\tilde{\nu}/\text{cm}^{-1}$ = 3006, 1491, 1460, 1450, 1382, 1243, 1208, 1192, 1162, 1092, 1040, 1009, 996, 977, 964, 868, 808, 782, 767, 732, 724, 674, 578, 537, 515, 465, 358, 334, 323, 288, 248, 211, 186, 151, 118. Raman (crystal, 1064 nm, 77 K) $\tilde{\nu}/\text{cm}^{-1}$ = 3010, 2957, 1467, 996, 770, 734, 674, 538, 521, 477, 437, 416, 387, 326, 295, 192, 155, 131, 93, 76. CCDC number: 2105582.

Acknowledgements

We gratefully acknowledge the ZEDAT at Freie Universität Berlin for providing computing resources. Additionally, we are grateful for donations of chemicals from the Solvay company. The ERC HighPotOx (Grant agreement ID:818862) is acknowledged for funding. Furthermore, P.P. acknowledges VCI for providing PhD funding (Kekulé Fellowship). Open Access funding enabled and organized by Projekt DEAL.

Conflict of Interest




The authors declare no conflict of interest.

Keywords: computational chemistry · fluorine chemistry · halogen chemistry · oxidation agents

- [1] R. Minkwitz, R. Bröchler, A. Kornath, R. Ludwig, F. Rittner, *Inorg. Chem.* **1997**, *36*, 2147.
- [2] J. D. O. Anderson, D. D. DesMarteau, *J. Fluorine Chem.* **1996**, *77*, 147.
- [3] J. H. Nissen, L. Wickemeyer, T. Stüker, S. Steinhauer, H. Beckers, S. Riedel, *J. Fluorine Chem.* **2019**, *230*, 109416.
- [4] T. Sandmeyer, *Ber. Dtsch. Chem. Ges.* **1886**, *19*, 857.
- [5] F. D. Chattaway, O. G. Backeberg, *J. Chem. Soc. Trans.* **1923**, *123*, 2999.
- [6] K. Seppelt, *Angew. Chem. Int. Ed.* **1979**, *18*, 186; *Angew. Chem.* **1979**, *91*, 199.
- [7] A. Yoshimura, V. V. Zhdankin, *Chem. Rev.* **2016**, *116*, 3328.
- [8] a) S. Ivlev, P. Woidy, F. Kraus, I. Gerin, R. Ostvald, *Eur. J. Inorg. Chem.* **2013**, *158*, 4984–4987; b) S. Rozen, *Adv. Synth. Catal.* **2010**, *352*, 2691.
- [9] J. P. Farr, W. L. Smith, D. S. Steichen in *Kirk-Othmer Encyclopedia of Chemical Technology*, John Wiley & Sons, Inc., Hoboken, NJ, USA, **2000**, S. 83.
- [10] a) W. Breuer, H. J. Frohn, *J. Fluorine Chem.* **1987**, *34*, 443; b) H. J. Frohn, M. Giesen, *J. Fluorine Chem.* **1984**, *24*, 9.
- [11] a) R. Minkwitz, R. Bröchler, *Z. Anorg. Chem.* **1997**, *623*, 487; b) R. Minkwitz, R. Bröchler, R. Ludwig, *Inorg. Chem.* **1997**, *36*, 4280.
- [12] M. Lustig, J. K. Ruff, *Inorg. Chem.* **1966**, *5*, 2124.
- [13] M. Lustig, G. H. Cady, *Inorg. Chem.* **1962**, *1*, 714.
- [14] K. O. Christe, C. J. Schack, *Inorg. Chem.* **1972**, *11*, 1682.
- [15] K. O. Christe, C. J. Schack, *Inorg. Chem.* **1974**, *13*, 1452.
- [16] K. O. Christe, D. Naumann, *Spectrochim. Acta A* **1973**, *29*, 2017.
- [17] K. Seppelt, *Angew. Chem. Int. Ed.* **2019**, *58*, 18928; *Angew. Chem.* **2019**, *131*, 19104.
- [18] F. Topić, J. M. Marrett, T. H. Borchers, H. M. Titi, C. J. Barrett, T. Friscic, *Angew. Chem. Int. Ed.* **2021**, <https://doi.org/10.1002/anie.202108843>.
- [19] X. Zhang, K. Seppelt, *Z. Anorg. Allg. Chem.* **1997**, *623*, 491.
- [20] I. M. Riddlestone, A. Kraft, J. Schaefer, I. Krossing, *Angew. Chem. Int. Ed.* **2018**, *57*, 13982; *Angew. Chem.* **2018**, *130*, 14178.
- [21] I. Krossing, I. Raabe, *Angew. Chem. Int. Ed.* **2004**, *43*, 2066; *Angew. Chem.* **2004**, *116*, 2116.
- [22] P. Pröhm, J. R. Schmid, K. Sonnenberg, S. Steinhauer, C. J. Schattnerberg, R. Müller, M. Kaupp, P. Voßnacker, S. Riedel, *Angew. Chem. Int. Ed.* **2020**, *59*, 16002; *Angew. Chem.* **2020**, *132*, 16136.
- [23] J. R. Schmid, P. Pröhm, P. Voßnacker, G. Thiele, M. Ellwanger, S. Steinhauer, S. Riedel, *Eur. J. Inorg. Chem.* **2020**, *2020*, 4497.
- [24] W. W. Wilson, K. O. Christe, *Inorg. Chem.* **1989**, *28*, 4172.
- [25] J. H. Nissen, T. Stüker, T. Drews, S. Steinhauer, H. Beckers, S. Riedel, *Angew. Chem. Int. Ed.* **2019**, *58*, 3584; *Angew. Chem.* **2019**, *131*, 3622–3626.
- [26] D. E. Young, L. R. Anderson, D. E. Gould, W. B. Fox, *J. Am. Chem. Soc.* **1970**, *92*, 2313.
- [27] A. Reisinger, D. Himmel, I. Krossing, *Angew. Chem. Int. Ed.* **2006**, *45*, 6997–7000; *Angew. Chem.* **2006**, *45*, 7156–7156.
- [28] R. K. Harris, E. D. Becker, S. M. Cabral de Menezes, P. Granger, R. E. Hoffman, K. W. Zilm, *Pure Appl. Chem.* **2008**, *80*, 59.
- [29] G. M. Sheldrick, *Acta Crystallogr. Sect. A* **2015**, *71*, 3.
- [30] G. M. Sheldrick, *Acta Crystallogr. Sect. C* **2015**, *71*, 3.
- [31] O. V. Dolomanov, L. J. Bourhis, R. J. Gildea, J. A. K. Howard, H. Puschmann, *J. Appl. Crystallogr.* **2009**, *42*, 339.
- [32] K. Brandenburg, *DIAMOND*, Crystal Impact GbR, Bonn, **2014**.
- [33] TURBOMOLE GmbH, *TURBOMOLE V7.3*. a) *development of University of Karlsruhe and Forschungszentrum Karlsruhe GmbH*, **2018**.
- [34] a) A. D. Becke, *J. Chem. Phys.* **1993**, *98*, 1372; b) C. Lee, W. Yang, R. G. Parr, *Phys. Rev. B* **1988**, *37*, 785; c) P. J. Stephens, F. J. Devlin, C. F. Chabalowski, M. J. Frisch, *J. Phys. Chem.* **1994**, *98*, 11623.
- [35] S. Grimme, J. Antony, S. Ehrlich, H. Krieg, *J. Chem. Phys.* **2010**, *132*, 154104.
- [36] S. Grimme, S. Ehrlich, L. Goerigk, *J. Comput. Chem.* **2011**, *32*, 1456.
- [37] F. Weigend, R. Ahlrichs, *Phys. Chem. Chem. Phys.* **2005**, *7*, 3297.
- [38] K. A. Peterson, D. Figgen, E. Goll, H. Stoll, M. Dolg, *J. Chem. Phys.* **2003**, *119*, 11113.
- [39] M. J. Frisch, G. W. Trucks, H. B. Schlegel, G. E. Scuseria, M. A. Robb, J. R. Cheeseman, G. Scalmani, V. Barone, G. A. Petersson, H. Nakatsuji, X. Li, M. Caricato, A. V. Marenich, J. Bloino, B. G. Janesko, R. Gomperts, B. Mennucci, H. P. Hratchian, J. V. Ortiz, A. F. Izmaylov, J. L. Sonnenberg, D. Williams-Young, F. Ding, F. Lipparini, F. Egidi, J. Goings, B. Peng, A. Petrone, T. Henderson, D. Ranasinghe, V. G. Zakrzewski, J. Gao, N. Rega, G. Zheng, W. Liang, M. Hada, M. Ehara, K. Toyota, R. Fukuda, J. Hasegawa, M. Ishida, T. Nakajima, Y. Honda, O. Kitao, H. Nakai, T. Vreven, K. Throssell, J. A. Montgomery, Jr., J. E. Peralta, F. Ogliaro, M. J. Bearpark, J. J. Heyd, E. N. Brothers, K. N. Kudin, V. N. Staroverov, T. A. Keith, R. Kobayashi, J. Normand, K. Raghavachari, A. P. Rendell, J. C. Burant, S. S. Iyengar, J. Tomasi, M. Cossi, J. M. Millam, M. Klene, C. Adamo, R. Cammi, J. W. Ochterski, R. L. Martin, K. Morokuma, O. Farkas, J. B. Foresman, D. J. Fox, *Gaussian 16*, Gaussian, Inc., Wallingford CT, **2016**.
- [40] E. D. Glendening, J. K. Badenhoop, A. E. Reed, J. E. Carpenter, J. A. Bohmann, C. M. Morales, P. Karafiloglou, C. R. Landis, F. Weinhold, *NBO 7.0*, Theoretical Chemistry Institute, University of Wisconsin, Madison, WI, **2018**.

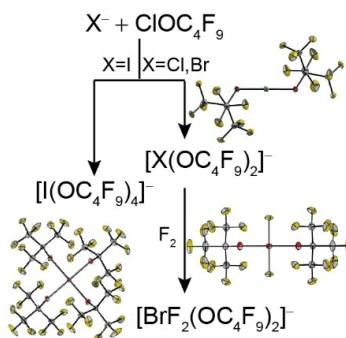
Manuscript received: September 13, 2021

Accepted manuscript online: October 14, 2021

Version of record online:   

FULL PAPER

Chemistry with halogens in positive oxidation states, especially the lighter halogens, is challenging due to their high oxidation potential. An ensemble of halogen +I and +III compounds with a comparatively large ligand system was synthesized and characterized with experimental and quantum-chemical methods. This study is envisioned as an example for the diverse but sometimes overlooked chemistry of group 17.



*P. Pröhm, W. R. Berg, S. M. Rupf, P. Voßnacker, Prof. Dr. S. Riedel**

1 – 7

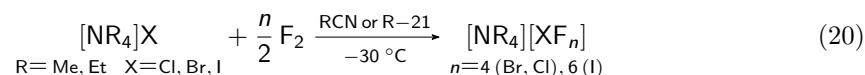
Investigation of Bis(Perfluoro-*tert*-Butoxy) Halogenates(I/III)



4. Conclusion and Outlook

4.1. Conclusion

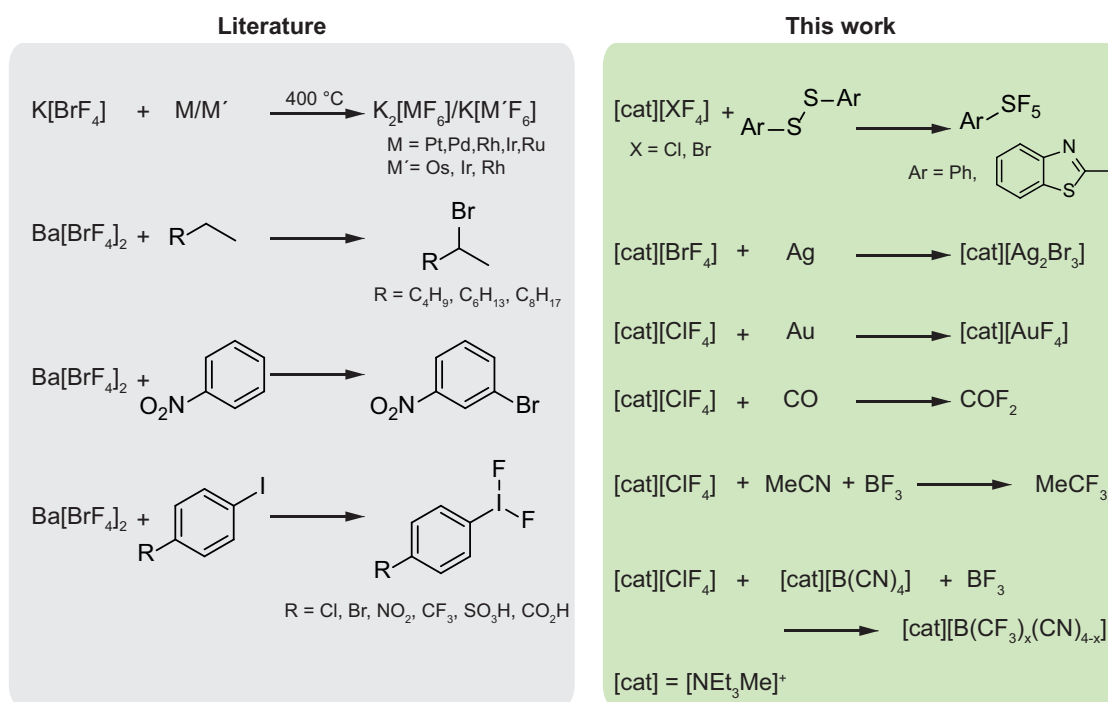
This thesis is concerned with anionic group 17 complexes with halogens in positive oxidation states. Novel synthetic pathways for their syntheses as well as their follow-up chemistry were studied. The first major step was the development of a straightforward method for the synthesis of organo-soluble tetraalkylammonium tetrafluoridochlorate(III) and -bromate(III) as well as hexafluoridoiodate(V) salts. For this purpose, the reaction of tetraalkylammonium chloride, bromide or iodide salts and dilute fluorine (10 % in Ar) in MeCN, EtCN or dichlorofluoromethane (R-21) at low temperatures (Eq. 20) was developed and optimized. This new protocol represents a one-step procedure to $[\text{XF}_4]^-$ -containing organic solutions without the need of further cation metathesis or workup. Secondly, the reaction proceeds without the use of BrF_3 or ClF_3 and instead uses less dangerous diluted fluorine^[196,197] which can be handled in standard laboratory glassware. The reactions can be performed on a multi-gram scale and the obtained solutions have concentrations up to $8 \text{ mol}\cdot\text{l}^{-1}$. This new methodology for the easy preparation of tetrafluoridohalogenate(III)-containing solutions enabled the investigation of their follow-up chemistry (Scheme 2).



Inspired by the unique reactivity of ClF_3 , the reaction of a tetrafluoridochlorate(III) $[\text{ClF}_4]^-$ with a tetracyanidoborate $[\text{B}(\text{CN})_4]^-$ salt and an additional Lewis acid (BF_3) led to a mixture of borate anions with trifluoromethyl and cyanido ligands $[\text{B}(\text{CF}_3)_x(\text{CN})_{4-x}]^-$. This indicates that the inherent reactivity of ClF_3 is preserved in $[\text{ClF}_4]^-$. The same reaction with $[\text{BrF}_4]^-$ was not successful. A similar reaction was investigated with organic nitriles such as acetonitrile, which showed the conversion of the nitrile group into a trifluoromethyl group, a reaction that is known with BrF_3 as a reagent.^[198] As a more technical application the dissolution of noble metals was studied. Gold metal was dissolved at room temperature in a $[\text{ClF}_4]^-$ -containing MeCN solution under formation of tetrafluoridoaurate(III) $[\text{AuF}_4]^-$. The dissolution of gold with $[\text{BrF}_4]^-$ under the same conditions is less efficient and only traces of $[\text{AuF}_4]^-$ can be obtained. However, the dissolution of silver in a $[\text{BrF}_4]^-$ -containing solution under formation of $[\text{Ag}_2\text{Br}_3]^-$ is much faster. This process (metal leaching) is a vital step for the recovery of metals and was previously demonstrated with other polyhalides and polyinterhalides. The selectivity for specific metals can be used for their separation, which otherwise requires a second process. The reaction of carbon monoxide with a solution of $[\text{ClF}_4]^-$ leads selectively to carbonyl fluoride COF_2 , analogous to the reaction of a trichloride with CO to phosgene COCl_2 (*vide supra*). A reactivity pattern more relevant in organic chemistry is the transformation of aromatic disulfides (Ar-S-S-Ar) to pentafluorosulfanyl-functionalized molecules which find widespread application in medical, agro

4. Conclusion and Outlook

and materials chemistry.^[199–204] This transformation can be accomplished in a one-step reaction by $[\text{XF}_4]^-$ ($\text{X} = \text{Cl}, \text{Br}$) containing solutions. Procedures reported in the literature usually use a two-step reaction.^[205] In the reaction of $[\text{BrF}_4]^-$ with 2,2'-dithiobis(benzothiazole) selectively the disulfide moiety was oxidized. The reactivity studies presented here, in combination with the literature-known examples (Scheme 2), show that the high reactivity of tetrafluoridochlorate(III) and -bromate(III) can be used for a variety of reactions in inorganic and organic synthesis.



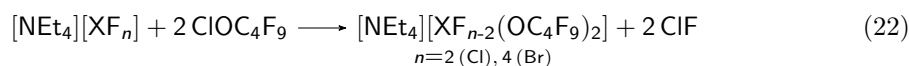
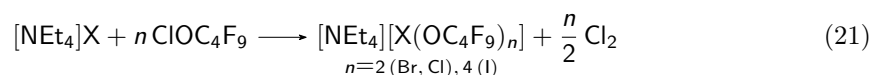
Scheme 2. Different reactivities of $[\text{XF}_4]^-$ ($\text{X} = \text{Cl}, \text{Br}$) salts.

In addition, the far less characterized difluoridohalogenates(I) of bromine and chlorine were studied. Previously, only vibrational spectroscopic data hinted at the linear structure of the anions. Two significantly different ^{19}F NMR chemical shifts are reported for $[\text{BrF}_2]^-$, while for $[\text{ClF}_2]^-$ no NMR data are known at all. During the fluorination reactions of X^- to $[\text{XF}_4]^-$ ($\text{X} = \text{Cl}, \text{Br}$) the observed intermediates were $[\text{XF}_2]^-$. Substoichiometric usage of fluorine led to mixtures of $[\text{XF}_2]^-$ and $[\text{XF}_4]^-$. In case of bromine the structure $[\text{NEt}_3\text{Me}][\text{BrF}_2]$ was determined crystallographically. In case of chlorine, a crystal containing both anionic moieties $[\text{ClF}_2]^-$ and $[\text{ClF}_4]^-$ was analyzed by X-Ray diffraction. However, pure samples of $[\text{NR}_4][\text{ClF}_2]$ were obtained when ClF was used as a fluorination reagent instead of elemental fluorine. The determination of the structures of $[\text{XF}_2]^-$ ($\text{X} = \text{Cl}, \text{Br}$) filled two out of four missing gaps amongst the known fluoridohalogenates, leaving only $[\text{ClF}_6]^-$ and $[\text{IF}_5]^{2-}$ without structural characterization. Furthermore, the ^{19}F NMR chemical shifts were experimentally determined, which refute MINKWITZ' report for $[\text{BrF}_2]^-$. Quantum-chemical calculations of the ^{19}F NMR chemical shifts showed accurate results for tetra- and hexafluoridohalogenates with only implicit solvent modeling. However, for difluoridohalogenate(I) anions explicit modeling of the first solvent shell was necessary to obtain accurate results due to strong interactions between solute and solvent.

So far, the di- and tetrafluoridohalogenates were only used as reagents. However, they also bear potential as substrates in ligand exchange reactions and therefore serve as a source for positively charged halogens. Table 19 shows an overview of the known anionic halogenate complexes with polyatomic oxygen-based ligands. Up to now (Section 3.4), only one structure of this type was literature-known. In this work, halogenate complexes with perfluoro-*tert*-butoxy ligands of chlorine, bromine and iodine were systematically studied, as well as structurally and spectroscopically characterized. The first chlorate anion with polyatomic ligands could be described. The perfluoro-*tert*-butoxy ligands were introduced from their hypochlorite by reaction with either a halide salt (Eq. 21) or a classical fluoridohalogenate (Eq. 22) under elimination of chlorine or chlorine monofluoride, depending on the employed starting material. In case of the I(I) containing salt, the perfluoro-*tert*-butoxy ligands were introduced by reaction of its silver(I) salts with dichloridoiodate (Eq. 23). Overall, the perfluoro-*tert*-butoxy halogenate compounds are somewhat comparable with the corresponding fluoridohalogenates with regard to the halogen-ligand-bonding. Both can be described by a 3c-4e bond and the natural charges of the central halogen atoms are very similar. Differences became obvious when comparing their reactivities. The perfluoro-*tert*-butoxy ligand itself is not stable in the presence of a chlorine(III) center, which oxidized the oxygen atom under generation of bisperfluoro-*tert*-butyl peroxide or perfluoro-*tert*-butyl hypofluorite. For iodine(III) the steric bulk of the ligands prevented any further fluorination.

Table 19. Known halogenate anions with polyatomic ligands. Entries marked with an asterisk are not structurally characterized. Green entries represent findings from this work, gray from the literature.

	Cl	Br	I
+I	[Cl(OC ₄ F ₉) ₂] ⁻	[Br(OC ₄ F ₉) ₂] ⁻	[I(OC ₄ F ₉) ₂] ⁻
		[Br(NO ₃) ₂] ⁻	[I(NO ₃) ₂] ^{-*}
		[Br(ClO ₄) ₂] ^{-*}	[I(ClO ₄) ₂] ^{-*}
		[Br(OCF ₃) ₂] ^{-*}	
+III	-	[BrF ₂ (OC ₄ F ₉) ₂] ⁻	[I(OC ₄ F ₉) ₄] ⁻
		[Br(SO ₃ F) ₄] ^{-*}	[I(SO ₃ F) ₄] ^{-*}
			[I(NO ₃) ₄] ^{-*}
			[I(O ₂ CCF ₃) ₄] ^{-*}



In the last project the non-classical fluoridochlorate [NMe₄][F(ClF)₃] was synthesized. After Cs[F(ClF₃)₃], it is only the second non-classical polyinterhalide based on these two elements. In comparison to similar polyhalides and -interhalides with other halogens, especially with other central atoms (e.g. [Cl₇]⁻ or [Cl(BrCl)₃]⁻), these compounds have the remarkable feature that

their calculated gas-phase structures are not pyramidal as predicted by the VSEPR model and found for several other seven atomic polyhalides and polyinterhalides. Instead, their calculated structures have a trigonal planar shape. The solid-state structures show some degree of pyramidalization. Generally, there are only small energy differences between pyramidal and planar $[\text{F}(\text{ClF})_3]^-$. Additionally, the cation forms three hydrogen bonds to the apical fluorine atom, meaning that the distortion of the minimum gas-phase structure can be traced back to intermolecular cation anion interactions in the solid state. Quantum-chemical calculations on $[\text{F}(\text{ClF})_3]^-$, $[\text{F}(\text{Cl}_2)_3]^-$ and $[\text{Cl}(\text{ClF})_3]^-$ revealed the central fluorine atom as the structure determining factor. Its bonding to the ClF ligands is more ionic than for a central chlorine atom and additionally bears a high charge-shift character.

Overall, this thesis expanded the field of polyhalide chemistry, especially chlorine and fluorine containing compounds, by simplifying synthetic access, studying their reactivity, and synthesizing unprecedented examples.

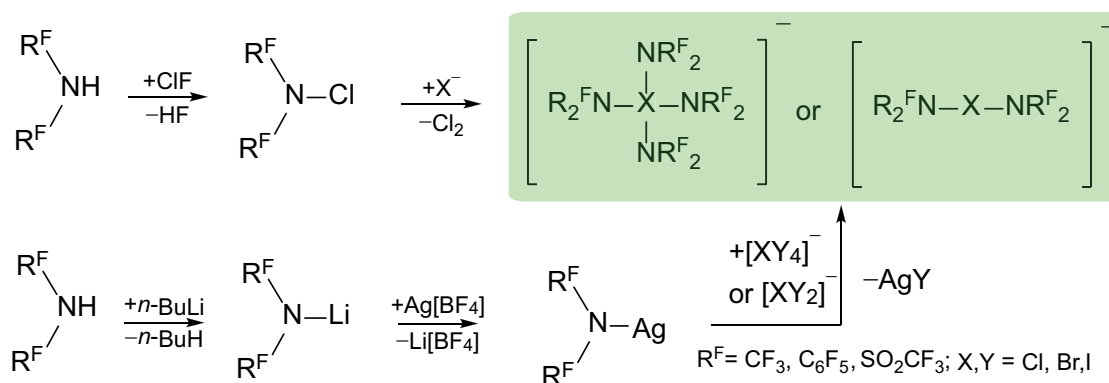
4.2. Outlook

As presented above, tetrafluoridohalogenates have potential as reagents in urban mining processes. In combination with other polyhalides and polyinterhalides, a reaction cascade for the extraction and separation of specific metals or groups of metals could be possible, depending on their redox potential, solubility of the formed complexes and passivation properties. To realize that, further data especially on the dissolution kinetics of metals in polyhalide and -interhalide solutions and ionic liquids need to be acquired. These substances might contribute to solve the globally relevant problem of excessive e-waste production and exploitation of natural resources. Additionally, the easy availability of soluble tetrafluoridohalogenates reported in Section 3.1 and 3.2 paves the way for more in-depth studies of the reactivity of tetrafluoridohalogenates(III). To make them viable reagents in synthetic organic and inorganic chemistry, the functional group tolerance has to be evaluated and reaction conditions have to be further optimized.

The study presented in Section 3.4 is the first systematic approach to polyatomic halogenate complexes with positively charged central halogen atoms. For these compounds a deeper understanding of the bonding has to be developed along the existing models for polyhalides. This requires sophisticated computational studies, benchmarked by precise experimental data, such as vibrational spectroscopic measurements, as well as determination of experimental electron densities analogously to the existing investigations of polyhalides.

Especially nitrogen based ligands are rare. Therefore, halogenate complexes with ligand systems such as triflimide, perfluorodimethylamide or perfluorodiphenylamide could be synthetic targets. Analogous to the perfluoro-*tert*-butoxy halogenates, which were synthesized from the corresponding hypochlorite, the ligands could be introduced from the *N*-chloro-compounds (Scheme 3). They are known for *N*-chloro-triflimide and *N*-chloro-perfluorodimethylamine and generally synthesized from the amine or amide with ClF or Cl₂.^[206,207] A second potential synthetic route is the usage of silver(I) salts, which are commercially available or can probably be prepared by cation metathesis from the corresponding lithium compounds, analogous to silver(I) alcoholates.^[208]

With only two precedents of non-classical chlorido fluorido polyinterhalides, these are certainly



Scheme 3. Proposed synthetic path to halogenate complexes with N-based ligands.

understudied compounds. This is most likely a result of the experimentally challenging handling of chlorine fluorides. However, as Section 3.3 has shown, unexpected observations are found amongst these compounds. To fully understand the unique electronic and structure-giving properties of fluorine in polyhalides, further examples have to be prepared and theoretically investigated. The refinement of experimental techniques for the synthesis of such reactive molecules could potentially lead to the synthesis of the long-studied trifluoride anion on a preparative scale.

5. References

- [1] N. G. Connelly, *Nomenclature of inorganic chemistry: IUPAC Recommendations 2005*, Royal Society of Chemistry, Cambridge, **2005**.
- [2] H. Haller, S. Riedel, *Z. Anorg. Allg. Chem.* **2014**, *640*, 1281–1291.
- [3] D. Mootz, D. Boenigk, *Z. Anorg. Allg. Chem.* **1987**, *544*, 159–166.
- [4] D. Mootz, J. Hocken, *Angew. Chem. Int. Ed.* **1989**, *28*, 1697–1698.
- [5] A. Deeg, Th. Dahlems, D. Mootz, *Z. Kristallogr. NCS* **1997**, *212*, 401–402.
- [6] R. Hagiwara, T. Hirashige, T. Tsuda, Y. Ito, *J. Electrochem. Soc.* **2002**, *149*, D1–D6.
- [7] D. Mootz, J. Hocken, *Z. Naturforsch. B* **1989**, *44b*, 1239–1246.
- [8] D. Wiechert, D. Mootz, R. Franz, G. Siegemund, *Chem. Eur. J.* **1998**, *4*, 1043–1047.
- [9] A. Deeg, D. Mootz, *Z. Naturforsch. B* **1993**, *48b*, 571–576.
- [10] D. Mootz, W. Poll, *Z. Naturforsch. B* **1984**, *39b*, 1300–1305.
- [11] H. Yoshino, K. Matsumoto, R. Hagiwara, Y. Ito, K. Oshima, S. Matsubara, *J. Fluorine Chem.* **2006**, *127*, 29–35.
- [12] P. Vořnacker, S. Steinhauer, J. Bader, S. Riedel, *Chem. Eur. J.* **2020**, *26*, 13256–13263.
- [13] A. Lauterbach, G. Uber in *Kirk-Othmer Encyclopedia of Chemical Technology, Vol. 91*, John Wiley & Sons, Inc, Hoboken, NJ, USA, **2000**, p. 5.
- [14] R. Frim, S. D. Ukeles in *Kirk-Othmer Encyclopedia of Chemical Technology, Vol. 55*, John Wiley & Sons, Inc, Hoboken, NJ, USA, **2000**, p. 1406.
- [15] S. K. Mendiratta, R. L. Dotson, R. T. Brooker, Updated by Staff in *Kirk-Othmer Encyclopedia of Chemical Technology, Vol. 52*, John Wiley & Sons, Inc, Hoboken, NJ, USA, **2000**, p. 197.
- [16] S. K. Mendiratta, B. L. Duncan in *Kirk-Othmer Encyclopedia of Chemical Technology, Vol. 138*, (Ed.: I. John Wiley & Sons), Wiley, **2000**, p. 399.
- [17] J. A. Wojtowicz in *Kirk-Othmer Encyclopedia of Chemical Technology, Vol. 213*, John Wiley & Sons, Inc, Hoboken, NJ, USA, **2000**, p. 237.
- [18] B. S. Ault, L. Andrews, *J. Am. Chem. Soc.* **1976**, *98*, 1591–1593.
- [19] B. S. Ault, L. Andrews, *Inorg. Chem.* **1977**, *16*, 2024–2028.
- [20] A. A. Tuinman, A. A. Gakh, R. J. Hinde, R. N. Compton, *J. Am. Chem. Soc.* **1999**, *121*, 8397–8398.
- [21] A. Artau, K. E. Nizzi, B. T. Hill, L. S. Sunderlin, P. G. Wenthold, *J. Am. Chem. Soc.* **2000**, *122*, 10667–10670.

- [22] S. Riedel, T. Köchner, X. Wang, L. Andrews, *Inorg. Chem.* **2010**, *49*, 7156–7164.
- [23] F. A. Redeker, H. Beckers, S. Riedel, *RSC Adv.* **2015**, *5*, 106568–106573.
- [24] F. D. Chattaway, G. Hoyle, *J. Chem. Soc. Trans.* **1923**, *123*, 654–662.
- [25] R. Brückner, Dissertation, Freie Universität Berlin, Berlin, **2016**.
- [26] F. A. Redeker, H. Beckers, S. Riedel, *Chem. Commun.* **2017**, *53*, 12958–12961.
- [27] M. P. Bogaard, J. Peterson, A. D. Rae, *Acta Cryst. B* **1981**, *37*, 1357–1359.
- [28] R. T. Boeré, A. W. Cordes, S. L. Craig, R. T. Oakley, R. W. Reed, *J. Am. Chem. Soc.* **1987**, *109*, 868–874.
- [29] T. Chivers, J. F. Richardson, N. R. M. Smith, *Inorg. Chem.* **1985**, *24*, 2453–2458.
- [30] M. Jansen, S. Strojek, *Z. Naturforsch.* **1995**, *50b*, 1171–1174.
- [31] J. C. Evans, G. Y. S. Lo, *J. Chem. Phys.* **1966**, *44*, 3638–3639.
- [32] H. Keil, K. Sonnenberg, C. Müller, R. Herbst-Irmer, H. Beckers, S. Riedel, D. Stalke, *Angew. Chem. Int. Ed.* **2021**, *60*, 2569–2573.
- [33] X. Li, A. van den Bossche, T. Vander Hoogerstraete, K. Binnemans, *Chem. Commun.* **2018**, *54*, 475–478.
- [34] X. Li, Z. Li, M. Orefice, K. Binnemans, *ACS Sustain. Chem. Eng.* **2019**, *7*, 2578–2584.
- [35] P. Voßnacker, A. Wüst, T. Keilhack, C. Müller, S. Steinhauer, H. Beckers, S. Yogendra, Y. Schiesser, R. Weber, M. Reimann, R. Müller, M. Kaupp, S. Riedel, *Sci. Adv.* **2021**, *7*, eabj5186.
- [36] A. Yao, F. Qu, Y. Liu, G. Qu, H. Lin, S. Hu, X. Wang, T. Chu, *Dalton Trans.* **2019**, *48*, 16249–16257.
- [37] K. Sonnenberg, L. Mann, F. A. Redeker, B. Schmidt, S. Riedel, *Angew. Chem. Int. Ed.* **2020**, *59*, 5464–5493.
- [38] F. Pichierri, *Chem. Phys. Lett.* **2011**, *515*, 116–121.
- [39] M. Schneider, G. P. Rajarathnam, M. E. Easton, A. F. Masters, T. Maschmeyer, A. M. Vassallo, *RSC Adv.* **2016**, *6*, 110548–110556.
- [40] C. H. Winter, Y.-H. Han, R. L. Ostrander, A. L. Rheingold, *Angew. Chem. Int. Ed.* **1993**, *32*, 1161–1163.
- [41] C. Chiappe, E. Leandri, D. Pieraccini, *Chem. Commun.* **2004**, 2536–2537.
- [42] R. E. Buckles, J. P. Yuk, *J. Am. Chem. Soc.* **1953**, *75*, 5048–5052.
- [43] C. Djerassi, C. R. Scholz, *J. Am. Chem. Soc.* **1948**, *70*, 417.
- [44] J. Salazar, R. Dorta, *Synlett* **2004**, 1318–1320.
- [45] J. Pelletier, J. B. Caventou, *Ann. Chim. Phys.* **1819**, 142–177.
- [46] S. M. Jørgensen, *J. prakt. Chem.* **1870**, *2*, 433–458.
- [47] S. S. Block, *Disinfection, sterilization and preservation*, 5th Ed., Lippincott Williams & Wilkins, Philadelphia, **2001**.
- [48] R. C. Teitelbaum, S. L. Ruby, T. J. Marks, *J. Am. Chem. Soc.* **1980**, *102*, 3322–3328.

-
- [49] R. Kawano, M. Watanabe, *Chem. Commun.* **2005**, 2107–2109.
- [50] V. Vitske, H. Herrmann, M. Enders, E. Kaifer, H.-J. Himmel, *Chem. Eur. J.* **2012**, *18*, 14108–14116.
- [51] M. A. Beno, U. Geiser, K. L. Kostka, H. H. Wang, K. S. Webb, M. A. Firestone, K. D. Carlson, L. Nunez, M. H. Whangbo, J. M. Williams, *Inorg. Chem.* **1987**, *26*, 1912–1920.
- [52] K.-F. Tebbe, R. Buchem, *Z. Anorg. Allg. Chem.* **1998**, *624*, 671–678.
- [53] K. Neupert-Laves, M. Dobler, *Helv. Chim. Acta* **1975**, *58*, 432–442.
- [54] A. J. Blake, R. O. Gould, W.-S. Li, V. Lippolis, S. Parsons, C. Radek, M. Schröder, *Inorg. Chem.* **1998**, *37*, 5070–5077.
- [55] P. H. Svensson, L. Kloo, *Chem. Rev.* **2003**, *103*, 1649–1684.
- [56] J. Taraba, Z. Zak, *Inorg. Chem.* **2003**, *42*, 3591–3594.
- [57] C. Ercolani, J. Jubb, G. Pennesi, U. Russo, G. Trigiane, *Inorg. Chem.* **1995**, *34*, 2535–2541.
- [58] H. Stegemann, A. Oprea, K. Nagel, K.-F. Tebbe, *Z. Anorg. Chem.* **1997**, *623*, 89–103.
- [59] A. Hills, D. L. Hughes, G. J. Leigh, J. R. Sanders, *J. Chem. Soc. Dalton Trans.* **1991**, *25*, 61–64.
- [60] T. Vent-Schmidt, F. Brosi, J. Metzger, T. Schlöder, X. Wang, L. Andrews, C. Müller, H. Beckers, S. Riedel, *Angew. Chem. Int. Ed.* **2015**, *54*, 8279–8283.
- [61] P. Voßnacker, T. Keilhack, N. Schwarze, K. Sonnenberg, K. Seppelt, M. Malischewski, S. Riedel, *Eur. J. Inorg. Chem.* **2021**, *2021*, 1034–1040.
- [62] M. Wolff, A. Okrut, C. Feldmann, *Inorg. Chem.* **2011**, *50*, 11683–11694.
- [63] F. B. Alhanash, N. A. Barnes, S. M. Godfrey, R. Z. Khan, R. G. Pritchard, *Polyhedron* **2013**, *65*, 102–109.
- [64] R. Poli, J. C. Gordon, R. K. Khanna, P. E. Fanwick, *Inorg. Chem.* **1992**, *31*, 3165–3167.
- [65] M. W. Renner, K. M. Barkigia, Y. Zhang, C. J. Medforth, K. M. Smith, J. Fajer, *J. Am. Chem. Soc.* **1994**, *116*, 8582–8592.
- [66] H. Haller, M. Ellwanger, A. Higelin, S. Riedel, *Angew. Chem. Int. Ed.* **2011**, *50*, 11528–11532.
- [67] H. Haller, M. Ellwanger, A. Higelin, S. Riedel, *Z. Anorg. Allg. Chem.* **2012**, *638*, 553–558.
- [68] H. Haller, M. Hog, F. Scholz, H. Scherer, I. Krossing, S. Riedel, *Z. Naturforsch.* **2013**, *68b*, 1103–1107.
- [69] T. M. Beck, H. Haller, J. Streuff, S. Riedel, *Synthesis* **2014**, *46*, 740–747.
- [70] K. Sonnenberg, P. Pröhm, N. Schwarze, C. Müller, H. Beckers, S. Riedel, *Angew. Chem. Int. Ed.* **2018**, *57*, 9136–9140.
- [71] H. Haller, J. Schröder, S. Riedel, *Angew. Chem. Int. Ed.* **2013**, *52*, 4937–4940.
- [72] M. L. Munzarová, R. Hoffmann, *J. Am. Chem. Soc.* **2002**, *124*, 4787–4795.
- [73] G. C. Pimentel, *J. Chem. Phys.* **1951**, *19*, 446–448.
- [74] R. E. Rundle, *J. Am. Chem. Soc.* **1963**, *85*, 112–113.

- [75] G. A. Landrum, N. Goldberg, R. Hoffmann, *J. Chem. Soc. Dalton Trans.* **1997**, 3605–3613.
- [76] K. O. Christe, J. P. Guertin, *Inorg. Chem.* **1965**, *4*, 905–908.
- [77] D. E. Woon, T. H. Dunning, *Comput. Theor. Chem.* **2011**, *963*, 7–12.
- [78] M. Häser, *J. Am. Chem. Soc.* **1996**, *118*, 7311–7325.
- [79] L. Chen, D. E. Woon, T. H. Dunning, *Comput. Theor. Chem.* **2017**, *1116*, 73–85.
- [80] C. Wang, D. Danovich, S. Shaik, Y. Mo, *Chem. Eur. J.* **2017**, *23*, 8719–8728.
- [81] R. Brückner, H. Haller, M. Ellwanger, S. Riedel, *Chem. Eur. J.* **2012**, *18*, 5741–5747.
- [82] S. Shaik, D. Danovich, W. Wu, P. C. Hiberty, *Nat. Chem.* **2009**, *1*, 443–449.
- [83] T. Brinck, J. S. Murray, P. Politzer, *Int. J. Quantum Chem.* **1992**, *44*, 57–64.
- [84] T. Clark, M. Hennemann, J. S. Murray, P. Politzer, *J. Mol. Model.* **2007**, *13*, 291–296.
- [85] P. Politzer, J. S. Murray, T. Clark, *Phys. Chem. Chem. Phys.* **2013**, *15*, 11178–11189.
- [86] B. Schmidt, K. Sonnenberg, H. Beckers, S. Steinhauer, S. Riedel, *Angew. Chem. Int. Ed.* **2018**, *57*, 9141–9145.
- [87] F. A. Redeker, A. Kropman, C. Müller, S. E. Zewge, H. Beckers, B. Paulus, S. Riedel, *J. Fluorine Chem.* **2018**, *216*, 81–88.
- [88] R. C. L. Mooney, *Z. Kristallogr.* **1938**, *38*, 324–333.
- [89] O. J. Curnow, M. S. Abdelbassit, *Chem. Eur. J.* **2019**, *25*, 13294–13298.
- [90] T. Surles, L. A. Quarterman, H. H. Hyman, *J. Inorg. Nucl. Chem.* **1973**, *35*, 668–670.
- [91] X. Zhang, K. Seppelt, *Z. Anorg. Allg. Chem.* **1997**, *623*, 491–500.
- [92] S. Siegel, *Acta Cryst.* **1956**, *9*, 493–495.
- [93] K. O. Christe, W. W. Wilson, G. W. Drake, D. A. Dixon, J. A. Boatz, R. Z. Gnann, *J. Am. Chem. Soc.* **1998**, *120*, 4711–4716.
- [94] K. O. Christe, W. W. Wilson, R. V. Chirakal, J. C. P. Sanders, G. J. Schrobilgen, *Inorg. Chem.* **1990**, *29*, 3506–3511.
- [95] A. R. Mahjoub, A. Hoser, J. Fuchs, K. Seppelt, *Angew. Chem. Int. Ed.* **1989**, *28*, 1526–1527.
- [96] A. R. Mahjoub, K. Seppelt, *Angew. Chem. Int. Ed.* **1991**, *30*, 323–324.
- [97] A. R. Mahjoub, K. Seppelt, *Angew. Chem. Int. Ed.* **1991**, *30*, 876–878.
- [98] K. O. Christe, J. P. Guertin, *Inorg. Chem.* **1965**, *4*, 1785–1787.
- [99] K. O. Christe, W. Sawodny, J. P. Guertin, *Inorg. Chem.* **1967**, *6*, 1159–1162.
- [100] E. D. Whitney, R. O. MacLaren, T. J. Hurley, C. E. Fogle, *J. Am. Chem. Soc.* **1964**, *86*, 4340–4342.
- [101] E. D. Whitney, R. O. MacLaren, C. E. Fogle, T. J. Hurley, *J. Am. Chem. Soc.* **1964**, *86*, 2583–2586.
- [102] L. B. Asprey, J. L. Margrave, M. E. Silverthorn, *J. Am. Chem. Soc.* **1961**, *83*, 2955–2956.
- [103] D. H. Kelly, B. Post, R. W. Mason, *J. Am. Chem. Soc.* **1963**, *85*, 307–308.

-
- [104] W. W. Wilson, K. O. Christe, *Inorg. Chem.* **1989**, *28*, 4172–4175.
- [105] B. Scheibe, S. I. Ivlev, A. J. Karttunen, F. Kraus, *Eur. J. Inorg. Chem.* **2020**, 1319–1324.
- [106] K. S. Thanthiriwatte, M. Vasiliu, D. A. Dixon, K. O. Christe, *Inorg. Chem.* **2012**, *51*, 10966–10982.
- [107] K. O. Christe, W. Sawodny, *Z. Anorg. Allg. Chem.* **1970**, *374*, 306–309.
- [108] K. O. Christe, J. P. Guertin, *Inorg. Chem.* **1966**, *5*, 473–476.
- [109] K. O. Christe, W. Sawodny, *Z. Anorg. Allg. Chem.* **1968**, *357*, 125–133.
- [110] D. E. Ibbotson, J. A. Mucha, D. L. Flamm, J. M. Cook, *J. Appl. Phys.* **1984**, *56*, 2939–2942.
- [111] Y. Saito, T. Nishizawa, M. Hamaguchi, *Appl. Surf. Sci.* **2005**, *240*, 381–387.
- [112] Y. Saito, T. Kosuge, *Sol. Energy Mater. Sol. Cells* **2007**, *91*, 1800–1804.
- [113] H. Habuka, T. Sukenobu, H. Koda, T. Takeuchi, M. Aihara, *Jpn. J. Appl. Phys.* **2004**, *151*, G783.
- [114] H. Habuka, H. Koda, D. Saito, T. Suzuki, A. Nakamura, T. Takeuchi, M. Aihara, *J. Cryst. Growth* **2003**, *150*, G461.
- [115] Y. Saito, O. Yamaoka, A. Yoshida, *J. Electrochem. Soc.* **1990**, *56*, 1119–1121.
- [116] H. A. Bernhardt, E. J. Barber, R. A. Gustison, *Ind. Eng. Chem.* **1959**, *51*, 179–184.
- [117] E. Bernhardt, G. Henkel, H. Willner, G. Pawelke, H. Bürger, *Chem. Eur. J.* **2001**, *7*, 4696–4705.
- [118] K. R. Brower, *J. Org. Chem.* **1987**, *52*, 798–802.
- [119] D. A. Dixon, D. J. Grant, K. O. Christe, K. A. Peterson, *Inorg. Chem.* **2008**, *47*, 5485–5494.
- [120] T. Surles, L. A. Quarterman, H. H. Hyman, *J. Inorg. Nucl. Chem.* **1973**, 668–670.
- [121] A. G. Maki, R. Forneris, *Spectrochim. Acta Part A* **1967**, *23*, 867–880.
- [122] G. C. Hayward, P. J. Hendra, *Spectrochim. Acta Part A* **1967**, *23*, 2309–2314.
- [123] W. Gabes, H. Gerding, *Recl. Trav. Chim. Pays-Bas* **1971**, *90*, 157–164.
- [124] R. Minkwitz, R. Bröchler, R. Ludwig, *Inorg. Chem.* **1997**, *36*, 4280–4283.
- [125] S. I. Ivlev, R. V. Ostvald, F. Kraus, *Monatsh. Chem.* **2016**, *147*, 1661–1668.
- [126] S. Siegel, *Acta Cryst.* **1957**, *10*, 380.
- [127] W. G. Sly, R. E. Marsh, *Acta Cryst.* **1957**, *10*, 378–379.
- [128] A. J. Edwards, G. R. Jones, *J. Chem. Soc. A* **1969**, 1936.
- [129] I. Sheft, A. F. Martin, J. J. Katz, *J. Am. Chem. Soc.* **1956**, *78*, 1557–1559.
- [130] K. O. Christe, C. J. Schack, *Inorg. Chem.* **1970**, *9*, 1852–1858.
- [131] S. I. Ivlev, F. Kraus, *IUCrData* **2018**, *3*, 2493.
- [132] S. I. Ivlev, A. J. Karttunen, R. Ostvald, F. Kraus, *Z. Anorg. Allg. Chem.* **2015**, *641*, 2593–2598.

- [133] J. Shamir, I. Yaroslavsky, *Isr. J. Chem.* **1969**, *7*, 495–497.
- [134] S. I. Ivlev, P. Woidy, I. I. Zherin, R. V. Ostvald, F. Kraus, M. Voytenko, V. V. Shagalov, *Procedia Chem.* **2014**, *11*, 35–42.
- [135] A. V. Malin, S. I. Ivlev, R. V. Ostvald, F. Kraus, *IUCrData* **2020**, *5*, 2846–2869.
- [136] A. G. Sharpe, H. J. Emeléus, *J. Chem. Soc.* **1948**, 2135–2138.
- [137] K. O. Christe, W. W. Wilson, *Inorg. Chem.* **1986**, *25*, 1904–1906.
- [138] S. Ivlev, V. Sobolev, M. Hoelzel, A. J. Karttunen, T. Müller, I. Gerin, R. Ostvald, F. Kraus, *Eur. J. Inorg. Chem.* **2014**, 6261–6267.
- [139] S. Kaza, L. Yao, P. Bhada-Tata, F. van Woerden, *What a Waste 2. 0: A Global Snapshot of Solid Waste Management To 2050*, World Bank Publications, Washington, D. C, **2018**.
- [140] V. Forti, C. P. Baldé, R. Kuehr, Bel G., *The Global E-waste Monitor 2020: Quantities, flows and the circular economy potential. United Nations University (UNU)/United Nations Institute for Training and Research (UNITAR) – co-hosted SCYCLE Programme, International Telecommunication Union (ITU) & International Solid Waste Association (ISWA)*, Bonn/Geneva/Rotterdam.
- [141] A. M. Mamatova, A. M. Shakimova, K. I. Merkel, A. V. Malin, R. V. Ostvald, *J. Phys.: Conf. Ser.* **2020**, *1443*, 012021.
- [142] S. I. Ivlev, A. V. Malin, A. J. Karttunen, R. V. Ostvald, F. Kraus, *J. Fluorine Chem.* **2019**, *218*, 11–20.
- [143] S. Ivlev, P. Woidy, F. Kraus, I. Gerin, R. Ostvald, *Eur. J. Inorg. Chem.* **2013**, *158*, 4984–4987.
- [144] V. I. Sobolev, R. V. Ostvald, I. I. Zherin, T. V. Shushpanova, V. D. Filimonov, *Russ. J. Org. Chem.* **2021**, *57*, 297–299.
- [145] V. I. Sobolev, V. D. Filimonov, R. V. Ostvald, V. B. Radchenko, I. I. Zherin, *J. Fluorine Chem.* **2016**, *192*, 120–123.
- [146] M. A. Samakbaeva in *Chemistry and Chemical Technology in the XXI Century: Materials of the XX International Scientific and Practical Conference Named after Professor LP Kulev of Students and Young Scientists*, **2017**, pp. 449–450.
- [147] R. Bougon, P. Charpin, J. Soriano, *C. R. Acad. Sci. Ser. C* **1971**, *272*, 565–568.
- [148] K. O. Christe, W. W. Wilson, *Inorg. Chem.* **1989**, *28*, 3275–3277.
- [149] A. R. Mahjoub, X. Zhang, K. Seppelt, *Chem. Eur. J.* **1995**, *1*, 261–265.
- [150] H. Meinert, H. Klamm, *Z. Chem.* **1965**, *5*, 468–469.
- [151] D. Naumann, A. Meurer, *J. Fluorine Chem.* **1995**, *70*, 83–84.
- [152] K. O. Christe, W. W. Wilson, G. W. Drake, M. A. Petrie, J. A. Boatz, *J. Fluorine Chem.* **1998**, *88*, 185–189.
- [153] K. O. Christe, W. W. Wilson, R. D. Wilson, R. Bau, J. A. Feng, *J. Am. Chem. Soc.* **1990**, *112*, 7619–7625.
- [154] H. Sun, S. G. DiMagno, *J. Am. Chem. Soc.* **2005**, *127*, 2050–2051.

-
- [155] M. Schmeißer, P. Sartori, D. Naumann, *Chem. Ber.* **1970**, *103*, 590–593.
- [156] J. H. Miller, L. Andrews, *Inorg. Chem.* **1979**, *18*, 988–992.
- [157] K. O. Christe, D. Naumann, *Inorg. Chem.* **1973**, *12*, 59–62.
- [158] G. B. Hargreaves, R. D. Peacock, *J. Chem. Soc.* **1960**, 2373–2374.
- [159] M. Schmeißer, W. Ludovici, D. Naumann, P. Sartori, E. Scharf, *Chem. Ber.* **1968**, *101*, 4214–4220.
- [160] K. O. Christe, E. C. Curtis, D. A. Dixon, H. P. Mercier, J. C. P. Sanders, G. J. Schrobilgen, *J. Am. Chem. Soc.* **1991**, *113*, 3351–3361.
- [161] K. O. Christe, *Inorg. Chem.* **1972**, *11*, 1215–1219.
- [162] C. J. Adams, *Inorg. Nucl. Chem. Lett.* **1974**, *10*, 831–835.
- [163] F. Seel, M. Pimpl, *J. Fluorine Chem.* **1977**, *10*, 413–430.
- [164] K. O. Christe, J. C. P. Sanders, G. J. Schrobilgen, W. W. Wilson, *J. Chem. Soc. Chem. Commun.* **1991**, *28*, 837–840.
- [165] A. Lashgari, S. Ghammamy, R. Ramirez-Tagle, G. Salgado-Moran, *J. Struct. Chem.* **2015**, *56*, 1505–1513.
- [166] D. D. Desmarteau, T. Grelbig, S.-H. Hwang, K. Seppelt, *Angew. Chem. Int. Ed.* **1990**, *29*, 1448–1449.
- [167] T. Drews, R. Marx, K. Seppelt, *Chem. Eur. J.* **1996**, *2*, 1303–1307.
- [168] B. M. Powell, K. M. Heal, B. H. Torrie, *Mol. Phys.* **1984**, *53*, 929–939.
- [169] G. L. Breneman, R. D. Willett, *Acta Cryst. B* **1969**, *25*, 1073–1076.
- [170] F. Lovas, Diatomic Spectral Database, NIST Standard Reference Database 114, **2002**.
- [171] L. Stein, *J. Fluorine Chem.* **1985**, *27*, 249–256.
- [172] S. Ivlev, P. Woidy, V. Sobolev, I. Gerin, R. Ostvald, F. Kraus, *Z. Anorg. Allg. Chem.* **2013**, *639*, 2846–2850.
- [173] S. I. Ivlev, A. J. Karttunen, R. V. Ostvald, F. Kraus, *Chem. Commun.* **2016**, *52*, 12040–12043.
- [174] J. Bandemehr, M. Sachs, S. I. Ivlev, A. J. Karttunen, F. Kraus, *Eur. J. Inorg. Chem.* **2020**, *2020*, 64–70.
- [175] J. Linnera, S. I. Ivlev, F. Kraus, A. J. Karttunen, *Z. Anorg. Allg. Chem.* **2019**, *645*, 284–291.
- [176] J. Bandemehr, S. I. Ivlev, A. J. Karttunen, F. Kraus, *Eur. J. Inorg. Chem.* **2020**, *2020*, 4568–4576.
- [177] D. W. Magnuson, *J. Chem. Phys.* **1957**, *27*, 223–226.
- [178] B. Scheibe, A. J. Karttunen, U. Müller, F. Kraus, *Angew. Chem. Int. Ed.* **2020**, *59*, 18116–18119.
- [179] J. A. Berry, D. W. Sharp, J. M. Winfield, *Inorg. Nucl. Chem. Lett.* **1976**, *12*, 869–871.
- [180] A. D. McNaught, A. Wilkinson, *IUPAC. Compendium of Chemical Terminology (the "Gold Book")*, 2nd ed., Blackwell Scientific Publications, Oxford, **1997**.

- [181] J. P. Farr, W. L. Smith, D. S. Steichen in *Kirk-Othmer Encyclopedia of Chemical Technology*, Vol. 5, John Wiley & Sons, Inc, Hoboken, NJ, USA, **2000**, p. 83.
- [182] K. Seppelt, *Angew. Chem. Int. Ed.* **1979**, *18*, 186–202.
- [183] K. O. Christe, C. J. Schack, *Adv. Inorg. Chem. Radiochem.* **1976**, *18*, 319–398.
- [184] U. Müller, R. Dübgen, K. Dehnicke, *Z. Anorg. Allg. Chem.* **1980**, *463*, 7–13.
- [185] R. Dübgen, K. Dehnicke, *Naturwissenschaften* **1978**, *65*, 535.
- [186] M. Lustig, J. K. Ruff, *Inorg. Chem.* **1966**, *5*, 2124–2125.
- [187] M. Lustig, G. H. Cady, *Inorg. Chem.* **1962**, *1*, 714–715.
- [188] K. O. Christe, C. J. Schack, *Inorg. Chem.* **1974**, *13*, 1452–1455.
- [189] K. O. Christe, C. J. Schack, *Inorg. Chem.* **1972**, *11*, 1682–1685.
- [190] D. Naumann, M. Schmeisser, R. Scheele, *J. Fluorine Chem.* **1972**, *1*, 321–326.
- [191] F. Aubke, H. A. Carter, S. P. L. Jones, *Inorg. Chem.* **1970**, *9*, 2485–2488.
- [192] K. Seppelt, *Angew. Chem. Int. Ed.* **2019**, *58*, 18928–18930.
- [193] W. W. Wilson, K. O. Christe, *Inorg. Chem.* **1987**, *26*, 1573–1580.
- [194] K. O. Christe, D. Naumann, *Spectrochim. Acta Part A* **1973**, *29*, 2017–2024.
- [195] R. Minkwitz, R. Bröchler, *Z. Anorg. Chem.* **1997**, *623*, 487–490.
- [196] S. Rozen, *Acc. Chem. Res.* **1996**, *29*, 243–248.
- [197] S. Rozen, *Eur. J. Org. Chem.* **2005**, *2005*, 2433–2447.
- [198] T. Stevens, *J. Org. Chem.* **1961**, *26*, 1627–1630.
- [199] P. R. Savoie, J. T. Welch, *Chem. Rev.* **2015**, *115*, 1130–1190.
- [200] M. F. Sowaileh, R. A. Hazlitt, D. A. Colby, *ChemMedChem* **2017**, *12*, 1481–1490.
- [201] J. M. W. Chan, *J. Mater. Chem. C* **2019**, *7*, 12822–12834.
- [202] A. M. Sipyagin, V. S. Enshov, S. A. Kashtanov, C. P. Bateman, B. D. Mullen, Y.-T. Tan, J. S. Thrasher, *J. Fluorine Chem.* **2004**, *125*, 1305–1316.
- [203] D. S. Lim, J. S. Choi, C. S. Pak, J. T. Welch, *J. Pestic. Sci.* **2007**, *32*, 255–259.
- [204] P. Kirsch, M. Bremer, *Angew. Chem. Int. Ed.* **2000**, *39*, 4216–4235.
- [205] C. R. Pitts, D. Bornemann, P. Liebing, N. Santschi, A. Togni, *Angew. Chem. Int. Ed.* **2019**, *58*, 1950–1954.
- [206] J. Foropoulos, D. D. Desmarteau, *Inorg. Chem.* **1984**, *23*, 3720–3723.
- [207] H. J. Emeléus, B. W. Tattershall, *Z. Anorg. Allgem. Chem.* **1964**, *327*, 147–150.
- [208] A. Reisinger, D. Himmel, I. Krossing, *Angew. Chem. Int. Ed.* **2006**, *45*, 6997–7000.

6. List of Publications

- Publications** **Investigation of bis(perfluoro-*tert*-butoxy) halogenates(I/III)**
Patrick Pröhm, Willi Berg, Susanne M. Rupf, Patrick Voßnacker, Sebastian Riedel *Chem. Eur. J.* **2021** DOI: 10.1002/chem.202103325.
- Non-classical polyinterhalides of chlorine monofluoride: experimental and theoretical characterization of $[\text{F}(\text{ClF})_3]^-$**
Patrick Pröhm, Nico Schwarze, Carsten Müller, Simon Steinhauer, Helmut Beckers, Susanne M. Rupf, Sebastian Riedel *Chem. Commun.* **2021**, 57, 4843-4846.
- Soluble Fluoridobromates as Well-Behaved Strong Fluorination Reagents**
Jonas R. Schmid[‡], Patrick Pröhm[‡], Patrick Voßnacker, Günter Thiele, Mathias Ellwanger, Simon Steinhauer, Sebastian Riedel *Eur. J. Inorg. Chem.* **2020**, 4497-4500.
- Improved Access to Organo-Soluble Di- and Tetrafluoridochlorate(I)/(III) Salts**
Patrick Pröhm, Jonas R. Schmid, Karsten Sonnenberg, Patrick Voßnacker, Simon Steinhauer, Caspar J. Schattenberg, Robert Müller, Martin Kaupp, Sebastian Riedel *Angew. Chem. Int. Ed.* **2020**, 59, 16002-16006.
- The [2+2] cycloaddition product of perhalogenated cyclopentadienyl cations: structural characterization of salts of the $[\text{C}_{10}\text{Cl}_{10}]^{2+}$ and $[\text{C}_{10}\text{Br}_{10}]^{2+}$ dications**
Susanne M. Rupf, Patrick Pröhm, Moritz Malischewski *Chem. Commun.* **2020**, 56, 9834-9837.
- Conformational Control in Main Group Phosphazane Anion Receptors and Transporters**
Alex J. Plajer, Jinbo Zhu, Patrick Pröhm, Felix J. Rizzuto, Ulrich F. Keyser, Dominic S. Wright *J. Am. Chem. Soc.* **2020**, 142, 1029-1037.
- Hydrogen-Bond-Assisted Symmetry Breaking in a Network of Chiral Metal–Organic Assemblies**
Felix J. Rizzuto[‡], Patrick Pröhm[‡], Alex J. Plajer, Jake L. Greenfield, Jonathan R. Nitschke *J. Am. Chem. Soc.* **2019**, 141, 1707-1715.
- Tailoring the Binding Properties of Phosphazane Anion Receptors and Transporters**

Alex J. Plajer, Jinbo Zhu, Patrick Pröhm, Andrew D. Bond, Ulrich F. Keyser, Dominic S. Wright, *J. Am. Chem. Soc.* **2019**, *141*, 8807-8815.

Beyond the limit: Investigation of large polychloride anions $[\text{Cl}_{11}]^-$, $[\text{Cl}_{12}]^{2-}$ and $[\text{Cl}_{13}]^-$

Karsten Sonnenberg, Patrick Pröhm, Nico Schwarze, Carsten Müller, Helmut Beckers, Sebastian Riedel *Angew. Chem. Int. Ed.* **2018**, *57*, 9136-9140.

How Changing the Bridgehead Can Affect the Properties of Tripodal Ligands

Alex J. Plajer, Annie L. Colebatch, Felix J. Rizzuto, Patrick Pröhm, Andrew D. Bond, Raúl Garcia-Rodriguez, Dominic S. Wright *Angew. Chem. Int. Ed.* **2018**, *57*, 6648-6652 .

Closing the gap: Structural evidence for the missing hexabromide dianion $[\text{Br}_6]^{2-}$

Karsten Sonnenberg, Patrick Pröhm, Carsten Müller, Helmut Beckers, Simon Steinhauer, Dieter Lentz, Sebastian Riedel *Chem. Eur. J.* **2018**, *24*, 1-5.

Formation and Characterization of $[\text{BrC}(\text{NMe}_2)_2][\text{Br}_3]$ and $[\text{BrC}(\text{NMe}_2)_2]_2[\text{Br}_8]$ in Ionic Liquids

Karsten Sonnenberg, Patrick Pröhm, Simon Steinhauer, Anja Wiesner, Carsten Müller, Sebastian Riedel *Z. Anorg. Allg. Chem.* **2017**, *643*, 101-105.

Structural Proof for the First Dianion of a Polychloride: Investigation of $[\text{Cl}_8]^{2-}$

Robin Brückner, Patrick Pröhm, Anja Wiesner, Simon Steinhauer, Carsten Müller, Sebastian Riedel, *Angew. Chem.* **2016**, *128*, 11064-11068.

Conferences

- 08/2021 GDCh-Wissenschaftsforum Chemie (online)
Poster: Halogens in positive oxidation states: From fluoro to $\text{OC}(\text{CF}_3)_3$ ligands
- 12/2019 FCI Fellowship Meeting, Berlin
Talk: A potpourri of polyhalides: Synthesis and application (Speaker prize)
- 09/2019 GDCh-Wissenschaftsforum Chemie, Aachen
Poster: Providing highly reactive, soluble fluorochlorates(I)/(III) as promising oxidation and fluorination reagents
- 09/2019 HalChem IX, Perugia, Italy
Talk: A potpourri of polyhalides: Synthesis and application
- 08/2019 19th European Symposium on Fluorine Chemistry, Warsaw, Poland
Poster: Soluble fluorochlorates(I)/(III) as fluorination reagents
- 04/2018 Dalton2018, Coventry, United Kingdom

Poster: Novelties from Polyhalide Chemistry

09/2017

GDCh–Wissenschaftsforum Berlin, Germany

Poster: Investigation of Higher Polychloride Structures

(GDCh Poster prize)

March 21, 2022

A. Supporting Information of Publications

A.1. Improved Access to Organo-Soluble Di- and Tetrafluoridochlorate(I/III) Salts



Supporting Information

Improved Access to Organo-Soluble Di- and Tetrafluoridochlorate-(I)/(III) Salts

*P. Pröhm, J. R. Schmid, K. Sonnenberg, P. Voßnacker, S. Steinhauer, C. J. Schattenberg, R. Müller, M. Kaupp, and S. Riedel**

[anie_202006268_sm_miscellaneous_information.pdf](#)

SUPPORTING INFORMATION

Supporting Information

Table of Contents

Experimental Section	3
Reactivity Studies	7
Crystallographic Section	15
Computational Section	16
References	17

Caution!

Fluorine, even under dilute conditions, is extraordinarily reactive and can react violently with organic materials under the formation of HF. Similarly, tetrafluoridochlorate(III) and difluoridochlorate(I) are strongly oxidizing compounds, which can decompose violently under certain conditions when exposed to organic materials. Exposure to acidic compounds (e.g. water or boron trifluoride) greatly enhances the reactivity due to the *in-situ* formation of ClF₃. Additionally, precipitation also greatly enhances the reactivity of tetrafluoridochlorate(III) and difluoridochlorate(I) compounds, leading to explosions at temperatures above -40 °C. Usage of PFA, FEP or PTFE may lower the risk of injury.

General Information

All experiments were performed under rigorous exclusion of moisture and oxygen using standard Schlenk techniques. Solids were handled in a dry box under argon atmosphere (O₂ < 0.5 ppm, H₂O < 0.5 ppm). HF addition experiments were performed in 3.8 mm PFA tubes with a stainless steel vacuum line. Acetonitrile and propionitrile were dried over Sicapent® prior to use. [NEt₄]Cl and [NEt₃Me]Cl were dried over night at 120 °C under dynamic vacuum. All other chemicals were used as purchased. ClF was synthesized according to literature.^[1]

Raman spectra were recorded on a Bruker MultiRAM II equipped with a low-temperature Ge detector (1064 nm, 30-80 mW, resolution, 4 cm⁻¹). NMR spectra were recorded on a JEOL 400 MHz ECS or ECZ spectrometer. All reported chemical shifts are referenced to the δ values given in IUPAC recommendations of 2008 using the ²H signal of the deuterated solvent as internal reference.^[2] For external locking acetone-d₆ was flame sealed in a glass capillary and the lock oscillator frequency was adjusted to give $\delta(^1\text{H}) = 7.26$ ppm for a CHCl₃ sample locked on the capillary. Crystal data were collected on a Bruker D8 Venture diffractometer with a Photon 100 CMOS area detector with MoK α radiation. Single crystal were picked at -80 °C under nitrogen atmosphere and mounted on a 0.15 mm Mitegen micromount using perfluoroether oil diluted with perfluorohexane. The structures were solved with the ShelXT^[3] structure solution program using intrinsic phasing and refined with the ShelXL^[4] refinement package using least squares minimizations by using OLEX2.^[5] For visualization the Diamond V3.0 program was used.^[6]

Structure optimizations and nonrelativistic shielding calculations for the [XF_n]⁻ (X = Cl, Br, I; n=2, 4, 6) anions and the CFCl₃ reference standard were performed using a developers' version of the TURBOMOLE program, release 7.4.^[7] Overall four sets of structures were optimized using def2-TZVPPD^[8] basis sets (including an effective core potential, ECP, for iodine^[9]) and TURBOMOLE standard grid setting 3. Two sets of structures were obtained at the BP86^[9]-D3(BJ)^[10] level, either in the gas phase or using the Conductor-like Screening Model (COSMO)^[11] with $r_{\text{solvent}} = 2.76$ [Å] and $\epsilon = 35.94$ (parameters for the solvent radius and finite permittivity of acetonitrile).

SUPPORTING INFORMATION

The other two sets were obtained at the B3LYP^[12]-D3(BJ)^[10] level of theory, also without and with COSMO solvent model. D3(BJ) stands for D3 atom-pairwise dispersion corrections with Becke-Johnson damping.^[10]

Subsequent nonrelativistic nuclear-shielding calculations at these structures used a recent improved DFT-GIAO^[13] implementation in Turbomole,^[14] extended to allow the use of local hybrid functionals.^[15] We used two functionals, which had previously been demonstrated to provide accurate ¹⁹F shieldings,^[15,16] the global hybrid B3LYP,^[12b,17] and the LH12ct-SsifPW92.^[18] local hybrid functional with position-dependent exact-exchange admixture.^[19] These computations used pcSseg-4 basis sets^[20] for F, Cl, and Br and ANO-RCC-unc^[21] basis sets for I. For each of the abovementioned sets of structures, shielding calculations with these two functionals were performed without or with COSMO. This allows the evaluation of the role of solvent effects acting either indirectly via the structure or directly. The nonrelativistic shielding/shift results are given in Tables S3, S4.

To evaluate the role of spin-orbit and scalar relativistic effects, we also carried out four-component relativistic computations (at the BP86-D3(BJ)(COSMO,CH₃CN)/def2-TZVPPD optimized structures) using the matrix Dirac-Kohn-Sham (mDKS) method^[22] implemented in the ReSpect program, version 5.1.0.^[23] As neither local hybrids nor B3LYP are currently available for shielding computations in ReSpect, we used a modified B3LYP functional with 50% admixture of exact Hartree-Fock exchange (B3LYP50), which should give results that are close to B3LYP data. Uncontracted Dyall valence quadruple- ζ (Dyall-VQZ)^[24] basis sets were used for all atoms. Relativistic shielding/shift results are shown in Table S5.

Experimental Section

Synthesis of [NEt₃Me][ClF₄] in solution (low concentration)

[NEt₃Me]Cl (100 mg, 0.659 mmol, 1 eq.) was dissolved in dried acetonitrile or propionitrile or CHFCl₂ (1 ml) and cooled to -35 °C (MeCN) or -55 °C (EtCN, CHFCl₂). Dilute F₂ (10 % in Ar) was bubbled through the solution (16 min, 20 ml·min⁻¹, 2 eq). Pure Ar (20 ml·min⁻¹) was bubbled through the solution for 15 min in order to remove residual amounts of reactive gases. A colorless solution was obtained.

¹H NMR (400 MHz, EtCN, ext. acetone-d₆, 20 °C) δ [ppm]= 3.87 (q, ³J(¹H,¹H)=7.30 Hz, 6H, CH₂), 3.48 (s, 3H N-CH₃), 1.85 (t, ³J(¹H,¹H)=7.30 Hz, ³J(¹⁴N,¹H)=1.84 Hz, CH₃). ¹⁹F NMR (377 MHz, EtCN, ext. acetone-d₆, 20 °C) δ [ppm]= 67 (ClF₄⁻); FT-Raman (EtCN, -196 °C): $\tilde{\nu}$ = [ClF₄]⁻: 500 (a_{1g}), 407(b_{1g}), 278 cm⁻¹ (b_{2g}).

Synthesis of [NEt₃Me][ClF₄] in solution (high concentration)

[NEt₃Me][Cl₃] was prepared by the addition of 1 eq. of Cl₂ to [NEt₃Me]Cl. [NEt₃Me][Cl₃] (0.621 g, 2.79 mmol, 1 eq.) was diluted with acetonitrile (0.3 ml) and cooled to -30 °C. Dilute F₂ (10 % in Ar) was bubbled through the solution (68 min, 20 ml min⁻¹, 2 eq). To remove residual amounts of reactive gases, Ar was bubbled through the solution for (15 min, 20 ml min⁻¹). A colorless solution was obtained. Analytics was identical to samples with low concentration.

Crystal growth of [NEt₄][ClF₄]

The synthetic procedure is similar to [NEt₃Me][ClF₄]. Single crystals were obtained by slowly cooling a propionitrile solution to -80 °C over 1 week in a freezer. An ethanol bath in a Dewar was used to reduce the cooling rate.

Synthesis of [NEt₄]₃[ClF₄][ClF₂]₂ in solution

[NEt₄]Cl (300 mg, 1.81 mmol, 1 eq.) was dissolved in acetonitrile (3 ml) and cooled to -30 °C. Dilute F₂ (10 % in Ar) was bubbled through the solution (20 min, 20 ml min⁻¹, 1.2 eq). To remove residual amounts of reactive gases, Ar was bubbled through the solution for 15 min. A colorless solution was obtained.

¹H NMR (400 MHz, MeCN, ext. acetone-d₆, -40 °C) δ [ppm]= 3.11 (q, ³J(¹H,¹H)=7.18 Hz, 8H, CH₂), 1.12 (t, ³J(¹H,¹H)=7.18 Hz, ³J(¹⁴N,¹H)=1.84 Hz, 12H, CH₃). ¹⁹F NMR (377 MHz, MeCN, ext. acetone-d₆, -40 °C) δ [ppm]= 67 (s, [ClF₄]⁻), -125 (s, [ClF₂]⁻) FT-Raman (MeCN, -196 °C): $\tilde{\nu}$ = [ClF₄]⁻: 500 (a_{1g}), 407(b_{1g}), 278 (b_{2g}), [ClF₂]⁻: 455 cm⁻¹ (a_{1g}).

Crystal growth of [NEt₃Me]₃[ClF₄][ClF₂]₂

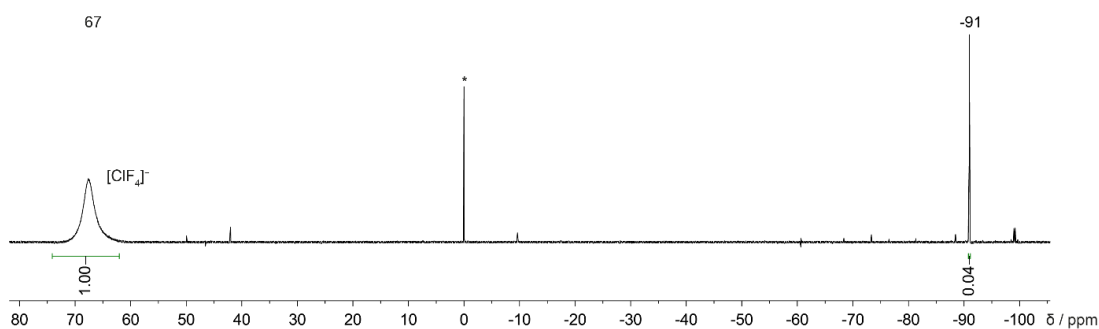
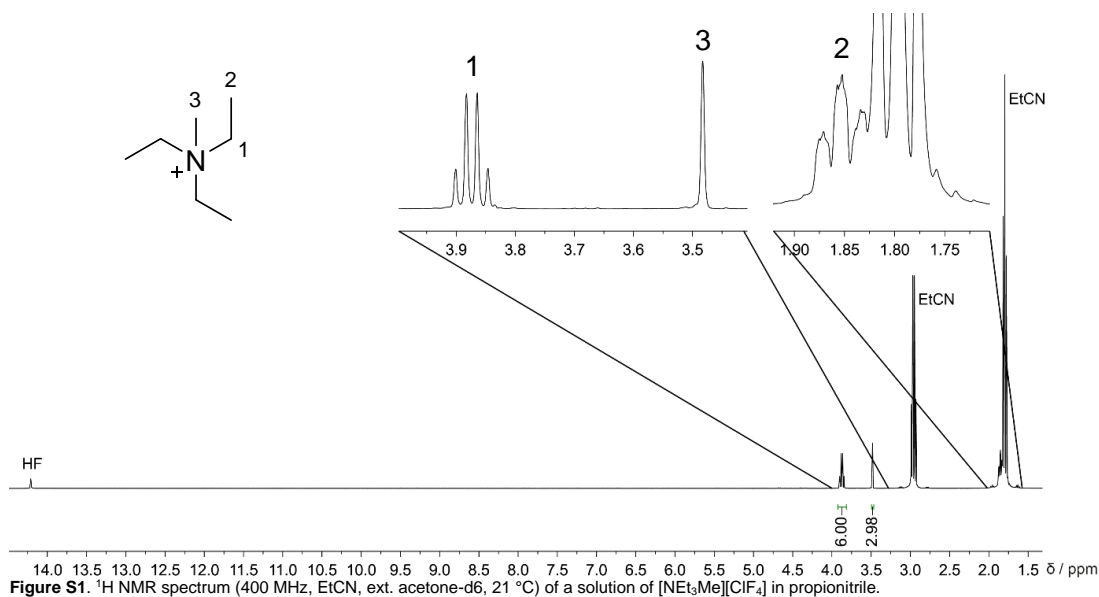
The synthetic procedure is similar to [NEt₄]₃[ClF₄][ClF₂]₂. Single crystals were obtained by slowly cooling a propionitrile solution to -35 °C over 2 days in a freezer. An ethanol bath in a Dewar was used to reduce the cooling rate.

SUPPORTING INFORMATION

Synthesis of $[\text{NEt}_3\text{Me}][\text{ClF}_2]$ in solution

$[\text{NEt}_3\text{Me}]\text{Cl}$ (50 mg, 0.330 mmol, 1 eq) was dissolved in propionitrile (0.5 ml) and cooled to $-50\text{ }^\circ\text{C}$. Dilute ClF (10 % in Ar) was bubbled through the solution (8.5 min, 20 ml min^{-1} , 2 eq). To remove residual amounts of reactive gases, Ar was bubbled through the solution for 15 min. A colorless solution was obtained. The reaction mixture was allowed to warm to $-10\text{ }^\circ\text{C}$ and subsequently slowly cooled to $-80\text{ }^\circ\text{C}$ in an ethanol bath Dewar to reduce the cooling rate. Single crystals were obtained after 4 days.

Raman (crystal, $-196\text{ }^\circ\text{C}$): $\tilde{\nu} = [\text{ClF}_2]^-$: 457 cm^{-1} (a_{1g}).



SUPPORTING INFORMATION

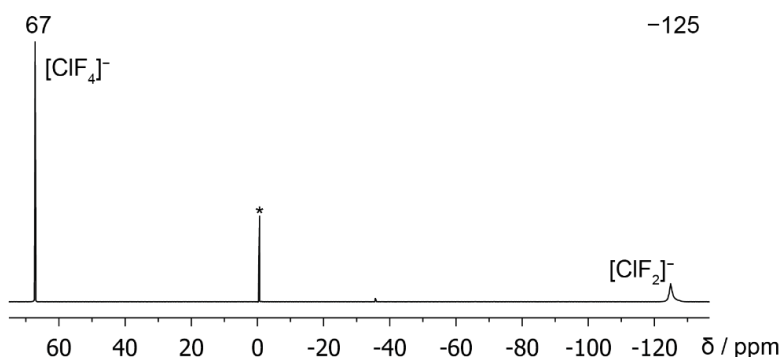


Figure S3. ^{19}F NMR spectrum (377 MHz, MeCN, ext. acetone- d_6 , $-40\text{ }^\circ\text{C}$) of a solution of $[\text{NEt}_3\text{Me}]_3[\text{ClF}_4][\text{ClF}_2]_2$ in acetonitrile. Asterisk (*) denotes CFCl_3 .

We realized that the ^{19}F NMR signal of $[\text{NEt}_3\text{Me}][\text{ClF}_4]$ shows different line broadening under certain conditions. Therefore, we studied the influence of temperature and HF impurities on the line width. Figure S4 shows the ^{19}F NMR spectra at $-20\text{ }^\circ\text{C}$ and $-40\text{ }^\circ\text{C}$ prior and after addition of 1 eq of HF. Raising the temperature from $-40\text{ }^\circ\text{C}$ to $-20\text{ }^\circ\text{C}$ leads to a significant line broadening ($-40\text{ }^\circ\text{C}$: FWHM = 164.8 Hz, $-20\text{ }^\circ\text{C}$ = 414.8 Hz). Addition of HF also leads to line broadening at $-20\text{ }^\circ\text{C}$ and $-40\text{ }^\circ\text{C}$ ($-40\text{ }^\circ\text{C}$ + HF addition: FWHM = 251.6 Hz; $-20\text{ }^\circ\text{C}$ + HF addition: FWHM = 637.7 Hz).

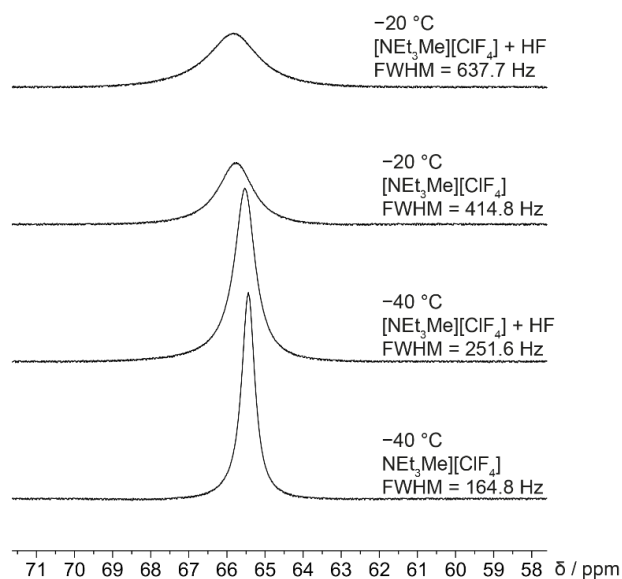


Figure S4. ^{19}F NMR spectra (377 MHz, EtCN, ext. acetone- d_6) of a solution of $[\text{NEt}_3\text{Me}][\text{ClF}_4]$ in propionitrile at $-20\text{ }^\circ\text{C}$ and $-40\text{ }^\circ\text{C}$ prior and after addition of 1 eq HF.

SUPPORTING INFORMATION

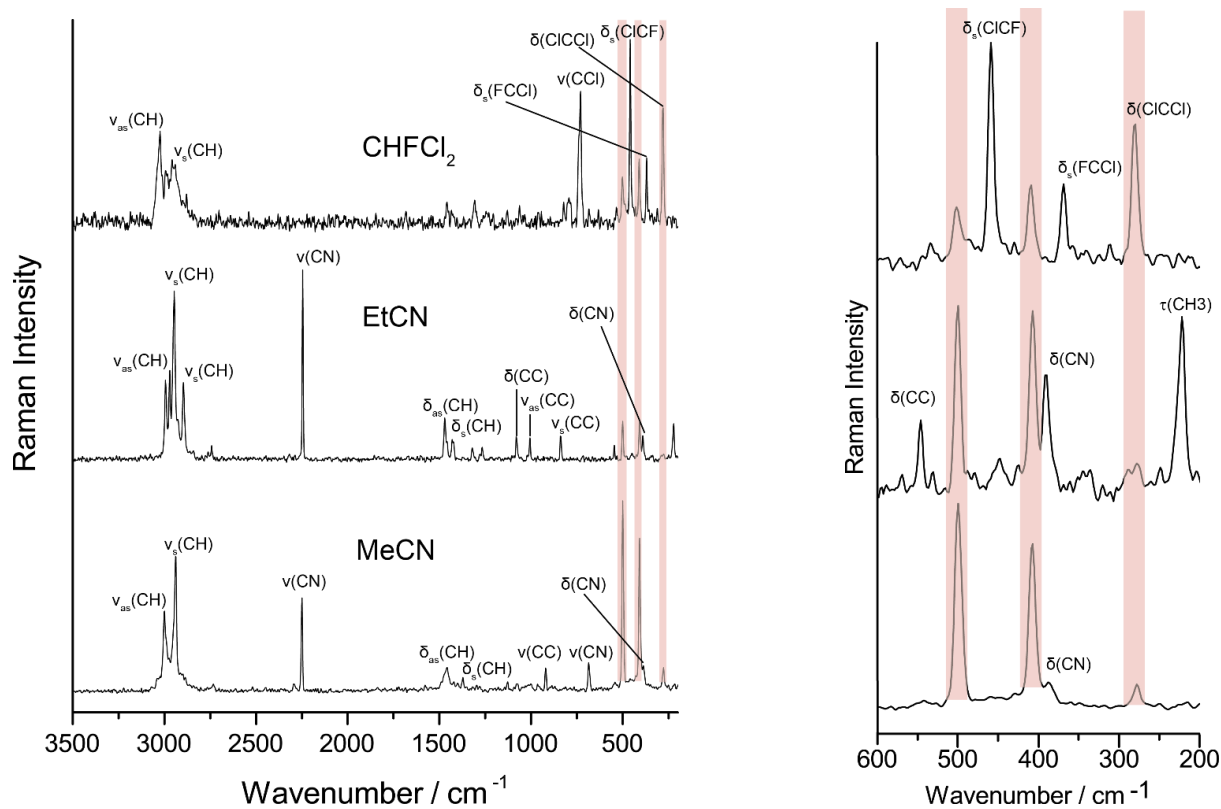


Figure S5. Raman spectra ($-196\text{ }^{\circ}\text{C}$) of $[\text{NEt}_3\text{Me}][\text{ClF}_4]$ in different solvents: CHFCℓ_2 (top), EtCN (middle), MeCN (bottom). Left: full spectrum, right: Extract from $200\text{--}600\text{ cm}^{-1}$. $[\text{ClF}_4]^-$ bands are highlighted in red.

$[\text{NEt}_3\text{Me}][\text{ClF}_4]$ in different solvents, CHFCℓ_2 (top), propionitrile (middle) and acetonitrile (bottom). The three characteristic bands for $[\text{ClF}_4]^-$ (500 cm^{-1} (a_{1g}), 407 cm^{-1} (b_{1g}), 278 cm^{-1} (b_{2g})) are highlighted in red. The different intensities are due to different concentrations. In case of propionitrile the concentration is too low ($0.32\text{ mol}\cdot\text{l}^{-1}$) to observe the b_{2g} vibration. In case of CHFCℓ_2 the band of the b_{2g} vibration is superimposed by a solvent band.

SUPPORTING INFORMATION

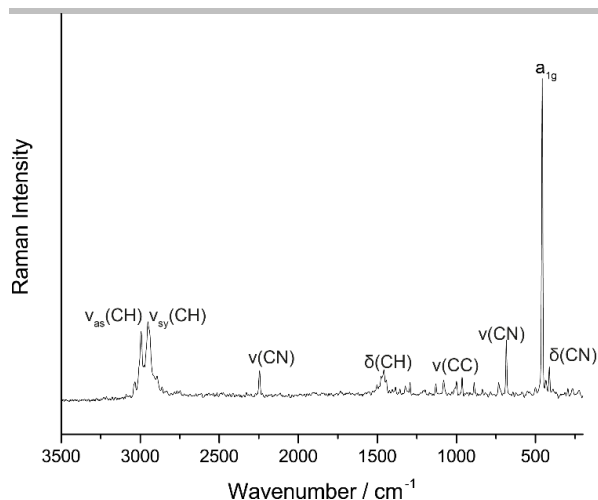
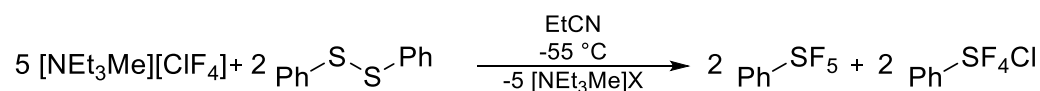


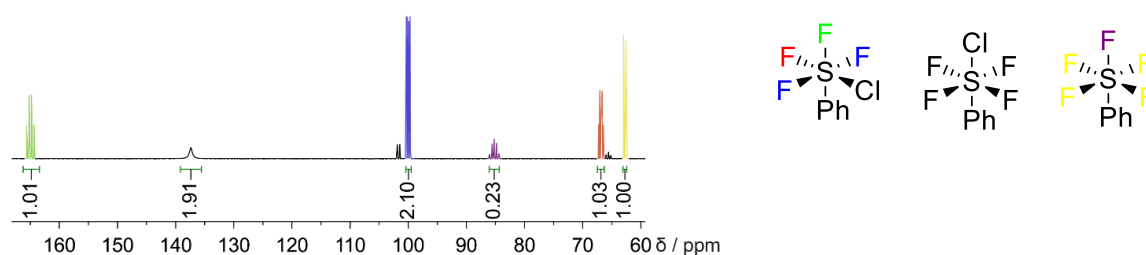
Figure S6. Raman spectrum ($-196\text{ }^{\circ}\text{C}$) of $[\text{NEt}_3\text{Me}][\text{ClF}_2]$. Anion band a_{1g} 457 cm^{-1} .

Reactivity Studies

Disulfide activation



To a cooled ($-55\text{ }^{\circ}\text{C}$) solution of $[\text{NEt}_3\text{Me}][\text{ClF}_4]$ in propionitrile (1 ml, $0.659\text{ mol}\cdot\text{l}^{-1}$, 1 eq.) a solution of phenyl disulphide (28.8 mg, 0.132 mmol, 0.2 eq) in propionitrile (2 ml) was added dropwise. The solution was stirred for 15 min at $-55\text{ }^{\circ}\text{C}$, then allowed to warm to r.t. and stirred over night. A 1 : 4 : 2 mixture of Ph-SF_5 : *cis*- PhSF_4Cl : *trans*- PhSF_4Cl was obtained. After addition of H_2O (0.5 ml) *trans*- PhSF_4Cl was selectively hydrolysed to PhSO_2F . Addition of dilute potassium hydroxide solution (1 ml) and heating to $90\text{ }^{\circ}\text{C}$ over night led to the hydrolysis of *cis*- PhSF_4Cl and PhSO_2F . Products were identified by ^{19}F NMR spectroscopy. NMR yield PhSF_5 : 17 %
 ^{19}F NMR (377 MHz, EtCN, ext. acetone- d_6 , $21\text{ }^{\circ}\text{C}$) δ = 85 (quin, $^2J(^{19}\text{F}, ^{19}\text{F})=148\text{ Hz}$, 1F, PhSF_5 *trans*-F), 63 (d, 4F, PhSF_5 *cis*-F), 165 (td, $^2J(^{19}\text{F}, ^{19}\text{F})=164\text{ Hz}$, $^2J(^{19}\text{F}, ^{19}\text{F})=149\text{ Hz}$, 1F, *cis*- PhSF_4 *trans*-F), 100 (dd, $^2J(^{19}\text{F}, ^{19}\text{F})=81\text{ Hz}$, 2F, *cis*- PhSF_4 *cis*-F), 67 (dt, 2F, *cis*- PhSF_4 *cis*-F), 137 (s, 4F, *trans*- PhSF_4Cl), 64 ppm (s, 1F PhSO_2F).



SUPPORTING INFORMATION

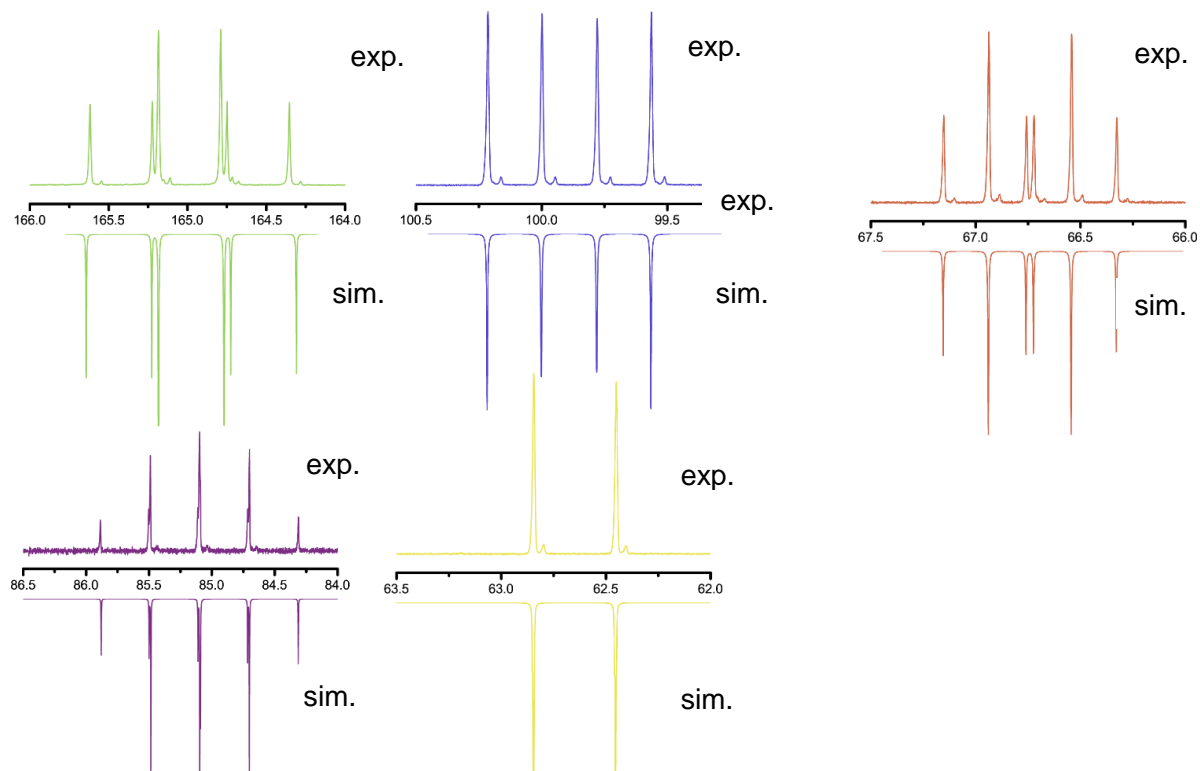


Figure S7. ^{19}F NMR spectra (377 MHz, EtCN, ext. acetone- d_6 , 21 $^{\circ}\text{C}$) of the reaction mixture after the reaction of $[\text{NEt}_3\text{Me}][\text{ClF}_4]$ with Ph_2S_2 showing three products: PhSF_5 , *cis*- PhSF_4Cl and *trans*- PhSF_4Cl . Experimental spectra shown with positive intensities, simulated spectra shown with negative intensities.

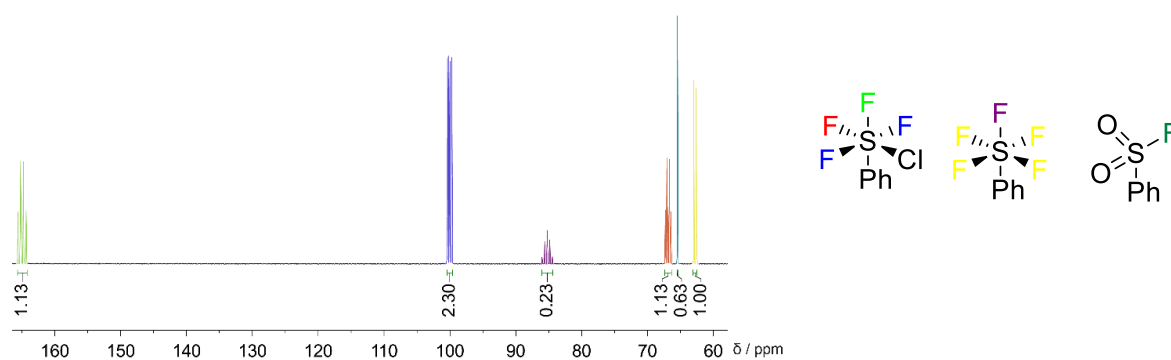


Figure S8. ^{19}F NMR spectrum (377 MHz, EtCN, ext. acetone- d_6 , 21 $^{\circ}\text{C}$) of the hydrolysed reaction mixture (H_2O , r.t., 15 min) after the reaction of $[\text{NEt}_3\text{Me}][\text{ClF}_4]$ with Ph_2S_2 showing three products: PhSF_5 , *cis*- PhSF_4Cl and PhSO_2F .

SUPPORTING INFORMATION

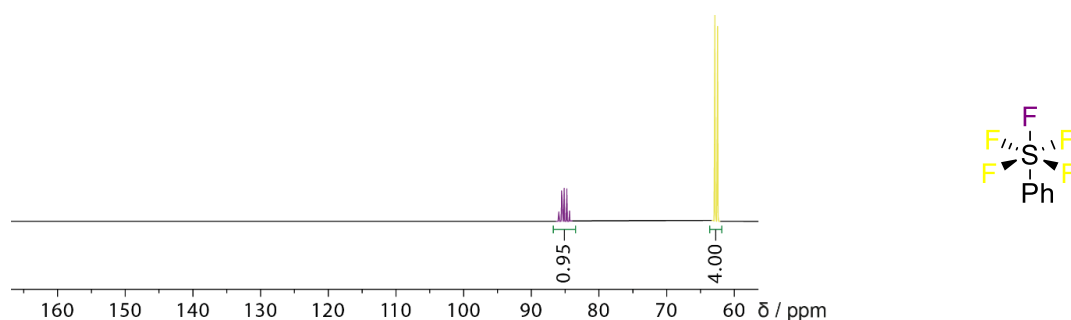
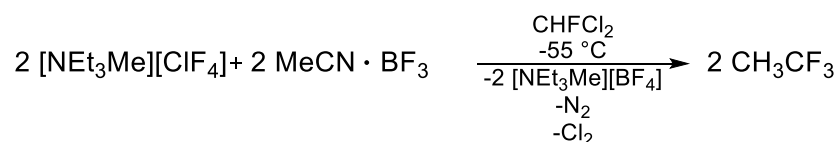


Figure S9. ^{19}F NMR spectrum (377 MHz, EtCN, ext. acetone- d_6 , 21 °C) of the hydrolysed reaction mixture (KOH_{aq} , 90 °C, 8 h) after the reaction of $[\text{NEt}_3\text{Me}][\text{ClF}_4]$ with Ph_2S_2 showing only PhSF_5 .

Nitrile activation



The acetonitrile boron trifluoride complex was synthesized by the addition of BF_3 to acetonitrile at r.t. followed by removal of residual acetonitrile under reduced pressure.

To solid acetonitrile boron trifluoride complex (35.9 mg, 0.330 mmol, 0.5 eq) a solution of $[\text{NEt}_3\text{Me}][\text{ClF}_4]$ (150 mg, 0.659 mmol, 1 eq) in dichlorofluoromethane (1 ml) was added at -60°C . The reaction mixture was analyzed by ^{19}F NMR spectroscopy (Figure S9). The reaction equation suggests the equimolar formation of CH_3CF_3 and $[\text{BF}_4]^-$. The ^{19}F NMR spectrum shows a ratio of 1:230 in favour of $[\text{BF}_4]^-$ this can be rationalised due to several reasons: First, CH_3CF_3 has a boiling point of -50°C . During the reaction and the transfer of the reaction mixture probably significant amounts of the product evaporated. Secondly, during the reaction highly reactive ClF_3 is formed leading to side products which are evident in the ^{19}F NMR spectrum. The signal at -129 ppm can be identified as $[\text{SiF}_6]^{2-}$ from a reaction with the glass vessel.

SUPPORTING INFORMATION

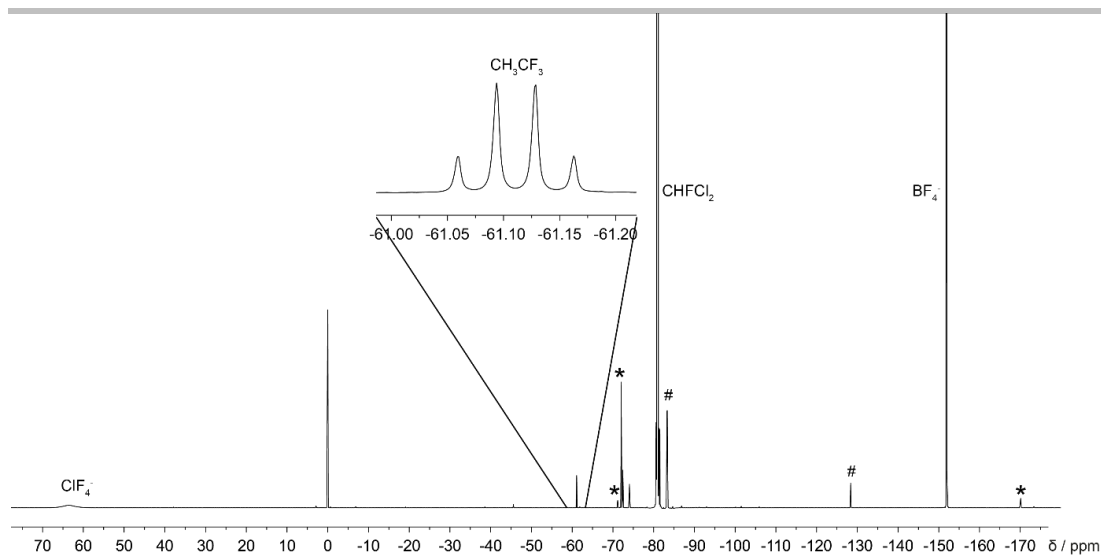
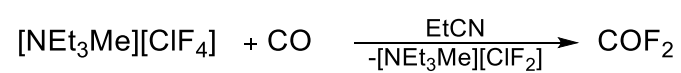


Figure S10. ^{19}F NMR spectrum (377 MHz, EtCN, ext. acetone- d_6 , 21 °C) of the reaction mixture. Symbols denote solvent impurities (*), side products generated during the reaction (#).

CO activation



SUPPORTING INFORMATION

A solution of $[\text{NEt}_3\text{Me}][\text{ClF}_4]$ (150 mg, 0.659 mmol, 1 eq) was stirred under a CO atmosphere for 30 min at r.t. Then the gas-phase was analyzed via FT-IR spectroscopy. The FT-IR spectrum (Figure S7) only shows the presence of starting material (CO) solvent (EtCN) and product (COF_2). The formation of COCl_2 or COCIF was not observed.

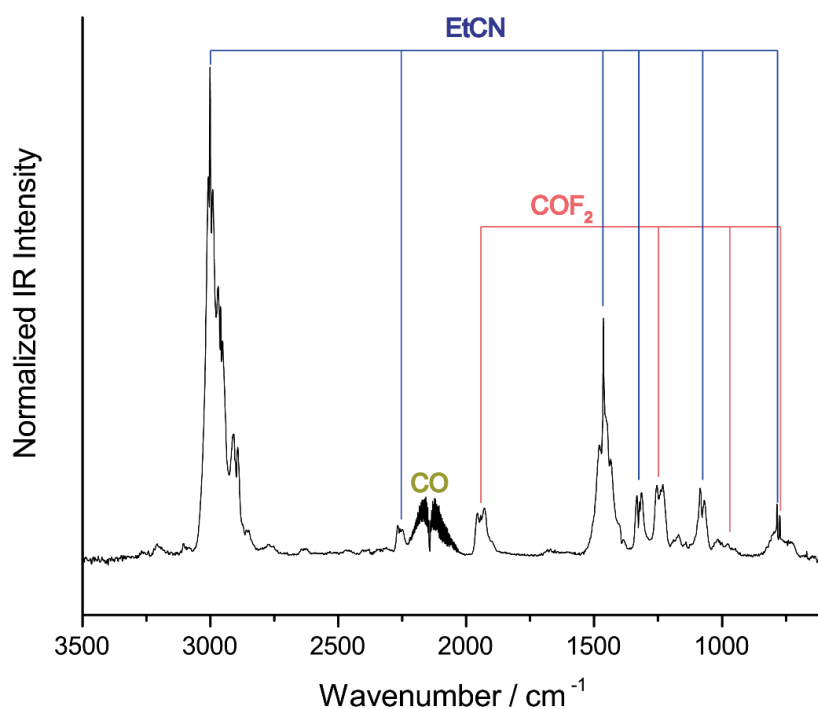
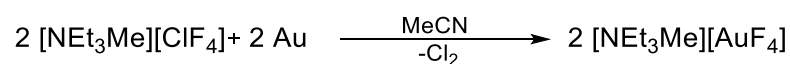


Figure S11. Gas-phase FT-IR spectrum (50 mbar, 10 cm) of the reaction mixture showing only solvent (EtCN, blue), starting material (CO, green) and product (COF_2 , red).

Dissolution of gold



Gold metal (16 mg) was dissolved over 2 days in a solution of $[\text{NEt}_3\text{Me}][\text{ClF}_4]$ in acetonitrile (0.5 ml, 8 mol l^{-1}) at r.t. The solution was analyzed with ^{19}F NMR spectroscopy. The major product is $[\text{AuF}_4]^-$ (95 %) but traces of $[\text{AuF}_3\text{Cl}]^-$ (3%) and *cis*- $[\text{AuF}_2\text{Cl}_2]^-$ (2 %) were also present in the reaction mixture.

SUPPORTING INFORMATION

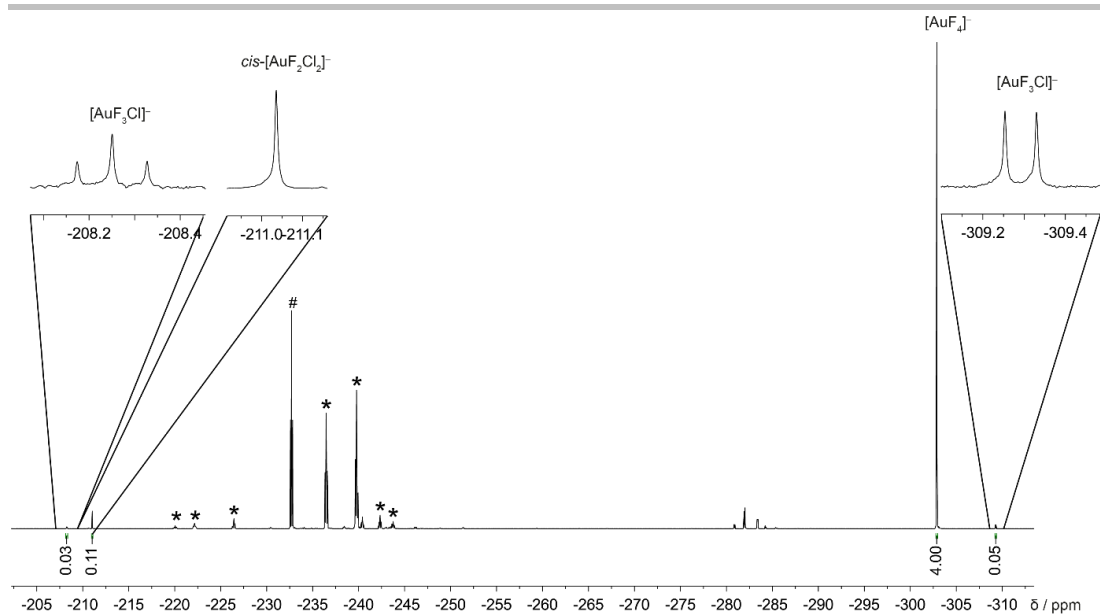
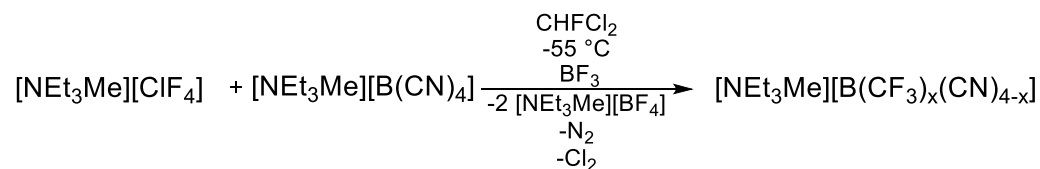


Figure S12. ^{19}F NMR spectrum (377 MHz, MeCN, ext. acetone- d_6 , 21 °C) of the reaction mixture after the reaction of $[\text{NEt}_3\text{Me}][\text{ClF}_4]$ with Au. Symbols denote fluorinated impurities: # fluorinated solvent (FCH_2CN), * halogenated cations.

SUPPORTING INFORMATION

Tetracyanoborate activation



Potassiumtetracyanoborate (500 mg, 3.25 mmol, 1 eq) was dissolved in acetonitrile (10 ml). A solution of triethylmethylammonium chloride (0.493 mg, 3.25 mmol, 1 eq) in acetonitrile (5 ml) was added. The colourless precipitated was filtrated and the solvent was removed under reduced pressure to yield tetramethylammonium tetracyanoborate.

Triethylmethylammonium tetracyanoborate (76.0 mg, 0.330 mmol, 0.5 eq) was dissolved in CH₂Cl₂ (1 ml) and boron trifluoride (67.0 mg, 0.989 mmol, 1.5 eq) was added. The solution was cooled to -60 °C. A cooled solution of Triethylmethylammonium tetrafluoridochlorate(III) (1 ml, 0.659 mol⁻¹, 1 eq) was added at -60 °C, stirred for 5 min at -60 °C and let allowed to warm to r.t. Volatiles were removed and the residue was dissolved in CD₃CN and analyzed via ¹⁹F and ¹¹B NMR spectroscopy. [B(CF₃)_x(CN)_{4-x}]⁻ anions were identified according to literature.

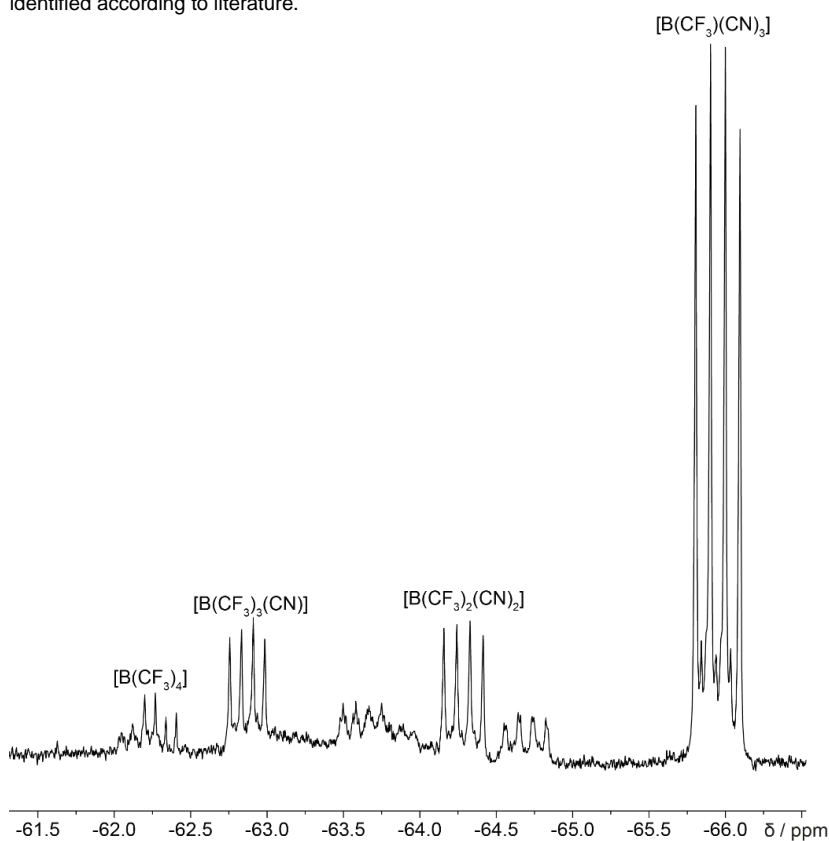


Figure S13. ¹⁹F NMR spectrum (377 MHz, CD₃CN, 21 °C) of the reaction mixture after the reaction of [NEt₃Me][ClF₄] with [NEt₃Me][B(CN)₄].

SUPPORTING INFORMATION

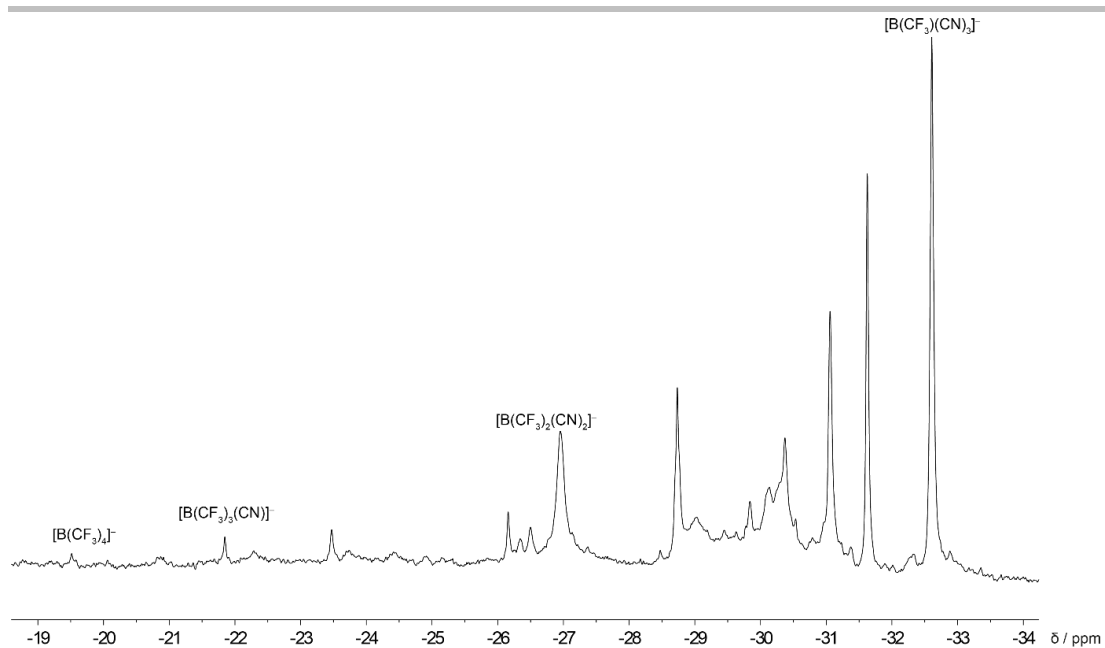
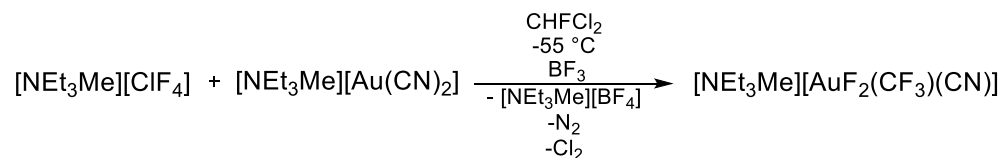


Figure S14. $^{11}\text{B}\{^{19}\text{F}\}$ NMR spectrum (129 MHz, CD_3CN , 21 °C) of the reaction mixture after the reaction of $[\text{NEt}_3\text{Me}][\text{ClF}_4]$ with $[\text{NEt}_3\text{Me}][\text{B}(\text{CN})_4]$.

SUPPORTING INFORMATION

Difluoroaurate activation



Cation metathesis was achieved in a similar procedure to triethylmethylammonium tetracyanoaurate.

Triethylmethylammonium dicyanoaurate (43 mg, 0.118 mmol, 0.18 eq) was dissolved in CHFC_2 (1 ml). Boron trifluoride (19 mg, 0.280 mmol, 0.42 eq) was added. The solution was cooled to -60 °C. A cooled solution of triethylmethylammonium tetrafluoridochlorate(III) (1 ml, 0.659 mol^{-1} , 1 eq) was added at -60 °C, stirred for 5 min at -60 °C and let allowed to warm to r.t and analyzed via ^{19}F NMR spectroscopy.

Cis-cyanodifluorido(trifluoromethyl)aurate(III) was identified using ^{19}F NMR spectroscopy in comparison with literature values.^[25] Due to the low concentration of *cis*-cyanodifluorido(trifluoromethyl)aurate(III) the region between -80 and -170 ppm in the NMR spectrum is not shown. It contains solvent signal CHFC_2 at -81 ppm, $[\text{SiF}_6]^{2-}$ at -129 ppm and $[\text{BF}_4]^-$ at -152 ppm
 $\delta[\text{ppm}] = -58.29$ (dd, $^3J(^{19}\text{F}, ^{19}\text{F}) = 5.8$ Hz, $^3J(^{19}\text{F}, ^{19}\text{F}) = 2.5$ Hz, 3F), -196.66 (dq, $^2J(^{19}\text{F}, ^{19}\text{F}) = 65.3$ Hz, $^3J(^{19}\text{F}, ^{19}\text{F}) = 2.5$ Hz, 1F), -254.31 (dq, $^2J(^{19}\text{F}, ^{19}\text{F}) = 65.3$ Hz, $^3J(^{19}\text{F}, ^{19}\text{F}) = 5.8$, 1F)

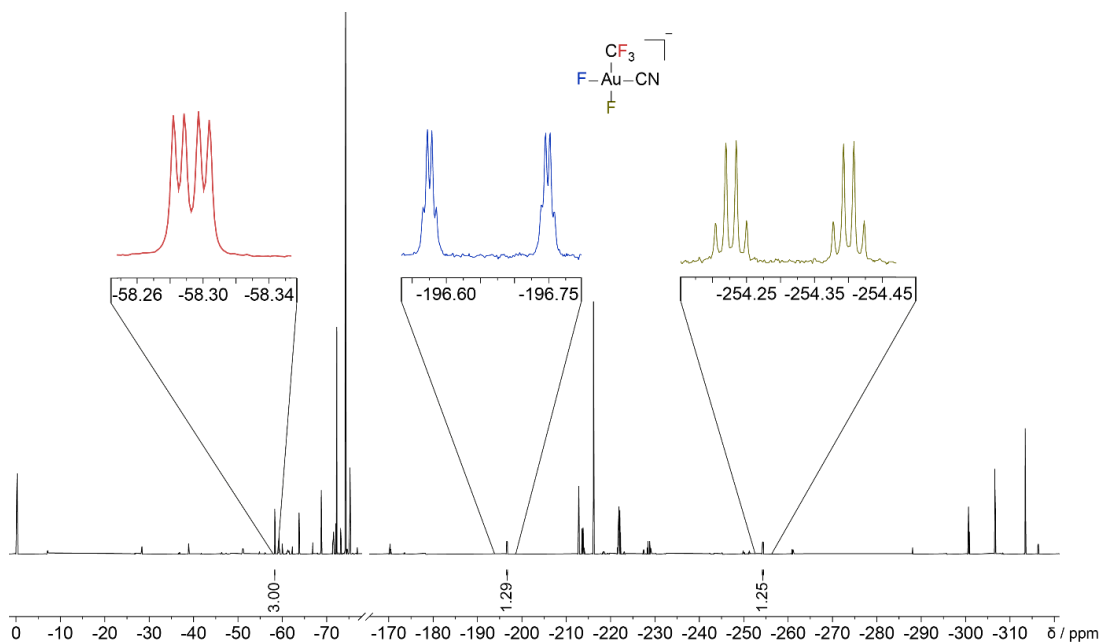


Figure S15. ^{19}F NMR spectrum (377 MHz, CHFC_2 , ext. acetone- d_6 , 21 °C) of the reaction mixture after the reaction of $[\text{NEt}_3\text{Me}][\text{ClF}_4]$ with $[\text{NEt}_3\text{Me}][\text{Au}(\text{CN})_2]$. Omitted spectral area between -80 and -170 ppm contains solvent CHFC_2 (-81 ppm), $[\text{SiF}_6]^{2-}$ (-129 ppm) and $[\text{BF}_4]^-$ (-152 ppm).

SUPPORTING INFORMATION

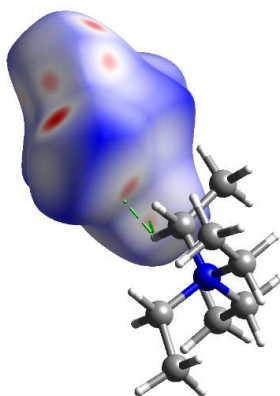
Crystallographic section

Table S1. Crystallographic details of [NEt₃Me]₃[ClF₄][ClF₂]₂ and [NEt₄][ClF₄].

Compound	[NEt ₃ Me] ₃ [ClF ₄][ClF ₂] ₂	[NEt ₄][ClF ₄]	[NMe ₃ Me][ClF ₂]
Empirical formula	C ₂₁ H ₅₄ Cl ₃ F ₈ N ₃	C ₈ H ₂₀ ClF ₄ N	C ₇ H ₁₈ ClF ₂ N
Formula weight	607.02	241.70	189.67
Temperature/K	100.0	99.92	100.0
Crystal system	triclinic	monoclinic	monoclinic
Space group	<i>P</i> $\bar{1}$	<i>C</i> 2/ <i>c</i>	<i>P</i> 2 ₁ / <i>c</i>
<i>a</i> /Å	6.9802(8)	11.4818(9)	11.2608(4)
<i>b</i> /Å	14.6749(16)	7.5474(5)	6.9954(2)
<i>c</i> /Å	15.3580(16)	14.3613(11)	12.6412(4)
<i>α</i> /°	97.190(4)	90	90
<i>β</i> /°	92.017(4)	110.877(3)	102.6650(10)
<i>γ</i> /°	102.608(4)	90	90
Volume/Å ³	1520.0(3)	1162.81(15)	971.57(5)
Z	2	4	4
ρ_{calc} /cm ³	1.326	1.381	1.297
μ /mm ⁻¹	0.366	0.347	0.367
F(000)	648.0	512.0	408.0
Crystal size/mm ³	0.34 × 0.23 × 0.18	0.32 × 0.16 × 0.04	0.293 × 0.216 × 0.154
Radiation	MoK α (λ = 0.71073)	MoK α (λ = 0.71073)	MoK α (λ = 0.71073)
2 θ range for data collection/°	5.358 to 57.15	6.072 to 56.738	3.708 to 61.112
Index ranges	-9 ≤ <i>h</i> ≤ 9, -19 ≤ <i>k</i> ≤ 19, -20 ≤ <i>l</i> ≤ 20	-15 ≤ <i>h</i> ≤ 15, -9 ≤ <i>k</i> ≤ 10, -19 ≤ <i>l</i> ≤ 19	16 ≤ <i>h</i> ≤ 16, -9 ≤ <i>k</i> ≤ 10, -18 ≤ <i>l</i> ≤ 18
Reflections collected	85154	25147	24557
Independent reflections	7678 [R _{int} = 0.0626, R _{sigma} = 0.0322]	1453 [R _{int} = 0.0452, R _{sigma} = 0.0173]	2961 [R _{int} = 0.0275, R _{sigma} = 0.0157]
Data/restraints/parameters	7678/0/331	1453/0/68	2961/0/117
Goodness-of-fit on F ²	1.059	1.172	1.065
Final R indexes [<i>I</i> > 2 σ (<i>I</i>)]	R ₁ = 0.0372, wR ₂ = 0.0810	R ₁ = 0.0300, wR ₂ = 0.0752	R ₁ = 0.0268, wR ₂ = 0.0751
Final R indexes [all data]	R ₁ = 0.0517, wR ₂ = 0.0878	R ₁ = 0.0334, wR ₂ = 0.0766	R ₁ = 0.0316, wR ₂ = 0.0804
Largest diff. peak/hole / e Å ⁻³	0.34/-0.44	0.32/-0.38	0.34/-0.34
CCDC deposition number	1948997	1948998	2004243

Table S2. Bond lengths and angles of [ClF₄]⁻ anions in [NEt₄][ClF₄] and [NEt₃Me]₃[ClF₄][ClF₂]₂ in comparison with the literature known compounds [pyr][ClF₄], [NO][ClF₄], Cs[ClF₄], Rb[ClF₄] and K[ClF₄].^[26] Lengths in pm, angles in °.

Bond/Angle	[NEt ₄][ClF ₄]	[NEt ₃ Me] ₃ [ClF ₄][ClF ₂] ₂	[pip][ClF ₄]	[NO][ClF ₄]	Cs[ClF ₄]	Rb[ClF ₄]	K[ClF ₄]
C1-F1	179.3(1)	178.8(1)	175.9(2)	187.4(1)	179.4(4)	180.34(9)	179.82(6)
C1-F2	180.6(1)	179.4(1)	181.4(1)	172.7(1)	179.2(4)	179.30(9)	-
C1-F3	-	180.0(1)	177.1(1)	-	-	-	-
C1-F4	-	180.8(1)	181.3(1)	-	-	-	-
F1-C1-F2	90.01(5)	89.78(5)	-	-	89.1(2)	89.33(4)	89.79(4)
F2-C1-F1'	89.99(5)	-	-	-	90.9(2)	90.67(4)	90.21(4)
F2-C1-F3	-	89.66(5)	-	-	-	-	-
F3-C1-F4	-	90.21(5)	-	-	-	-	-
F4-C1-F1	-	90.35(5)	-	-	-	-	-

**Figure S16.** Hirshfeld surface of of the [ClF₄]⁻ anion in [NEt₃Me]₃[ClF₄][ClF₂]₂. Color code: blue = N, grey = C, white H, green dashed line displays hydrogen bond.^[27]

SUPPORTING INFORMATION

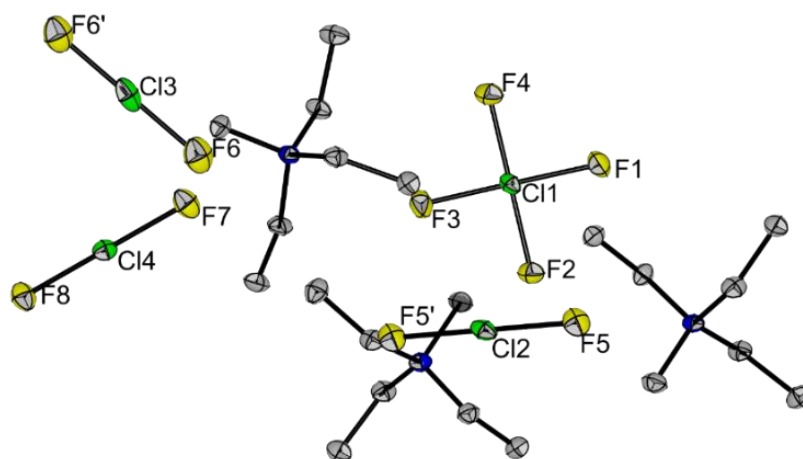


Figure S17. Crystal structure of $[\text{NEt}_3\text{Me}]_3[\text{ClF}_4][\text{ClF}_2]_2$. Color code: yellow = F, green = Cl, blue = N, grey = C. Displacement ellipsoids are shown at 50 % probability at 100 K. Selected bond lengths [pm] and bond angles [°]: F1–Cl1 178.8(1), F2–Cl1 179.4(1), F3–Cl1 180.0(1), F4–Cl1 180.8(2), F5–Cl2 185.4(1), F6–Cl3 184.1(2), F7–Cl4 184.9(1), F8–Cl4 185.4(1), F7–Cl4–F8 179.66(5). Hydrogen atoms omitted for clarity.

By slowly cooling a reaction mixture of $[\text{NEt}_3\text{Me}]\text{Cl}$ with 1.2 eq. fluorine in acetonitrile, single crystals of $[\text{NEt}_3\text{Me}]_3[\text{ClF}_4][\text{ClF}_2]_2$ were obtained (Figure S16). This compound crystallizes in the space group $P\bar{1}$. In the asymmetric unit are four anionic moieties. One is a $[\text{ClF}_4]^-$ anion, the second is an asymmetric $[\text{ClF}_2]^-$ (F7Cl4F8) anion. Furthermore, there are two $[\text{ClF}_2]^-$ units with the chlorine atom on centers of inversion ($\text{F6Cl3F6}'$ and $\text{F5Cl2F5}'$) (Figure 4). The bond lengths and angles in the $[\text{ClF}_4]^-$ anion in $[\text{NEt}_3\text{Me}]_3[\text{ClF}_4][\text{ClF}_2]_2$ are very similar to the ones found in $[\text{NEt}_4][\text{ClF}_4]$. The Cl–F bond lengths of the $[\text{ClF}_2]^-$ anions vary between 184.1(2) pm and 185.4(1) pm. The bond angle of the $[\text{ClF}_2]^-$ anion (F7Cl4F7) is 179.66(5) °.

SUPPORTING INFORMATION

Computational section

Table S3. Calculated ^{19}F NMR chemical shifts relative to CFCl_3 (in ppm) of $[\text{XF}_n]^-$ ($\text{X} = \text{Cl, Br, I; } n=2, 4, 6$) in comparison with experimental values, at BP86-D3 structures.^a

opt. NMR	BHLYP				LH12ct-SsifPW92				δ_{exp}
	gas. gas	gas COSMO	COSMO. gas	COSMO COSMO	gas. gas	gas COSMO	COSMO. gas	COSMO COSMO	
$[\text{ClF}_2]^-$	-193.2	-200.0	-196.6	-202.4	-166.3	-170.1	-171.5	-174.4	-125
$[\text{ClF}_4]^-$	80.6	76.1	71.9	67.8	71.8	68.6	63.3	60.5	67
$[\text{ClF}_6]^-$	284.3	286.8	275.0	277.6	255.1	257.3	246.6	248.9	-
$[\text{BrF}_2]^-$	-284.4	-294.6	-286.2	-295.5	-262.6	-270.7	-265.4	-272.7	-210
$[\text{BrF}_4]^-$	-32.2	-38.3	-36.3	-42.0	-36.6	-41.6	-40.7	-45.4	-37
$[\text{BrF}_6]^-$	131.9	135.0	126.0	129.2	114.6	117.4	109.0	111.9	94
$[\text{IF}_2]^-$	-350.1	-359.3	-351.4	-360.1	-338.1	-346.7	-339.5	-347.8	-282
$[\text{IF}_4]^-$	-103.1	-109.5	-105.1	-111.1	-109.8	-115.5	-111.8	-117.3	-106
$[\text{IF}_6]^-$	31.1	33.3	28.1	30.5	14.8	16.9	11.9	14.1	13
$\sigma(\text{CFCl}_3)$	185.4	189.7	183.8	183.8	195.2	198.8	193.7	197.5	

^a At BP86-D3(BJ)/def2-TZVPPD optimized structures. CFCl_3 reference shieldings at the same level have been used to obtain the relative shifts. Nonrelativistic results with pcSseg-4 basis sets for F, Cl, Br, and ANO-RCC-unc for I.

Table S4. Calculated ^{19}F NMR chemical shifts relative to CFCl_3 (in ppm) of $[\text{XF}_n]^-$ ($\text{X} = \text{Cl, Br, I; } n=2, 4, 6$) in comparison with experimental values, at B3LYP-D3 structures.^a

opt. NMR	BHLYP				LH12ct-SsifPW92				δ_{exp}
	gas. gas	gas COSMO	COSMO. gas	COSMO COSMO	gas. gas	gas COSMO	COSMO. gas	COSMO COSMO	
$[\text{ClF}_2]^-$	-190.6	-196.4	-193.4	-198.4	-169.8	-171.0	-173.3	-169.8	-125
$[\text{ClF}_4]^-$	65.3	61.3	58.5	54.9	56.5	53.8	49.9	47.5	67
$[\text{ClF}_6]^-$	250.8	252.9	243.0	245.3	224.7	226.7	217.5	219.7	-
$[\text{BrF}_2]^-$	-279.4	-288.5	-281.1	-289.5	-260.0	-267.1	-262.3	-268.9	-210
$[\text{BrF}_4]^-$	-38.2	-43.7	-41.5	-46.7	-43.3	-47.8	-46.6	-50.8	-37
$[\text{BrF}_6]^-$	113.8	116.4	108.5	111.4	97.6	100.0	92.7	95.3	94
$[\text{IF}_2]^-$	-343.0	-351.5	-344.6	-352.9	-332.4	-340.3	-333.9	-341.8	-282
$[\text{IF}_4]^-$	-99.5	-105.5	-101.3	-107.1	-107.0	-112.5	-108.8	-114.1	-106
$[\text{IF}_6]^-$	29.3	31.1	26.5	28.4	12.7	14.4	9.9	11.7	13
CFCl_3	190.77	194.77	189.11	193.25	200.31	203.63	198.72	202.17	

^a At B3LYP-D3(BJ)/def2-TZVPPD optimized structures. CFCl_3 reference shieldings at the same level have been used to obtain the relative shifts. Nonrelativistic results with pcSseg-4 basis sets for F, Cl, Br, and ANO-RCC-unc for I.

Table S5. Fully relativistic 4c-mDKS/B3LYP50/Dyall-VQZ results for ^{19}F NMR nuclear shieldings and chemical shifts of $[\text{XF}_n]^-$ ($\text{X} = \text{Cl, Br, I; } n=2, 4, 6$).^a

	$[\text{ClF}_2]^-$	$[\text{ClF}_4]^-$	$[\text{ClF}_6]^-$	$[\text{BrF}_2]^-$	$[\text{BrF}_4]^-$	$[\text{BrF}_6]^-$	$[\text{IF}_2]^-$	$[\text{IF}_4]^-$	$[\text{IF}_6]^-$	CFCl_3
σ^{iso}	389.0	126.2	-78.8	471.3	236.1	75.0	539.6	321.5	192.1	192.4
δ	-196.5	66.2	271.2	-278.9	-43.7	117.4	-347.2	-129.2	0.3	0
δ_{exp}	-125	67	—	-210	-37	94	-282	-106	13	0

^a Gas-phase results relative to CFCl_3 at the same level, at BP86-D3(BJ)(COSMO, CH_3CN)/def2-TZVPPD structures.

SUPPORTING INFORMATION

References

- [1] M. Baudler, G. Brauer, *Handbuch der Präparativen Anorganischen Chemie in drei Bänden, Bd 1*, Vol 5., Ferdinand Enke, Stuttgart, **1975**, p.166.
- [2] R. K. Harris, E. D. Becker, S. M. Cabral de Menezes, P. Granger, R. E. Hoffman, K. W. Zilm, *Pure Appl. Chem.* **2008**, *80*, 59.
- [3] G. M. Sheldrick, *Acta Crystallogr. A* **2008**, *A64*, 112.
- [4] G. M. Sheldrick, *Acta Crystallogr. C* **2015**, *C71*, 3.
- [5] O. V. Dolomanov, L. J. Bourhis, R. J. Gildea, J. A. K. Howard, H. Puschmann, *J. Appl. Cryst.* **2009**, *42*, 339.
- [6] K. Brandenburg, *Crystal Impact GbR* **2009**.
- [7] Local version derived from Turbomole version 7.4, Turbomole GmbH, 2017. Turbomole is a development of University of Karlsruhe and Forschungszentrum Karlsruhe 1989–2007, Turbomole GmbH since 2007.
- [8] a) A. D. Becke *Phys. Rev. A* **1988**, *38*, 3098; b) J. P. Perdew *Phys. Rev. B* **1986**, *33*, 8822.
- [9] a) F. Weigend, R. Ahlrichs, *Phys. Chem. Chem. Phys.* **2005**, *7*, 3297; b) D. Rappoport, F. Furche, *J. Chem. Phys.* **2010**, *133*, 134105; c) K. A. Peterson, D. Figgen, E. Goll, H. Stoll, M. Dolg, *J. Chem. Phys.* **2003**, *119*, 11113.
- [10] a) S. Grimme, J. Antony, S. Ehrlich, H. Krieg, *J. Chem. Phys.* **2010**, *132*, 154104; b) S. Grimme, S. Ehrlich, L. Goerigk, L. *J. Comput. Chem.* **2011**, *32*, 1456–1465.
- [11] A. Klamt, G. Schüürmann, *J. Chem. Soc. Perkin Trans.* **1993**, *2*, 799.
- [12] a) A. D. Becke, *J. Chem. Phys.* **1993**, *98*, 5648; b) C. Lee, W. Yang, R. G. Parr, *Phys. Rev. B* **1988**, *37*, 785.
- [13] a) F. London, *J. Phys. Radium* **1937**, *8*, 397; b) R. Ditchfield, *Mol. Phys.* **1974**, *27*, 789; c) K. Wolinski, J. F. Hinton, P. Pulay, *J. Am. Chem. Soc.* **1990**, *112*, 8251.
- [14] K. Reiter, F. Mack, F. Weigend, *J. Chem. Theory Comput.* **2018**, *14*, 191.
- [15] C. J. Schattenberg, K. Reiter, F. Weigend, M. Kaupp *J. Chem. Theory Comput.* **2020**, *16*, 931.
- [16] T. Kupka, *Magn. Reson. Chem.* **2009**, *47*, 959.
- [17] A. D. Becke, *J. Chem. Phys.* **1993**, *98*, 1372.
- [18] A. V. Arbuznikov, M. Kaupp, *J. Chem. Phys.* **2012**, *136*, 014111.
- [19] T. M. Maier, A. V. Arbuznikov, M. Kaupp *WIREs Comp. Mol. Sci.* **2019**, *9*, e1378.
- [20] F. Jensen, *J. Chem. Theory Comput.* **2015**, *11*, 132.
- [21] B. O. Roos, R. Lindh, P.-Å. Malmqvist, V. Veryazov, P.-O. Widmark, *J. Phys. Chem. A* **2005**, *108*, 2851.
- [22] S. Komorovský, M. Repiský, O. L. Malkina, V. G. Malkin, I. Malkin Ondík, M. Kaupp *J. Chem. Phys.* **2008**, *128*, 104101/1-15.
- [23] M. Repisky, S. Komorovsky, V. G. Malkin, O. L. Malkina, M. Kaupp, K. Ruud, R. Bast, R. Di Remigio, U. Ekstrom, M. Kadek, S. Knecht, L. Konecny, E. Malkin, I. Malkin-Ondik, ReSpect 5.1.0 (2019) Relativistic Spectroscopy DFT program <http://www.respectprogram.org>.
- [24] K. G. Dyall, *Theor. Chem. Acc.* **2006**, *115*, 441.
- [25] E. Bernhardt, M. Finze, H. Willner, *J. Fluor. Chem.* **2004**, *125*, 967.
- [26] a) X. Zhang, K. Seppelt, *Z. Anorg. Allg. Chem.* **1997**, *623*, 491; b) B. Scheibe, S. I. Ivlev, A. J. Karttunen, F. Kraus, *Eur. J. Inorg. Chem.* **2020**, *37*, 477.
- [27] M. J. Turner, J. J. McKinnon, S. K. Wolff, D. J. Grimwood, P. R. Spackman, D. Jayatilaka and M. A. Spackman, *CrystalExplorer17*, University of Western Australia, **2017**.

A.2. Soluble Fluoridobromates as Well-Behaved Strong Fluorination Reagents

European Journal of Inorganic Chemistry

Supporting Information

Soluble Fluoridobromates as Well-Behaved Strong Fluorination Reagents

Jonas R. Schmid, Patrick Pröhm, Patrick Voßnacker, Günter Thiele,
Mathias Ellwanger, Simon Steinhauer, Sebastian Riedel*

Content:

General information	1
Experimental section	2
Crystallographic section	9
Computational section	12
Author contribution	13
References	13

Caution!

Fluorine, even under dilute conditions, is extraordinarily reactive and can react violently with organic materials under the formation of HF. Similarly, difluoridobromate(I), tetrafluoridobromate(III) and heptafluoridodibromate(III) are strongly oxidizing compounds, which can decompose violently under certain conditions when exposed to organic materials. Exposure to acidic compounds (e.g. water or boron trifluoride) enhances the reactivity due to the *in-situ* formation of BrF₃. Additionally, precipitation also enhances the reactivity of organic difluoridobromate(I), tetrafluoridobromate(III) and heptafluoridodibromate(III) salts.

General Information

All experiments were performed under rigorous exclusion of moisture and oxygen using standard Schlenk techniques. Solids were handled in a dry box under argon atmosphere (O₂ < 0.5 ppm, H₂O < 0.5 ppm). Acetonitrile and propionitrile were dried over Sicapent® prior to use. Bromine was dried over molecular sieve (3 Å). SO₂ClF was dried over CaH₂ and stored over fresh CaH₂. [NEt₃Me]Br was dried overnight at 120 °C under dynamic vacuum. Metals were heated to 500 °C under reduced pressure for several minutes. All other chemicals were used as purchased.

Raman spectra were recorded on a Bruker MultiRAM II equipped with a low-temperature Ge detector (1064 nm, 30-180 mW, resolution, 4 cm⁻¹). NMR spectra were recorded on a JEOL 400 MHz ECS or ECZ spectrometer or on a Bruker AVANCE III 700 MHz spectrometer. All reported chemical shifts are referenced to the δ values given in IUPAC recommendations of 2008 using the ²H signal of the deuterated solvent as internal reference.^[1] For external locking acetone-d₆ was flame sealed in a glass capillary and the lock oscillator frequency was adjusted to give $\delta(^1\text{H}) = 7.26$ ppm for a CHCl₃ sample locked on the capillary. Crystal data were collected on a Bruker D8 Venture diffractometer with a Photon 100 CMOS area detector with MoK α radiation. Single crystals were picked at -80 °C under nitrogen atmosphere and mounted on a 0.15 mm Mitegen micromount using perfluoroether oil diluted with perfluorohexane. The structures were solved with the ShelXT^[2] structure solution program using intrinsic phasing and refined with the ShelXL^[3] refinement package using least squares minimizations by using OLEX2.^[4] For visualization the Diamond V3.0 program was used.^[5]

Structure optimizations were performed using the Turbomole V7.3 program package^[6] at DFT level with the B3LYP hybrid functional^[7,8] and the triple- ζ basis set def2-TZVPP^[9,10] on an m5 grid. Dispersion correction by Grimme (D3)^[11] and Becke-Johnson damping (BJ)^[12] was employed for the calculations as implemented. Minimum structures were confirmed by frequency analysis within the harmonic approximation as implemented in the Turbomole code. NBO analysis was carried out using the NBO7.0 program^[13] in the Gaussian 16^[14] interface. For visualization the program VMD V1.9.3 was used.^[15]

Bis(triethylmethylammonium) hexabromide [NEt₃Me]₂[Br₆]

Triethylmethylammonium bromide (0.1 g, 0.5 mmol, 1.0 eq.) was combined with bromine (0.08 g, 0.5 mmol, 1.0 eq.) in a dried Schlenk tube. The reaction mixture was allowed to warm to r.t., propionitrile (0.5 mL) was added and slowly cooled to -80 °C. Single crystals suitable for X-ray diffraction were obtained after 12 days.

FT-Raman (298 K): $\tilde{\nu}$ [cm⁻¹] = 2986 (w, CH), 2943 (w, CH), 257 (s, [Br₆]²⁻), 211 (m, [Br₆]²⁻), 201 (m, [Br₆]²⁻), 160 (s, [Br₆]²⁻).

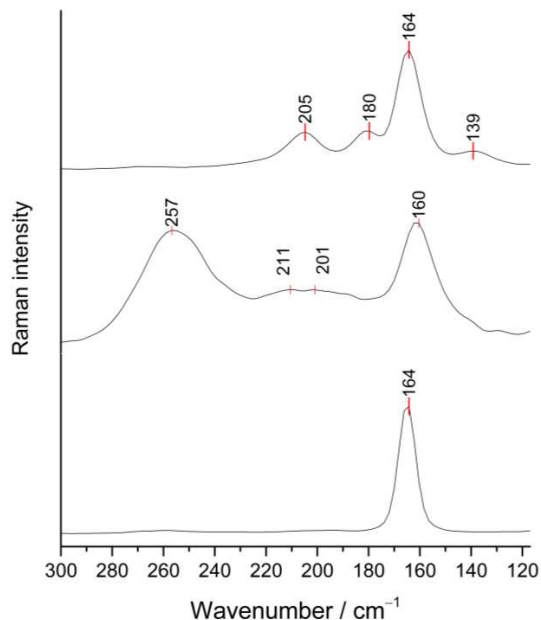


Figure S1. Raman spectra of [NEt₃Me]₂[Br₆] in MeCN solution at -77 K (bottom), [NEt₃Me]₂[Br₆] single crystal at 298 K (middle) and the known compound [C₅H₁₁N₂Br₂][Br₆] (top).^[16]

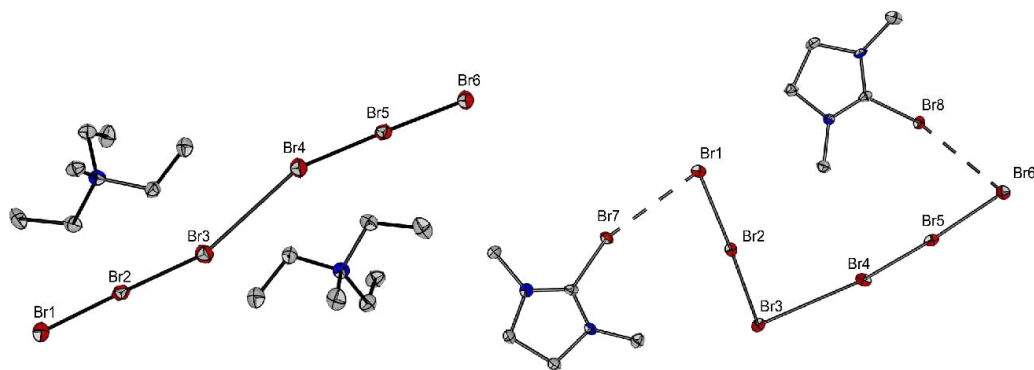


Figure S2. Solid state structures of [NEt₃Me]₂[Br₆] (left) and [C₅H₁₀N₂Br₂][Br₆] (right).^[16] Thermal ellipsoids are shown at 50 % probability at 100 K. Color code: red = bromine, grey = carbon, blue = nitrogen.

Figure S2 shows the solid-state structures of the two [Br₆]²⁻ anions (left: new; right: previously reported). However, the structure reported in this work (Figure S2 left) significantly differs from the previously reported structure (Figure S2 right).^[16] The structure reported by our group in 2018 shows an L-shape motive whereas the structure we are reporting here exhibits a zig-zag chain geometry. This is due to the different cation-anion interactions. The bromine atoms of [C₅H₁₀N₂Br₂]⁺ form halogen bonds with the terminal bromine atoms on the anion (340.1(1) pm, 345.6(1) pm).^[16] The bond angles are Br₂-Br₁-Br₇ = 76.56(3)° (Br₂-Br₁-Br₇) and 72.81(2)° (Br₅-Br₆-Br₈).^[16] A similar directional interaction is not present in the [Br₆]²⁻ anion presented in this work. Both [Br₆]²⁻ units can be interpreted as two end-on connected [Br₃]⁻ fragments (Br₁-Br₂-Br₃ and Br₄-Br₅-Br₆). The bond angles between the two [Br₃]⁻ moieties in [NEt₃Me]₂[Br₆] of 159.9(2)° (Br₂-Br₃-Br₄) and 162.6(2)° (Br₃-Br₄-Br₅) are significantly wider than in the reported structure (87.7°) (Br₂-Br₃-Br₄).

Interestingly, the distance between the two $[\text{Br}_3]^-$ fragments (Br3–Br4) in this structure is with 342.8(9) pm shorter than in the reported structure (359.3(1) pm). The four Raman bands in the Br–Br region (257, 211, 201, 160 cm^{-1}) are found at higher wavenumbers in comparison to the known structure (205, 181, 165 and 139 cm^{-1}). Therefore, we assume that the overall bonding in the anion is stronger.

Triethylmethylammonium difluoridobromate(I) $[\text{NEt}_3\text{Me}][\text{BrF}_2]$

Triethylmethylammonium bromide (0.1 g, 0.5 mmol, 1.0 eq.) and bromine (0.08 g, 0.5 mmol, 1.0 eq.) were dissolved in propionitrile (1.5 ml) and cooled to $-40\text{ }^\circ\text{C}$. Dilute fluorine (10 % in Ar, 20 ml min^{-1} , 7.5 min, 1 eq.) was bubbled through the reaction mixture. Subsequently, Ar (20 ml min^{-1} , 7.5 min) was passed through the reaction mixture to get rid of any excess fluorine gas. The reaction mixture was slowly cooled to $-80\text{ }^\circ\text{C}$. Single crystals suitable for X-ray diffraction were obtained after one and a half months.

^1H NMR (401 MHz, EtCN, ext. acetone- d_6 , 298 K) δ [ppm] = 3.83 (q, $^3J(^1\text{H}, ^1\text{H}) = 7.3\text{ Hz}$, 6H, CH_2); 3.44 (s, 3H, NCH_3), 1.82 (tt, $^3J(^1\text{H}, ^1\text{H}) = 7.3$, $^2J(^{14}\text{N}, ^1\text{H}) = 2.0\text{ Hz}$, 9H, CH_3); ^{19}F NMR (377 MHz, EtCN, ext. acetone- d_6 , 22 $^\circ\text{C}$) δ [ppm] = -216.74 .

Raman (crystal, 77 K): $\tilde{\nu}$ [cm^{-1}] = 3024 (w), 2982 (m), 2941 (m), 2910 (w), 2247 (w), 1460 (w), 1321 (w), 1126 (w), 1076 (w), 999 (w), 963 (w), 885 (w), 685 (m), 546 (w), 467 (vs).

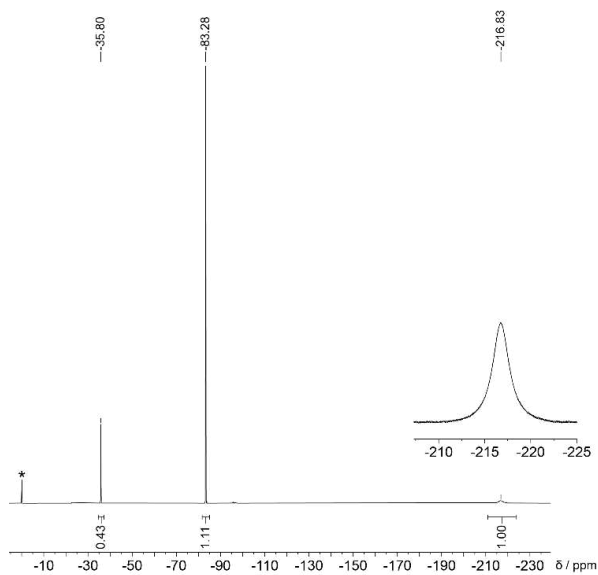


Figure S3. ^{19}F NMR spectrum (377 MHz, EtCN, ext. acetone- d_6 , 298 K) of $[\text{NEt}_3\text{Me}][\text{BrF}_2]$. Asterisk denotes CFCl_3 . Signals at 35.8 ppm = $[\text{BrF}_4]^-$, 83.3 ppm = fluorinated solvent, 216.8 ppm = $[\text{BrF}_2]^-$.

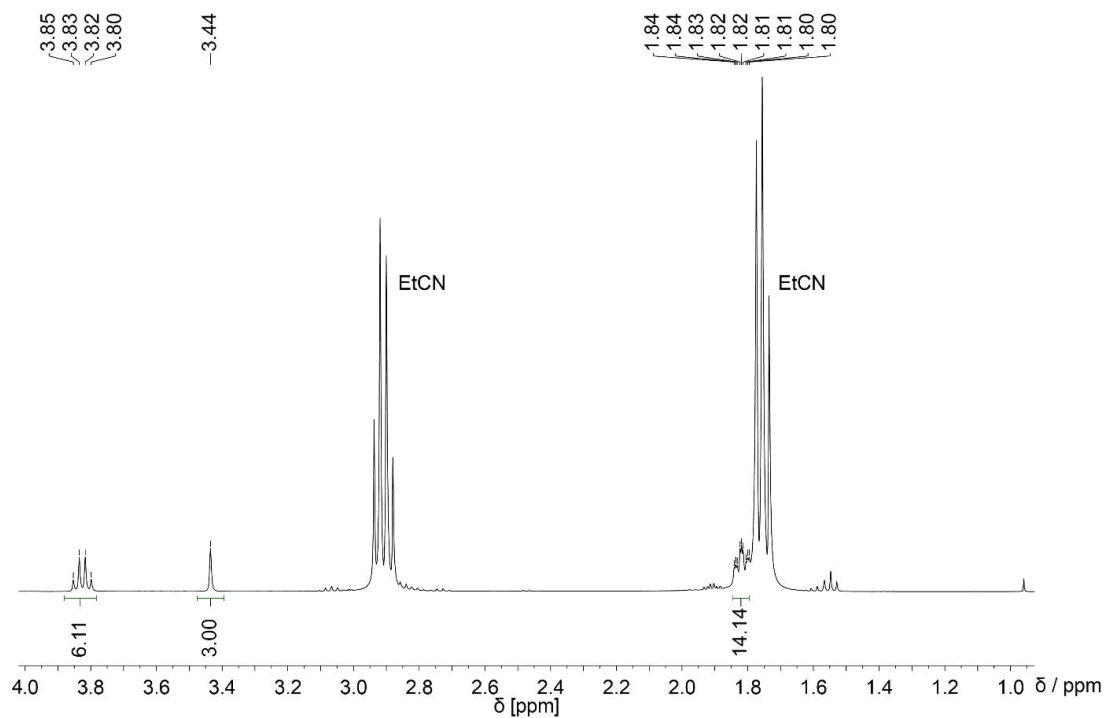


Figure S4. ^1H NMR spectrum (401 MHz, EtCN, ext. acetone- d_6 , 298 K) of $[\text{NEt}_3\text{Me}][\text{BrF}_2]$.

Triethylmethylammonium tetrafluoridobromate(III) [NEt₃Me][BrF₄]

Triethylmethylammonium bromide (0.1 g, 0.5 mmol, 1.0 eq.) was dissolved in acetonitrile or propionitrile or bromine (1.5 ml) and cooled to -30 °C (MeCN) or -55 °C (EtCN) or 0 °C (Br₂). Dilute fluorine (10 % in Ar, 20 ml min⁻¹, 15 min, 2.4 eq.) was bubbled through the reaction mixture. Subsequently, Ar (20 ml min⁻¹, 7.5 min) was passed through the reaction mixture to get rid of any excess fluorine gas. Single crystals were obtained by slowly cooling [NEt₃Me][BrF₄] in a 2:1 mixture of CFCI₃:MeCN to -40 °C.

¹H NMR (400 MHz, MeCN, ext. acetone-d₆, 238 K) δ[ppm] = 2.95 (q, ³J(¹H, ¹H) = 7.3 Hz, 6H, CH₂), 2.57 (s, 3H, NCH₃), 0.95 (tt, ³J(¹H, ¹H) = 7.3, ²J(¹⁴N, ¹H) = 2.0 Hz, 9H, CH₃); ¹⁹F NMR (376 MHz, MeCN, ext. acetone-d₆, 298 K) δ[ppm] = -35.1. Raman (crystal, 77 K): $\tilde{\nu}$ [cm⁻¹] = 2989 (m), 2953 (m), 1512 (m), 1472 (w), 685 (m), 519 (s), 442 (m), 247 (w).

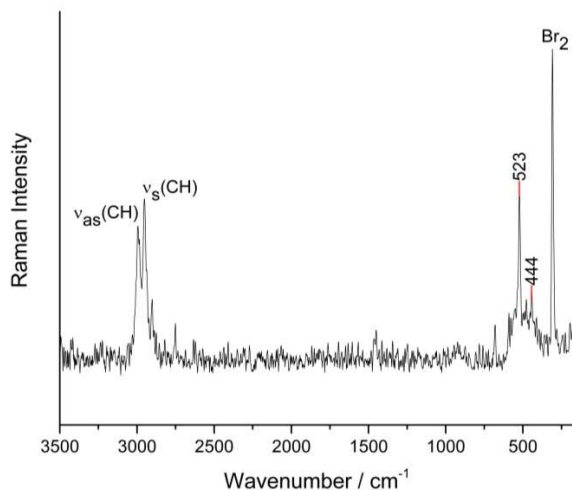


Figure S5. Raman spectrum of [NEt₃Me][BrF₄] in Br₂ solution at 77 K.

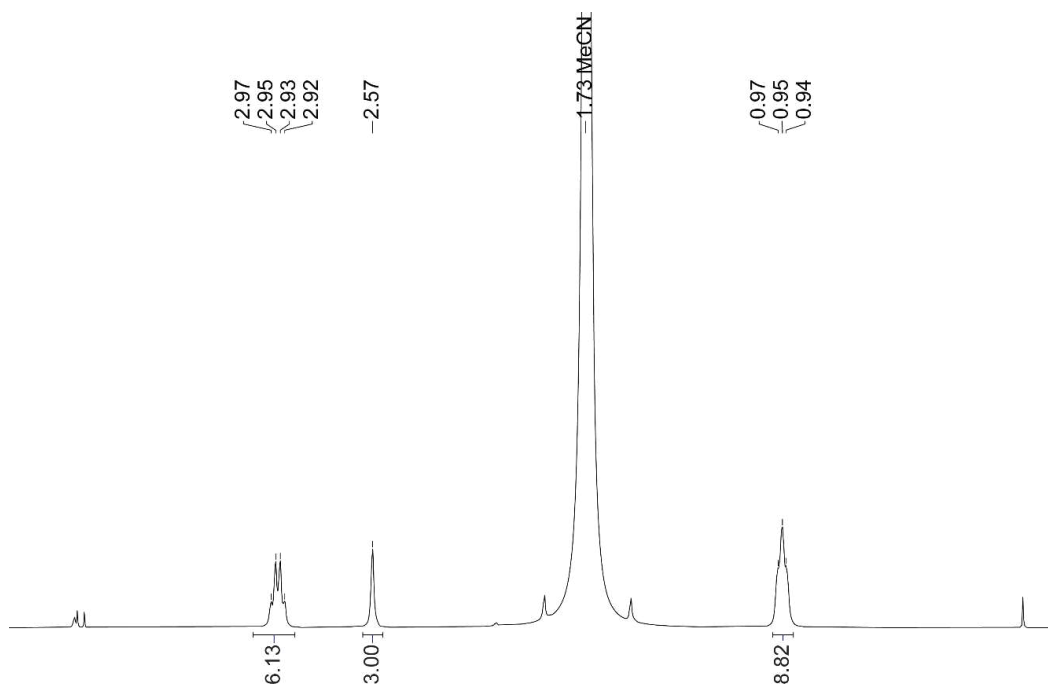


Figure S6. ¹H NMR spectrum (400 MHz, MeCN, ext. acetone-d₆, 238 K) of [NEt₃Me][BrF₄].

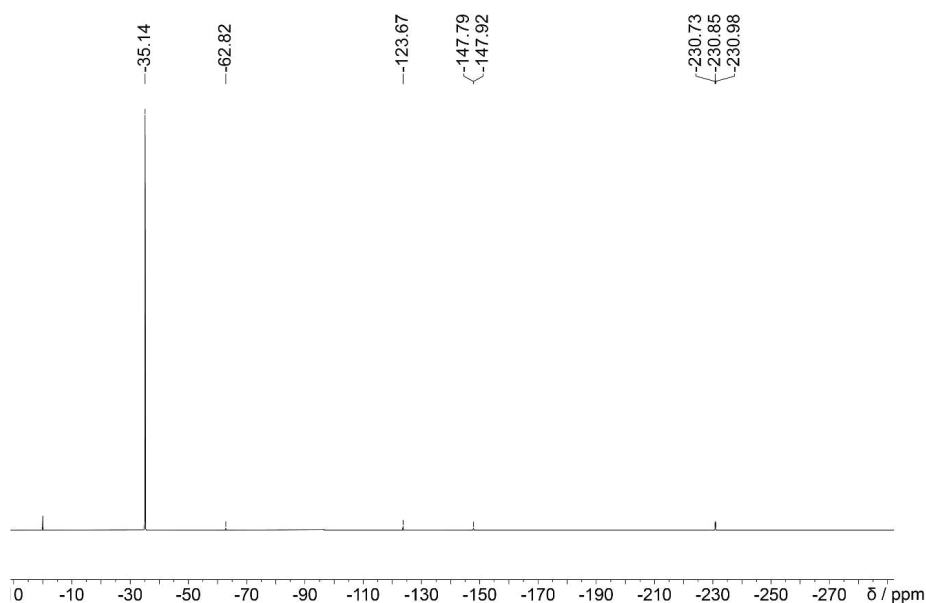


Figure S7. ^{19}F NMR spectrum (377 MHz, MeCN, ext. acetone- d_6 , 238 K) of $[\text{NEt}_3\text{Me}][\text{BrF}_4]$.

Triethylmethylammonium heptafluorodibromate(III) $[\text{NEt}_3\text{Me}][\text{Br}_2\text{F}_7]$

Triethylmethylammonium bromide (0.1 g, 0.5 mmol, 1.0 eq.) was dissolved in bromine (3.8 g) and cooled to 0 °C. Dilute fluorine (10 % in Ar, 20 ml min^{-1} , 26.5 min, 4 eq.) was bubbled through the reaction mixture. Subsequently, Ar (20 ml min^{-1} , 7.5 min) was passed through the reaction mixture to get rid of any excess fluorine gas. Excess bromine was removed under reduced pressure at 0 °C. Single crystals were obtained from an SO_2ClF solution by slow cooling from -20 °C to -80 °C.

Raman (crystal, 77 K): $\tilde{\nu}$ [cm^{-1}] = 3001 (w), 2961 (w), 683 (w), 610 (s), 573 (m), 513 (s), 505 (s) 477 (w).

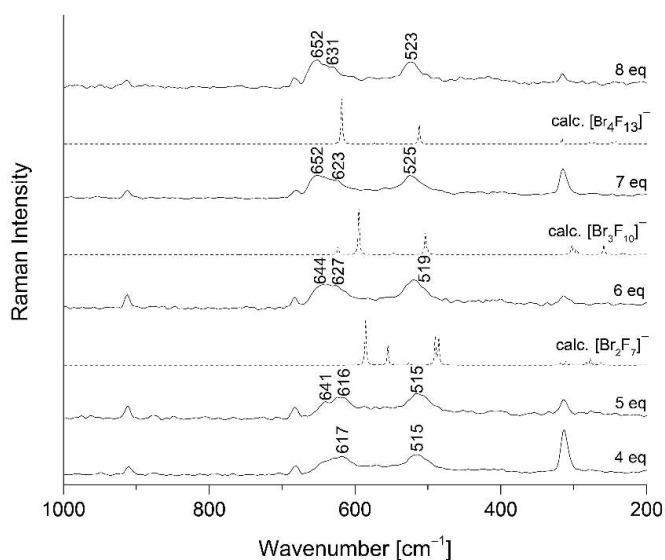


Figure S8. Experimental Raman spectra (solid lines) of the reaction between $[\text{NEt}_3\text{Me}]\text{Br}$ with different amounts of fluorine in liquid bromine in comparison with calculated Raman spectra (dashed lines) of $[\text{Br}_x\text{F}_{(3x+1)}]^-$ ($x = 2-4$). Note, to achieve sufficient sensitivity for Br-F containing species in the Raman spectrum the excess Br_2 had to be removed at low temperatures.

Reactivity studies with noble metals

An aliquot of noble metal sponge was treated with excess of a $[\text{NEt}_3\text{Me}][\text{BrF}_4]$ solution in acetonitrile. The reaction vessels were exposed to ultrasonic to accelerate the dissolution process. The reaction solutions were studied with ^{19}F NMR spectroscopy, revealing the formation of $[\text{AuF}_4]^-$. In the case of silver it was possible to grow single crystals of $[\text{NEt}_3\text{Me}][\text{Ag}_2\text{Br}_3]$.

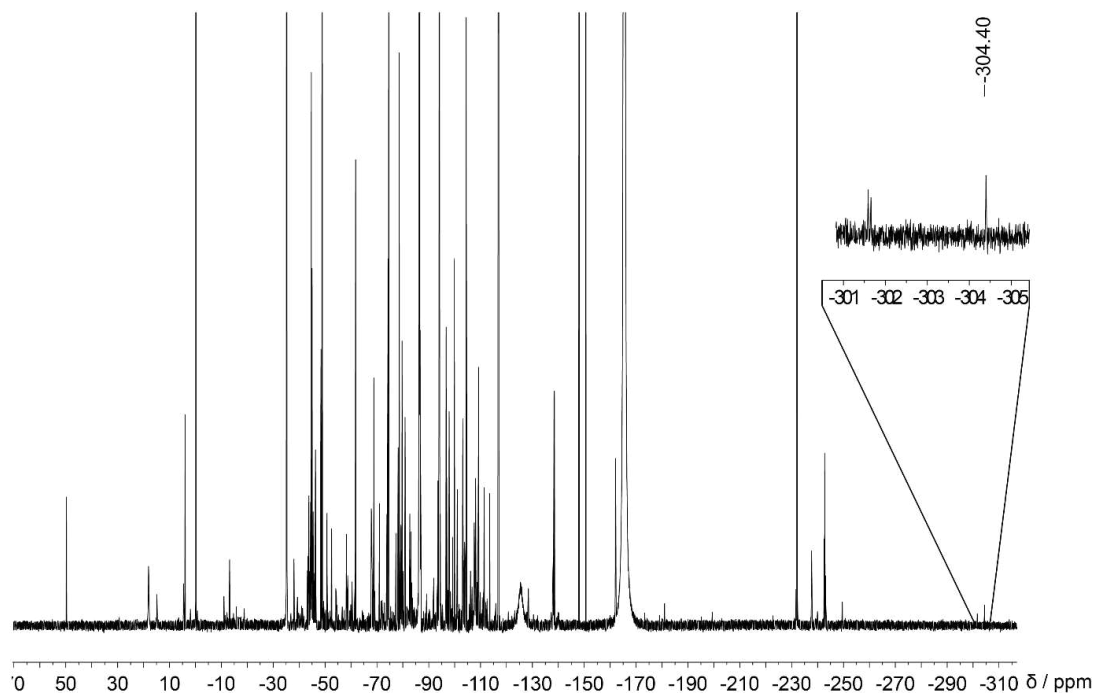


Figure S9. ^{19}F NMR spectrum (377 MHz, MeCN, ext. acetone- d_6 , 298 K) of the reaction mixture of $[\text{NEt}_3\text{Me}][\text{BrF}_4]$ with Au.

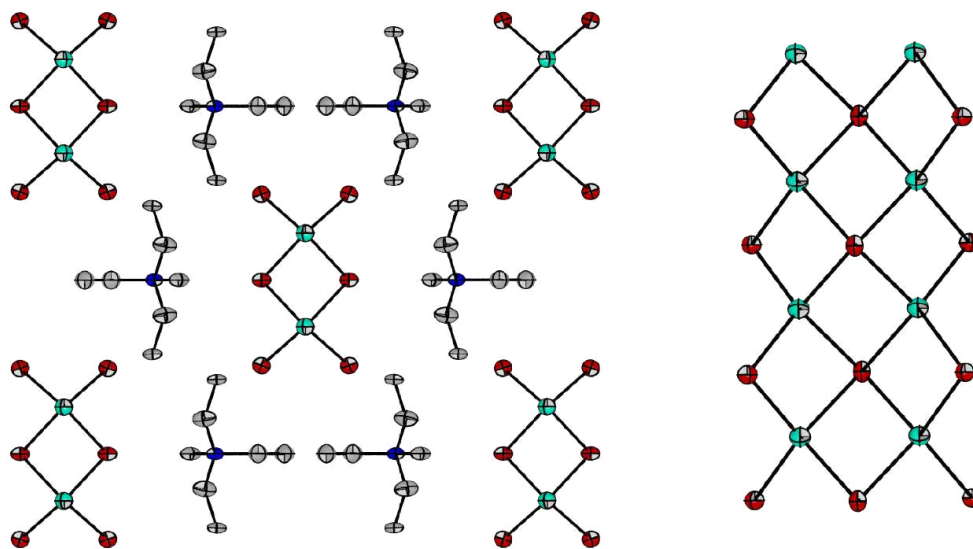
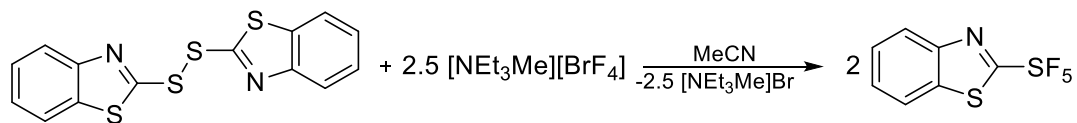


Figure S10. Solid state structure of $[\text{NEt}_3\text{Me}][\text{Ag}_2\text{Br}_3]$. Left: unit cell; right: anionic moiety. Color code: red = Br, teal = Ag, blue = N, grey = C. Hydrogen atoms are omitted for clarity, disorder is omitted for clarity. Thermal ellipsoids shown at 50 % probability at 100 K.

Reaction of [NEt₃Me][BrF₄] with a disulfide

2,2'-Dibenzothiazolyl disulfide (80.0 mg, 0.25 mmol, 1.0 eq.) was cooled to $-20\text{ }^{\circ}\text{C}$. A $-40\text{ }^{\circ}\text{C}$ cold solution of [NEt₃Me][BrF₄] in acetonitrile (4 mL, 0.38 mol/L, 1.5 mmol, 6.0 eq.) was added, the reaction mixture allowed to warm up to r.t. and stirred overnight. The obtained yellow solution was washed with water (30 ml), extracted with dichloromethane (3 x 40 ml), dried over magnesium sulfate and concentrated in vacuo. Purification by column chromatography over silica gel (eluent = *n*-pentane:DCM, 10:1) afforded 2-(pentafluoro-λ⁶-sulfanyl)benzo[d]thiazole as a colourless solid. No yield was determined due to volatility and solvent impurities.

¹H NMR (700 MHz, CDCl₃, 298 K) δ [ppm] = 8.18 (d, ³*J*(¹H, ¹H) = 8.2 Hz, 1H), 7.95 (d, ³*J*(¹H, ¹H) = 8.0 Hz, 1H), 7.63 (d, ³*J*(¹H, ¹H) = 8.3 Hz, 1H), 7.59 (d, ³*J*(¹H, ¹H) = 8.3 Hz, 1H); ¹³C NMR (176 MHz, CDCl₃, 298 K) δ [ppm] = 170.62 (C_q), 148.78 (C_q), 135.23 (C_q), 128.22 (CH), 127.71 (CH), 125.55 (CH), 121.82 (CH); ¹⁹F NMR (377 MHz, CDCl₃, 298 K) δ [ppm] = 74.2 (XY₄, 1F, SF₅ axial ²*J*(¹⁹F, ¹⁹F) = 153.68 Hz), 62.4 (XY₄, 4F, SF₅ equatorial, ²*J*(¹⁹F, ¹⁹F) = 153.68 Hz). LRMS (ESI+, quadrupol, MeCN) = 262.0 ([M-H]⁺)

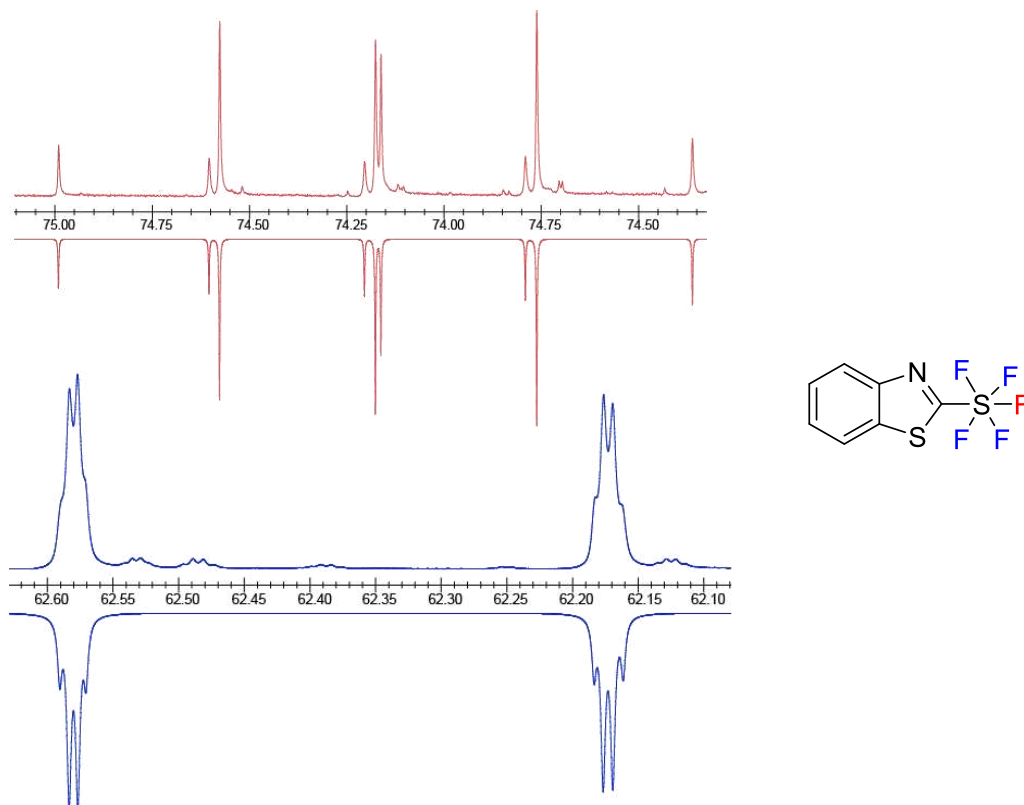


Figure S11. ¹⁹F NMR spectrum (377 MHz, CDCl₃ ext. acetone-d₆, 298 K) of 2-(pentafluoro-λ⁶-sulfanyl)benzo[d]thiazole. Experimental spectrum with positive intensities, simulated spectrum with negative intensities.

Crystallographic section

Compound	[NEt ₃ Me] ₂ [Br ₆]	[NEt ₃ Me][BrF ₂]
Empirical formula	C ₇ H ₁₈ Br ₃ N	C ₇ H ₁₈ BrF ₂ N
Formula weight	355.95	234.13
Temperature/K	100	100
Crystal system	monoclinic	orthorhombic
Space group	<i>P</i> 2 ₁ / <i>c</i>	<i>P</i> 2 ₁ 2 ₁ 2 ₁
<i>a</i> /Å	25.2785(18)	7.5791(7)
<i>b</i> /Å	7.0747(5)	10.9890(9)
<i>c</i> /Å	13.9597(10)	12.4680(11)
<i>α</i> /°	90	90
<i>β</i> /°	97.279(3)	90
<i>γ</i> /°	90	90
Volume/Å ³	2476.4(3)	1038.42(16)
Z	8	4
$\rho_{\text{calc}}/\text{cm}^{-3}$	1.909	1.498
μ/mm^{-1}	9.727	3.935
F(000)	1376	480
Crystal size/mm ³	0.186 × 0.12 × 0.054	0.508 × 0.111 × 0.105
Radiation	MoK α (λ = 0.71073)	MoK α (λ = 0.71073)
2 θ range for data collection/°	4.874 to 56.618	4.942 to 66.298
Index ranges	-33 ≤ <i>h</i> ≤ 33, -9 ≤ <i>k</i> ≤ 9, -18 ≤ <i>l</i> ≤ 18	-11 ≤ <i>h</i> ≤ 11, -16 ≤ <i>k</i> ≤ 16, -19 ≤ <i>l</i> ≤ 19
Reflections collected	78418	22854
Independent reflections	6169 [R _{int} = 0.0427, R _{sigma} = 0.0182]	3962 [R _{int} = 0.0322, R _{sigma} = 0.0307]
Data/restraints/parameters	6169/9/263	3962/0/104
Goodness-of-fit on F ²	1.093	1.06
Final R indexes [<i>I</i> ≥ 2 σ (<i>I</i>)]	<i>R</i> ₁ = 0.0289, <i>wR</i> ₂ = 0.0581	<i>R</i> ₁ = 0.0185, <i>wR</i> ₂ = 0.0422
Final R indexes [all data]	<i>R</i> ₁ = 0.0384, <i>wR</i> ₂ = 0.0611	<i>R</i> ₁ = 0.0220, <i>wR</i> ₂ = 0.0430
Largest diff. peak/hole / e Å ⁻³	0.75/-0.45	0.35/-0.30
Flack parameter		0.024(4)
CCDC deposition number	2015010	2015013

A. Supporting Information of Publications

Compound	[NEt ₃ Me][BrF ₄]	[NEt ₃ Me][Br ₂ F ₇]	[NEt ₃ Me][Ag ₂ Br ₃]
Empirical formula	C ₇ H ₁₈ BrF ₄ N	C ₇ H ₁₈ Br ₂ F ₇ N	C ₇ H ₁₈ Ag ₂ Br ₃ N
Formula weight	272.13	409.04	571.69
Temperature/K	100	100	100
Crystal system	monoclinic	triclinic	orthorhombic
Space group	<i>P</i> 2 ₁ / <i>m</i>	<i>P</i> $\bar{1}$	<i>Cmcm</i>
<i>a</i> /Å	6.8683(4)	7.3028(5)	11.9394(6)
<i>b</i> /Å	13.5094(7)	8.0345(6)	16.5964(10)
<i>c</i> /Å	11.8934(6)	12.1132(6)	6.8858(4)
α /°	90	74.228(2)	90
β /°	97.294(2)	79.170(3)	90
γ /°	90	86.849(2)	90
Volume/Å ³	1094.62(10)	671.79(8)	1364.43(13)
Z	4	2	4
$\rho_{\text{calc}}/\text{cm}^{-3}$	1.651	2.022	2.783
μ/mm^{-1}	3.77	6.095	11.618
F(000)	552	400	1064
Crystal size/mm ³	0.48 × 0.332 × 0.292	0.433 × 0.332 × 0.238	0.105 × 0.082 × 0.015
Radiation	MoK α (λ = 0.71073)	MoK α (λ = 0.71073)	MoK α (λ = 0.71073)
2 θ range for data collection/°	4.584 to 90.766	5.268 to 61.254	4.202 to 50.712
Index ranges	-13 ≤ <i>h</i> ≤ 13, -27 ≤ <i>k</i> ≤ 27, -23 ≤ <i>l</i> ≤ 23	-10 ≤ <i>h</i> ≤ 10, -11 ≤ <i>k</i> ≤ 11, -17 ≤ <i>l</i> ≤ 17	-14 ≤ <i>h</i> ≤ 14, -20 ≤ <i>k</i> ≤ 20, -8 ≤ <i>l</i> ≤ 8
Reflections collected	121643	61797	75881
Independent reflections	9419 [<i>R</i> _{int} = 0.0440, <i>R</i> _{sigma} = 0.0187]	4137 [<i>R</i> _{int} = 0.0293, <i>R</i> _{sigma} = 0.0125]	715 [<i>R</i> _{int} = 0.0553, <i>R</i> _{sigma} = 0.0069]
Data/restraints/parameters	9419/0/131	4137/0/158	715/0/52
Goodness-of-fit on <i>F</i> ²	1.041	1.108	1.195
Final <i>R</i> indexes [<i>I</i> ≥ 2 σ (<i>I</i>)]	<i>R</i> ₁ = 0.0199, <i>wR</i> ₂ = 0.0450	<i>R</i> ₁ = 0.0139, <i>wR</i> ₂ = 0.0323	<i>R</i> ₁ = 0.0271, <i>wR</i> ₂ = 0.0649
Final <i>R</i> indexes [all data]	<i>R</i> ₁ = 0.0262, <i>wR</i> ₂ = 0.0463	<i>R</i> ₁ = 0.0153, <i>wR</i> ₂ = 0.0329	<i>R</i> ₁ = 0.0374, <i>wR</i> ₂ = 0.0777
Largest diff. peak/hole / e Å ⁻³	0.45/-0.93	0.39/-0.53	1.53/-1.37
Flack parameter			
CCDC deposition number	2015014	2015012	2015008

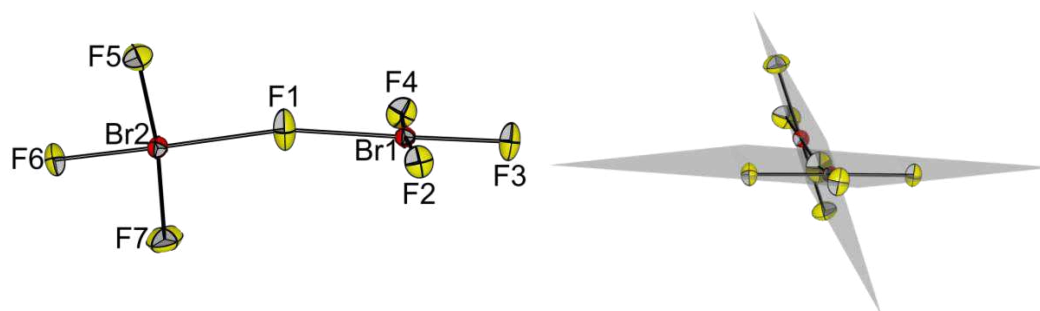


Figure S12. Solid-state structure of the anionic moiety in $[\text{NEt}_3\text{Me}][\text{Br}_2\text{F}_7]$ (left) and with two planes including all atoms of the two $[\text{BrF}_4]^-$ fragments (F1F2F3F4Br1 and F1F5F6F7Br2).

Table S1. Comparison of structural parameters of the solid state structures of $[\text{NEt}_3\text{Me}][\text{Br}_2\text{F}_7]$, $[\text{PbF}][\text{Br}_2\text{F}_7]^{[17]}$, $\text{Rb}[\text{Br}_2\text{F}_7]^{[18]}$, $\text{Cs}[\text{Br}_2\text{F}_7]^{[18]}$ and of the optimized structure of $[\text{Br}_2\text{F}_7]^-$ at B3-LYP-D3BJ/def2-TZVPP.

Object ^a	$[\text{PbF}][\text{Br}_2\text{F}_7]^{[17]}$	$\text{Rb}[\text{Br}_2\text{F}_7]^{[18]}$	$\text{Cs}[\text{Br}_2\text{F}_7]^{[18]}$	$[\text{NEt}_3\text{Me}][\text{Br}_2\text{F}_7]$	Optimized structure
Br1—F1	220.0(11)	214.5(2)	214.30(12)	206.68(7)	215.7
Br2—F1	225.4(10)	211.5(2)	211.26(12)	218.61(7)	215.7
Br1—F2	179.8(11)	185.5(2)	185.81(12)	188.10(7)	188.3
Br1—F3	175.3(12)	176.7(2)	176.86(11)	179.18(7)	181.8
Br1—F4	194.2(12)	187.1(2)	186.81(12)	185.78(7)	188.8
Br2—F5	184.5(12)	1.845(2)	184.88(12)	185.85(7)	188.8
Br2—F6	173.6(12)	178.0(2)	188.46(12)	176.38(7)	181.8
Br2—F7	186.3(12)	189.0(2)	177.86(12)	184.76(8)	188.3
$\angle(\text{Br1}-\text{F1}-\text{Br2})$	105.6(5)	134.75(9)	140.27(6)	166.86(5)	128.0
$\Theta(\text{F4}-\text{Br1}-\text{F1}-\text{Br2})^b$	85.2(3)	65.31(6)	61.90(4)	70.40(4)	84.983

^asee Figure S12 left ^b torsion angle between planes shown in Figure 12 right

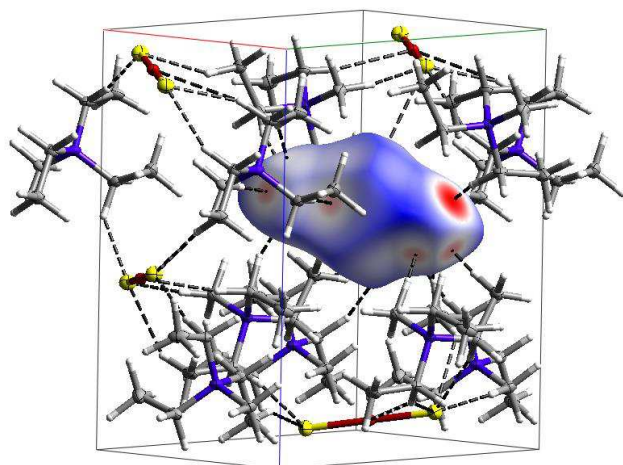


Figure S13. Hirshfeld surface calculated for $[\text{NEt}_3\text{Me}][\text{BrF}_2]$ showing various short cation-anion contacts.

Computational section

To gain a deeper understanding of the bonding and the electronic situation in $[\text{Br}_2\text{F}_7]^-$ in general, we analyzed the wavefunction with an NBO analysis based on the optimized structure (B3LYP-D3-BJ/def2-TZVPP) as well as on the solid-state structure of $[\text{NEt}_3\text{Me}][\text{Br}_2\text{F}_7]$ reported in this work and the solid state structure of $\text{Cs}[\text{Br}_2\text{F}_7]$ reported by Kraus *et al.*^[17] The structural parameters of the optimized structure are given in Table S1.

The NBO analysis reveals that a 3-centre-4-electron bond is present in the F1-Br-F2 fragment (Figure S14). A large energy gain (452 kJ/mol) is associated with the delocalization of the F2 lone pair in the Br-F1 antibonding orbital.

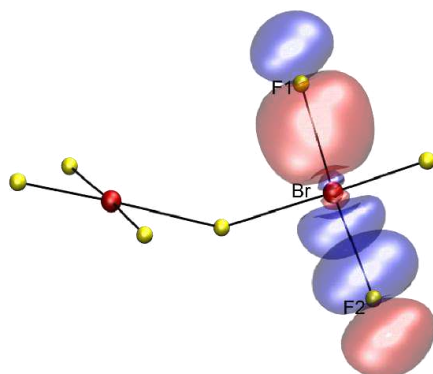


Figure S14. 3-centre-4-electron bond in $[\text{Br}_2\text{F}_7]^-$ (optimized structure) in the F1-Br-F2 fragment.

In an MO treatment, the F_b -Br interaction is largely due to the interaction between two F_b lone pairs with the $\sigma^*(\text{Br}-\text{F}')$. The graphical representation of the larger interaction (102 kJ/mol) is shown in Figure 5. The smaller contribution is computed to 58 kJ/mol, resulting from a perpendicular lone pair with the same $\sigma^*(\text{Br}-\text{F}')$.

The NBO analyses of the solid state structures of $\text{Cs}[\text{Br}_2\text{F}_7]$ reported by Kraus and $[\text{NEt}_3\text{Me}][\text{Br}_2\text{F}_7]$ in this work did not show any fundamentally different results. The 3c-4e⁻ bond is comparable (delocalization energies: optimized: 452 kJ/mol, $\text{Cs}[\text{Br}_2\text{F}_7]$: 432 kJ/mol, $[\text{NEt}_3\text{Me}][\text{Br}_2\text{F}_7]$: 452 kJ/mol). The interaction energies of the bridging fluorine atom F_b with the $\sigma^*(\text{Br}-\text{F}')$ in the case of $\text{Cs}[\text{Br}_2\text{F}_7]$ are: 43 kJ/mol, 85 kJ/mol 48kJ/mol, and 68 kJ/mol. (Note: due to the different bond lengths between F_b and the two bromine centers the two fragments are no longer equal and therefore have different interaction energies.) In the case of the crystal structure reported in this work the interaction energies between the F_b lone pair the $\sigma^*(\text{Br}-\text{F}')$ are computed to: 169 kJ/mol, 43 kJ/mol, 85 kJ/mol and 34 kJ/mol. Notably, due to the significantly different bond lengths between the bromine centers and the bridging fluorine atom $\Delta d(\text{Br}-\text{F}_b) = 12$ pm the interactions on one side of the molecule are significantly stronger than on the other side.

The natural charges are similar within the range of $\Delta\text{NPA} = \pm 0.02$ in all three cases (Figure S15).

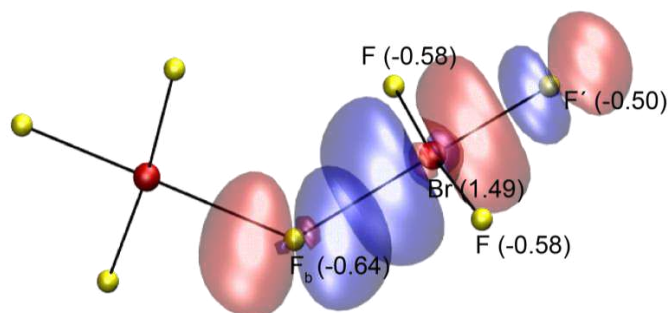


Figure S15. MOs corresponding to the interaction of the lone pair of F_b with the $\sigma^*(\text{Br}-\text{F}')$ orbital in the optimized $[\text{Br}_2\text{F}_7]^-$ structure. NPAs of the optimized structure in brackets.

Author Contribution

Jonas R. Schmid: preparative work, Raman measurements, NMR measurements, data interpretation

Patrick Pröhm: manuscript preparation, VT NMR measurements, computational chemistry, data interpretation, project supervision

Patrick Voßnacker: Crystallography, Raman measurements

Günther Thiele: Crystallography

Simon Steinhauer: Crystallography, project supervision

Mathias Ellwanger: Project supervision, data interpretation

Sebastian Riedel: General supervision

References

- [1] R. K. Harris, E. D. Becker, S. M. Cabral de Menezes, P. Granger, R. E. Hoffman, K. W. Zilm, *Pure Appl. Chem.* **2008**, *80*, 59.
- [2] G. M. Sheldrick, *Acta Cryst. A* **2008**, *A64*, 112.
- [3] G. M. Sheldrick, *Acta Cryst. C* **2015**, *C71*, 3.
- [4] O. V. Dolomanov, L. J. Bourhis, R. J. Gildea, J. A. K. Howard, H. Puschmann, *J. Appl. Cryst.* **2009**, *42*, 339.
- [5] K. Brandenburg, *Crystal Impact GbR* **2009**.
- [6] TURBOMOLE GmbH, *TURBOMOLE V7.3. a development of University of Karlsruhe and Forschungszentrum Karlsruhe GmbH*, **2018**.
- [7] A. D. Becke, *Phys. Rev. A* **1988**, *38*, 3098.
- [8] C. Lee, W. Yang, R. G. Parr, *Phys. Rev. B* **1988**, *37*, 785.
- [9] F. Weigend, M. Häser, H. Patzelt, R. Ahlrichs, *Chem. Phys. Lett.* **1998**, *294*, 143.
- [10] F. Weigend, R. Ahlrichs, *Phys. Chem. Chem. Phys.* **2005**, *7*, 3297.
- [11] S. Grimme, J. Antony, S. Ehrlich, H. Krieg, *J. Chem. Phys.* **2010**, *132*, 154104.
- [12] S. Grimme, S. Ehrlich, L. Goerigk, *J. Comput. Chem.* **2011**, *32*, 1456.
- [13] E. D. Glendening, J. K. Badenhoop, A. E. Reed, J. E. Carpenter, J. A. Bohmann, C. M. Morales, P. Karafiloglou, C. R. Landis, and F. Weinhold, *NBO 7.0*, Theoretical Chemistry Institute, University of Wisconsin, Madison, WI, **2018**.
- [14] M. J. Frisch, G. W. Trucks, H. B. Schlegel, G. E. Scuseria, M. A. Robb, J. R. Cheeseman, G. Scalmani, V. Barone, G. A. Petersson, H. Nakatsuji, X. Li, M. Caricato, A. V. Marenich, J. Bloino, B. G. Janesko, R. Gomperts, B. Mennucci, H. P. Hratchian, J. V. Ortiz, A. F. Izmaylov, J. L. Sonnenberg, D. Williams-Young, F. Ding, F. Lipparini, F. Egidi, J. Goings, B. Peng, A. Petrone, T. Henderson, D. Ranasinghe, V. G. Zakrzewski, J. Gao, N. Rega, G. Zheng, W. Liang, M. Hada, M. Ehara, K. Toyota, R. Fukuda, J. Hasegawa, M. Ishida, T. Nakajima, Y. Honda, O. Kitao, H. Nakai, T. Vreven, K. Throssell, J. A. Montgomery, Jr., J. E. Peralta, F. Ogliaro, M. J. Bearpark, J. J. Heyd, E. N. Brothers, K. N. Kudin, V. N. Staroverov, T. A. Keith, R. Kobayashi, J. Normand, K. Raghavachari, A. P. Rendell, J. C. Burant, S. S. Iyengar, J. Tomasi, M. Cossi, J. M. Millam, M. Klene, C. Adamo, R. Cammi, J. W. Ochterski, R. L. Martin, K. Morokuma, O. Farkas, J. B. Foresman, and D. J. Fox, *Gaussian 16*, Gaussian, Inc., Wallingford CT, **2016**.
- [15] W. Humphrey, A. Dalke, K. Schulten, *J. Molec. Graphics* **1996**, *14*, 33.
- [16] K. Sonnenberg, P. Pröhm, C. Müller, H. Beckers, S. Steinhauer, D. Lentz, S. Riedel, *Chem. Eur. J.* **2018**, *24*, 1072.
- [17] J. Bandemehr, M. Sachs, S. I. Ivlev, A. J. Karttunen, F. Kraus, *Eur. J. Inorg. Chem.* **2020**, *2020*, 64.
- [18] S. I. Ivlev, A. J. Karttunen, R. V. Ostvald, F. Kraus, *Chem. Commun.* **2016**, *52*, 12040.

**A.3. Non-classical polyinterhalides of chlorine monofluoride:
experimental and theoretical characterization of
 $[\text{F}(\text{ClF})_3]^-$**

Electronic Supplementary Material (ESI) for ChemComm.
This journal is © The Royal Society of Chemistry 2021

Supporting Information

Non-classical polyinterhalides of chlorine monofluoride: Experimental and theoretical characterization of $[F(ClF)_3]^-$

Patrick Pröhm,^a Nico Schwarze,^a Carsten Müller,^a Simon Steinhauer,^a Helmut Beckers,^a Susanne M. Rupf,^a and Sebastian Riedel^{*a}

We present the synthesis and characterization of the first non-classical Cl(I) polyinterhalide $[NMe_4][F(ClF)_3]$ as well as the homologous polychloride $[NPr_3Me][Cl_7]$. Both salts were obtained from the reaction of the corresponding ammonium chlorides with ClF or Cl₂, respectively. Quantum-chemical investigations predict an unexpected planar structure for the $[F(ClF)_3]^-$ anion.

Contents

General Information	2
Experimental Section	3
Crystallographic Section	5
Computational Section	7
References	14

Caution!

Chlorine monofluoride is extraordinarily reactive and can react violently with organic materials under the formation of HF. Similarly, $[\text{NMe}_4][\text{Cl}_3\text{F}_4]$ can decompose violently under certain conditions when exposed to organic materials. Exposure to acidic compounds (e.g. water or boron trifluoride) greatly enhances the reactivity.

General Information

All experiments were performed under rigorous exclusion of moisture and oxygen using standard Schlenk techniques. Solids were handled in a dry box under argon atmosphere ($\text{O}_2 < 0.5$ ppm, $\text{H}_2\text{O} < 0.5$ ppm). CIF experiments were performed in 8 mm PFA tubes with a stainless steel vacuum line, previously passivated with F_2 . Propionitrile was dried over Sicapent[®] prior to use. $[\text{NMe}_4]\text{Cl}$, and $[\text{NPr}_2\text{Me}]\text{Cl}$ were dried overnight at 120 °C under dynamic vacuum. All other chemicals were used as purchased. CIF was synthesized as described elsewhere.¹

Raman spectra were recorded on a Bruker MultiRAM II equipped with a low-temperature Ge detector (1064 nm, 30-80 mW, resolution, 4 cm^{-1}). Spectra of single crystals were recorded at -196 °C using the Bruker RamanScope III. Crystal data were collected on a Bruker D8 Venture diffractometer with a Photon 100 CMOS area detector with MoK_α radiation. Single crystals were picked at -80 °C under nitrogen atmosphere and mounted on a 0.15 mm Mitegen micromount using perfluoroether oil diluted with perfluorohexane. The structures were solved with the ShelXT² structure solution program using intrinsic phasing and refined with the ShelXL³ refinement package using least squares minimizations by using OLEX2.⁴ For visualization the Diamond V3.0 program was used.⁵

For -structure optimizations the program packages Turbomole V7.3,⁶ Gaussian G16⁷ and Molpro2019⁸ were used. Thermochemical data on second-order Møller-Plesset perturbation theory (MP2) with spin-component scaling (SCS)⁹ and on DFT level with the hybrid functional B3¹⁰LYP¹¹ and dispersion correction by Grimme (D3)¹² and Becke-Johnson damping (BJ)¹³ with the triple- ζ basis set def2-TZVPP¹⁴ were obtained with the Turbomole V7.3. As a validation for minimum structures, harmonic frequencies were calculated as implemented. Relaxed surface scans and NBO analyses¹⁵ were performed with the Gaussian G16 software package with tight convergence criteria. Structure optimizations on CCSD(T) level were done with the Molpro2019 program. For fluorine the triple ζ basis set aug-cc-pVTZ¹⁶ was used. For chlorine an individually parametrized basis set with the following ECP was used:

```
s,Cl,104.3829980,10.9005580,2.2685170,0.9567350,0.3943800,0.1380120,0.0591000;
c,1.3,0.0031560,0.0239720,-0.3310080;
p,Cl,17.9293820,3.2048610,1.5221960,0.6753990,0.2541180,0.0787660,0.0376000;
c,1.3,0.0029790,-0.0600800,0.0690590;
d,Cl,1.0460000,0.3440000,0.1350000;
f,Cl,0.7060000,0.3120000;
```

```
ECP,Cl,10,3;
1;                               ! f-ul potential
2,1.000000000,0.000000000;
2;                               ! s-ul potential
2,6.394300000,33.136632000;
2,3.197100000,16.270728000;
2;                               ! p-ul potential
2,5.620700000,24.416993000;
2,2.810300000,7.683050000;
1;                               ! d-ul potential
2,5.338100000,-8.587649000;
```

All periodic solid-state calculations as well as molecular calculations were performed with the CRYSTAL17¹⁷ program, using the B3LYP DFT functional. An energy-consistent, multi-electron fit, quasi relativistic Stuttgart–Cologne pseudo potential with a chemically inactive [Ne] core was utilized for chlorine.¹⁸ The valence electrons of chlorine were represented by a triple- ζ basis set, (6s5p2d)/[4s3p2d], that was applied successfully for polychloride systems before¹⁹ as well as for solid chlorine²⁰ and was derived from a (6s6p)/[3s3p] basis set by Dolg²¹ (for details about this basis set and its derivation, see Ref.²⁰ and the corresponding Supporting Information). For all other atoms Dunning's cc-pVDZ²² basis set was used. In the periodic calculations, the first Brillouin zone was sampled using an $6 \times 6 \times 6$ Monkhorst-Pack grid. Coulomb and exchange integral thresholds were set to 8, 8, 8, and 16 using the TOLINTEG keyword. QTAIM Analysis was performed

with the TOPOND code developed by Gatti²³ and recently implemented in CRYSTAL17; data for 2D-maps of the ELF were calculated with the CRYSTAL17 program and visualized with Gri.²⁴

Experimental Section

Synthesis of $[NMe_4][Cl_3F_4]$

Tetramethylammonium (20 mg, 0.18 mmol, 1 eq) was dissolved in dichlorofluoromethane (0.15 ml) in a 20 cm long 8 mm PFA reactor. Chlorine monofluoride (5 eq) was added at -196°C and the reactor was flame-sealed. Then it was allowed to warm to -20°C until the solid was fully dissolved and subsequently slowly cooled to -80°C . An ethanol filled Dewar was used to slow the cooling rate. Single crystals were obtained after 2 weeks.

Raman: $\tilde{\nu}$ [cm^{-1}] = 3043 (m), 2960 (m), 2328(s), 950 (m), 675 (s), 641 (s), 615 (s).

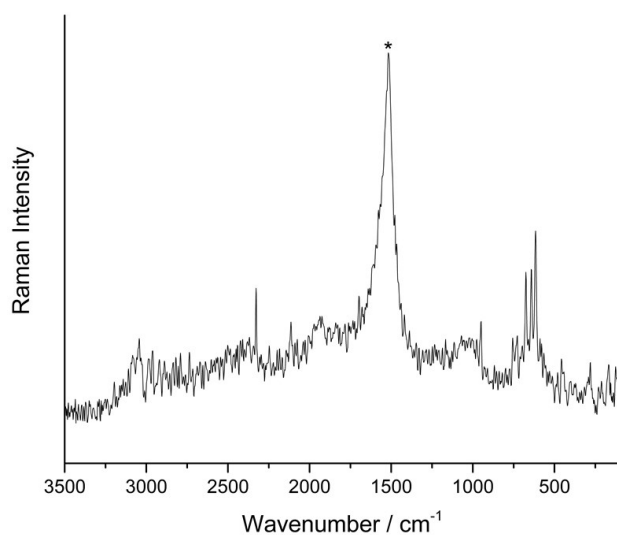


Figure S1 Raman spectrum (77 K) of $[NMe_4][Cl_3F_4]$. Band highlighted with asterisk corresponds to liquid oxygen from the measurement setup.

Synthesis of $[\text{NPr}_3\text{Me}][\text{Cl}_7]$

Tripropylmethylammonium chloride (660 mg, 3.42 mmol, 1 eq) was dissolved in an excess of chlorine (1.23 g, 17.6 mmol, 5.1 eq) by condensing Cl_2 onto the solid and subsequently allowing it to warm to r.t. For the growth of single crystals, the sample was slowly cooled to -40°C . An ethanol filled Dewar was used to slow the cooling rate. Single crystals were obtained after several days.

Raman: $\tilde{\nu}$ [cm^{-1}] = 2989 (w), 2948 (w), 2935 (w), 1458 (w), 467 (vs), 444 (vs), 151 (w).

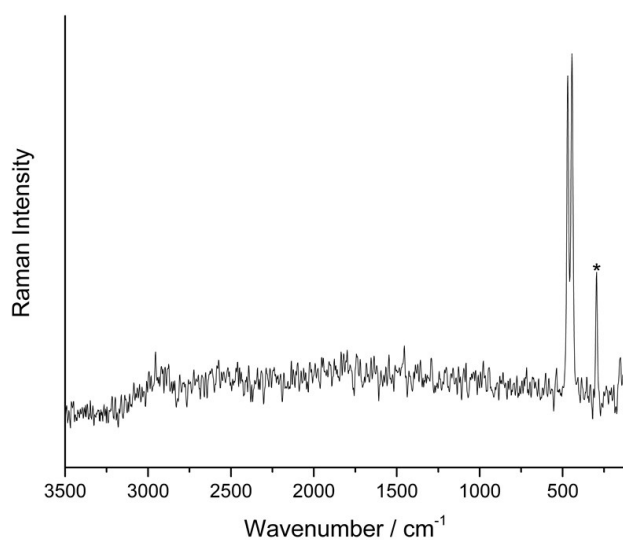


Figure S2 Raman spectrum (77 K) of $[\text{NPr}_3\text{Me}][\text{Cl}_7]$. Band highlighted with asterisk corresponds to decomposition product $[\text{Cl}_3]$.

Crystallographic section:

Table S1. Crystallographic details

Empirical formula	$C_{10}H_{24}Cl_7N_7$	$C_4H_{12}Cl_3F_4N$
Formula weight	406.45	256.50
Temperature/K	100.0	100.0
Crystal system	triclinic	orthorhombic
Space group	$P-1$	$Pna2_1$
a/Å	9.2183(6)	11.8381(2)
b/Å	9.6315(6)	10.0385(2)
c/Å	11.5543(8)	9.3211(2)
$\alpha/^\circ$	67.512(2)	90
$\beta/^\circ$	88.551(2)	90
$\gamma/^\circ$	89.108(2)	90
Volume/Å ³	947.53(11)	1107.69(4)
Z	2	4
$\rho_{\text{calc}}/\text{cm}^3$	1.425	1.538
μ/mm^{-1}	1.033	7.675
F(000)	420.0	520.0
Crystal size/mm ³	0.3 × 0.22 × 0.15	0.547 × 0.334 × 0.296
Radiation	MoK α ($\lambda = 0.71073$)	CuK α ($\lambda = 1.54178$)
2 θ range for data collection/ $^\circ$	4.42 to 52.812	11.558 to 144.478
Reflections collected	27183	17449
Independent reflections	3889 [$R_{\text{int}} = 0.0283$, $R_{\text{sigma}} = 0.0168$]	2178 [$R_{\text{int}} = 0.0491$, $R_{\text{sigma}} = 0.0251$]
Data/restraints/parameters	3889/0/167	2178/1/114
Goodness-of-fit on F^2	1.131	1.069
Final R indexes [$I \geq 2\sigma(I)$]	$R_1 = 0.0301$, $wR_2 = 0.0762$	$R_1 = 0.0199$, $wR_2 = 0.0517$
Final R indexes [all data]	$R_1 = 0.0325$, $wR_2 = 0.0777$	$R_1 = 0.0204$, $wR_2 = 0.0523$
Largest diff. peak/hole / e Å ⁻³	0.97/-0.85	0.17/-0.15
Flack parameter	-	-
BASF	-	0.495(15)
CCDC deposition numbers	2031712	2060326

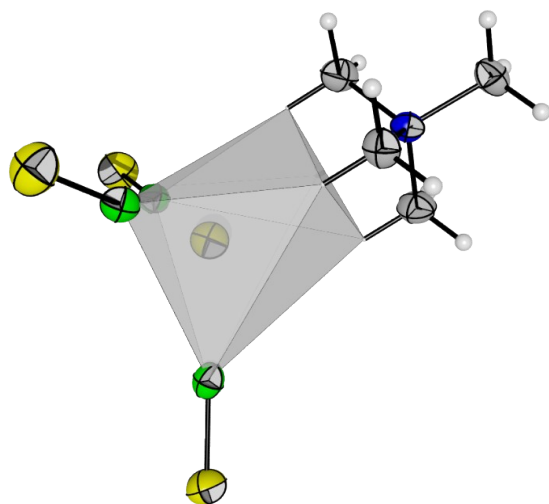


Figure S3. Coordination octahedron of the central fluoride ion in $[NMe_4][Cl_3F_4]$ with three ClF ligands and three hydrogen bonds.

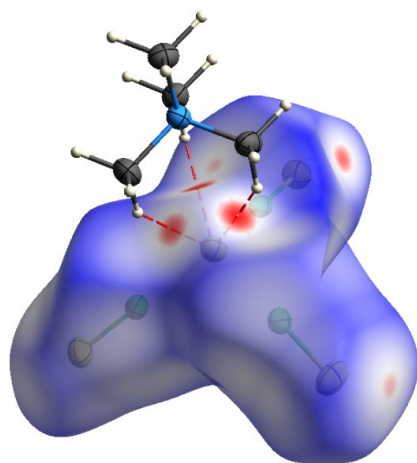


Figure S4. Hirshfeld surface of [NMe₄][Cl₃F₄], showing three close cation-anion contacts via hydrogen bonding.

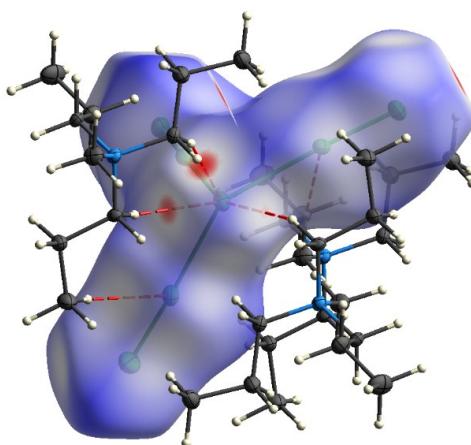


Figure S5. Hirshfeld surface of [NPr₃Me][Cl₇], showing five close cation-anion contacts via hydrogen bonding.

Computational Section

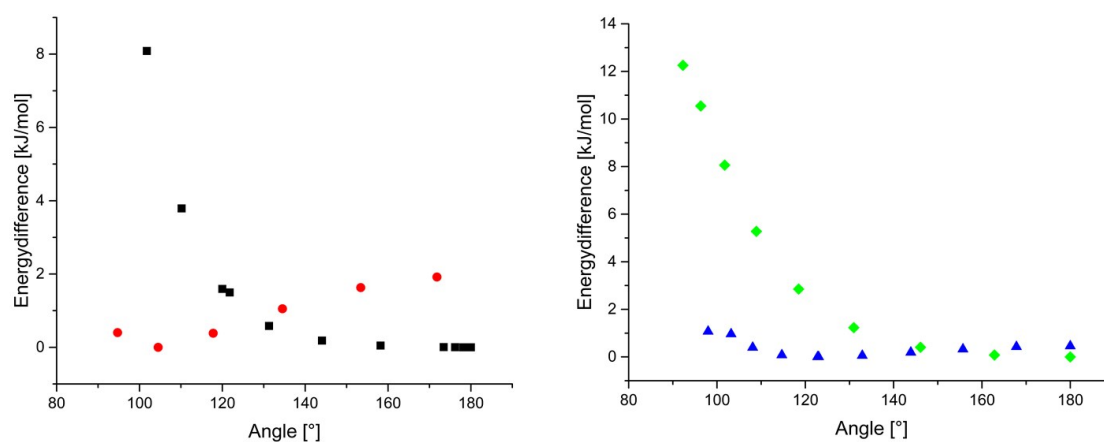


Figure S6. Relaxed surface scans (MP2/def2-TZVPP) of $[\text{F}(\text{ClF})_3]^-$ (left, black squares), $[\text{Cl}(\text{Cl}_2)_3]^-$ (left, red circles), $[\text{F}(\text{HF})_3]^-$ (right, green diamonds) and $[\text{Cl}(\text{HF})_3]^-$ (right, blue triangles) depending on the dihedral angle.

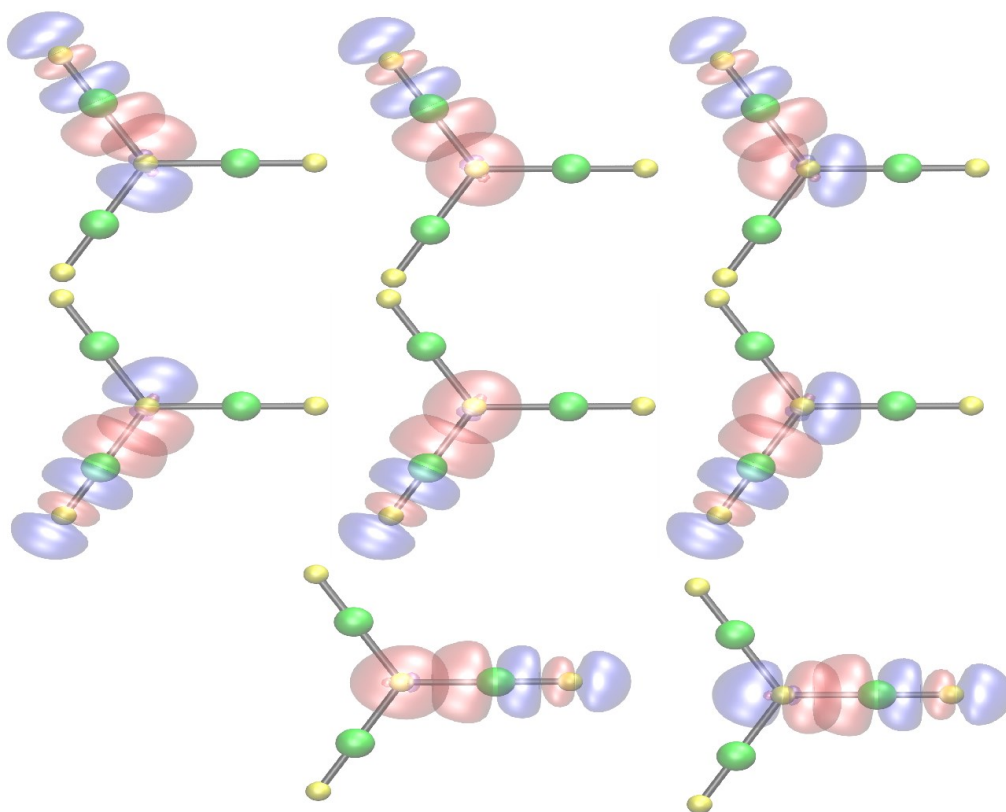


Figure S7. NBOs showing the bonding interactions between the central fluoride ion and the ClF ligands.

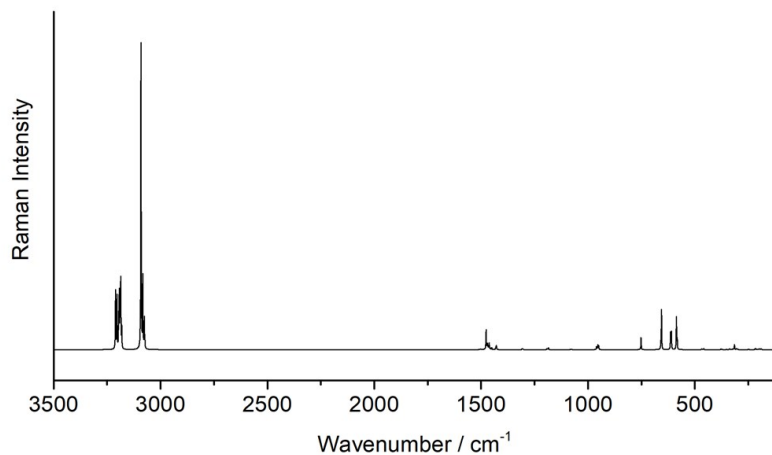


Figure S8 Calculated Raman spectrum of $[\text{NMe}_4][\text{F}(\text{CF})_3]$ (periodic solid-state calculation B3LYP-D2).

Frequency [cm^{-1}]	Raman Intensity [arb. u.]	Description
54.18	0.06	
61.37	2.82	
66.68	4.53	
73.62	0.79	
85.79	0.20	
86.88	---	
89.23	1.17	
91.00	0.64	
91.27	0.57	
93.98	0.10	
104.38	0.01	
107.30	---	
116.09	0.34	
117.42	0.23	
125.03	0.06	
188.33	1.98	
118.90	---	
189.01	1.28	
192.66	0.98	
193.81	1.54	
199.02	1.89	
212.73	0.63	
212.96	1.12	
216.99	4.05	
217.56	0.02	
246.73	1.47	
248.88	0.89	
297.90	1.22	
302.08	2.55	
304.05	0.03	
305.62	3.34	
314.42	7.07	
314.55	0.21	
315.11	10.54	
317.35	0.49	
321.81	2.80	
325.53	0.14	
333.73	0.42	
333.86	0.27	
334.63	0.09	
337.30	3.00	
339.03	0.52	
348.02	---	
352.09	0.07	
460.25	0.11	
463.98	0.49	
467.01	2.51	
467.36	0.17	
582.73	33.49	
583.78	0.24	
586.45	106.13	

A.3. Non-classical polyinterhalides of chlorine monofluoride: experimental and theoretical characterization of $[F(ClF)_3]^-$

609.82	56.86	
611.31	1.02	
613.15	17.63	
613.83	43.89	
656.16	132.40	
658.95	6.01	
659.16	12.91	
663.30	0.75	
751.77	40.83	
949.45	4.53	
950.34	10.49	
950.52	0.54	
951.63	0.24	
954.45	14.63	
955.33	0.14	
956.21	2.12	
959.44	3.92	
960.58	6.68	
1184.71	5.82	
1191.68	2.56	
1427.62	6.34	
1429.14	5.74	
1429.19	5.54	
1430.93	4.72	
1431.39	0.03	
1431.77	0.34	
1450.07	5.69	
1450.31	0.14	
1450.57	0.17	
1461.82	5.66	
1462.13	1.38	
1462.21	10.78	
1462.47	3.76	
1464.68	8.00	
1465.47	3.13	
1468.94	14.73	
1470.25	9.30	
1472.66	9.20	
1475.41	3.37	
1476.82	44.90	
1477.08	20.16	
1486.44	0.96	
1495.49	0.05	
1495.67	1.61	
1500.47	0.03	
1501.38	0.45	
1502.64	1.28	
1504.18	0.07	
1504.89	0.67	
1507.70	0.95	
3073.62	9.35	
3074.00	10.50	
3076.25	96.88	
3076.35	4.38	
3076.87	1.46	
3082.07	5.75	
3082.47	4.59	
3083.33	233.97	
3090.52	5.21	
3091.10	0.26	
3091.92	1000.00	
3181.37	5.19	
3181.45	2.78	
3181.47	4.67	
3181.90	18.77	
3181.93	33.14	
3181.95	3.30	
3186.49	178.15	
3186.60	15.41	
3186.63	6.47	
3186.65	17.76	
3189.56	116.07	
3189.70	0.79	
3189.86	19.73	
3189.89	10.73	
3193.25	32.58	
3193.38	17.95	
3193.43	119.82	
3193.47	3.96	

A. Supporting Information of Publications

3195.95	49.18
3196.17	5.65
3195.22	29.74
3196.25	11.77
3203.93	78.12
3204.02	9.88
3204.08	84.65
3210.69	113.60
3210.69	29.39
3210.79	55.78

xyz-coordinates of optimized (SCS-MP2/def2-TZVPP) $[\text{Cl}_3\text{F}_4]^-$ anion.

```
F 0.0030253 0.0054886 0.0014566
Cl -0.3592242 -0.6223461 2.0362951
Cl 1.8007373 -0.6231479 -1.0177774
Cl -1.4400692 1.2481127 -1.0179147
F -0.6450901 -1.1177886 3.6423700
F -2.5791231 2.2289924 -1.8223426
F 3.2197440 -1.1193112 -1.8220871
```

xyz-coordinates of optimized (B3LYP-D3BJ/def2-TZVPP) $[\text{Cl}_3\text{F}_4]^-$ anion.

```
F -0.1536391 -0.2668807 -0.1115889
Cl -0.3802044 -0.6581485 2.0014337
Cl 1.7637205 -0.6601486 -1.0267206
Cl -1.4531163 1.1971881 -1.0259917
F -0.5675361 -0.9811748 3.6837986
F -2.4976014 2.3547186 -1.7599470
F 3.2883767 -0.9855541 -1.7609839
```

xyz-coordinates of optimized (CCSD(T)) $[\text{Cl}_3\text{F}_4]^-$ anion.

```
Cl 0.0009904861 2.1531833330 0.1643768064
F -0.0047317888 3.8610420453 0.2948078648
F 0.0085650425 -0.0005862369 -0.0001350683
Cl 0.0010431428 -0.9344525242 -1.9478674402
F -0.0047897103 -1.6748187581 -3.4924261114
Cl 0.0010481618 -1.2190292316 1.7834399958
F -0.0047944861 -2.1850801623 3.1978478107
```

xyz-coordinates of optimized (SCS-MP2/def2-TZVPP) $[\text{Cl}_2\text{F}_3]^-$ anion.

```
F -0.9339776 0.6604305 -0.0000001
Cl -1.1316617 -1.3729277 -0.0000002
Cl 0.9171898 1.5245794 0.0000003
F 2.4829014 2.2932242 -0.0000002
F -1.3344518 -3.1053063 0.0000001
```

A.3. Non-classical polyinterhalides of chlorine monofluoride: experimental and theoretical
characterization of $[F(ClF)_3]^-$

xyz-coordinates of optimized (B3LYP-D3BJ/def2-TZVPP) $[Cl_2F_3]^-$ anion.

F	-0.9379490	0.6632979	-0.0000001
Cl	-1.1361637	-1.3813141	-0.0000013
Cl	0.9235012	1.5316916	0.0000015
F	2.5047300	2.3217379	-0.0000008
F	-1.3541185	-3.1354134	0.0000007

xyz-coordinates of optimized (CCSD(T)) $[Cl_2F_3]^-$ anion.

Cl	0.0000000000	0.1017656146	1.7597803656
F	0.0000000000	-0.7689394000	3.2780644604
F	0.0000000000	1.1580619590	-0.0000008778
Cl	0.0000000000	0.1017754626	-1.7597836751
F	0.0000000000	-0.7689514221	-3.2780574067

xyz-coordinates of optimized (SCS-MP2/def2-TZVPP) $[Cl_6F]^-$ anion.

F	-0.0003182	0.0000011	0.0016983
Cl	-1.1137745	1.9294117	0.0003593
Cl	-1.1137778	-1.9294109	0.0003517
Cl	-2.1487445	-3.7227928	-0.0008831
Cl	-2.1487433	3.7227934	-0.0008684
Cl	2.2273872	-0.0000136	0.0003203
Cl	4.2979711	0.0000110	-0.0009432

xyz-coordinates of optimized (B3LYP-D3BJ/def2-TZVPP) $[Cl_6F]^-$ anion.

F	0.5361256	0.5360421	0.5356411
Cl	-0.1946310	-0.1945864	2.5106608
Cl	2.5110957	-0.1948964	-0.1947234
Cl	-0.1948466	2.5110478	-0.1946218
Cl	4.3675824	-0.8929151	-0.8921457
Cl	-0.8924256	-0.8922506	4.3671269
Cl	-0.8929006	4.3675586	-0.8919379

xyz-coordinates of optimized (CCSD(T)) $[Cl_6F]^-$ anion.

Cl	1.1363609971	0.0004079770	1.9182020100
Cl	2.1988605108	-0.0007146636	3.7121474025
F	0.0003207373	0.0016776927	-0.0000108523
Cl	1.0928094777	0.0004266974	-1.9433573152
Cl	2.1145455680	-0.0007243406	-3.7608277747
Cl	-2.2289554554	0.0004324577	0.0251499828
Cl	-4.3137929736	-0.0007271627	0.0486915100

xyz-coordinates of optimized (B3LYP-D3BJ/def2-TZVPP) $[Cl_4F]^-$ anion.

F	-0.0000000	0.0000001	-1.2096049
Cl	-1.8478920	0.0000000	-0.1916745
Cl	1.8478920	-0.0000002	-0.1916745
Cl	3.7666507	0.0000001	0.7964769
Cl	-3.7666507	-0.0000000	0.7964769

A. Supporting Information of Publications

xyz-coordinates of optimized (CCSD(T)) [Cl₄F]⁻ anion.

Cl	0.0000000000	1.8222671175	0.3342801156
Cl	0.0000000000	3.6777510085	-0.7106616237
F	0.0000000000	-0.0000016207	1.4047356203
Cl	0.0000000000	-1.8222634965	0.3342776012
Cl	0.0000000000	-3.6777537610	-0.7106598486

xyz-coordinates of optimized (SCS-MP2/def2-TZVPP) [Cl₄F₃]⁻ anion.

Cl	-0.5610671	-0.9720259	-0.3968604
Cl	-0.4565580	-0.7905466	2.1485504
Cl	1.8736258	-0.7906509	-1.1466457
Cl	-1.6213855	1.2272003	-1.1464218
F	-0.3959032	-0.6851468	3.8620393
F	-2.3480901	2.6965036	-1.6601356
F	3.5093781	-0.6853337	-1.6605263

xyz-coordinates of optimized (B3LYP-D3BJ/def2-TZVPP) [Cl₄F₃]⁻ anion.

Cl	-0.1826938	-0.3205968	-0.1312649
Cl	-0.1243599	-0.2125720	2.3966331
Cl	2.2206795	-0.2140995	-0.9166975
Cl	-1.2936933	1.8142015	-0.9138059
F	-0.1029684	-0.1689759	4.1418649
F	-2.0856681	3.2672041	-1.4702005
F	3.8738851	-0.1724934	-1.4765202

xyz-coordinates of optimized (CCSD(T)) [Cl₄F₃]⁻ anion.

Cl	-0.6061668304	-1.0498807873	-0.4286255048
Cl	-0.4555742123	-0.7890568463	2.0886221555
Cl	1.8173179784	-0.7890608114	-1.1257134650
Cl	-1.5919781281	1.1793553813	-1.1257072247
F	-0.3592491688	-0.6222299765	3.8063425420
F	-2.2732606998	2.6931074752	-1.6074556285
F	3.4689110610	-0.6222344348	-1.6074629744

xyz-coordinates of optimized (SCS-MP2/def2-TZVPP) [Cl₃F₂]⁻ anion.

Cl	0.0000000	-0.0000003	-1.5754267
Cl	-1.9645902	0.0000004	-0.1182676
Cl	1.9645902	0.0000004	-0.1182676
F	3.3979807	-0.0000002	0.9059811
F	-3.3979807	-0.0000002	0.9059811

xyz-coordinates of optimized (B3LYP-D3BJ/def2-TZVPP) [Cl₃F₂]⁻ anion.

Cl	-0.1636318	-0.0000018	-0.1158603
Cl	-0.2006988	0.0000013	2.3316518
Cl	2.1313584	0.0000025	-0.9665130
F	3.7914329	-0.0000013	-1.6460291
F	-0.2881518	-0.0000007	4.1234376

A.3. Non-classical polyinterhalides of chlorine monofluoride: experimental and theoretical
characterization of $[F(ClF)_3]^-$

xyz-coordinates of optimized (CCSD(T)) $[Cl_3F_2]^-$ anion.

Cl	-0.0000000000	-0.0000001980	-1.5957441585
Cl	-1.9418740298	0.0000002739	-0.1256930692
Cl	1.9418740298	0.0000002739	-0.1256930693
F	3.3706197564	-0.0000001249	0.9235652985
F	-3.3706197564	-0.0000001249	0.9235652984

xyz-coordinates of optimized (B3LYP-D3BJ/def2-TZVPP) $[Cl_7]^-$ anion.

Cl	-0.5234752	0.9072869	-0.3718812
Cl	-0.4856117	0.8398819	2.2585893
Cl	1.9696101	0.8410976	-1.2114195
Cl	-1.7130635	-1.2849912	-1.2106431
Cl	-0.4926385	0.8526057	4.3837772
Cl	3.9716452	0.8554413	-1.9244998
Cl	-2.7264664	-3.0113221	-1.9239229

xyz-coordinates of optimized (B3LYP-D3BJ/def2-TZVPP) $[Cl_5]^-$ anion.

Cl	-0.2372058	-0.0000048	-0.4214092
Cl	-0.1667735	-0.0000003	2.0979990
Cl	2.1849543	0.0000056	3.0041587
Cl	-0.3772537	0.0000023	-2.6045621
Cl	4.1965717	-0.0000028	3.8637926

xyz-coordinates of optimized (SCS-MP2/def2-TZVPP) ClF.

Cl	0.0000000	0.0000000	-0.8174630
F	0.0000000	0.0000000	0.8174630

xyz-coordinates of optimized (B3LYP-D3BJ/def2-TZVPP) ClF.

Cl	0.0000000	0.0000000	-0.0054183
F	0.0000000	0.0000000	1.6354183

xyz-coordinates of optimized (CCSD(T)) ClF.

Cl	0.0000000000	0.0000000000	-0.8217078447
F	0.0000000000	0.0000000000	0.8217078447

xyz-coordinates of optimized (SCS-MP2/def2-TZVPP) Cl_2 .

Cl	0.0000000	0.0000000	-0.9987069
Cl	0.0000000	0.0000000	0.9987069

xyz-coordinates of optimized (B3LYP/def2-TZVPP) Cl_2 .

Cl	0.0000000	0.0000000	-1.0069131
Cl	0.0000000	0.0000000	1.0069131

xyz-coordinates of optimized ((CCSD(T)) Cl₂.

Cl	0.0000000000	0.0000000000	-1.0063722385
Cl	0.0000000000	0.0000000000	1.0063722385

References

- M. Baudler and G. Brauer, *Handbuch der Präparativen Anorganischen Chemie in drei Bänden, Bd1*, Ferdinand Enke, Stuttgart, 3rd edn., 1975–1981.
- G. M. Sheldrick, *Acta Cryst. A*, 2015, **71**, 3–8.
- G. M. Sheldrick, *Acta Cryst.*, 2015, **C71**, 3–8.
- O. V. Dolomanov, L. J. Bourhis, R. J. Gildea, J. A. K. Howard and H. Puschmann, *J. Appl. Cryst.*, 2009, **42**, 339–341.
- K. Brandenburg, *DIAMOND*, Crystal Impact GbR, Bonn, 2014.
- TURBOMOLE GmbH, *TURBOMOLE V7.3. a development of University of Karlsruhe and Forschungszentrum Karlsruhe GmbH*, 2018.
- M. J. Frisch, G. W. Trucks, H. B. Schlegel, G. E. Scuseria, M. A. Robb, J. R. Cheeseman, G. Scalmani, V. Barone, G. A. Petersson, H. Nakatsuji, X. Li, M. Caricato, A. V. Marenich, J. Bloino, B. G. Janesko, R. Gomperts, B. Mennucci, H. P. Hratchian, J. V. Ortiz, A. F. Izmaylov, J. L. Sonnenberg, D. Williams-Young, F. Ding, F. Lipparini, F. Egidi, J. Goings, B. Peng, A. Petrone, T. Henderson, D. Ranasinghe, V. G. Zakrzewski, J. Gao, N. Rega, G. Zheng, W. Liang, M. Hada, M. Ehara, K. Toyota, R. Fukuda, J. Hasegawa, M. Ishida, T. Nakajima, Y. Honda, O. Kitao, H. Nakai, T. Vreven, K. Throssell, J. A. Montgomery, Jr., J. E. Peralta, F. Ogliaro, M. J. Bearpark, J. J. Heyd, E. N. Brothers, K. N. Kudin, V. N. Staroverov, T. A. Keith, R. Kobayashi, J. Normand, K. Raghavachari, A. P. Rendell, J. C. Burant, S. S. Iyengar, J. Tomasi, M. Cossi, J. M. Millam, M. Klene, C. Adamo, R. Cammi, J. W. Ochterski, R. L. Martin, K. Morokuma, O. Farkas, J. B. Foresman, and D. J. Fox, *Gaussian 16*, Gaussian, Inc., Wallingford CT, 2016.
- H.-J. Werner, P. J. Knowles, G. Knizia, F. R. Manby, M. Schütz, P. Celani, W. Gyrffly, D. Kats, T. Korona, R. Lindh, A. Mitrushenkov, G. Rauhut, K. R. Shamasundar, T. B. Adler, R. D. Amos, S. J. Bennie, A. Bernhardsson, A. Berning, D. L. Cooper, M. J. O. Deegan, A. J. Dobby, F. Eckert, E. Goll, C. Hampel, A. Hesselmann, G. Hetzer, T. Hrenar, G. Jansen, C. Köppl, S. J. R. Lee, Y. Liu, A. W. Lloyd, Q. Ma, R. A. Mata, A. J. May, S. J. McNicholas, W. Meyer, T. F. Miller III, M. E. Mura, A. Nicklass, D. P. O'Neill, P. Palmieri, D. Peng, K. Pflüger, R. Pitzer, M. Reiher, T. Shiozaki, H. Stoll, A. J. Stone, R. Tarroni, T. Thorsteinsson, M. Wang and M. Welborn, *MOLPRO, version 2019.2, a package of ab initio programs*, molpro_address, 2019.
- A. Hellweg, S. A. Gruen and C. Hättig, *Phys. Chem. Chem. Phys.*, 2008, **10**, 4119–4127.
- A. D. Becke, *J. Chem. Phys.*, 1993, **98**, 1372–1377.
- C. Lee, W. Yang and R. G. Parr, *Phys. Rev. B*, 1988, **37**, 785–789.
- S. Grimme, J. Antony, S. Ehrlich and H. Krieg, *J. Chem. Phys.*, 2010, **132**, 154104.
- S. Grimme, S. Ehrlich and L. Goerigk, *J. Comput. Chem.*, 2011, **32**, 1456–1465.
- a) F. Weigend and R. Ahlrichs, *Phys. Chem. Chem. Phys.*, 2005, **7**, 3297–3305; b) F. Weigend, M. Häser, H. Patzelt and R. Ahlrichs, *Chem. Phys. Lett.*, 1998, **294**, 143–152;
- E. D. Glendening, J. K. Badenhoop, A. E. Reed, J. E. Carpenter, J. A. Bohmann, C. M. Morales, P. Karafiloglou, C. R. Landis and F. Weinhold, *NBO 7.0*, Theoretical Chemistry Institute, University of Wisconsin, Madison, WI, 2018.
- F. Weigend, A. Köhn and C. Hättig, *J. Chem. Phys.*, 2002, **116**, 3175–3183.
- R. Dovesi, A. Erba, R. Orlando, C. M. Zicovich-Wilson, B. Civalleri, L. Maschio, M. Rérat, S. Casassa, J. Baima, S. Salustro and B. Kirtman, *WIREs Comput Mol Sci*, 2018, **8**, e1360.
- A. Bergner, M. Dolg, W. Küchle, H. Stoll and H. Preuß, *Mol. Phys.*, 1993, **80**, 1431–1441.
- a) R. Brückner, P. Pröhm, A. Wiesner, S. Steinhauer, C. Müller and S. Riedel, *Angew. Chem. Int. Ed.*, 2016, **55**, 10904–10908; b) R. Brückner, H. Haller, S. Steinhauer, C. Müller and S. Riedel, *Angew. Chem. Int. Ed.*, 2015, **54**, 15579–15583;
- K. G. Steenbergen, N. Gaston, C. Müller and B. Paulus, *J. Chem. Phys.*, 2014, **141**, 124707.
- M. Dolg, Universität Stuttgart, 1989.
- T. H. Dunning, *J. Chem. Phys.*, 1989, **90**, 1007–1023.
- C. Gatti, *Acta Crystallogr A Found Crystallogr*, 1996, **52**, C555–C556.
- Dan E. Kelley, *gri – scientific graphic program*, 2017.

**A.4. Investigation of
Bis(Perfluoro-*tert*-Butoxy)Halogenates(I/III)**

SUPPORTING INFORMATION

Table of Contents

Low Temperature IR Setup	1
IR Data	2
Raman Data	4
[NEt ₃ Me][IF ₆]	6
Crystal Data	7
Computational Data	11
References	15

Low Temperature IR Setup

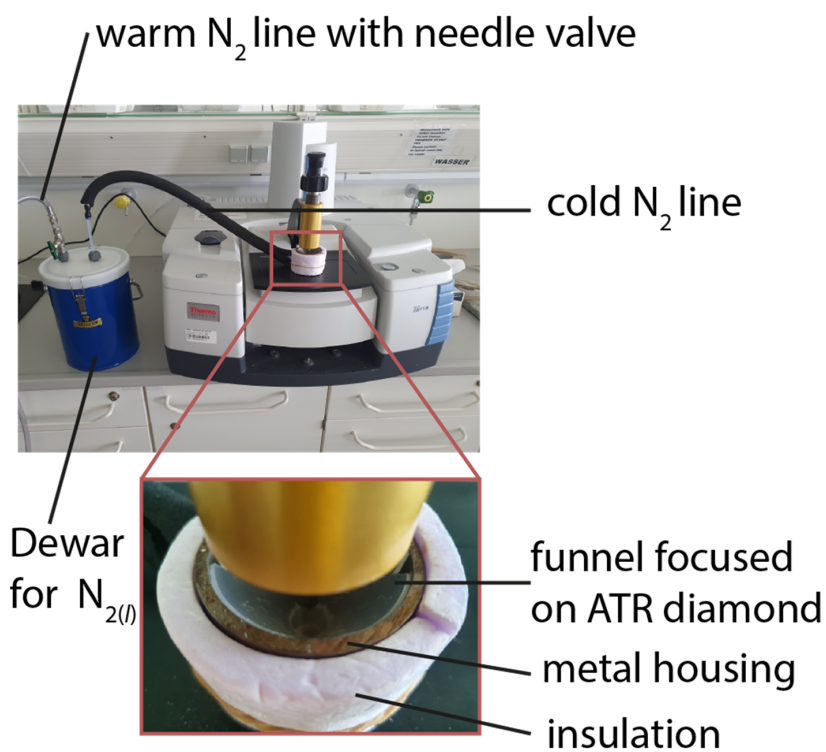


Figure S1. Experimental setup for measuring IR spectra at low temperatures.

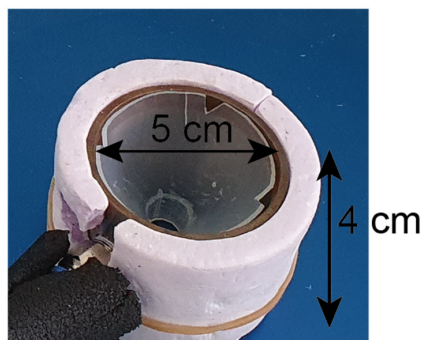


Figure S2. Experimental setup for measuring IR spectra at low temperatures.

SUPPORTING INFORMATION

Raman Data

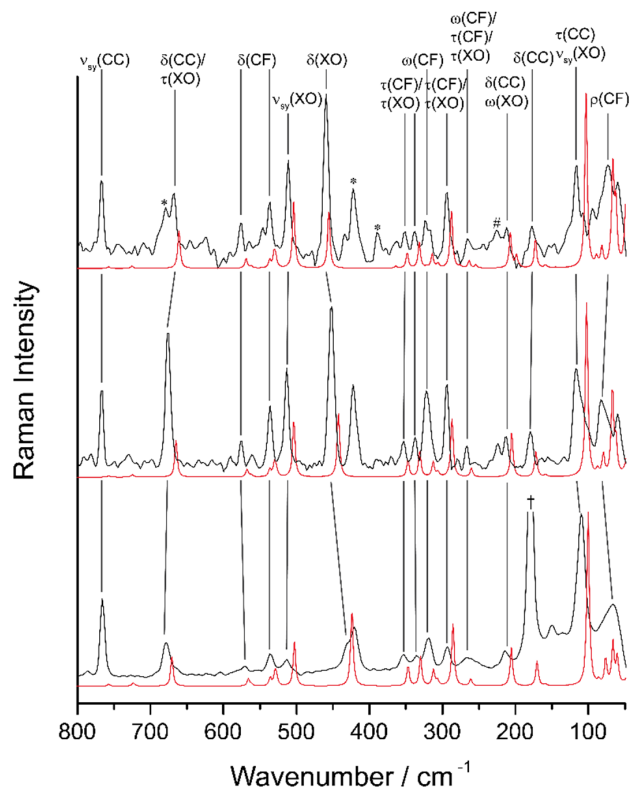


Figure S3. Raman spectra (1064 nm) of $[\text{NEt}_4][\text{Cl}(\text{OC}_4\text{F}_9)_2]$ **1** (top, 77 K), $[\text{NEt}_4][\text{Br}(\text{OC}_4\text{F}_9)_2]$ (middle, 77 K) and $[\text{NEt}_4][\text{I}(\text{OC}_4\text{F}_9)_2]$ (bottom, 298 K). Experimental spectra (black), calculated spectra of the anion (red, B3LYP-D3BJ/def2-TZVPP). Asterisk highlights cation bands, hash denotes residual solvent bands of EtCN, dagger highlights iodine impurity.

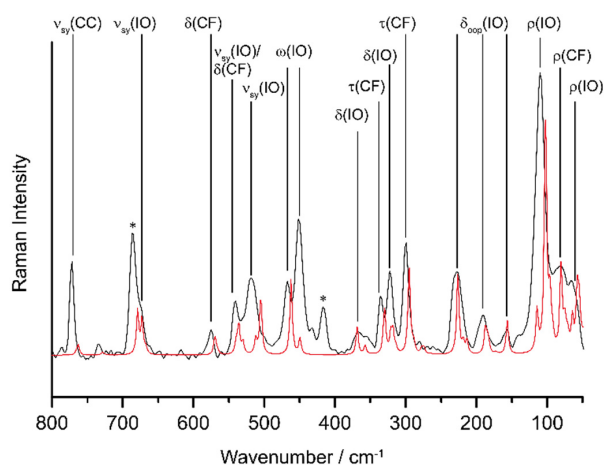


Figure S4. Raman spectrum (1064 nm, 298 K) of $[\text{NEt}_4][\text{I}(\text{OC}_4\text{F}_9)_4]$. Experimental spectrum (black), calculated spectrum of the anion (red, B3LYP-D3BJ/def2-TZVPP). Asterisk highlights cation bands.

SUPPORTING INFORMATION

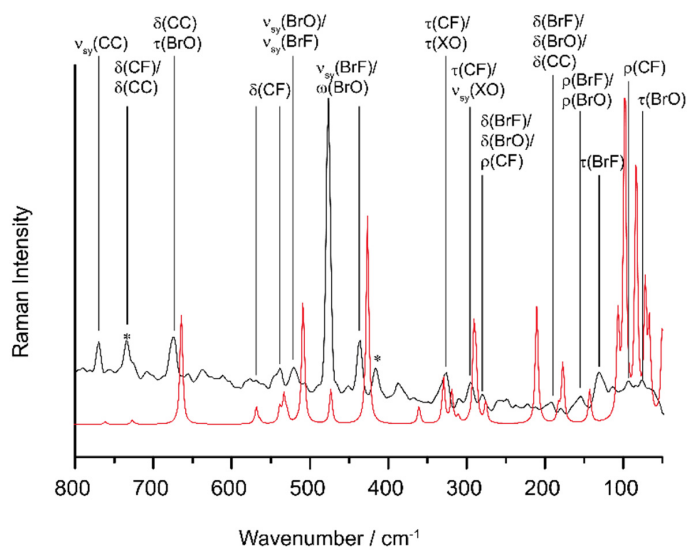


Figure S5. Raman spectrum (1064 nm, 77 K) of $[\text{NEt}_4][\text{BrF}_2(\text{OC}_4\text{F}_9)_2]$. Experimental spectrum (black), calculated spectrum of the anion (red, B3LYP-D3BJ/def2-TZVPP). Asterisk highlights cation bands.

SUPPORTING INFORMATION

IR Data

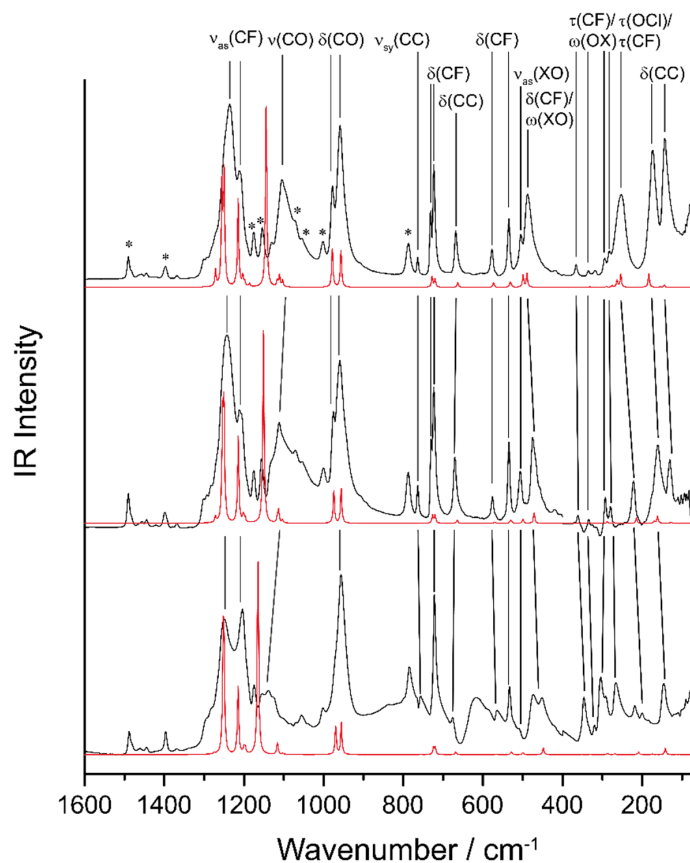


Figure S6. IR spectra (ATR) of $[\text{NEt}_4][\text{Cl}(\text{OC}_4\text{F}_9)_2]$ (top, 233 K), $[\text{NEt}_4][\text{Br}(\text{OC}_4\text{F}_9)_2]$ (middle 233 K) and $[\text{NEt}_4][\text{I}(\text{OC}_4\text{F}_9)_2]$ (bottom, 298 K). Experimental spectra (black), calculated spectra of the anion (red). Discontinuity at 400 cm^{-1} due to a different beam splitter. Bands highlighted with an asterisk correspond to the cation.

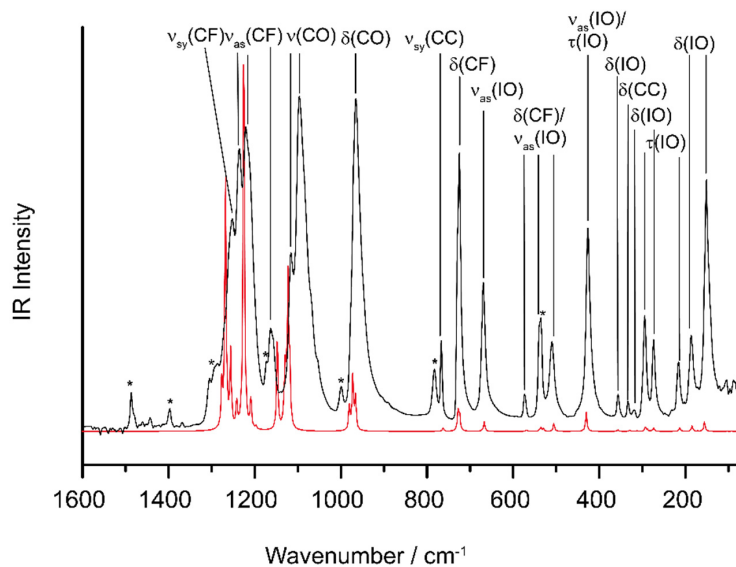


Figure S7. IR spectrum (ATR, 233 K) of $[\text{NEt}_4][\text{I}(\text{OC}_4\text{F}_9)_4]$. Experimental spectrum (black), calculated spectrum of the anion (red). Discontinuity at 400 cm^{-1} due to a different beam splitter. Bands highlighted with an asterisk correspond to the cation.

SUPPORTING INFORMATION

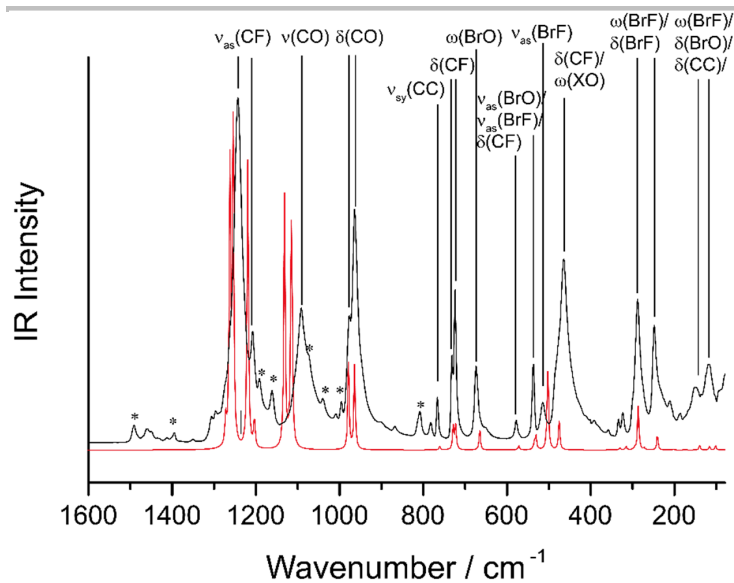
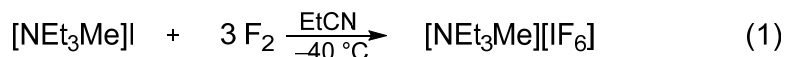


Figure S8. IR spectrum (ATR, 233 K) of $[NEt_4][BrF_2(OC_4F_9)_2]$. Experimental spectrum (black), calculated spectrum of the anion (red). Discontinuity at 400 cm⁻¹ due to a different beam splitter. Bands highlighted with an asterisk correspond to the cation.

SUPPORTING INFORMATION

[NEt₃Me][IF₆] 6

Analogous to the reactions of quaternary tetraalkylammonium chlorides^[1] and bromides^[2] the iodide salt [NEt₃Me]I can be fluorinated using dilute fluorine (10 % in Ar) to yield the corresponding hexafluoridoiodate(V) salt (eq. 1).



We were able to obtain single crystals by cooling the reaction mixture slowly to $-80\text{ }^\circ\text{C}$ (Figure S7 and S8). As expected, the structure is largely in agreement with the known structure of [NMe₄][IF₆] which was synthesized from [NMe₄]F and IF₅.^[3]

[NEt₃Me]I (100 mg, 0.411 mmol, 1 eq) was dissolved in propionitrile (2 ml) and cooled to $-40\text{ }^\circ\text{C}$. Dilute fluorine (10 % in Ar, 20 ml min⁻¹, 15 min, 1 eq) was bubbled through the reaction solution. Afterwards, Ar was bubbled through the solution for 15 min to remove any residual reactive gas. The reaction mixture was slowly cooled to $-80\text{ }^\circ\text{C}$ and the product was obtained as a crystalline solid. Raman (crystal, 1064 nm, 77 K) $\tilde{\nu} / \text{cm}^{-1} = 3050, 3000, 2946, 1507, 1077, 1008, 961, 683, 628, 565, 496, 460, 386$. CCDC number: 2105587

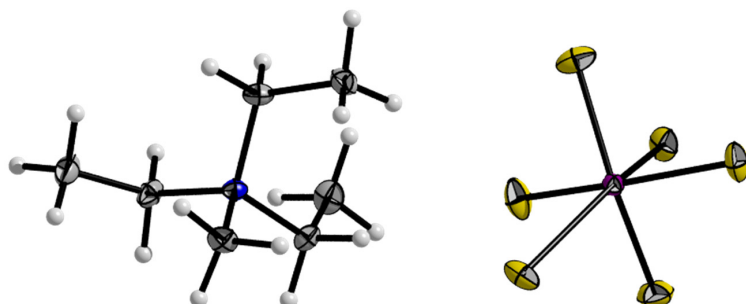


Figure S9. Solid-state structure of [NEt₃Me][IF₆]. Displacement ellipsoids are shown at 50 % probability level. Color code: yellow = fluorine, grey = carbon, purple = iodine, blue = nitrogen.

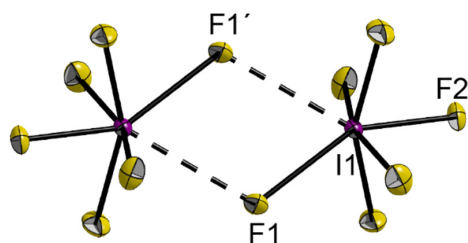


Figure S10. Solid-state structure of [NEt₃Me][IF₆] showing two bridged anions. Cations omitted for clarity. Displacement ellipsoids are shown at 50 % probability level. Color code: yellow = fluorine, purple = iodine. Selected bond lengths [pm]: I1-F1 222.4(2), I1-F2 186.6(2), I1-F1' 269.0(2).

SUPPORTING INFORMATION

Crystal Data

Compound	1	2	3
Identification code	fullp21m_b	P21_twin_final	P2(1)_multiscan
Empirical formula	C ₁₆ H ₂₀ ClF ₁₈ NO ₂	C ₁₆ H ₂₀ BrF ₁₈ NO ₂	C ₁₆ H ₂₀ F ₁₈ INO ₂
Formula weight	635.78	680.24	727.23
Temperature/K	100	100.0	100
Crystal system	monoclinic	monoclinic	monoclinic
Space group	<i>P</i> 2 ₁	<i>P</i> 2 ₁	<i>P</i> 2 ₁
<i>a</i> /Å	9.8030(5)	9.9124(5)	10.1009(6)
<i>b</i> /Å	12.2085(7)	12.0667(6)	11.8498(7)
<i>c</i> /Å	10.5701(4)	10.5647(6)	10.7012(5)
α /°	90	90	90
β /°	113.137(2)	112.206(2)	111.355(2)
γ /°	90	90	90
Volume/Å ³	1163.28(10)	1169.92(11)	1192.92(12)
<i>Z</i>	2	2	2
ρ_{calc} g/cm ³	1.815	1.931	2.025
μ /mm ⁻¹	0.324	1.916	1.499
<i>F</i> (000)	636.0	672.0	708.0
Crystal size/mm ³	0.938 × 0.521 × 0.517	0.59 × 0.23 × 0.19	0.353 × 0.167 × 0.143
Radiation	MoK α (λ = 0.71073)	MoK α (λ = 0.71073)	MoK α (λ = 0.71073)
2 θ range for data collection/°	4.19 to 56.65	4.164 to 56.612	4.086 to 50.716
Index ranges	-13 ≤ <i>h</i> ≤ 13, -16 ≤ <i>k</i> ≤ 16, -14 ≤ <i>l</i> ≤ 13	-13 ≤ <i>h</i> ≤ 13, -16 ≤ <i>k</i> ≤ 16, -14 ≤ <i>l</i> ≤ 14	-12 ≤ <i>h</i> ≤ 12, -14 ≤ <i>k</i> ≤ 14, -12 ≤ <i>l</i> ≤ 11
Reflections collected	53521	5805	20495
Independent reflections	5773 [<i>R</i> _{int} = 0.0329, <i>R</i> _{sigma} = 0.0182]	5805 [<i>R</i> _{int} = 0.0, <i>R</i> _{sigma} = 0.0309]	4350 [<i>R</i> _{int} = 0.0553, <i>R</i> _{sigma} = 0.0411]
Data/restraints/parameters	5773/1/348	5805/1/348	4350/1/336
Goodness-of-fit on <i>F</i> ²	1.051	1.019	1.039
Final <i>R</i> indexes [<i>I</i> ≥ 2 σ (<i>I</i>)]	<i>R</i> ₁ = 0.0382, <i>wR</i> ₂ = 0.1032	<i>R</i> ₁ = 0.0381, <i>wR</i> ₂ = 0.0886	<i>R</i> ₁ = 0.0410, <i>wR</i> ₂ = 0.1010
Final <i>R</i> indexes [all data]	<i>R</i> ₁ = 0.0407, <i>wR</i> ₂ = 0.1049	<i>R</i> ₁ = 0.0443, <i>wR</i> ₂ = 0.0925	<i>R</i> ₁ = 0.0510, <i>wR</i> ₂ = 0.1075
Largest diff. peak/hole / e Å ⁻³	0.79/-0.29	0.65/-0.58	1.91/-1.02
Flack parameter	0.41(9)	0.481(15)	0.33(5)

SUPPORTING INFORMATION

Compound	4	5	6
Identification code	P21_n	I2_m	P21_n
Empirical formula	C ₂₄ H ₂₀ F ₃₆ IINO ₄	C ₁₆ H ₂₀ BrF ₂₀ NO ₂	C ₇ H ₁₈ F ₆ IN
Formula weight	1197.31	718.24	357.12
Temperature/K	100	100.0	100.0
Crystal system	monoclinic	monoclinic	monoclinic
Space group	<i>P</i> 2 ₁ / <i>n</i>	<i>I</i> 2/ <i>m</i>	<i>P</i> 2 ₁ / <i>n</i>
<i>a</i> /Å	19.0494(7)	18.399(2)	8.3739(4)
<i>b</i> /Å	18.9420(5)	9.2277(9)	16.3141(8)
<i>c</i> /Å	20.5628(7)	6.9961(7)	9.6506(5)
α /°	90	90	90
β /°	96.6270(10)	95.600(4)	112.395(2)
γ /°	90	90	90
Volume/Å ³	7370.2(4)	1182.1(2)	1218.96(11)
<i>Z</i>	8	2	4
ρ_{calc} g/cm ³	2.158	2.018	1.946
μ /mm ⁻¹	1.088	1.914	2.675
<i>F</i> (000)	4640.0	708.0	696.0
Crystal size/mm ³	0.26 × 0.22 × 0.17	0.37 × 0.33 × 0.3	0.2 × 0.2 × 0.2
Radiation	MoK α (λ = 0.71073)	MoK α (λ = 0.71073)	MoK α (λ = 0.71073)
2 θ range for data collection/°	4.532 to 52.764	4.448 to 56.706	4.994 to 56.636
Index ranges	-23 ≤ <i>h</i> ≤ 23, -23 ≤ <i>k</i> ≤ 23, -25 ≤ <i>l</i> ≤ 25	-24 ≤ <i>h</i> ≤ 24, -12 ≤ <i>k</i> ≤ 12, -9 ≤ <i>l</i> ≤ 9	-11 ≤ <i>h</i> ≤ 10, -21 ≤ <i>k</i> ≤ 21, -12 ≤ <i>l</i> ≤ 12
Reflections collected	141718	12186	27477
Independent reflections	15060 [R _{int} = 0.0524, R _{sigma} = 0.0270]	1561 [R _{int} = 0.0348, R _{sigma} = 0.0213]	3029 [R _{int} = 0.0255, R _{sigma} = 0.0132]
Data/restraints/parameters	15060/0/1318	1561/0/116	3029/0/140
Goodness-of-fit on F ²	1.006	1.159	1.217
Final <i>R</i> indexes [<i>I</i> ≥ 2 σ (<i>I</i>)]	<i>R</i> ₁ = 0.0319, <i>wR</i> ₂ = 0.0714	<i>R</i> ₁ = 0.0268, <i>wR</i> ₂ = 0.0683	<i>R</i> ₁ = 0.0190, <i>wR</i> ₂ = 0.0461
Final <i>R</i> indexes [all data]	<i>R</i> ₁ = 0.0476, <i>wR</i> ₂ = 0.0778	<i>R</i> ₁ = 0.0268, <i>wR</i> ₂ = 0.0683	<i>R</i> ₁ = 0.0191, <i>wR</i> ₂ = 0.0462
Largest diff. peak/hole / e Å ⁻³	0.81/-0.61	0.42/-0.44	0.35/-1.28
Flack parameter	-	-	-

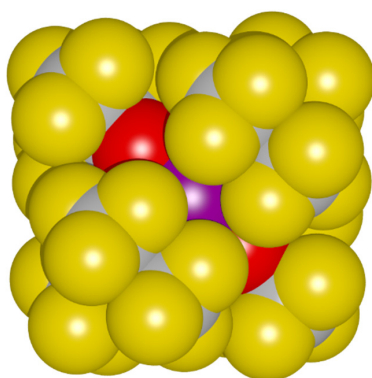


Figure S12. Space-filling representation of the anionic moiety of [NEt₄][I(OC₄F₉)₄] **4**, taken from its solid-state structure. Color code: yellow = fluorine, red = oxygen, purple = iodine.

SUPPORTING INFORMATION

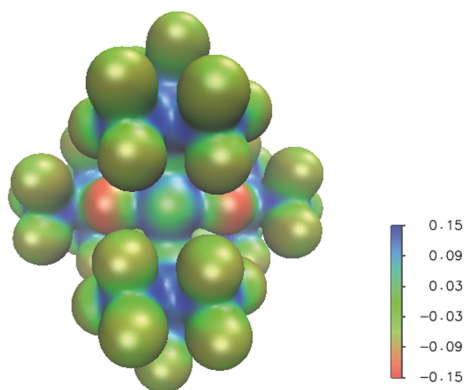


Figure S13. Electrostatic potential plotted in the electron density isosurface (iso = 0.025) of $[\text{I}(\text{OC}_4\text{F}_9)_4]^-$.

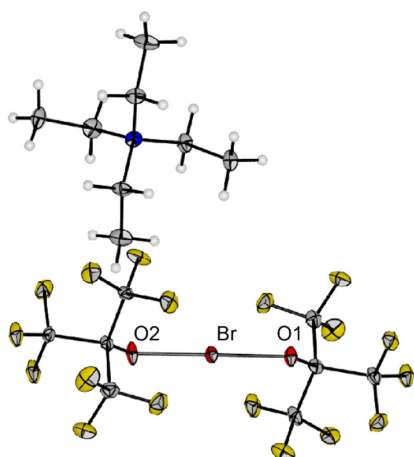


Figure S14. Molecular structure of $[\text{NEt}_4][\text{Br}(\text{OC}_4\text{F}_9)_2]$ **2**. Displacement ellipsoids are shown at 50 % probability level. Color code: yellow = fluorine, grey = carbon, red = oxygen, dark red = bromine, blue = nitrogen. Selected bond lengths [pm] and angles [°]: Br-O1 205.1(4), Br-O2 204.9(4); O1-Br-O2-179.5(2).

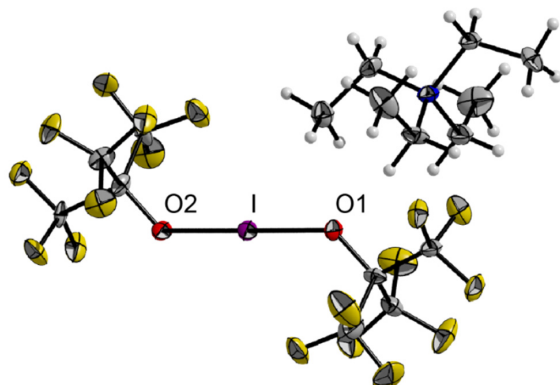


Figure S15. Molecular structure of $[\text{NEt}_4][\text{I}(\text{OC}_4\text{F}_9)_2]$ **3**. Displacement ellipsoids are shown at 50 % probability level. Disorder in the cation omitted for clarity. Color code: yellow = fluorine, grey = carbon, red = oxygen, purple = iodine, blue = nitrogen. Selected bond lengths [pm] and angles [°]: I-O1 218.5(6), I-O2 218.0(6), O1-I-O2 179.8(3).

SUPPORTING INFORMATION

The estimation of the thermochemical volume V_{therm} of the $[(OC_4F_9)_4]^-$ anion from the crystal structure was done according to a method presented by Passmore.^[4] Firstly, the thermochemical volume of the counterion $[NEt_4]^+$ was estimated from the crystal structure of $[NEt_4]Cl$ ^[5].

$$V([NEt_4]^+)_{therm} = \frac{\text{unit cell volume}}{Z} - V(Cl^-) = \frac{990.7}{4} - 25 = 223 \text{ \AA}^3$$

With this the thermochemical volume V_{therm} of the $[(OC_4F_9)_4]^-$ anion was estimated to 699 \AA^3 .

$$V([(OC_4F_9)_4]^-)_{therm} = \frac{\text{unit cell volume}}{Z} - V([NEt_4]^+) = \frac{7370.2}{8} - 223 = 698 \text{ \AA}^3$$

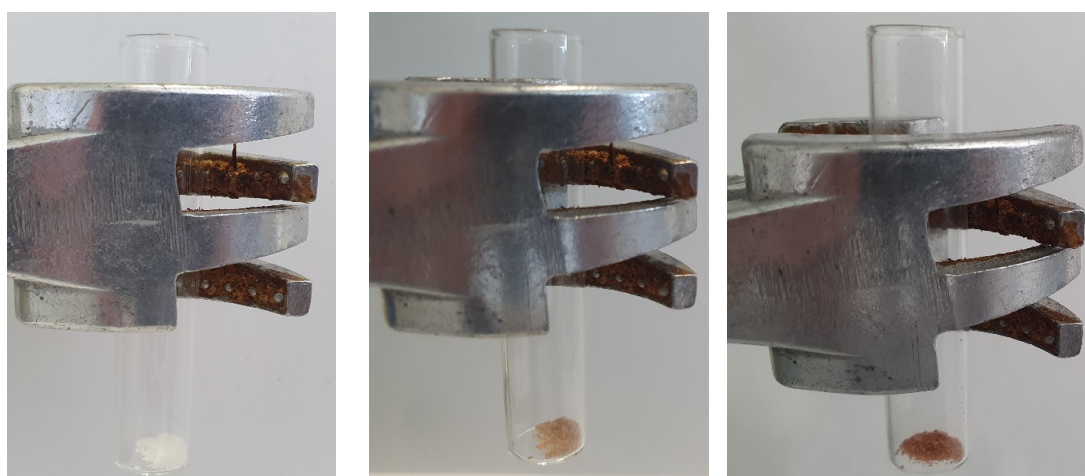


Figure S16. Photographs of the decomposition process of **4** at ambient atmosphere. Left: initial sample, middle: after 3.5 h, right: after 20 h. Increasingly dark color of the solid indicates formation of iodine.

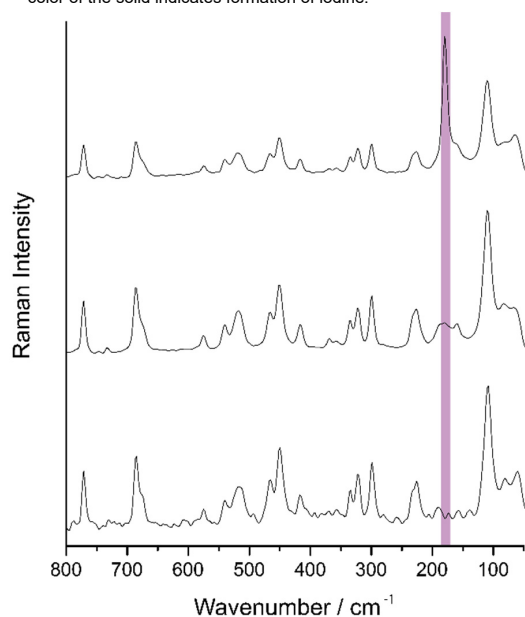


Figure S17. Raman spectra (1064 nm, 298 K) of the decomposition process of **4** at ambient atmosphere. bottom: initial sample, middle: after 3.5 h, top: after 20 h. Purple bar indicates formation of iodine.

SUPPORTING INFORMATION

Computational Data

NBO analysis:

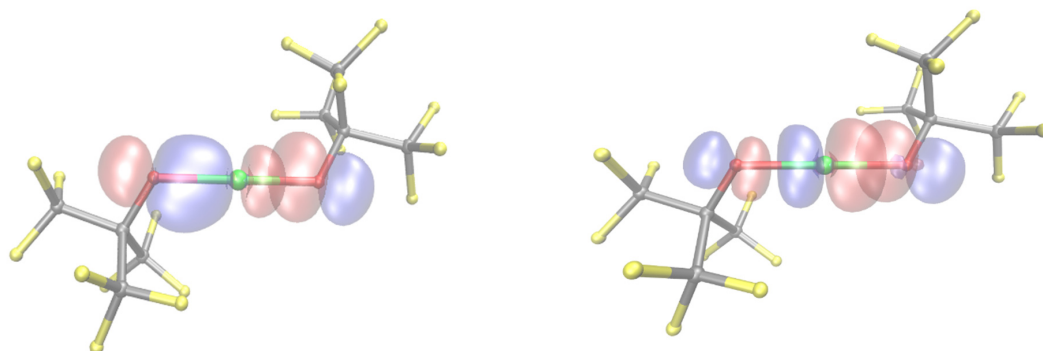


Figure S18. Results from the NBO analysis of $[\text{Cl}(\text{OC}_4\text{F}_9)_2]^-$. Left: NMOs of the O-Cl-O hyperbond. Right: Correlation between the oxygen lone pair and the $\sigma^*(\text{Cl-O})$ NMO.

Figure S18 (left) shows the orbitals taking part in the 3-center-4-electron bond according to the NBO analysis for $[\text{Cl}(\text{OC}_4\text{F}_9)_2]^-$. The occupancy is 3.9 all three derivatives $[\text{X}(\text{OC}_4\text{F}_9)_2]^-$. Figure S18 (right) shows the correlation between the antibonding $\sigma^*(\text{Cl-O})$ with the lone pair of the opposite oxygen atom. For $[\text{Cl}(\text{OC}_4\text{F}_9)_2]^-$ the occupancy of $\sigma^*(\text{Cl-O})$ which is mainly composed of p-type natural atomic orbitals is 0.38. For $[\text{Br}(\text{OC}_4\text{F}_9)_2]^-$ the occupancy is 0.34 and for $[\text{I}(\text{OC}_4\text{F}_9)_2]^-$ 0.27. The $\sigma^*(\text{X-O})$ orbital is mainly (Cl: 74%, Br: 79%, I 84%) composed of a p-type orbital of X.

NPA charges of neutral precursor species:

Molecule	ClF	ClOC ₄ F ₉	BrOC ₄ F ₉	IOC ₄ F ₉	I(OC ₄ F ₉) ₃	IF ₃
NPA at X	+0.33	+0.25	+0.34	+0.46	1.65	1.73

Xyz coordinates of $[\text{Br}(\text{OC}_4\text{F}_9)_2]^-$ optimized on B3LYP-D3BJ/def2-TZVPP:

29

Energy = -4826.751497174

```

Br  0.0010693  0.0127201 -0.0066797
F  -2.6646632  1.3074957 -3.2319725
F   3.8301136  1.3671272  3.6630571
F   4.2989331 -0.7649331  1.9857114
F  -2.2653308 -2.4413806 -0.2817040
F   2.3507356  2.7970357  2.9785983
F  -4.2257345 -1.9037999 -1.0239453
F   1.7480359  1.1050283  4.1752269
F  -2.5393345  1.6133139 -1.0996654
O   0.9695350  0.5984656  1.7449338
F  -1.7608547 -1.0656366 -4.1877347
F  -3.2008330 -0.6029086  0.3671572
F   3.2192564  0.5706322 -0.3617402
C  -2.9737767  0.7697044 -2.0372936
O  -0.9694993 -0.5704622 -1.7585113
F  -4.3237096  0.7380659 -1.9557791
F   4.2536542  1.8689460  1.0248017
C   2.5690661  1.4881897  3.1939618
F  -2.3234943 -2.7799184 -3.0033810
F  -3.8333876 -1.3688473 -3.6597706
F   2.5082474 -1.6181824  1.1205938
F   2.3088974  2.4309515  0.2597614
C  -2.3095348 -0.6512139 -1.8815783

```

SUPPORTING INFORMATION

C	3.0335636	1.3932592	0.6823965
C	-3.0106539	-1.4114909	-0.6870993
C	2.3098049	0.6573853	1.8785341
F	2.6181406	-1.2936645	3.2509998
C	2.9479623	-0.7729737	2.0543096
C	-2.5662086	-1.4729086	-3.2031881

Xyz coordinates of $[\text{BrF}_2(\text{OC}_4\text{F}_9)_2]^-$ optimized on B3LYP-D3BJ/def2-TZVPP:

31

Energy = -5026.366342161

C	-2.8898054	0.7101859	-1.9143302
C	-2.3459683	-0.7637351	-1.8044037
C	-2.5552561	-1.4814371	-3.1940197
F	-3.7874935	-1.2868168	-3.7063569
F	-2.4012581	1.3145823	-3.0053567
F	-2.5416036	1.4399662	-0.8534549
F	-4.2377505	0.7549357	-1.9994901
O	-1.0025552	-0.8201842	-1.5862474
Br	0.0008541	0.0005133	-0.0019380
O	1.0031595	0.8220860	1.5829530
C	2.3459069	0.7640554	1.8039404
C	2.8873607	-0.7104342	1.9172203
F	2.3959062	-1.3122503	3.0083044
C	-3.1600582	-1.5425255	-0.7031691
F	-3.2460791	-0.8209302	0.4240194
F	-2.5775859	-2.7009230	-0.4091027
F	-4.4256087	-1.8165318	-1.0968965
C	2.5535189	1.4836430	3.1928539
F	1.6716872	1.0471305	4.0942666
F	3.7838674	1.2866902	3.7088592
F	2.3823886	2.8091928	3.0714250
C	3.1635316	1.5399443	0.7032529
F	2.5827217	2.6982430	0.4052315
F	3.2518705	0.8160887	-0.4223977
F	4.4282685	1.8137271	1.0997120
F	4.2351472	-0.7570296	2.0049514
F	2.5400904	-1.4413328	0.8568806
F	-1.6770185	-1.0409773	-4.0970719
F	-2.3802441	-2.8066770	-3.0753554
F	0.3602261	1.5346641	-1.0661960
F	-0.3582202	-1.5338633	1.0619166

Xyz coordinates of $[\text{Cl}(\text{OC}_4\text{F}_9)_2]^-$ optimized on B3LYP-D3BJ/def2-TZVPP:

29

Energy = -2712.843989505

C	-3.1555319	0.8068693	-1.6109068
C	-2.3003365	-0.5150895	-1.6777069
C	-2.6287097	-1.2599176	-3.0279459
F	-3.9491589	-1.2967823	-3.3100621
F	-3.0866670	1.4722704	-2.7797429
F	-2.7085617	1.6288403	-0.6612824
F	-4.4661506	0.5796830	-1.3632436
O	-0.9757615	-0.2558845	-1.7228807
C	-2.7225698	-1.4573525	-0.4812155
F	-2.8803713	-0.7698998	0.6593606
F	-1.7997570	-2.3966411	-0.2709437
F	-3.8957190	-2.0932673	-0.7155734
F	-2.0244171	-0.6705724	-4.0633994
F	-2.1968449	-2.5319067	-2.9848563
Cl	-0.0102346	0.2623125	-0.0786941
O	0.9589950	0.8192657	1.5513204

SUPPORTING INFORMATION

C	2.2946218	0.6401322	1.6408994
C	2.6703877	-0.8610732	1.9384578
F	2.3090099	-1.1987154	3.1909228
C	2.7544577	1.5263550	2.8610313
F	1.9223431	1.3897213	3.8971357
F	3.9928828	1.2222294	3.3061601
F	2.7626917	2.8277580	2.5246217
C	3.0853262	1.1195947	0.3590327
F	2.5358365	2.2239647	-0.1485940
F	3.0905176	0.1825767	-0.6002120
F	4.3817603	1.4053062	0.6287636
F	3.9971998	-1.1052141	1.8317342
F	2.0447614	-1.6945630	1.1078193

Xyz coordinates of $[(OC_4F_9)_4]^-$ optimized on B3LYP-D3BJ/def2-TZVPP:

57

Energy = -4803.047330096

I	0.0002818	0.0002934	0.0006938
O	0.0336657	0.0057754	2.1481943
O	2.1473199	-0.0145156	-0.0335196
O	-0.0336918	0.0249478	-2.1463905
O	-2.1470894	-0.0155321	0.0335331
C	2.9947216	-1.0868966	-0.0405149
C	-0.0356127	1.1006438	-2.9896255
C	-2.9942989	-1.0881862	0.0304107
C	0.0350578	1.0744567	3.0004351
C	-0.0446265	0.4887126	-4.4417994
C	-1.3096693	2.0130889	-2.8147947
C	1.2529256	1.9902205	-2.8178365
F	-1.2116066	3.1685315	-3.5013141
F	-2.4116802	1.3871120	-3.2423191
F	-1.4944218	2.3320215	-1.5301228
F	-0.3145352	1.4100452	-5.3880128
F	1.1467271	-0.0509860	-4.7367275
F	-0.9600502	-0.4744620	-4.5484366
F	1.4225664	2.8589000	-3.8339455
F	1.1754783	2.7081204	-1.6833421
F	2.3467592	1.2393339	-2.7478058
C	-4.4442707	-0.4711756	0.0415445
C	-2.8249032	-1.9725788	-1.2619608
C	-2.8231957	-2.0066628	1.3006903
F	-3.5131747	-3.1595354	1.1974260
F	-1.5396696	-2.3304028	1.4849660
F	-3.2494609	-1.3839603	2.4050865
F	-5.3938438	-1.3907418	0.3056737
F	-4.5483018	0.4874214	0.9620926
F	-4.7364993	0.0760358	-1.1470278
F	-3.8424355	-2.8389495	-1.4347846
F	-2.7543499	-1.2172013	-2.3526842
F	-1.6915247	-2.6925902	-1.1881980
C	4.4447670	-0.4696953	-0.0468079
C	2.8260801	-1.9831217	1.2436842
C	2.8233040	-1.9935091	-1.3192380
F	3.5133141	-3.1473147	-1.2272279
F	1.5397293	-2.3154362	-1.5062006
F	3.2493456	-1.3601228	-2.4176040
F	5.3936835	-1.3857480	-0.3251080
F	4.5465614	0.5007557	-0.9550250
F	4.7399022	0.0619437	1.1481567
F	3.8442087	-2.8505101	1.4078270
F	2.7554926	-1.2379445	2.3414903

SUPPORTING INFORMATION

F	1.6930411	-2.7029836	1.1637311
C	0.0413365	0.4508600	4.4475575
C	1.3103684	1.9871723	2.8352431
C	-1.2524064	1.9664077	2.8335675
F	0.3104926	1.3647873	5.4011958
F	-1.1508279	-0.0901962	4.7366212
F	0.9558222	-0.5138675	4.5480505
F	1.2107346	3.1389956	3.5275083
F	2.4104198	1.3580356	3.2635708
F	1.5001154	2.3127651	1.5530840
F	-1.4223699	2.8284191	3.8552072
F	-1.1726514	2.6917757	1.7039430
F	-2.3470545	1.2172483	2.7571895

Xyz coordinates of $[\text{OC}_4\text{F}_9]^-$ optimized on B3LYP-D3BJ/def2-TZVPP:
14

Energy = -1126.383048342

O	0.1606553	0.1243953	-1.8147659
C	0.0471858	0.0365452	-0.5346221
C	1.4638150	0.1138407	0.2033967
C	-0.6306575	-1.3390026	-0.0823163
C	-0.8504350	1.2118307	0.0732536
F	2.1545307	-1.0400533	0.0489035
F	2.2244482	1.0860201	-0.3252964
F	1.4232129	0.3505025	1.5459543
F	-0.5041534	-1.6585331	1.2376013
F	-0.1167314	-2.3724414	-0.7686542
F	-1.9597553	-1.3317953	-0.3386093
F	-0.1765178	2.3857558	0.0729372
F	-1.9513577	1.4051529	-0.6709560
F	-1.2842400	1.0277825	1.3531737

Xyz coordinates of ClOC_4F_9 optimized on B3LYP-D3BJ/def2-TZVPP:
15

Energy = -1586.409178232

C	0.7394859	0.0431451	1.3047987
F	1.3636821	-1.1401044	1.3086897
C	-0.1179315	0.2222003	0.0032407
C	0.7022606	-0.1983228	-1.2713965
F	0.7265311	-1.5286733	-1.4036421
F	-0.0424247	0.1131604	2.3865405
F	1.6620711	1.0017873	1.4080856
C	-1.4293954	-0.6512033	0.0961645
F	-2.0076899	-0.7404558	-1.1044666
O	-0.6539266	1.5208972	-0.0835057
Cl	0.3903483	2.7894225	-0.5477707
F	-1.1515634	-1.8841156	0.5263841
F	-2.3032596	-0.1003982	0.9355823
F	1.9678446	0.2276773	-1.1915098
F	0.1539674	0.3249832	-2.3671945

Xyz coordinates of BrOC_4F_9 optimized on B3LYP-D3BJ/def2-TZVPP:
15

Energy = -3700.305358691

C	0.7361939	0.0318509	1.3053324
F	1.3604706	-1.1513770	1.3109693
C	-0.1211994	0.2172687	0.0044934
C	0.6988836	-0.2120028	-1.2672873
F	0.7273613	-1.5419986	-1.3974516
F	-0.0432753	0.1041231	2.3886638
F	1.6612267	0.9904200	1.4076474

SUPPORTING INFORMATION

C	-1.4323093	-0.6596866	0.0979541
F	-2.0120646	-0.7472290	-1.1025533
O	-0.6514586	1.5099078	-0.0808484
Br	0.4197796	2.9396219	-0.5759753
F	-1.1539431	-1.8944066	0.5249985
F	-2.3062258	-0.1127821	0.9395004
F	1.9646158	0.2184076	-1.1890526
F	0.1519447	0.3078828	-2.3663909

References

- [1] P. Pröhm, J. R. Schmid, K. Sonnenberg, S. Steinhauer, C. J. Schattenberg, R. Müller, M. Kaupp, P. Voßnacker, S. Riedel, *Angew. Chem. Int. Ed.* **2020**, *59*, 16002.
- [2] J. R. Schmid, P. Pröhm, P. Voßnacker, G. Thiele, M. Ellwanger, S. Steinhauer, S. Riedel, *Eur. J. Inorg. Chem.* **2020**, *2020*, 4497.
- [3] A. R. Mahjoub, K. Seppelt, *Angew. Chem. Int. Ed.* **1991**, *30*, 323.
- [4] T. S. Cameron, I. Krossing, J. Passmore, *Inorg. Chem.* **2001**, *40*, 4488.
- [5] Y. Yan, J. T. Mague, J. P. Donahue, *CCDC 741550: Experimental Crystal Structure Determination*, Cambridge Crystallographic Data Centre, **2009**.